

(27) N 10 K 500

UNCLASSIFIED

AD 638 916

PROCEEDINGS OF THE FIRST AEROSPACE
MECHANISMS SYMPOSIUM, May 19-20, 1966

Jet Propulsion Laboratory
and
Lockheed Missiles & Space Company

Processed for . . .

DEFENSE DOCUMENTATION CENTER
DEFENSE SUPPLY AGENCY

FACILITY FORM 204	N67 16901	N67 16927
	(ACCESSION NUMBER)	(THRU)
	350	1
	(PAGES)	(CODE)
	CR-81503	30
	(NASA CR OR TMX OR AD NUMBER)	(CATEGORY)
	AD-638916	

CLEARINGHOUSE
FOR FEDERAL SCIENTIFIC AND TECHNICAL INFORMATION

U. S. DEPARTMENT OF COMMERCE / NATIONAL BUREAU OF STANDARDS / INSTITUTE FOR APPLIED TECHNOLOGY

GPO PRICE \$ _____

CFSTI PRICE(S) \$ _____

Hard copy (HC) 3.00

Microfiche (MF) 3.90

Approved Document
EOT

AEROSPACE MECHANISMS

PROCEEDINGS of the FIRST SYMPOSIUM

May 19–20, 1966

University of Santa Clara • Santa Clara, California

Sponsored by

**Jet Propulsion Laboratory, University of Santa Clara,
and
Lockheed Missiles & Space Company**

Edited by George G. Herzl

**Clearing House for Federal, Scientific, and Technical Information
U. S. Department of Commerce
Washington, D. C.**

FOREWORD

The boundaries of space technology have been expanding at an ever-increasing rate as more and more successful orbital flights and other space achievements have been recorded. As a result, the scope of the design principles, details, and applications with which the aerospace mechanism designer must be familiar has grown in variety, complexity, and volume.

It has been difficult for the aerospace mechanism designer to maintain a satisfactory awareness and sophistication in the state-of-the-art since, in the past, aerospace mechanisms have been discussed at conferences only as secondary aspects of other main topics, such as guidance and control, gravity-gradient stabilization, or the measurement of magnetism in space. It has been impractical, in many instances, for the designer to attend the many such conferences, and sit through session after session of specialized theoretical discussion providing only nominal consideration of the various aspects of mechanism design and development.

To provide a better opportunity, therefore, for the aerospace mechanisms designer to compare and correlate the specific knowledge gained from a wide variety of important mechanism design efforts, the First Aerospace Mechanisms Symposium was held on 19-20 May 1966. This Symposium, dealing exclusively with aerospace mechanism design and development, was sponsored by the Jet Propulsion Laboratory of the California Institute of Technology, Lockheed Missiles & Space Company, and the University of Santa Clara. The first aerospace symposium with such broad sponsorship, is supplied the first forum for an extensive discussion in depth of ideas, problems, and accomplishments regarding aerospace mechanisms. It stressed the practical aspects, with emphasis on actual flight test data and correlation with analytical predictions.

This volume presents the papers offered at the Symposium in order to provide the aerospace mechanisms designer with a useful source of ideas and information and to serve as a stimulant to the continuance of a periodic professional interchange in the field of aerospace mechanisms.

The Chairman is especially appreciative of the preparation effort and cooperation of the Symposium participants whose papers are presented in this volume. In addition, special thanks for making the Symposium possible are due to the Very Reverend Patrick A. Donohue, S. J., President, University of Santa Clara; Dr. J. P. Nash, Vice-President, Lockheed Missiles & Space Company; and Dr. W. H. Pickering, Director, Jet Propulsion Laboratory, California Institute of Technology.

The contribution of all phases of the Symposium organization and planning by Messrs. R. K. Pefley, S. Weissenberger, and E. J. Fisher of the University of Santa Clara; W. J. Shimandle and J. L. Adams of the Jet Propulsion Laboratory; and A. L. Rinaldo of Lockheed Missiles & Space Company is greatly appreciated as is the assistance of L. H. Goldich, M. E. Markley, and Dr. W. A. Kozumplik of Lockheed Missiles & Space Company in the editorial preparation of this publication.

George G. Herzl
Symposium Chairman

CONTENTS

	Page
FOREWORD	iii
FLIGHT-PROVEN MECHANISMS ON THE NIMBUS WEATHER SATELLITE	
S. Chorp and S. Drabek, Spacecraft Department, General Electric Company	1 ✓
EXTENDIBLE BOOM DEVICE	
W. C. Gamble, Lockheed Missiles & Space Company	27 ✓
MARINER-IV STRUCTURAL DAMPERS	
P. T. Lyman, Jet Propulsion Laboratory, California Institute of Technology	37 ✓
MECHANISM FOR SPACECRAFT REFLECTANCE-DEGRADATION EXPERIMENT	
E. Cornish, R. K. Kissinger, and G. P. McCabe, Lockheed Missiles & Space Company	51 ✓
NONCONTAMINATING SEPARATION SYSTEMS FOR SPACECRAFT (PROJECT ZIP)	
A. B. Leaman, Lockheed Missiles & Space Company	61 ✓
A VIBRATION ISOLATION MOUNT	
R. E. Reed, Jr., Ames Research Center, National Aeronautics and Space Administration	73 ✓
GEMINI/AGENDA DOCKING MECHANISM	
P. H. Meyer, McDonnell Aircraft Corporation	81 ✓
DRAG MAKE-UP SENSOR FOR LOW-ALTITUDE SATELLITES	
W. R. Davis, Lockheed Missiles & Space Company	91 ✓
SPACECRAFT HYDRAULIC TIMERS	
H. D. Trimble, Jet Propulsion Laboratory, California Institute of Technology	101 ✓
SOLAR CELL GRAVITY-STABILIZATION BOOMS	
B. D. Osborne, Lockheed Missiles & Space Company	109 ✓

ANALYSIS OF AEROSPACE IMPACT PROBLEMS	Page
D. Hayes, C. Cawood, and T. Kertesz, University of Santa Clara	123 ✓
COMPRESSION-SPRING SEPARATION MECHANISMS	
T. G. Harrington, Lockheed Missiles & Space Company	137 ✓
MARINER IV SCIENCE PLATFORM STRUCTURE AND ACTUATOR DESIGN, DEVELOPMENT, AND PERFORMANCE	
G. Coyle and E. Floyd, Jet Propulsion Laboratory, California Institute of Technology	145 ✓
NONMAGNETIC EXPLOSIVE-ACTUATED INDEXING DEVICE	
J. P. Bauernschub, Jr., Goddard Space Flight Center, National Aeronautics and Space Administration	157 ✓
LOW-TEMPERATURE EFFECTS ON MATERIALS FOR AEROSPACE MECHANISMS	
Warren E. Henry, Lockheed Missiles & Space Company	167 ✓
HIGH-IMPACT-RESISTANT MECHANISMS	
J. L. Adams, Jet Propulsion Laboratory, California Institute of Technology	181 ✓
A PYROTECHNIC SHOCK ISOLATION MECHANISM	
A. L. Ikola, Lockheed Missiles & Space Company	189 ✓
CONICAL PIVOT BEARINGS FOR SPACE APPLICATIONS	
G. G. Herzl, Lockheed Missiles & Space Company	203 ✓
COMPRESSION SPRINGS AT ELEVATED TEMPERATURES	
M. J. Siegel, University of Southern California	223 ✓
SIMPLIFIED SPACE MECHANISMS USING SUBLIMING SOLIDS	
H. M. Kindsvater, Lockheed Missiles & Space Company	239 ✓
ZERO-G TESTING OF SATELLITE INSPECTION MECHANISMS	
R. N. Lahde, Lockheed Missiles & Space Company, and J. W. Lebold, Lockheed-California Company	251 ✓
A CONCEPT FOR THE DESIGN OF VARIABLE-VISCOSITY, VARIABLE-STIFFNESS DAMPERS	
J. J. Lohr, Ames Research Center, National Aeronautics and Space Administration	263 ✓

ANALYSIS OF A SATELLITE ANGLE-OF-ATTACK SENSOR

W. E. Frye, Lockheed Missiles & Space Company

277 ✓

**EXPLOSIVELY ACTUATED (PYROMECHANICAL) DEVICES
FOR SPACECRAFT APPLICATIONS**

A. G. Benedict, Jet Propulsion Laboratory, California Institute
of Technology

285 ✓

**DEVELOPMENT OF A PASSIVE DAMPER FOR A GRAVITY-
GRADIENT STABILIZED SPACECRAFT**

E. J. Buerger, Spacecraft Department, General Electric
Company

297 ✓

**AN EXTENDIBLE STRUCTURE FOR SOLAR ELECTRIC POWER
IN SPACE**

D. E. Lindberg, Lockheed Missiles & Space Company

311 ✓

FLIGHT-PROVEN MECHANISMS ON THE NIMBUS WEATHER SATELLITE

By S. Charp and S. Drabek
Spacecraft Department
General Electric Company

SUMMARY

N67 16902

The second Nimbus* weather satellite is scheduled to be launched in early 1966. The two satellites contain mechanical devices and subsystems of a complexity and number higher than previously flown on spacecraft. These include a continuous motion solar array drive, fluid thermal control sensors and drives, horizon scanners and momentum generators, stored energy springs, hydraulic dampers, explosive-actuated bolt and cable cutters, and pneumatic components. Designs for and performance of these elements are discussed.

INTRODUCTION

The Nimbus weather satellite (figure 1), one of the most complex spacecraft ever orbited, is best known for its functional characteristics pertaining to observation of the earth's cloud cover, radiation temperatures, and weather phenomena. Not so well known are the design and operating characteristics of its large number of mechanical devices, mechanisms, and subsystems (figure 2). Many of these were designed specifically for Nimbus; others were designed originally for earth use and were modified for spacecraft use.

*The National Aeronautics and Space Administration, Goddard Space Flight Center, Nimbus Project Office, Greenbelt, Md., has systems management responsibility for the Nimbus series of spacecraft. Under contract to this group, the General Electric Company, Spacecraft Department, designed and developed the 3-axis, active stabilization and attitude control system; designed, developed, and fabricated the spacecraft structure, temperature control, and various components; integrated experiments and meteorological sensors; and tested the complete spacecraft.

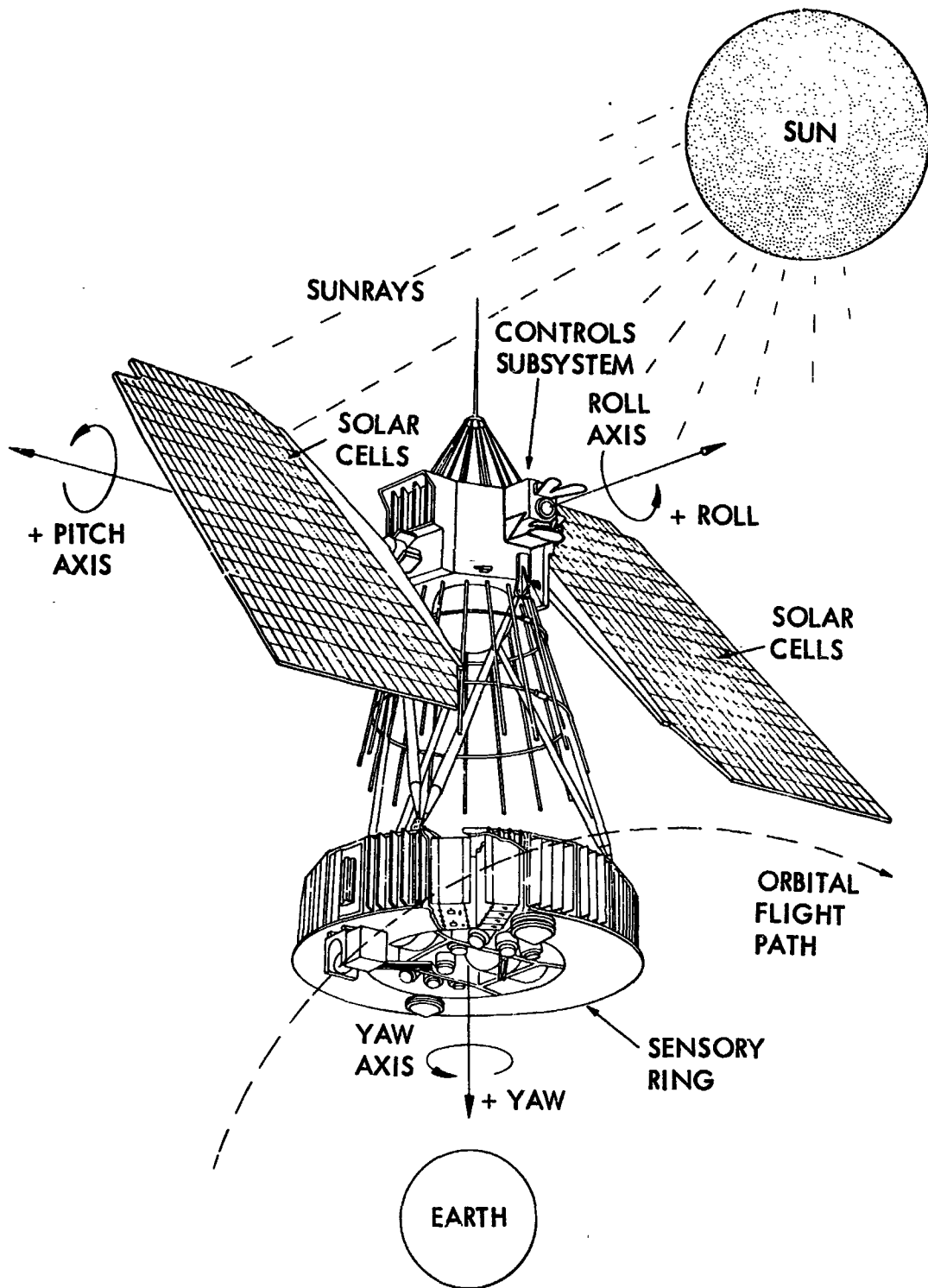
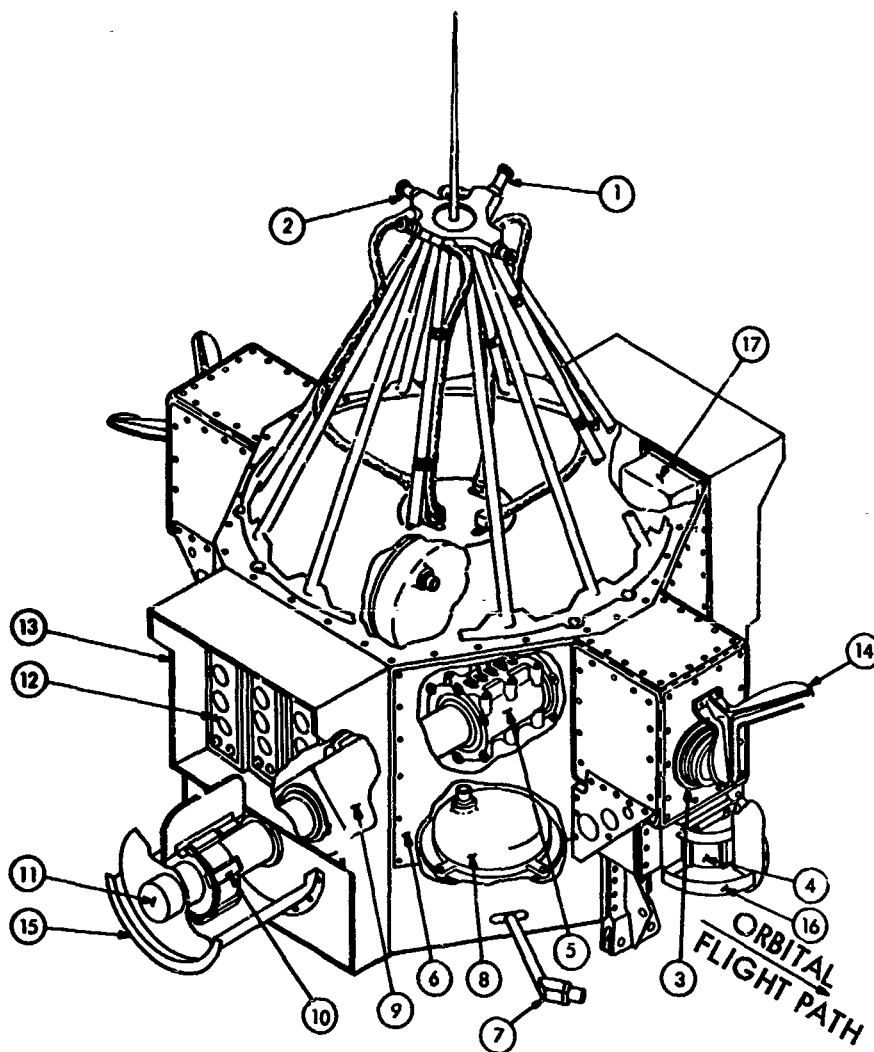


Figure 1 Nimbus Spacecraft



- | | |
|---|--|
| 1 ROLL NOZZLES (2) | 10 SOLAR ARRAY SUN SENSORS (2) |
| 2 PITCH NOZZLES (2) | 11 SOLAR ARRAY SHAFT |
| 3 IR HORIZON SCANNERS (2) | 12 SHUTTERS |
| 4 YAW SUN SENSORS (2) | 13 TEMPERATURE CONTROLS (2) |
| 5 SLIP RING ASSEMBLY | 14 IR SCANNER SUN SHADES (2) |
| 6 PANEL 1 (1 OF 6) CLOCKWISE
LOOKING FORWARD | 15 SOLAR ARRAY SENSOR
ALBEDO SHIELD |
| 7 YAW NOZZLES (4) | 16 YAW SUN SENSOR
ALBEDO SHIELD (2) |
| 8 FLYWHEELS (3) | 17 GYRO |
| 9 SOLAR ARRAY DRIVE MECHANISM | |

Figure 2 Nimbus Controls Package

Nimbus A orbited the earth for 26 days. The solar array drive then seized because of high-temperature deterioration of the lubricant in the motor drive. All other mechanisms operated in accordance with design. The second Nimbus satellite includes a redesigned solar array drive, a sample of which has been operating continuously, in simulated orbit cycling in a hard-vacuum environment, since May 1965.

The mechanisms on the spacecraft can be categorized as follows:

- Sealed components, continuous operation—horizon scanner, gyro, momentum generators, and pneumatic components
- Unsealed simple components, single operation—booster attachment, separation springs, paddle unfold system, and paddle support
- Sealed components, single operation—paddle dampers (launch vibration), bolt and cable cutters, switches
- Unsealed complex components, repeated operations—solar array drive
- Unsealed simple components, repeated operations—temperature controllers, shaft bearings, shutter position indicators and slip rings
- Other mechanical devices

These categories are treated in detail in the following sections of this paper.

SEALED COMPONENTS – CONTINUOUS OPERATION

Horizon Scanner

Two infrared horizon scanners (figure 3) are oriented parallel to the spacecraft body roll axis—one looking forward, one backward. These scanners continuously provide signals which, when processed, yield roll and pitch deviation angles between the spacecraft body axes and the local vertical.

The scanners operate in the 12 to 18 μ wavelength energy band, peaking at 14 μ . They detect the temperature difference, both day and night, between space and the relatively constant layer of carbon dioxide that surrounds the earth at an altitude of approximately 85 n. mi. An aperture 6 by 8 deg rotates conically about a 90-deg-apex angle. Optical

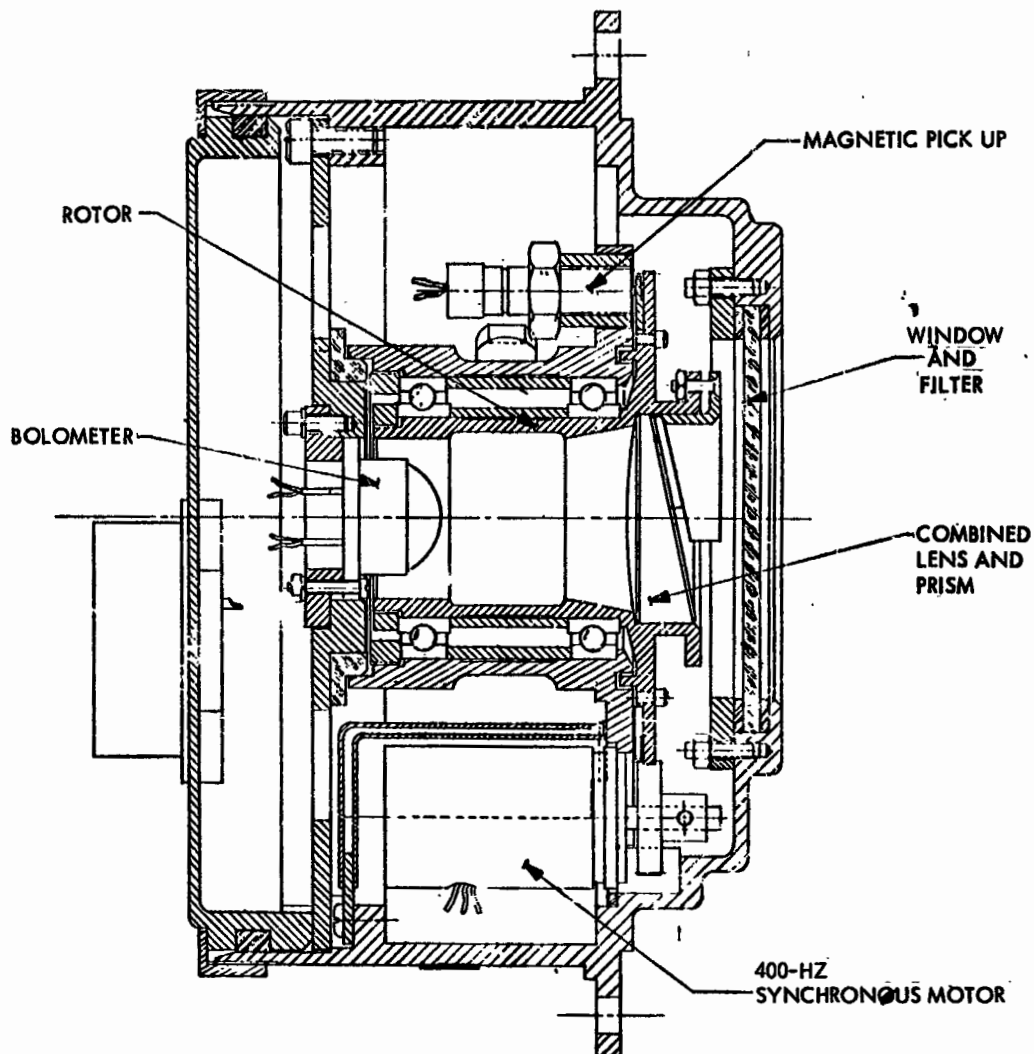


Figure 3 Horizon Scanner

scanning is provided by a prism mounted in a hollow shaft rotor, which rotates at 970 rpm following a single spur gear reduction of 8.25 to 1. A uniquely shaped sun-shade above each scanner keeps out the direct rays of the sun.

The accuracies of the computed error angles are within ± 0.2 deg. To ensure such accuracy, the scanner is aligned on the spacecraft to 3 min of arc in roll, 3 min of arc in pitch, and 18 min of arc in yaw.

An hysteresis synchronous two-phase motor operating at 8,000 rpm is driven from a 26-V, 400-Hz, square-wave power supply. It is a precision component having a

design life of 10,000 hr. The rotor is balanced to 20 μ in. oz at the synchronous speed. After addition of the pinion gear to the rotor shaft, this rotating assembly is dynamically balanced to better than 150 μ in. oz at 8,000 rpm. Rotor end play is held to less than 0.0003 in. with a reversing axial load of 1 lb. Radial play does not exceed 0.0005 in. when an 8-oz reversing load is applied not more than 0.25 in. from the bearing face.

The minimum motor pull-in torque is approximately 0.23 in. oz. The motor uses precision bearings and lubricants conforming to MIL-L-6085A. The preloaded bearings are double-shielded, Class ABEC-7 (or better) stainless steel hardened to Rockwell C58. The preloaded bearings (required for balance) are a major factor in the coast-down time of the complete rotor assembly. From full speed to rest, it is approximately 5 sec.

The optical system consists of a germanium window, a thermistor bolometer adhered to the back of a germanium lens, and the rotating prism. The prism rotor subassembly is dynamically balanced so that the unbalanced torque is no more than 150 μ in. oz at 970 rpm on its own bearings, and its slow-running torque must be below 0.20 in. oz.

The lubricant on prism rotor bearings and gears has low infrared absorption in the 12 to 18- μ wavelength region; it conforms to specification MIL-L-7870-A.

Yaw Gyro Reference Package

The gyro reference package consists of a floated, rate-integrating, single-degree-of-freedom inertial gyroscope; electronics sensing and driving circuits for rate mode operation; heater and heater-control circuits; and telemetry sensors and signal-conditioning circuits. The control current of a feedback null system is proportional to the angular velocity. For a 500 n. mi. altitude orbit, 1 deg of yaw error is sensed by the gyro as 3.564 deg/min.

No special design changes were made in the gyroscope to satisfy the needs of the program, although modifications were made in other parts of the package. The spin-

reference axis is kept perpendicular to the mounting surface within 0.5 mil. The output axis is perpendicular to the input axis to within 1.25 mil. The mounting surface finish is no rougher than 30 μ in. A coarse heater (20 w) is used for quick warmup; a fine heater (7.5 w) controls the temperature of the gyro flotation fluid to $162^{\circ} \pm 1^{\circ}\text{F}$.

The gyro measures angular rates over more than three orders of magnitude, from a threshold of 0.1 arc sec/sec (maximum) to 324 arc sec/sec, the maximum rate to be sensed. Hysteresis is less than 0.2 arc sec/sec so the gyro can respond rapidly to spacecraft oscillations. Linearity is better than ± 2 percent (6.48 arc sec/sec) to the maximum rate to be sensed. During its evaluation tests, the gyro measures angular rates to 7,200 arc sec/sec with a linearity of ± 0.5 percent (36 arc sec/sec).

Long-life tests on several gyro reference packages indicate the unit should exceed the design objective of 6 mo. continuous operation.

Momentum Generators

The fine attitude-control system includes three momentum generators, mounted one on each axis. Each is essentially a hermetically sealed "inside-out" motor, with integral speed sensors and flywheel having a high moment of inertia (41,400 gm/cm²). The two-phase, 400-Hz motor can be driven in two directions. The fixed phase has a single 26-v winding. The control phase has split, bifilar windings, each rated at 13 v. At no load, the motor speed is 1,250 rpm; the stall torque is 2 in. oz minimum with an input power of less than 4.8 w.

A two-phase tachometer signal is generated whose frequency is proportional to rotor speed. One cycle of signal is generated for each revolution of the rotor. Direction is detected by monitoring the lead/lag relationship between the signals from the two phases.

The momentum generator is required to operate for the full life period of the spacecraft. The quality of the bearings and the useful life of the lubricant are, therefore, important elements of design. The bearings, size R4, are double shielded and made of 440C stainless steel hardened to Rockwell C58. They have a two-piece retainer.

Two momentum generators were disassembled after approximately three years of combined shelf and service life. No significant deterioration that would affect in-orbit performance was observed in either the bearings or the lubricant (MIL-L-6085).

The momentum generator is a hermetically sealed unit; two cover halves are bolted together for strength, and each is soldered to a band for sealing. After initial assembly, it is evacuated to an internal pressure of 10^{-5} mm Hg, then filled with approximately 98 percent helium and 2 percent oxygen to a pressure of 0.5 atm. absolute, through a fill port that is crimped and sealed. The leakage rate does not exceed 10^{-5} standard cc/sec.

Pneumatic Components

The pneumatic system was originally intended for use with nitrogen at 2,500-psi storage pressure. It was converted, however, for use with Freon 14 at 1,400 psi to increase the strength safety margin of the tank and to obtain the increased propulsive capacity of this gas. The only change from the original design is the shape of the nozzles. The pressure regulator consists of a silicone rubber diaphragm on one side of which are ambient pressure and a calibrated spring, and on the other side are regulated (downstream) pressure of 35 psig and a balanced poppet valve. A tapered land on the stainless-steel poppet moves against a sharp-edged nylon seat to control the gas flow into the regulated pressure cavity in a single step. The poppet stem is sealed with two butyl rubber O-rings. It is ported internally to achieve a pressure-balanced design. Solenoid-driven pneumatic valves and the check valve have single, Buna-N rubber, O-ring seal seats. Static O-rings, including those in the filter and fittings, are also made of Buna-N. The tube fittings are a standard AN type with slightly tighter dimensional control. Flared tube fittings are used in all locations except for connections to the nozzles, where flareless fittings are used.

The major environmental influence is the pneumatic pressure within the components. The vacuum in space tends to aggravate any leakage rate over that existing at sea-level ambient. Carefully controlled tests under both types of laboratory environment, however, do not always indicate differences in leakage rate. This is probably because the total leakage is so low—usually less than 10 standard cc/hr—from the complete

system, including a regulator, seven valves, a check valve, a filter, and all tube fittings. The requirements of a space mission make it necessary to repeatedly prove such low leakage before, during, and after many environmental tests. The development of good shop practices in clean room areas and the elimination of bulkhead-type fittings have been the keys to success.

UNSEALED SIMPLE COMPONENTS- SINGLE OPERATION

Booster Attachment

An adapter section joins the spacecraft to the booster. The upper flange of the adapter mates with a stepped flange at the bottom of the spacecraft. The two flanges are held together by a segmented, circular vee-clamp assembly with a circumferential steel band tightened by two, tangential nut and bolt units located 180 deg apart (figure 4).

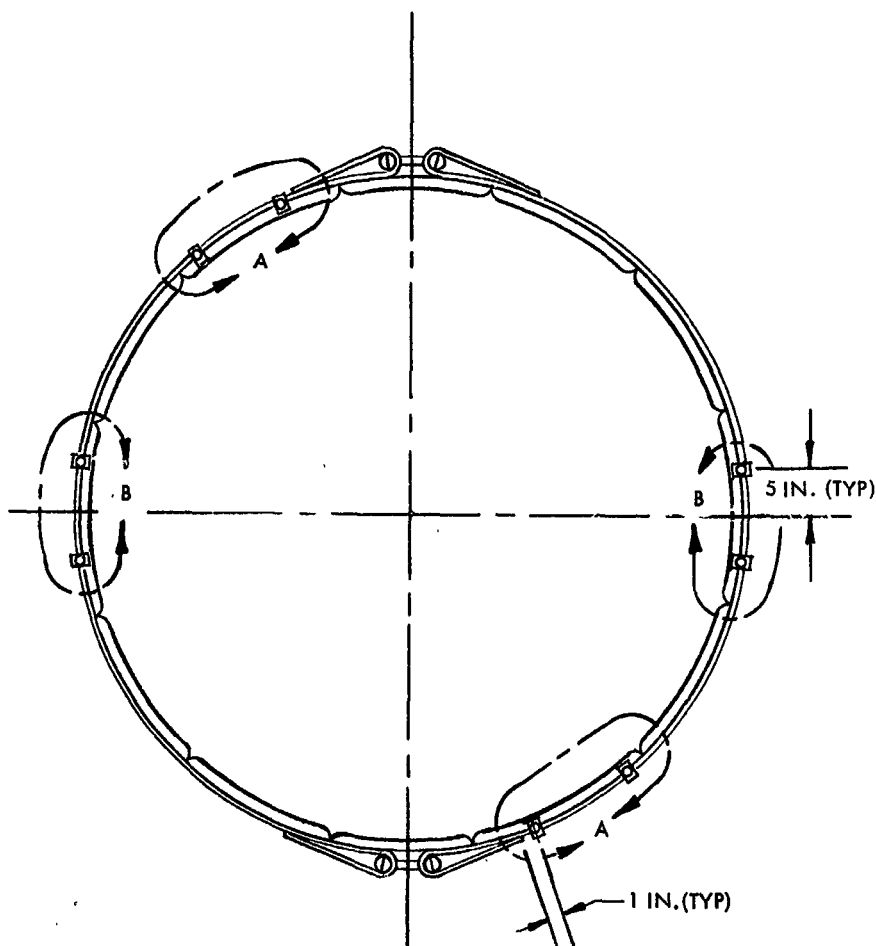


Figure 4 Vee-Clamp for Adapter/Spacecraft

The bolts are made of 8740 steel, hardened to Rockwell C 35 to C 40, and machined to a shank diameter of 0.270 in. The vee-clamp segments are Teflon-coated to assure low sliding friction against the flanges, and are coated lightly with silicone grease where they make contact with the band. The two bolts are cut by what are believed to be the most powerful bolt cutters qualified for space application. The cutter and anvil are specially designed to provide clean cutting, without shattering or debris. The explosive gas is contained behind an O-ring seal in a tight-clearance cutter assembly. Upon release, the steel band immediately contracts its 0.5-in. preloaded stretch and pulls the vee-clamp segments outward in a radial direction, providing instantaneous release around the complete periphery.

Separation Springs

Four spring cartridges located inside the adapter shell push apart the spacecraft and the adapter plus the Agena booster. The spring cartridges are carefully designed and adjusted for the spacecraft to achieve a relative separating velocity of 4 fps minimum and a tumble rate of less than 0.5 deg/sec around any axis.

The spring cartridges contain a central rod guided by two axial bearing assemblies. The ends of the coil springs are carefully machined normal to the axis of the spring. Although the springs can be compressed to solid height without taking a set, their travel is limited so as to achieve the most uniform and repeatable gradient. Their guide rods have screw and nut adjustments on each end to adjust for predetermined initial force settings and spring travel. The adjustments to the four springs are determined by digital computer analysis to assure low tumble rates even though the spacecraft center of gravity is not at its geometric center, and the four springs have different gradients as well as different force settings. The system is also designed to produce a total spring force slightly greater than the weight of the spacecraft. This condition causes a small gap between the two flanges when the spacecraft sits on the springs. The size of the gap near each spring is measured and compared with the calculated value obtained from the computer analysis. This serves as a check to ensure that the proper spring cartridge is located in its designated part of the adapter.

Paddle Unfold System

The two solar array paddles are folded toward each other so that the two outer edges touch at a series of points (figure 5). Each point has a hinge-like device with all the

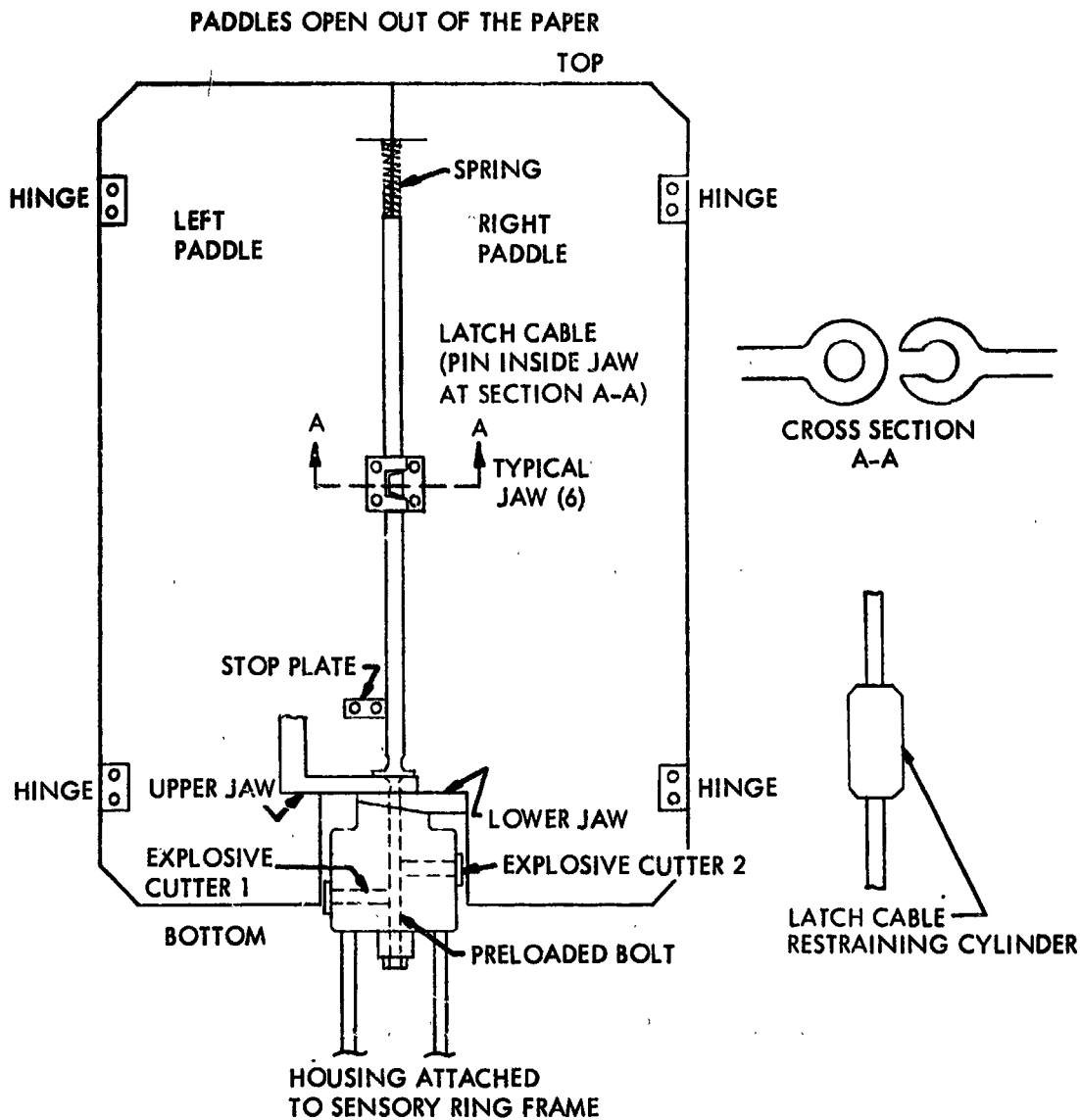


Figure 5 Paddle Unfold System

hinge pins of hard nickel-plated 303 Se stainless steel, tied together by a continuous cable. The hinge-like parts on one paddle contain two hollow cylindrical sections of 303 Se stainless steel to support the pins with about 0.002-in. diametral clearance.

The mating parts on the other paddle contain a single cylindrical section of 303 Se stainless steel, which fits loosely around the pin in the region between the two cylinders of the mating part. The single cylinders are slotted to let the cable slip through for separation during paddle-unfold, but still restrain the pin to withstand vibration during launch. After separation from the adapter section, the bottom end of the cable is cut by an explosive bolt cutter (figure 6). This permits a coil spring at the other end of the cable to pull the cable, moving all the pins out of position in the hinge-like devices.

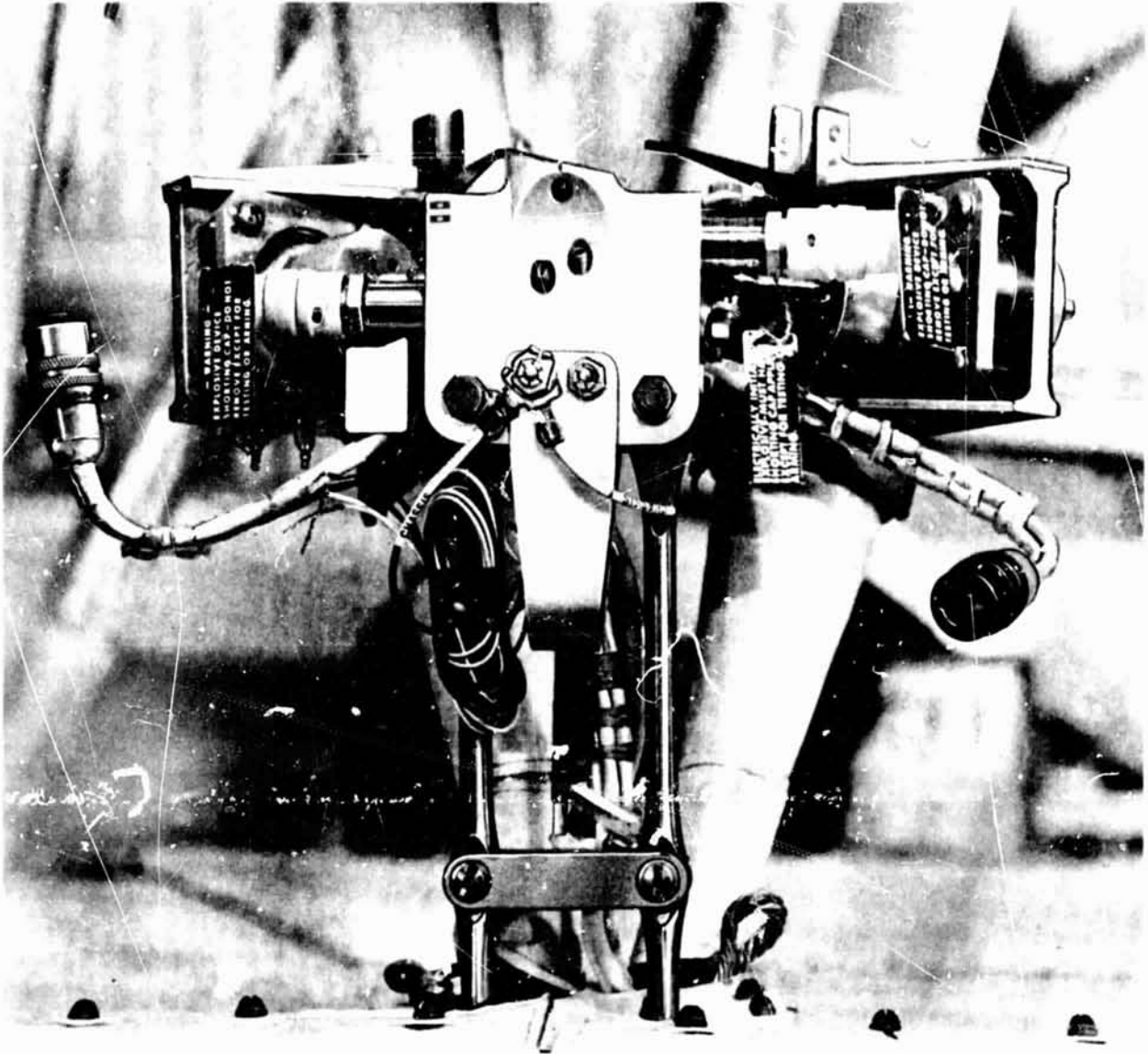


Figure 6 Paddle Bolt-Cutter Assembly

The hinge-like parts have been sprayed with MoS_2 to reduce friction. The slots in the single cylinder sections now easily pass over the cable, as the two paddles are pushed away from each other by a large number of coil and leaf springs. Gear motors, located on the hinge line of each paddle, control the rate of paddle movement. Latching devices engage and lock the paddles in full-open position.

Paddle Support

Because of the high vibration-induced loading into the paddles during launch, they are tied to a support to prevent destructive impact upon parts of the spacecraft and the shroud. The bottom hinge-like device is modified to represent two flat plates, one with a hole and one with a slotted hole. A modified, flanged pin fits through these holes. The flanged pin clamps the two flat plates against a block that is supported on two rods. The flanged pin is locked to this block with a nut tightened to a 2,000 lb pull. A strain-gage load cell is clamped in the assembly to monitor this loading. Locking the flanged pin in position automatically locates all the other pins in the paddle-unfold system in their hinge-like devices. This flanged pin is cut 2.5 sec after the spacecraft is separated from the booster rocket, initiating the paddle-unfold sequence. A microswitch on the supporting block, sensing the pulling of the cut pin from the locking position, powers the gear motors on the paddles. The system provides for a second (upper) bolt cutter to be fired in case the first (lower) bolt cutter is not successful.

The paddle-support system is stiff in the thrust direction but has loose pins to permit movement in the lateral direction. This requirement is dictated by paddle strength.

SEALED COMPONENT - SINGLE OPERATION (PADDLE DAMPER)

To restrain the lateral excursion of the solar paddles during launch vibration, the tie-down point is connected to two damper units (figure 7). Each is a single piston and cylinder assembly filled with Octoil-S oil. The periphery of the 2024 aluminum piston is sealed with a single O-ring against a 2024 aluminum cylinder having a 16- μ in. finish. A calibrated axial orifice through the piston permits a restricted

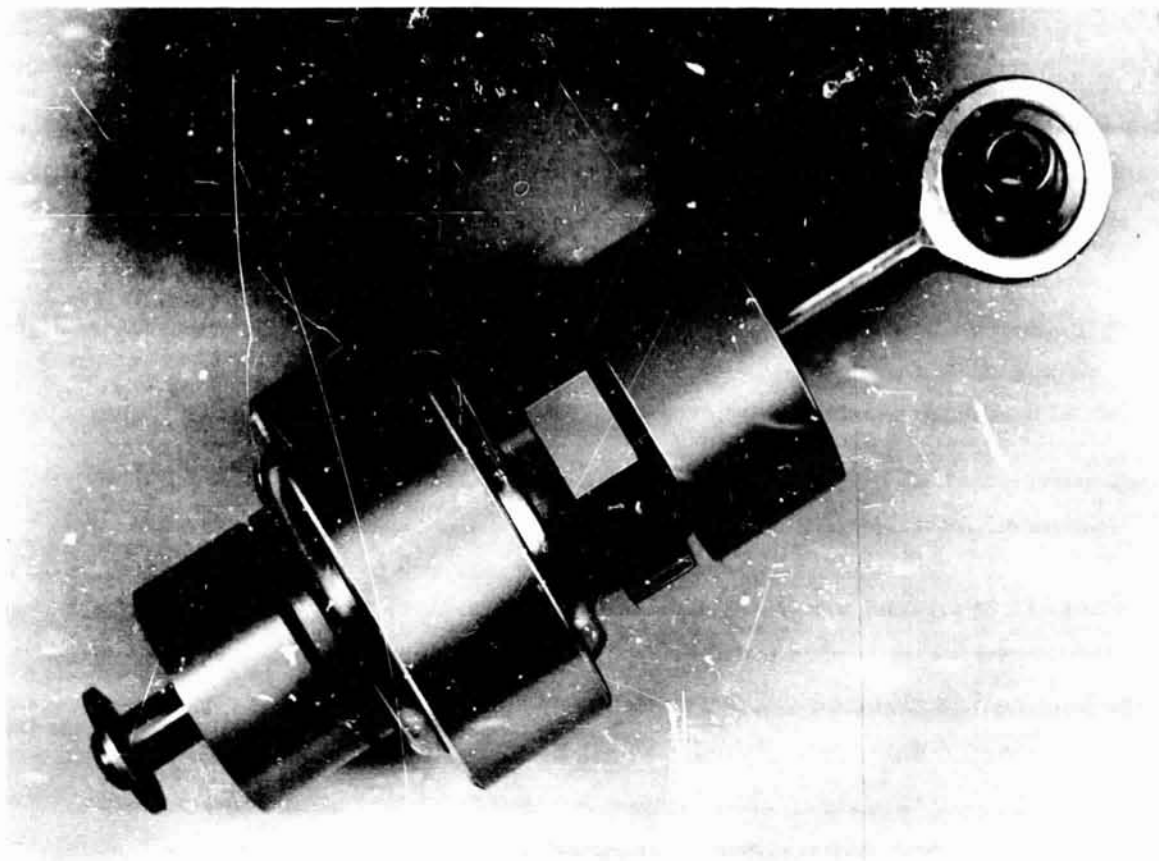


Figure 7 Paddle Damper

flow of oil to damp piston movement. The piston is pinned to a 303 stainless steel rod, which pierces both ends of the cylinder. One end of the rod has an integral mono-ball bearing for attachment to the paddle tie-down point. The cylinder is surrounded by a large mono-ball bearing for attachment to the spacecraft frame. Both bearings are lubricated with Versilube G-300 grease. The rod seals are parback-type backed by high-load bronze bushings to take the load. To assure the unit is completely filled with oil, all parts are individually wetted and all assembly, including final torquing of the end caps, is done while immersed in the oil.

Each unit is individually tested at 14 Hz to assure that its performance falls within the envelope (figure 8). This performance must be repeated after exposure to vacuum thermal testing to ensure that no degradation takes place after the spacecraft is put through its prelaunch test program.

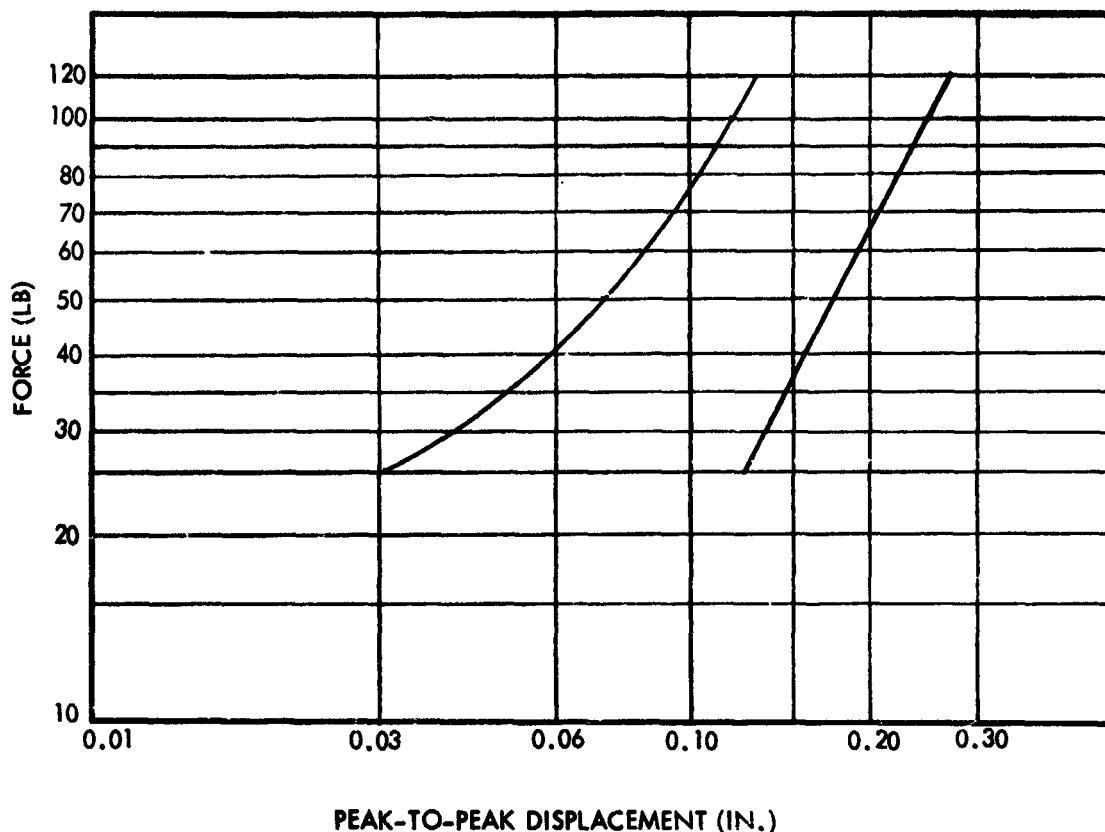


Figure 8 Paddle Damper Performance, Showing Limits of Displacement for a Given Force Oscillating at 14 Hz

UNSEALED COMPLEX COMPONENT— REPEATED OPERATION (SOLAR ARRAY DRIVE)

The solar array tracks the sun at 3.5 deg/min as the spacecraft is continuously oriented for its meteorological sensors to face the earth. A set of sun-sensors on each shaft provides signals that are amplified to control the drive motor. In the shadow of the earth, the drive slews the array at about six times normal speed to position it to the "dark period null," where it is ready to face the sun at the moment of "satellite sunrise."

The solar array drive used on the first spacecraft was based on a standard Size 8, two-phase, servo motor and a Size 15 servo gear box. Their primary adaptations for space environment included the use of Versilube G-300 grease in the gears and bearings and F-50 oil impregnated into a Nylasint cylinder slipped over the motor,

with a cover can over both the cylinder and the motor. Analysis of performance of the first flight indicated the motor rotor and bearings became too hot to benefit much from this configuration. An extensive redesign was undertaken.

The revised design (figures 9 and 10) eliminates the multipiece approach that used off-the-shelf servo hardware. The motor and gear assembly was redesigned as an integral unit. Gear alignment is greatly improved, and each gear mesh has controlled minimum clearance to eliminate binding at the expense of a greater minimum backlash than is tolerated on new servo units. The gears are hardened 4340 steel. The solar-array drive now consists of a Size 11 400-Hz, two-phase motor directly coupled to a 12,121 to 1, 7-mesh gear box. This unit is flange-mounted to a gear box containing a 2.33 to 1 gear reduction to a clutch shaft, followed by a 3 to 1 gear reduction to a drive shaft collar. The collar slips over, and is pinned to the shaft supporting the two solar array paddles. The motor gearhead contains size R-1, R-2, and R-4 shielded ball bearings, Class 7 ABEC, lubricated with G-300 silicone grease. The motor gearhead is given a 100-hr 'green run' at full speed, under load in vacuum. This is followed by complete teardown, inspection, cleaning, relubrication, and reassembly to ensure a perfectly clean unit without sign of degradation of any type. Only nominal provisions are made for sealing the assembly; no gaskets or O-rings are used. The attachment flanges are wetted with grease for thermal conductivity. Air and vapor leakage is permitted through a potentiometer assembly and two large bearings on the main shaft collar.

An eight-ball, detent-type, spring-loaded clutch is located between the last two gear meshes. This unit permits the paddle shaft to be rotated manually during handling in assembly and testing without transmitting a high, back-driving load into the motor gear box. It also prevents the accidental loading of full motor torque through the gears if the shaft is locked during special ground testing. The clutch slipping level, about 600 in. lb on the paddle shaft, in either direction, is high enough for the clutch to be fully locked during all operations in orbit.

Extensive investigations were conducted to confirm the cause of the malfunction on the first flight. The cause was soon determined to be excessive temperature in the

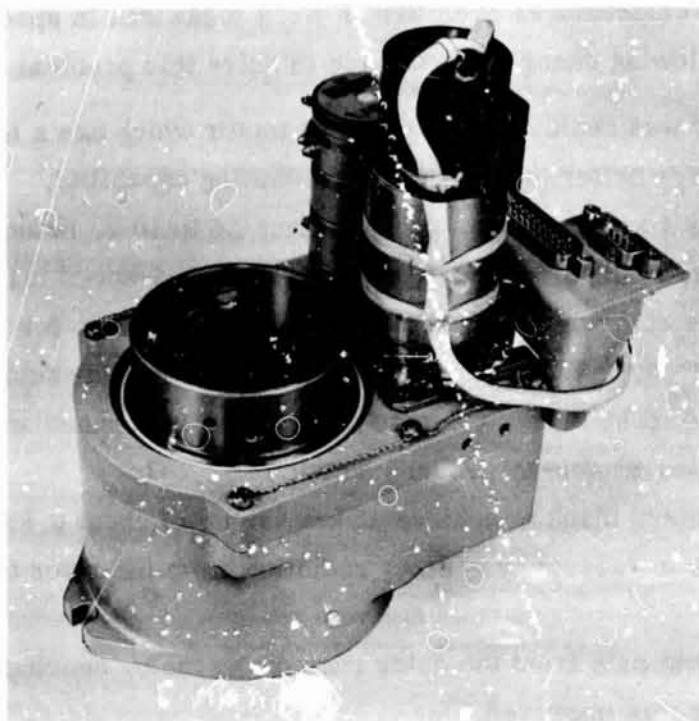


Figure 9 Solar Array Drive

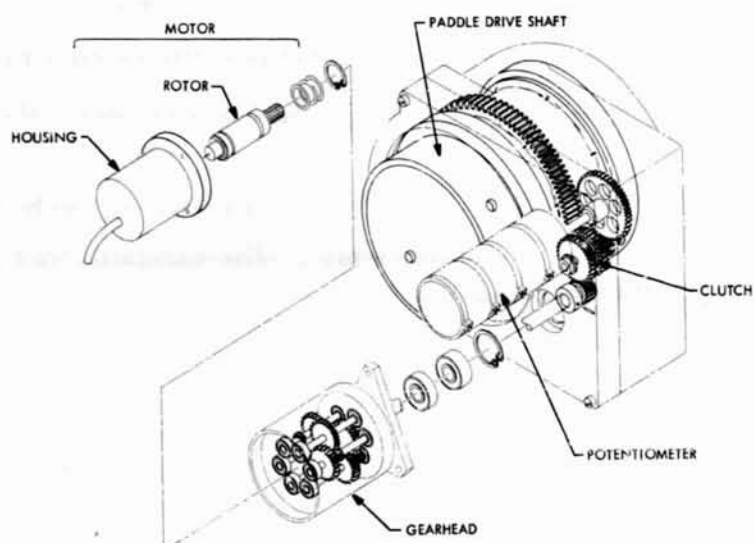


Figure 10 Solar Array Drive - Second Flight

rotor and its bearings. Temperatures over 300° F were measured in special laboratory tests. The following changes were made to solve this problem:

- The Size 8 motor was replaced with a Size 11 motor which has a longer rotor, providing for better torque and heat radiating capability.
- The voltage on the fixed phase was reduced from 26 to 10 v, reducing the electrical heating, at all times, for the required torque-speed loading. The voltage on the control phase was reduced from 18 to 12 v for maximum (slewing) speed, to further reduce the electrical heating during part of the orbit cycle. (The higher voltages on both the fixed phase and the control phase are available by ground control.)
- The rotor was painted black to achieve an emissivity of about 0.85, to improve heat loss in vacuum by greater radiation from the rotor to the stator.
- The conducting heat path from the outer race of the motor bearings to the stator housing was improved.
- A thermally conducting aluminum strap was wrapped around the motor and joined to the coldest spot in the control box.

With these changes, maximum inner-race bearing temperatures are expected to be below 160° F during normal orbiting cycles, based upon infrared temperature readings made in the laboratory in vacuum conditions. Two units have been on life test in vacuum conditions and exposed to maximum expected spacecraft temperatures. At this writing, one unit has been operating continuously in a simulated orbital cycle for 9 mo. and the other 5 mo. of actual time. At the beginning of these tests, each unit underwent "accelerated cycling" to achieve the equivalent of 6 mo. of cycles in 1 mo. of actual time. A recent examination of the G-300 grease in the bearings showed it to be almost entirely clean and milky-white. The exception was a faint yellowing in a small portion of one bearing.

UNSEALED SIMPLE COMPONENTS - REPEATED OPERATIONS

Temperature Controllers

Active temperature control is provided directly to 14 bays of the sensory ring and 2 parts of the control assembly. Further aided by internal heat conduction and balancing, plus passive temperature-controlling surfaces, the sensory ring and the control assembly are maintained at $25^{\circ} \pm 10^{\circ}\text{C}$. The active system (figure 11) consists of a set of insulated shutters, closing to reduce heat radiated to space, and opening to expose white-painted surfaces to cold black space to lose heat by radiation. The shutters consist of thin, lightweight frames covered with multiple layers of aluminum-coated mylar attached with adhesive tape. The assembly is fabricated with rivets and epoxy adhesive. The frames are hinged on two small flanged pins sitting in nylon bushings. Four or five shutters in each assembly are driven in unison through adjustable links with pin and bushing ends.

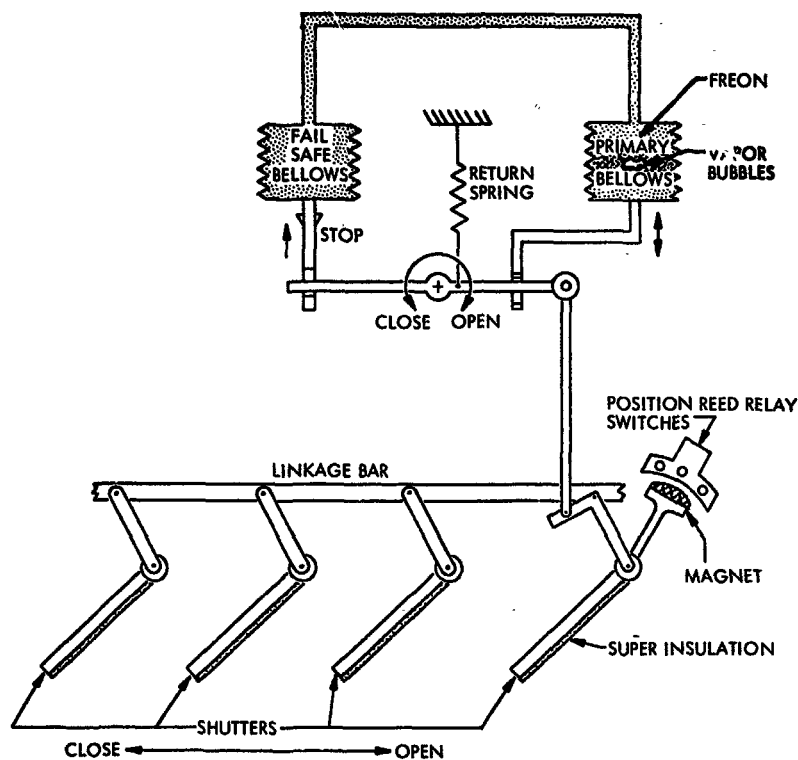


Figure 11 Active Temperature-Control System

The sensor and motive power for the actuator-controller originates in a liquid-vapor temperature-sensing and force producing system (figure 12). A Freon-filled bellows assembly, mounted directly on an aluminum plate, operates the linkage system that moves the shutters. This plate is spring-loaded against the side of the electronic packages in the sensory ring. (In the configuration used in the control box, the plate is an integral part of the structure, and electronic components are mounted directly on it.) The bellows assembly is also spring-loaded, and the output linkage system is adjusted to place it in the midpoint of its travel at a temperature of 25°C and to achieve

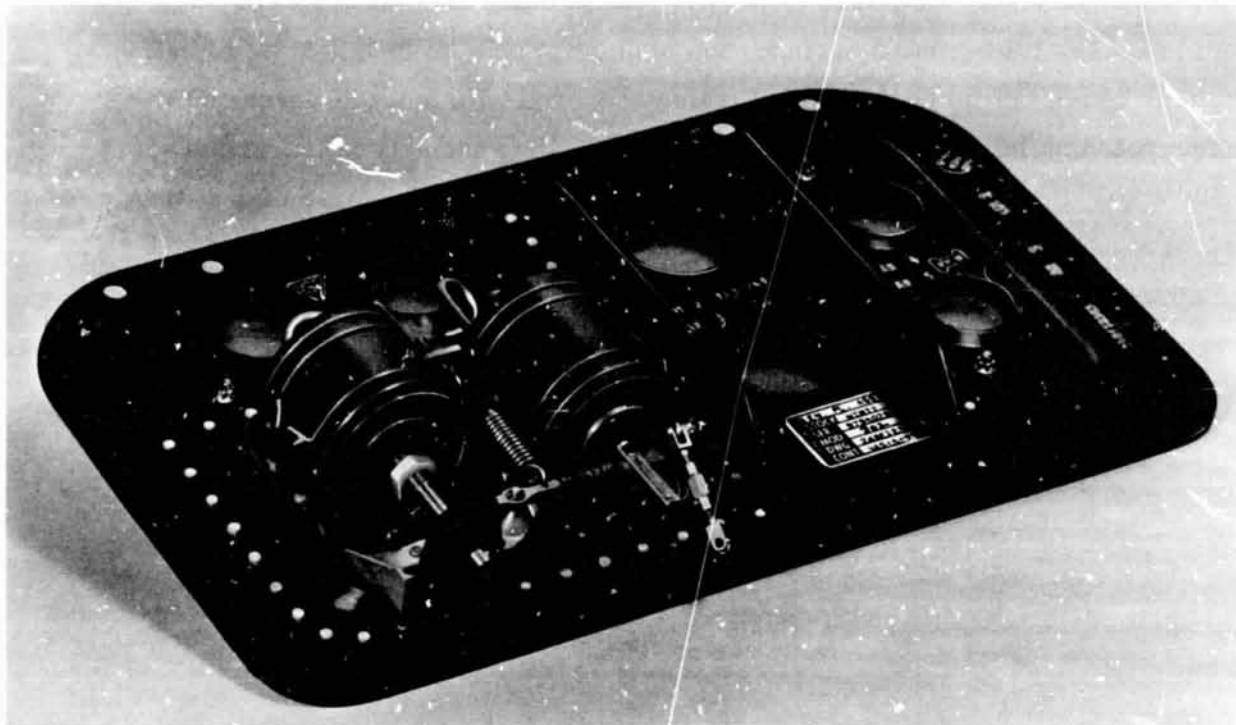


Figure 12 Temperature Controller

full stroke in about 6°C above and below this temperature. The linkage system is connected to one point off the hinge line of one of the shutters.

To provide against bellows-drive failure due to a leak, a second bellows is tied to the first through an open pipeline plus a free-running, slotted, linkage connection. During all normal operation, the fail-safe bellows is fully extended and has no effect on the linkage position. Should a leak occur, this fail-safe bellows would contract and pull the linkage system to place the shutters in a precalculated fail-safe position.

Shutter Position Indicator

To provide engineering performance data useful in verifying the thermal design, the orientation of the shutters for each active controller is measured, and the data are transmitted to the ground. Two types of position indicators have been used: The first flight spacecraft used an indicator assembly consisting of a ceramic magnet moved by the shutter actuator over a circular array of three magnetically actuated reed switches (figure 11). The three glass-enclosed switches and the magnet were encased in an epoxy compound for mechanical protection. The appeal of this design lay in the absence of friction and the slight opportunity for jamming, since a large clearance was maintained between the magnet and the reed switches. Because of the high incidence of breakage of the glass envelopes during manufacture, as well as the desire for more detailed information on the shutter position, the second flight spacecraft uses miniature potentiometers. These potentiometers (continuous film units lubricated with G-300 grease) are commercial stock units, except for minor changes to insure orbital operation following flight acceptance tests.

Slip Ring Assembly

Sun sensor signals and power are transferred from the rotating solar paddles to the stationary control system through a slip ring assembly on the drive shaft (figure 13). This consists of 4 power rings, 20 signal rings, brushes, brush holders, and associated hardware. Each slip ring is insulated electrically from other parts of the assembly by a mineral-filled epoxy glass laminate, which provides at least 1,000-M Ω resistance between mutually insulated points. The insulation is designed to prevent wear products from forming electrical conducting paths. Electrical leads are integral with each slip ring - No. AWG 16 for power, and No. AWG 22, shielded, for signals. Shields float at the slip rings.

Following extensive laboratory evaluation tests under simulated orbital conditions, the materials selected were rhenium-plated silver for the slip rings and a combination of 12 percent molybdenum disulfide and 88 percent silver for the brushes. These allow continuous direct currents to flow at maximum levels of 10 amp for the power rings

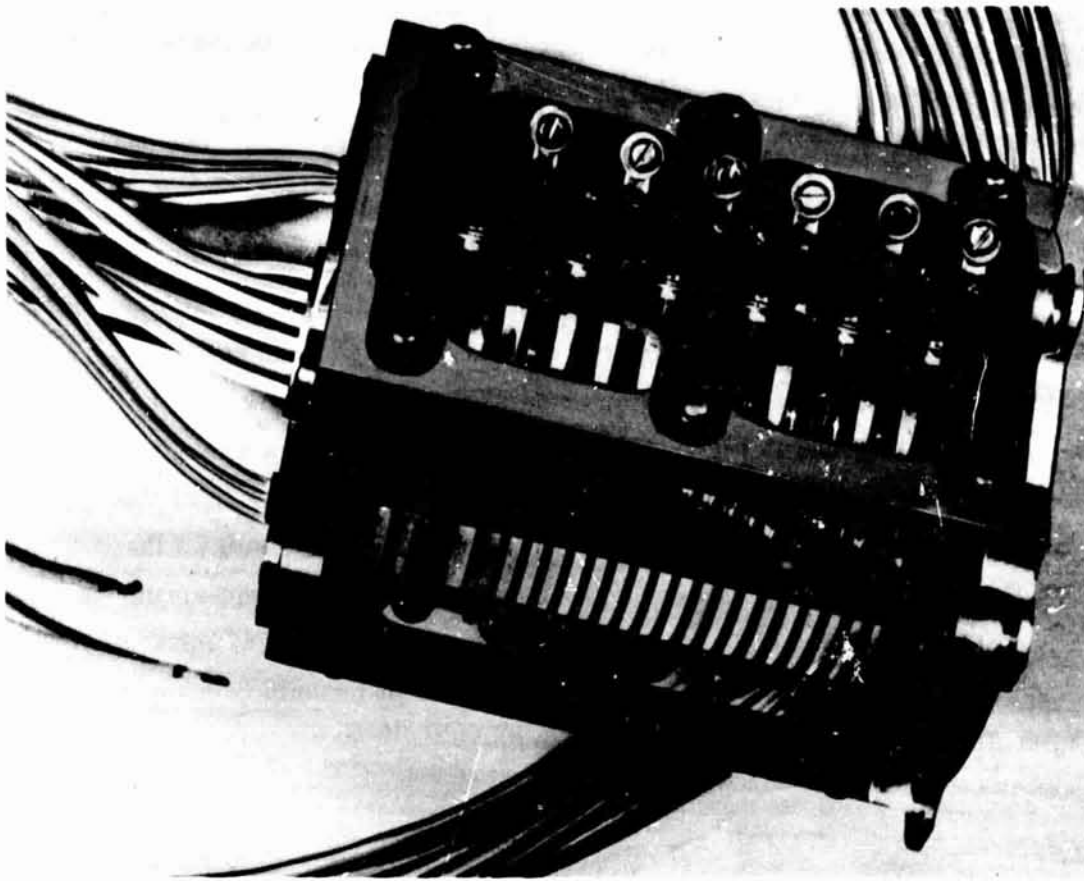


Figure 13 Slip Ring and Brush Assembly

and 1 amp for the signal rings, with brush-to-ring contact forces of 80 to 100 gm for the power rings and 40 to 60 gm for the signal rings. The actual current level passed through the signal rings is less than $20\mu\text{a}$. The electrical resistance between a slip ring and its associated brush contact is less than $10\text{ M}\Omega$ while carrying currents between 1 ma and rated current, and operating at speeds between 3.6 arc min/sec and 36 arc min/sec.

OTHER MECHANICAL DEVICES

In addition to the mechanisms associated with the spacecraft proper, there are electromechanical devices in several meteorological systems. The single-channel High Resolution Infrared Radiometer* has a single small motor (2-phase, 100 Hz.)

* International Telephone and Telegraph Company

that rotates a scan mirror and a radiation chopper. The five-channel Medium Resolution Infrared Radiometer* has two small motors (2-phase, 100Hz). One rotates a scan mirror, the other rotates an aperture plate which chops the radiation incident on each of the five detectors.

Each of the three cameras in the Advanced Vidicon Camera System** is equipped with a variable iris. Signals derived from a potentiometer on the solar array drive or from ground command actuate a small dc motor and gear mechanism (figure 14) in a null-seeking system, allowing the opening to vary from $f/16$ at the solar zenith to $f/4$ near the poles. In these cameras and the Automatic Picture Transmission System camera,** the vidicon is exposed for 40 ms by a two-bladed, solenoid-operated, focal plane shutter. Three tape recorders are carried for the first three

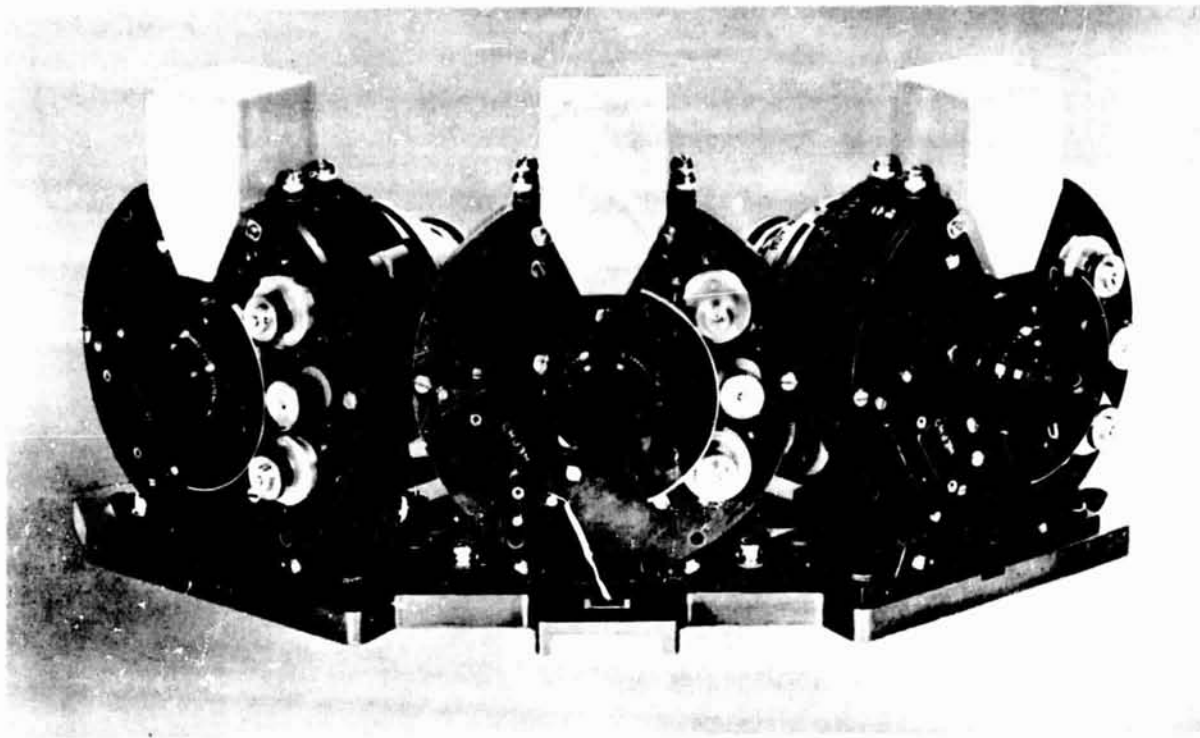


Figure 14 Cameras of Advanced Vidicon Camera System

*Santa Barbara Research Center

**Radio Corporation of America

systems above and the telemetry systems. All are in sealed containers, gas-filled to provide thermal convection and to reduce lubricant evaporation. Each is characterized by small size and a large ratio of playback to record speeds (approximately 30 to 1). (See figure 15.) Two recorders use endless tapes; the other requires reversal of direction of the recording medium. Momentum compensation is provided to minimize the effects of the tape-recorder rotating elements acting like flywheels or momentum generators to prevent disturbing the spacecraft attitude.

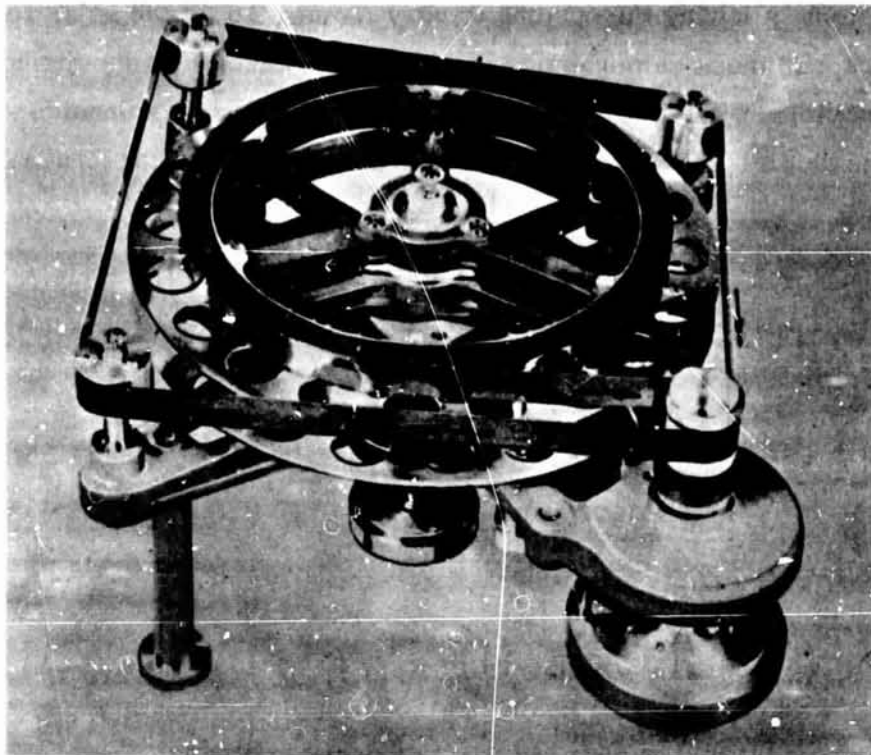


Figure 15 Tape Transport for the Advanced Vidicon Camera System

CONCLUSIONS

The influence of the space environment upon the design of devices and mechanisms, although significant in certain instances, is not severely limiting. The hard-vacuum environment influenced the choice of synthetic materials and lubricants, primarily as a function of their vaporization and outgassing characteristics. By controlling line-of-sight paths to the surfaces of sensitive optics, and by exposing subsystems and

the complete spacecraft to extensive vacuum testing to eliminate initial outgassing products, high confidence exists that this potential threat is controlled. While better lubricants for non-space applications are available, the Versilube G-300 silicone grease has proved most satisfactory for use with small, unsealed, motor-gear drives and large, slow-speed bearings. Hard-vacuum conditions also influenced the choice of materials for slip rings and brushes. The final choices did not result, however, in problems for the Nimbus application.

The high-energy proton and electron bombardment from the van Allen belt and from solar flares has not prevented the use of any mechanism or device on Nimbus, which orbits at a nominal altitude of 500 to 600 n.mi. Likewise, solar ultraviolet and low-energy proton and electron bombardment has not influenced design except with respect to the thermal coatings used on outside surfaces of the spacecraft.

Page intentionally left blank

EXTENDIBLE BOOM DEVICE

**By W. C. Gamble
Lockheed Missiles & Space Company**

SUMMARY

N67 16903

Requirements for extension devices for use in spacecraft configurations led to the preparation of a matrix analysis of all known mechanical means of deploying long booms from packaged extension systems. Requirements for high-density packaging, deployment in a 1-g field, multiple extension and retraction, and high strength prompted development of a unique device which forms a beam from three rolls of metal tape, with the metal tape edges joined by Velcro tapes and snap fasteners. The mechanism was designed, fabricated, and successfully tested.

INTRODUCTION

One of the pressing requirements of current spacecraft design involves the deployment or extension of booms or beams. In many cases, the terminal of the extension system must mount a device or several devices of varying masses and positional accuracies. The development of large deployable parabolic antennas, for example, has imposed the requirement for antenna feed booms of considerable length (e.g., 52 ft for an 80-ft parabola).

LMSC has participated in a number of NASA, USAF, and AEC programs and studies that require the use of long-extension booms or the deployment of devices at some distance from the parent vehicle. The NASA Advanced Technology Satellite - 4 Program (ATS-4), for example, includes the aforementioned deployable parabolic antenna which, in turn, necessitates the extension of a 52-ft antenna feed boom.

With these requirements in mind, LMSC conducted a matrix analysis of all known boom-extension devices. The result of this analysis is summarized in table 1. The 12 most promising types of extension devices were subjected to 8 evaluation criteria. Of these, the more important were the capacity to extend and retract in a 1-g environment; to extend and retract consecutively and consistently; to provide capacity for drawing cables, lines, and wiring during the extension operation; and the possession of low thermal-distortion characteristics as well as high dynamic damping.

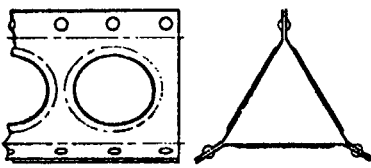
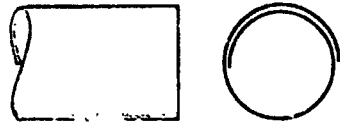
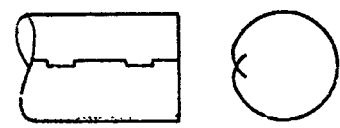
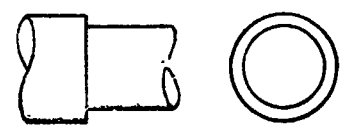


Although the summary table results are subjective, a detailed engineering analysis was made of each boom device listed in table 1. Booms 1, 2, 7, and 11 met most of the general requirements. Boom 2, the de Havilland system, was rejected because it did not demonstrate predictable twist after extension. This characteristic will not permit, for example, the terminal location of orbit-control gas jets. Further, the extension mechanism of the de Havilland boom has an extremely low L/D ratio, making the device difficult to mount in certain low L/D configurations and, in addition, the mandrel does not permit the enclosure of cables or tubing.

Booms 7 and 11 exhibited all necessary characteristics. Their durability is questionable, however, since multiple demonstrations revealed a progressive deterioration of structural properties.

For continued development, and for determining the problems inherent in deployment devices of this type, boom 1 was selected. Several working models were fabricated and tested. This device is shown in figures 1 and 2.

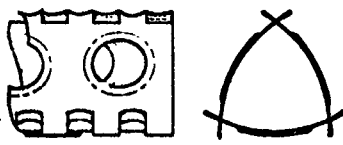
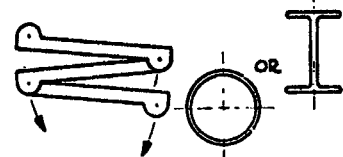
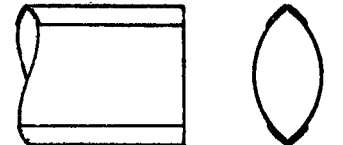
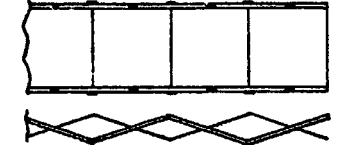
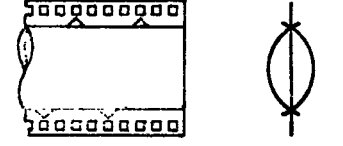
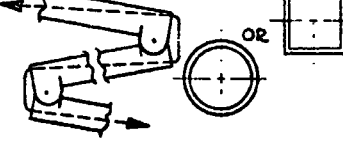
DESCRIPTION OF BOOM MECHANISM

The boom mechanism is designed to assemble, extend, retract, and disassemble a lightweight, thin-web beam of triangular, box, or other cross section. In the development model, the beam is made of three preformed webs which are flanged at 30 deg along both edges. The mating portions of strips of Velcro tape, as well as a series of mating fasteners at appropriate intervals, are bonded to each flange.

No.	Configuration	Illustration	Manufacturer	Description	Background and Manufacturing Experience	Flight Experience
1	Triangular Extendible Boom		MSC	Preformed sheet metal tapes unrolled from storage drums; assembled by pressing Velcro tape and snaps together	Working model 4 in. wide and 40 ft long, with aluminum panels; additional development continuing	None to date
2	Storage Tubular Extendible Member (Stem)		DeHavilland Aircraft Canada	Preformed spring sheet stock unrolled from drum; overlapped into tube through forming die for alignment	Many current applications up to 1,000 ft long and from 0.001 to 0.010 in. thick	Advanced Technology Satellite RAE, Gemini, and many other vehicles
3	Interlocking Extendible/Retractable Room		Melpar Inc., Virginia	Preformed spring sheet stock pulled from drum; edge teeth interlocked in forming die to maintain alignment	Engineering working model constructed; still undergoing development	None to date
4	Telescoping Cylinders		Several	Nested cylinders extended with gas; locked in end flanges to maintain alignment and rigidity in that position	Old concept used extensively in previous applications	Unknown
5	Self-Extruding Foam Cylinder		None	Fiberglas cloth pulled from storage drum by forming in die with foam filler, resulting in straight and rigid member	None; believed to be new concept which may prove applicable to this design	None to date
6	Inflatable Tripod		LMSC	Aluminized mylar tubes inflated with gas; aligned by a system of spacers and peripheral guy wires tied in place	Working model, 18-ft long, constructed and tested; further development proceeding	None to date

Structural Problems	Thermodynamic Problems	Ground Deployment Demonstration	Impact Upon Satellite Configuration	Requirement for Deployment Power	Comment
Slightly higher unit weight than cylindrical members, caused by material distribution	Requires external sock to minimize thermal gradients and deflections; Sheets isolated	Completely extendible and retractable many times in ground environment	Requires space about centerline of system for three storage drums and driving mechanism	Motor to pull tapes against brake and press flanges together	Probably one of the heavier systems. Detailed analysis may prove that offsetting illumination holes can eliminate thermal sock
Lacks torsional rigidity; unsymmetrical bending characteristics; unpredictable twist	Same as 1	Completely extendible and retractable many times in ground environment	Requires relatively long space on centerline for storage drum, form die, and driving mechanism	Motor to drive tubing through mandrel	Relatively heavy system with proven reliability record but twist unpredictable. Satellite arrangement will determine applicability of configuration
Limit on torsional and bending stiffness due to crippling in edge teeth	Same as 1	Progressive deterioration of structural properties with multiple demonstrations	Requires relatively long space on centerline for storage drum, form die, and driving mechanism	Motor to drive tubing through mandrel	Appears to offer relatively lightweight, stiff, and torsionally stable structure, but manufacturing tolerances critical and properties degrade with number of activation cycles
Physical property restriction due to diameter limitations; possible solution by use of graduated sections	Same as 1	Completely extendible and retractable many times, depending upon detail design	May require long space on centerline, depending upon relative dimensions of cylinder	Power for release squibs only; stored gas provides deployment energy	Relatively heavy weight because of joints and taper; strength and stiffness dependent upon fixity achievable in joints. Retraction can be designed into joints if required.
Latent problem areas possible with development of working model	Appears to offer minimum thermal deflection because of nonmetallic construction	Not repeatable; many samples can be made to demonstrate system	Space for cloth storage drum and foam tank required but forming die must align with centerline	Release of foam pressure theoretically will force cylinder through mandrel lubricated by resin	Relatively lightweight system with good potential stiffness and torsional stability; not retractable. However, system not developed and reliability must be established by multiple samples
Low torsional and bending stiffness after releasing inflation gas in space	Spacing and size of tubes may be varied to minimize thermal deflection	Ground aids required for demonstration purposes	Relatively small space needed; requires consideration of possible entanglement of adjacent spacecraft protuberances with strings.	Power for release squibs only; deployment energy provided by stored gas	Design probably lightest weight concept but adequate stiffness difficult to achieve. Ground demonstration relies greatly upon ground aids for deployment

Table 1 Extendible-Boom Selection Matrix

No.	Configuration	Illustration	Manufacturer	Description	Background and Manufacturing Experience	Flight Experience
7	Edge-Locked Triangular Boom		LMSC	Preformed spring sheet metal tapes unrolled from drums; assembled and aligned by pressing tabs into mating slots	None to date; concept believed new and offers promising solution to problem	None to date
8	Spring-Actuated Folding Boom		Several	Several hinged links swinging out and locking into straight beam by action of torsion, leaf, helical, or sheet-coil springs	One of oldest means of accomplishing function; used extensively	Unknown
9	Flattened Tube Boom		LMSC	Preformed sheet metal tapes joined with fabric tapes; assumes shape upon escape from storage drum	Aluminum working model, 20 ft long, constructed for demonstration purposes	None to date
10	Pantograph		LMSC	Structural panels hinged together and stabilized by attachment to hinged beams at edges; actuated by motor	Concept employed for several contemporary solar array systems with resulting high reliability	Programs 461 and 770, and several other vehicles
11	Instarect Reel-Stored Rigid Boom		Sanders Associates, Nashua, N. H.	Three-piece boom erected from flexible reel of stored material with required spring properties	Working prototype developed	Unknown
12	Cable-Actuated Folding Boom		Several	Several hinged links swinging out and locking into straight beam by applying tension to cable inside links	Classic mechanical device with many contemporary applications	Unknown

Structural Problems	Thermodynamic Problems	Ground Deployment Demonstration	Impact Upon Satellite Configuration	Requirement for Deployment Power	Comment
Latent problem areas possible with development of working model	Space illuminating holes or thermal sock usable as means of minimizing gradient and deflections	Progressive deterioration of structural properties with multiple demonstrations	Requires space about centerline of system for three storage drums and release mechanism	Necessary to press tapes together before flight; unrolling accomplished in space without aid	Design provides conduction path between sheets, self-indexing feature, and good stiffness; however, tolerances are critical and properties degrade after first activation cycle
Best combination of torsional and bending stiffness provided by cylinder; latching method critical	External thermal sock usable to minimize thermal gradients and deflections	No problem; completely extendible and retractable many times without degradation; requires aids	Requires some storage space and considerable clearance to allow arms to swing out	Power for release squibs only; necessary energy of deployment stored in springs	Very simple, direct, and well established method with many current and past applications. Only simple analysis needed, but requires adequate space and clearance and careful latch design to be efficient
Variation in bending stiffness around periphery, and dependence upon spring and joint properties	External sock required to minimize thermal gradients and deflections	Completely extendible and retractable many times; may require some ground aid	Must be wrapped about large-diameter rotating storage drum and guided during release	Motor to rotate storage drum and overcome drag in guides	Flexibility in joint to permit rolling for storage causes some torsional and bending softness. Relatively large cylindrical space is required for storage
Torsionally soft; weak in bending in one axis	Dependent upon application and detail design	Usually aided by drapery rod system, but extendible and retractable many times	Requires rectangular storage area for actuator and track	Customary use of small motor to actuate one end and overcome the hinge drag; squib release device	Concept quite reliable and suitable for solar array deployment. Torsional and bending softness may limit use to this application
Adequate tab-stiffness and hole-bearing strength requiring relatively high boom unit weight	Required external sock to minimize thermal gradients and deflections	Ground-aids requirement dependent on design; extendible and retractable many times	Requires space about centerline of system for storage drums and mechanism	Motor to drive storage drums, cams, and rollers	Relatively stiff member in both bending and torsion; can be made of several metallic or dielectric materials with required spring properties
Links designed to function as eccentric columns as well as beams and torsion members; matching important	External thermal sock to minimize thermal gradients and deflections	No problem; completely extendible and retractable many times	Requires some storage space and considerable clearance to allow arms to swing out	Motor release squib and tension spring	Very simple, direct, well established method with many applications; requires careful latch design; moderately heavy because of multiplicity of load conditions; considerable clearance required

Table 1 (Contd)

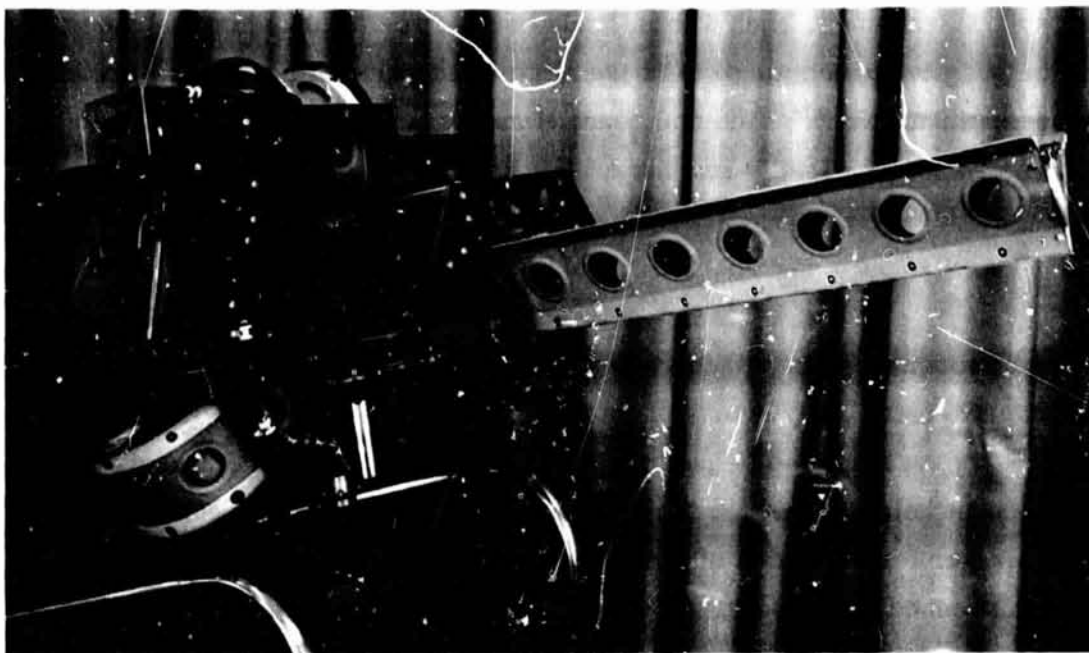


Figure 1 Extendible Boom Device - Side View

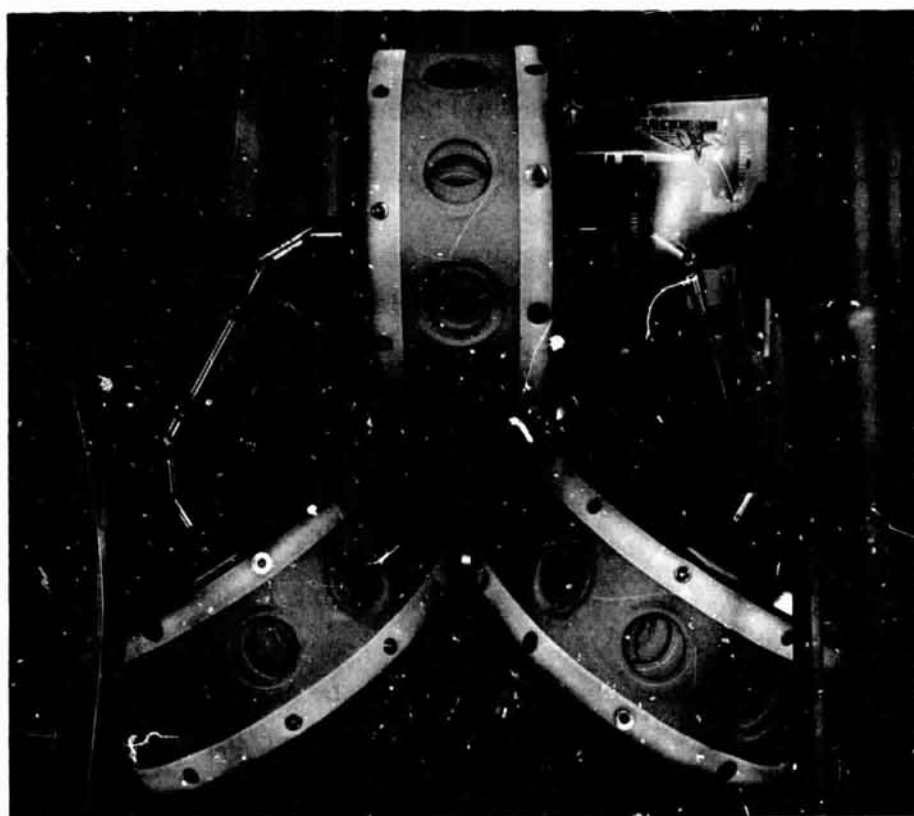


Figure 2 Extendible Boom Device - Rear View

As shown in table 1 sketches, each web is loaded onto a reel situated on the underside of a base plate. On the upper side of the base plate are three pairs of power-driven pressure rollers, through which the beam flanges are passed. Above these pressure rollers are three roller fair leads, one for each corner of the beam.

METHOD OF EXTENSION

The power-driven forming rolls pull the webs from the reels and press the flange edges together. Extension is by means of friction between the rubber roller surfaces and the web. Extension may also be accomplished by means of sprocket wheels and appropriate sprocket holes in the web flange. In the demonstration model, an electric motor provides power for extension of the boom. Power may also be derived from hydraulic or compressed air motors.

The three sets of forming wheels are linked by jointed shafts, thus making all three wheel sets drive at a constant rate. The three web reels are also linked by shafts. The rate at which the web is pulled from the reel is determined by clutches on these wheels, so that the tendency of the web to unwind because of spring tension is controlled.

The webs pass from the reel over a rotating disc. This disc keeps the Velcro tapes from touching until they are mated by the drive wheels. Between the disc and the drive wheels is a machined finger, positioned just before entrance of the flanges to the rollers. Adjustment of the position of this finger assists in alignment of the beam.

The length of beam that can be produced is dependent entirely on the length of the webbing supplied in the storage reels. In the demonstration model shown in the figures, the extension rate is 37 in./min. Beams exceeding 1,000 ft in length can be produced in a zero-g condition. Extension under a 1-g condition is limited by the strength of the beam, the type of material used in the web, and the attitude of the machine during extension. Vertically, the 4-in. beam described in the demonstration model can be erected up to 60 ft.

RETRACTION

Retraction is accomplished by energizing the motor driving the reels through the fully torqued electromagnetic clutch. Differences in gearing between the motors (constant gear rate at pressure rolls versus increasing radius at reels) is taken up by slippage of the electromagnetic clutches. The webs are separated by the fingers as they pass over the pressure rollers.

VELCRO TAPE FASTENERS

Velcro is a patented fabric fastener consisting of nylon tapes joined by hooks imbedded in a nylon pile. It is also produced from stainless steel. One tape contains rows of nylon hooks; the other tape contains the nylon pile. When the tapes are pressed together, they exhibit great adhesive strength in shear although they can be easily peeled apart.

A design problem in the original machine developed from the use of Velcro. It was found, during the tests, that though the metal tapes failed before the Velcro tapes were parted (even with 0.025-in. aluminum panels), the gradual take-up of the thousands of hooks permitted considerable distortion of the beam when torqued. For this reason, the snap fasteners were used to provide initial torsional rigidity. Since the snaps are imbedded in the Velcro, parting of one snap at a strain point is limited to that snap alone; no zippering effect is permitted.

MECHANISM DURABILITY AND TEST RESULTS

A complete series of structural tests is planned for both the booms and the extension device. In general, the tests will involve strength characteristics of sample booms fabricated of magnesium, aluminum, steel, and BeCu, in various cross sections. Tests with the mechanism will involve extension accuracies and retractions. The test model shown in figures 1 and 2 has been extended and retracted over 200 times with only one failure. This failure occurred in the Norden bombsight clutch (from World War II surplus) used in the retraction system.

CONCLUSIONS

Continued testing of development models of the extendible boom device has provided sufficient data to verify the validity of the original matrix analysis, and to lead to the conclusion that the extended boom has the characteristics of strength, dimensional accuracy, and reliability of operation necessary for a number of spacecraft applications. Should development funding become available, the structural tests of boom samples will verify the structural integrity data which so far has been based on calculations and extrapolation of design calculations.

Development work now under way by the Velcro Corporation in steel tapes appears to have direct application to the boom device program. While these tapes are basically intended for high-temperature applications, their use in the boom device should provide increased torsional rigidity and bending strength.

Successful testing of the device has continued, with the basic set of tapes. These tapes have shown no tendency to fail or warp; the extended boom is both rigid and straight. It is proposed to fabricate a device that will extend clinched tapes (without retraction) of various material types and gages. It will be evaluated for ground as well as space applications.

MARINER-IV STRUCTURAL DAMPERS*

By Peter T. Lyman**
Jet Propulsion Laboratory
California Institute of Technology

SUMMARY

Structural dampers employed on the Mariner-IV spacecraft were constructed of spring-centered struts consisting of two concentric tubes whose annulus was filled with a very viscous silicone fluid. From early testing throughout the spacecraft development program these dampers performed without difficulty. Since there were no telemetry measurements which yielded direct performance of the spacecraft structure, satisfactory flight performance by the dampers is inferred from the proper functioning of all Mariner-IV subsystems.

INTRODUCTION

The structural dampers employed on Mariner IV (ref. 1) consisted of a pair of spring-centered damper struts for each of the four solar panels, and two spring-centered damper struts supporting the low-gain antenna waveguide. Figure 1 shows the relative launch configuration of a solar panel and the associated damper struts during a development test. The solar panel dampers are attached to the solar panel by means of a pyrotechnic pinpuller which is actuated after the spacecraft is separated from the launch vehicle, permitting the panels to deploy to the cruise position. Figure 2 shows the low-gain antenna waveguide supported by its two dampers during a development test.

*This paper presents the results of one phase of research carried out at the Jet Propulsion Laboratory, California Institute of Technology, under Contract NAS7-100, sponsored by the National Aeronautics and Space Administration.

**The author acknowledges the efforts of William E. Layman of the Jet Propulsion Laboratory for his efforts in developing the damper concept used on Mariner II, and then demonstrating the feasibility of this concept for Mariner IV.



Figure 1 Development Test of Solar Panel Structure and Solar Panel Dampers

It is noted that the Mariner-IV spacecraft also had a set of dashpot-type mechanical dampers. These devices were used as snubbers during the terminal phase of solar-panel deployment, and also were used to prevent a deleterious servo-elastic coupling between the structure, the midcourse rocket motor, and the autopilot. These dampers will not be discussed here because they were of a conventional dashpot design.

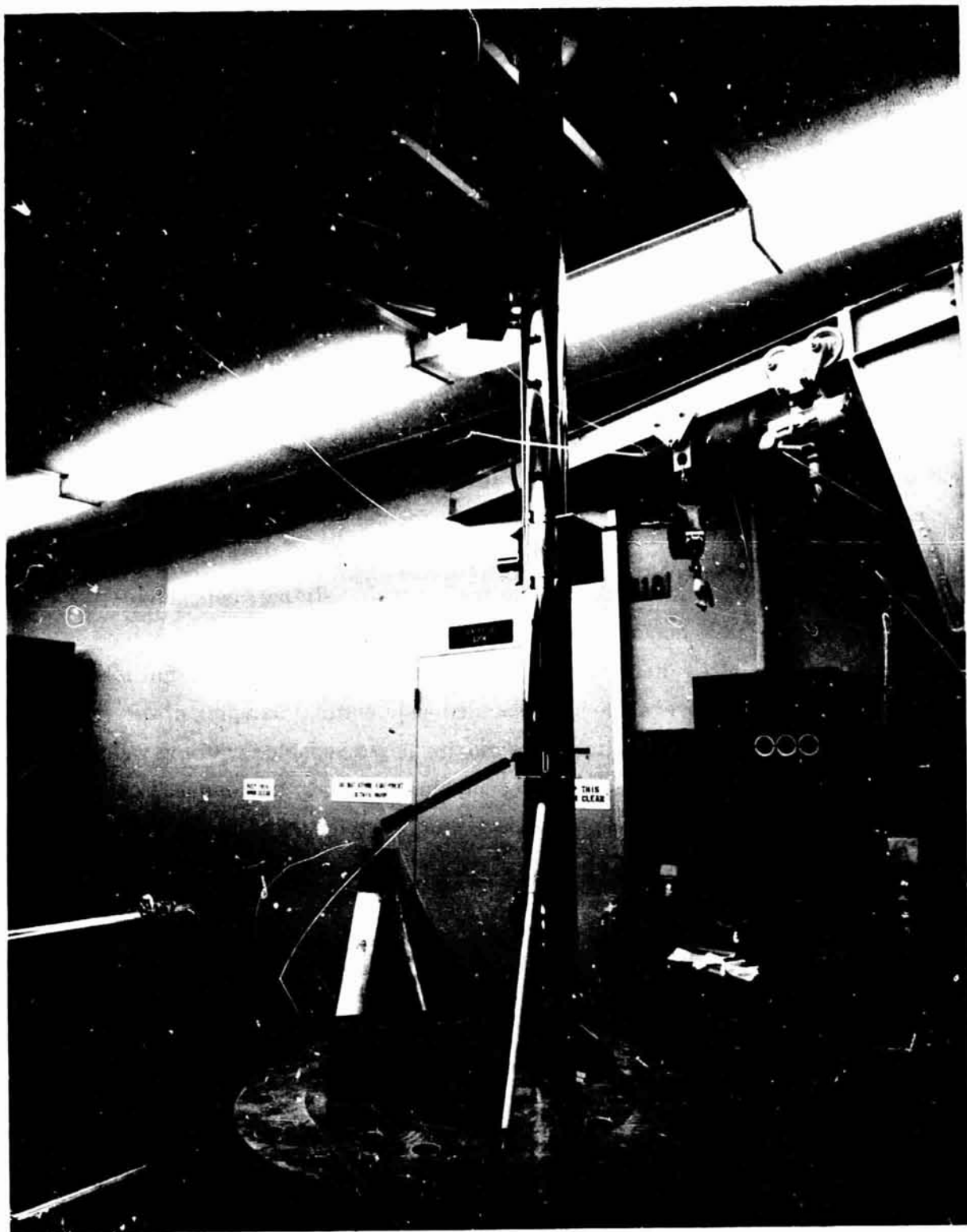


Figure 2 Development Test of Low-Gain Antenna Waveguide
and Low-Gain Antenna Dampers

DESCRIPTION OF THE PROBLEM

Mariner II

Midway through the development of the Mariner-II spacecraft, a low-frequency (2 cps) resonance of the extended high-gain antenna was observed which, it was feared, would interact with the spacecraft autopilot, creating a dynamic instability during the midcourse-maneuver rocket firing. The extremely short (9 mo) development time for Mariner II did not permit the sophisticated testing necessary to establish the significance of the antenna-autopilot interaction; therefore, it was decided that the resonance must be eliminated. The obvious solution was to apply some type of damping to the resonant antenna structure; however, no space-qualified dashpots were in existence at that time, and very little time was available for the development of such a unit. It was clear that whatever was to be used must be extremely simple, lightweight, easily manufactured, and thoroughly tested. It was decided to try a simple, sliding, concentric-tube device wherein viscous fluid contained in the annulus was sheared by relative motion of the tubes. Typical damper dimensions of 3/4-in. outside diameter, 15-mil tube walls, 5-mil annulus, and 6-in. overall length provided near critical damping of the 10-lb antenna structure, and the simplicity of two moving parts, coupled with the weight of 1/8 lb, made the concentric-tube damper an acceptable solution to the antenna resonance problem.

Shortly after the solution of the antenna resonance problem, a second and more severe problem arose. The earth sensor-package resonances during boost were so severe that the detector tube would be destroyed. Several unsuccessful attempts were made to damp this resonance by using bumper pads and additional support struts. Finally, a pair of auxiliary spring-loaded, concentric-tube dampers were attached to the earth sensor to reduce the detector-tube resonances to acceptable levels.

Ranger Block III

The success of heavy structural damping in the control of structural resonances led to a series of development tests on the Mariner-II structural test model spacecraft after

the Mariner-II flight to Venus. In this series of tests, dramatic resonance reductions were achieved in the spacecraft's solar panels and omni-antenna support tower. These tests led directly to the use of damped struts in the Ranger Block-III solar-panel support structure, with an associated reduction of panel tip excursions from 3 in. to 0.25 in. (ref. 2).

Mariner IV

During the development of the Mariner-IV spacecraft, it became clear that the solar-panel weight would be excessive if Mariner-II-type panels were used. Because of the panels' locations on the Mariner IV, it appeared they would have to withstand more vibration than the Mariner-II panels; yet, because the Mariner IV needed more panel area per spacecraft pound, heavy-panel construction led to an unbearable penalty in overall spacecraft weight. This resulted in the use of an unconventional damped-strut support system for the Mariner-IV panels which protected the panels from vibration, thereby allowing a significant weight reduction.

Concurrent with the development of the solar-panel damped support system, another utilization of heavily damped structure was investigated for the Mariner IV. In this case, both weight and space limitations required a very tall, slender structure for the low-gain antenna support. This structure, 7 ft tall and 4 in. in diameter, supported using conventional techniques, would have developed tip excursions in excess of 10 in. during spacecraft vibration qualification and would have induced excessive loads into the spacecraft upper structure. A damped support system was proposed for the control of this slender structure, and subsequent testing indicated that the damped support system would reduce the structure's loads and excursions by a factor of more than 20. The tests were conducted on a thin-walled aluminum tube controlled by previously described concentric-tube dampers. A variation of damping-coefficient test series revealed that the structure's resonant behavior was insensitive to reasonable variations in damping.

From the previously described test, it was concluded that the utilization of damped structures on the Mariner-IV spacecraft would result in large savings of structural weight, and would allow the use of a desirable, lightweight, slender, low-gain antenna support structure.

DEVELOPMENT

Essentially the solar-panel boost dampers and low-gain antenna dampers differ only in envelope constraints; therefore, the following discussion, while referring specifically to the solar-panel boost dampers, also applies to the low-gain antenna dampers. In arriving at a final damper design, the constraints considered included: function, envelope, strength and stiffness, thermal environment, and material. Some of these requirements were conflicting, making trade-offs necessary in order to arrive at a reasonable solution.

Viscous Damping

As described earlier, damping was accomplished by shearing a layer of viscous fluid in the annulus between two tubes. The expression for the damping force for this type of damper is

$$F = \mu \frac{V}{\Delta} \pi DL \quad (1)$$

where

- μ = the apparent viscosity
- V = the relative shearing velocity
- Δ = radial clearance between the tubes
- D = the mean diameter of the annulus
- L = the effective length of the piston

The damping coefficient is defined as the ratio of the peak damping force to the peak velocity. The damping coefficient is then given by

$$c = \mu \frac{\pi DL}{\Delta} \quad (2)$$

This is sufficient to design a viscous-type tube damper if the viscosity is a constant. Unfortunately, the viscosity, or more correctly, the apparent viscosity, is frequently a function of both shear rate and temperature. In other words,

$$\mu = \mu \left(\frac{V}{\Delta}, T \right) \quad (3)$$

where

V/Δ = the shear rate

T = the temperature

Damping Fluid

The first problem which had to be solved in the damper design was that of selecting the damping fluid. In selecting a fluid, a tradeoff had to be made between two effects: fluid shear rate and temperature. Typical hydrocarbon oils and greases show decreasing viscosity changes of the order of 10 or 20 over reasonable temperature operating limits, while typical silicone fluids (methyl-polysiloxanes) show decreases of the order of two over the same temperature limits (ref. 3). The damped structure feasibility tests demonstrated that changes in damping on the order of two or more could be tolerated without noticeable effects. On this primary basis a Dow Corning 210 silicone fluid was selected for the dampers. Additional considerations in selecting this fluid were its excellent high-temperature stability and its very low vapor pressure.

To obtain the desired damping rates, a very viscous fluid was required. A fluid with a nominal kinematic viscosity of 500,000 centistokes was selected. The shear-rate effects for this fluid were determined, over shear rates of interest, to be approximately:

$$\mu = 1.58 \times 10^6 \left(\frac{V}{\Delta} \right)^{-1/2} \text{ cs} \quad \frac{V}{\Delta} \geq 10 \quad (4)$$

or

$$\mu = 0.223 \left(\frac{V}{\Delta} \right)^{-1/2} \text{ lb-sec/in.}^2 \quad \frac{V}{\Delta} \geq 10 \quad (5)$$

When eq. (5) is substituted into eq. (3), the design equation for the damper with the chosen fluid is obtained:

$$c(V) = 0.223 \frac{\pi DL}{(V\Delta)^{1/2}} \text{ lb-sec/in.} \quad (6)$$

It is immediately obvious that the damper is nonlinear in behavior; in fact, it is clear that the damping force will be proportional to the square root of the velocity.

For the solar panel boost dampers, the following dimensions were selected:

$$D = 0.567 \text{ in.}, \quad L = 9.36 \text{ in.}, \quad \Delta = 0.005 \text{ in.}$$

When these dimensions were substituted into eq. (6), the following design value is obtained:

$$c(V) = 50.2 V^{-1/2} \text{ lb-sec/in.} \quad (7)$$

This can be compared to the following measured value from flight damper Serial No. C-142:

$$c(V) = 46.0 V^{-0.51} \quad (8)$$

Material

The materials used in the design of the dampers were all commonly used in spacecraft applications. The damper tubes were an anodic hard-coated 6061-T6 aluminum alloy. The damper spring was fabricated from beryllium-copper spring stock, and the damper spring plugs and various tube end fittings were fabricated from AZ-31B magnesium alloy. The fluid sealing devices were a combination of Viton O-rings and Teflon slipper seals. The various components were assembled using a common two-part, heat-cured epoxy (Epon 901/B3).

A Mylar boot was bonded over the spring assemblies on each end of the dampers to prevent potential outgassing of the damping fluid in case the sealing device leaked. The internal volume of the damper was vented through a hole, which was directed away from any part of the spacecraft, to prevent a buildup of internal pressure which, during the boost phase of the launch, would tend to cause seepage of the damping fluid past the seals. Except for the short, low-gain antenna damper, which was always in the shade of the high-gain antenna, the dampers were kept cool by coating them with a PV-100 temperature-control paint. This had the effect of maintaining a low vapor pressure in the damping fluid.

Figure 3 is a schematic drawing of the short, low-gain antenna damper.

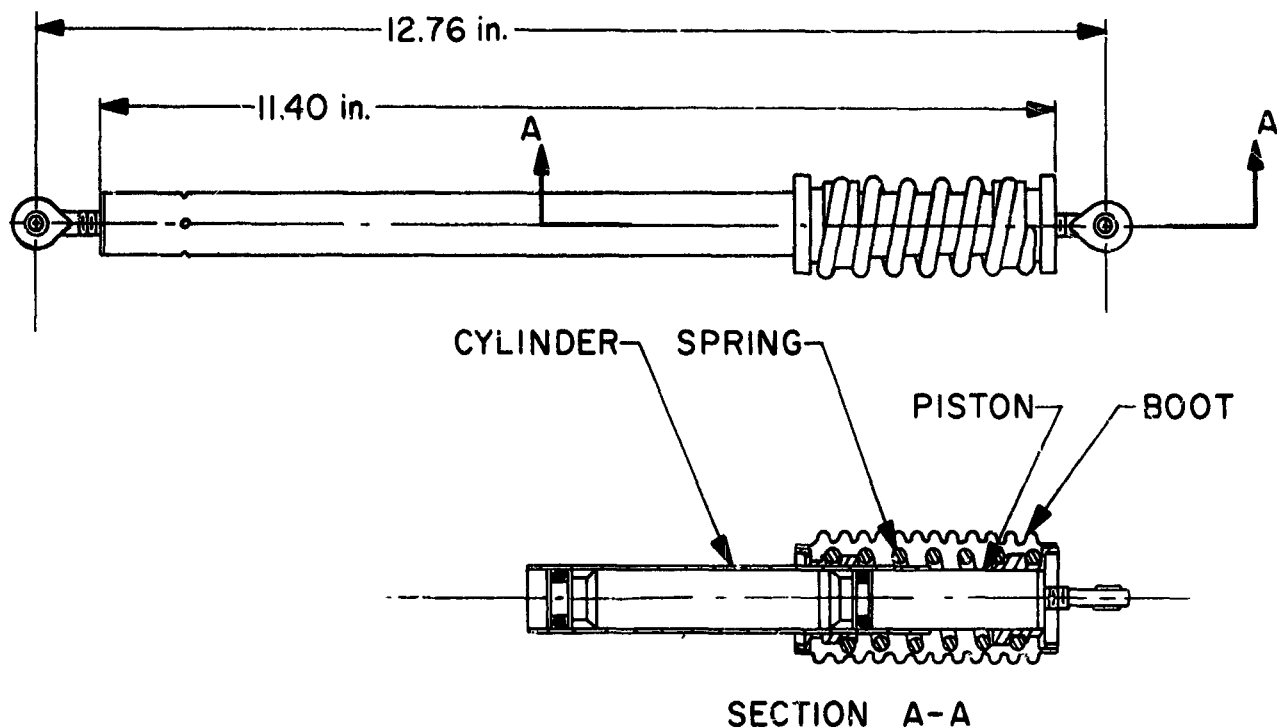


Figure 3 Short, Low-Gain Antenna Damper

Figures 4, 5, and 6 show the completed flight-type dampers. It should be noted in figure 5 that over one-half the length of the damper is a tube which provides the required damper length. This tube was fabricated of unidirectional filament, epoxy fiberglass cloth, which provided both a lightweight structure and a very low heat conduction path into the spacecraft bus.



Figure 4 Short, Low-Gain Antenna Damper

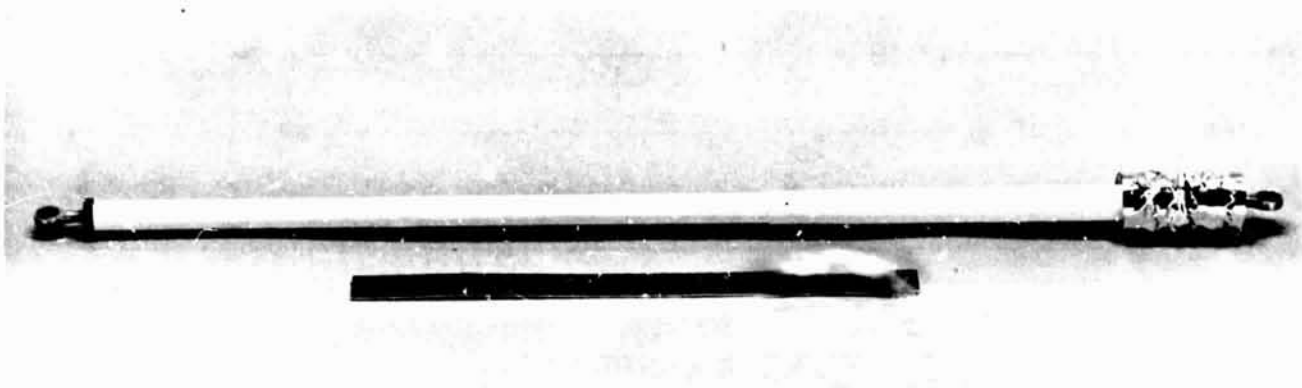


Figure 5 Long, Low-Gain Antenna Damper

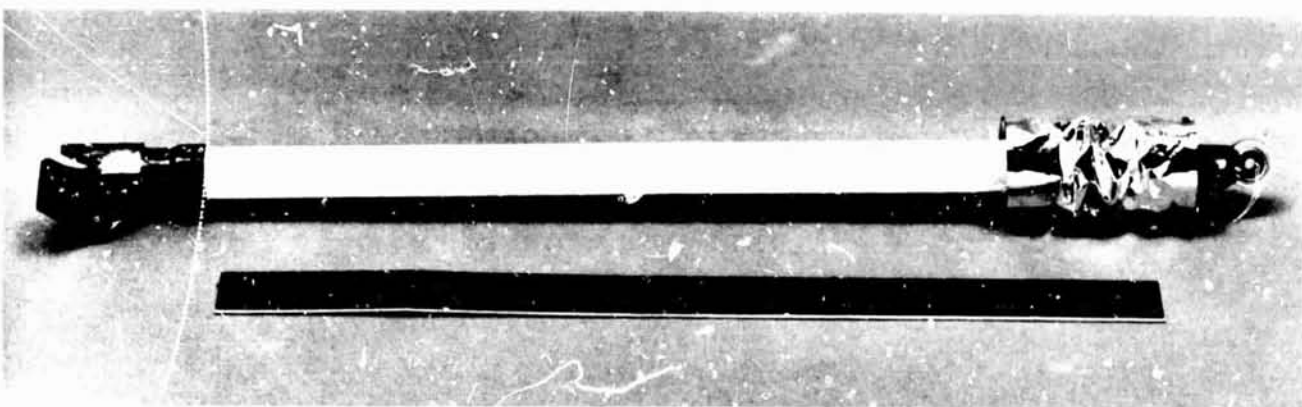


Figure 6 Solar-Panel Boost Damper

Testing

The functional testing of the boost dampers consisted of measuring the spring rate and the damping rate. The spring-rate measurement was performed on the spring, as received from the vendor, at the subassembly level with the spring plugs installed, and on the completed damper after environmental testing.

Damping-rate measurements were much more difficult to obtain than the spring-rate measurements. The early, damped-structure feasibility tests were conducted with untested dampers because proper test facilities were not available. As the resulting damper development program progressed, efforts were made to utilize electrodynamic shakers which were available in the environmental test lab as damper test devices. Testing was accomplished by attaching one end of the damper to the shaker armature and the other end to a rigid foundation. The shaker was then operated throughout the desired spectrum of frequencies and g levels. This test technique, which was necessary early in the program, had many serious disadvantages, including poor waveform control at low frequencies, undesirable low frequency suspensions of the electrodynamic shaker, dc shifts in the armature, and resonances in the foundation system. Most of the above characteristics are tolerable in normal vibration testing, but are disastrous when shaking against a rigid foundation. With the technical difficulties associated with this type of testing, it became imperative, because of facility scheduling, to develop some other test technique. This problem was further compounded because the Ranger Block-III damper program was also utilizing the facilities on a priority basis.

To solve these problems, a subcontractor was requested to develop a damper test machine to JPL specifications. This machine consisted of a variable-speed, variable-displacement scotch-yoke drive capable of a frequency range of zero to 70 cps, and a displacement range, dependent on the selected frequency, of ± 0.025 to ± 0.250 in. Figure 7 shows a solar-panel boost damper mounted in this test machine and figure 8 shows the test and control console used with the tester during the damper test program.

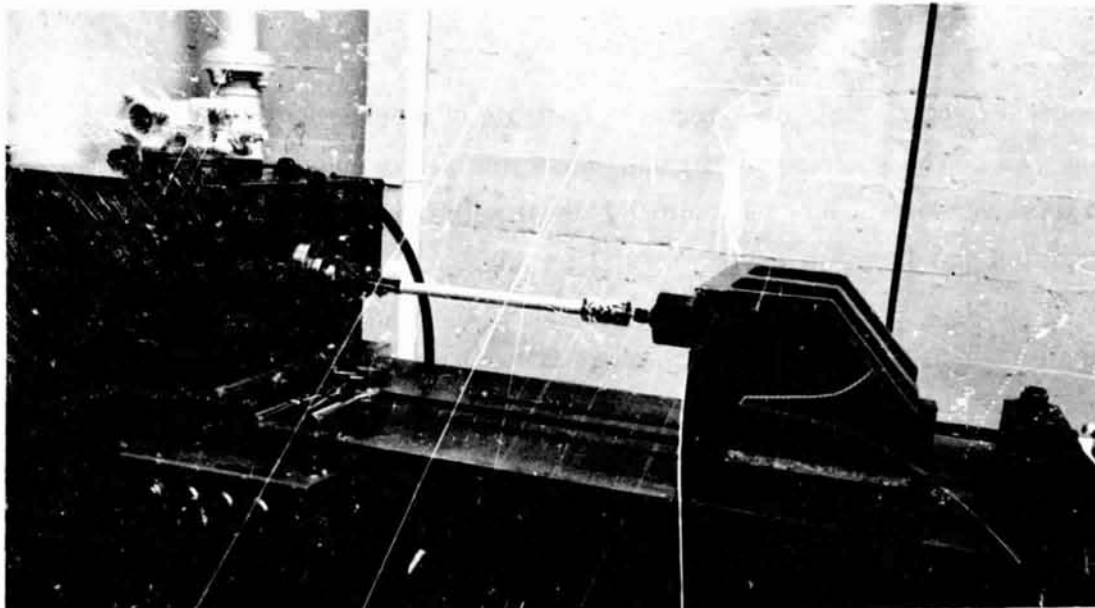


Figure 7 Solar-Panel Damper Under-
going Functional Testing in
Damper Tester

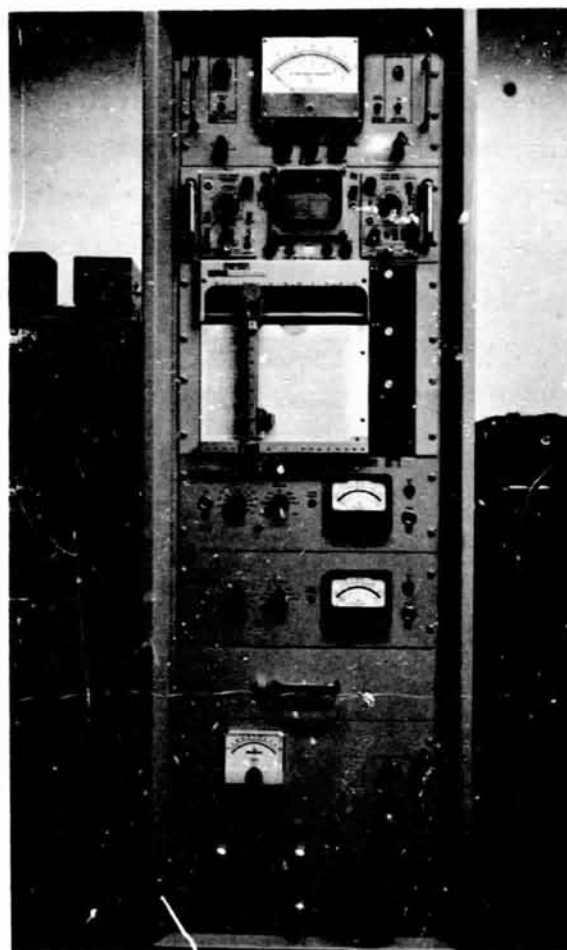


Figure 8 Damper Test Console

The test and control console provided a programmed speed-control signal to the test machine which, in conjunction with a preset displacement of the test machine, provided a programmed sinusoidal velocity to the damper. A feedback signal from the test machine tachometer was used to drive the X axis of an X-Y plotter. The Y axis of the plotter was driven by a signal from a load cell which was placed in series with the damper. The sinusoidal force signal was passed through an rms converter to obtain dc signal to drive the plotter. The resulting plot obtained from this test setup was the rms damping force versus peak sinusoidal velocity. The test console also contained an oscilloscope for waveform monitoring and a phase meter to determine the phase angle of the damping force relative to a velocity or displacement signal. Figure 9 shows the characteristic type of damping curve for the solar panel boost dampers; the curves for low-gain antenna dampers are of the same shape, but different amplitude.

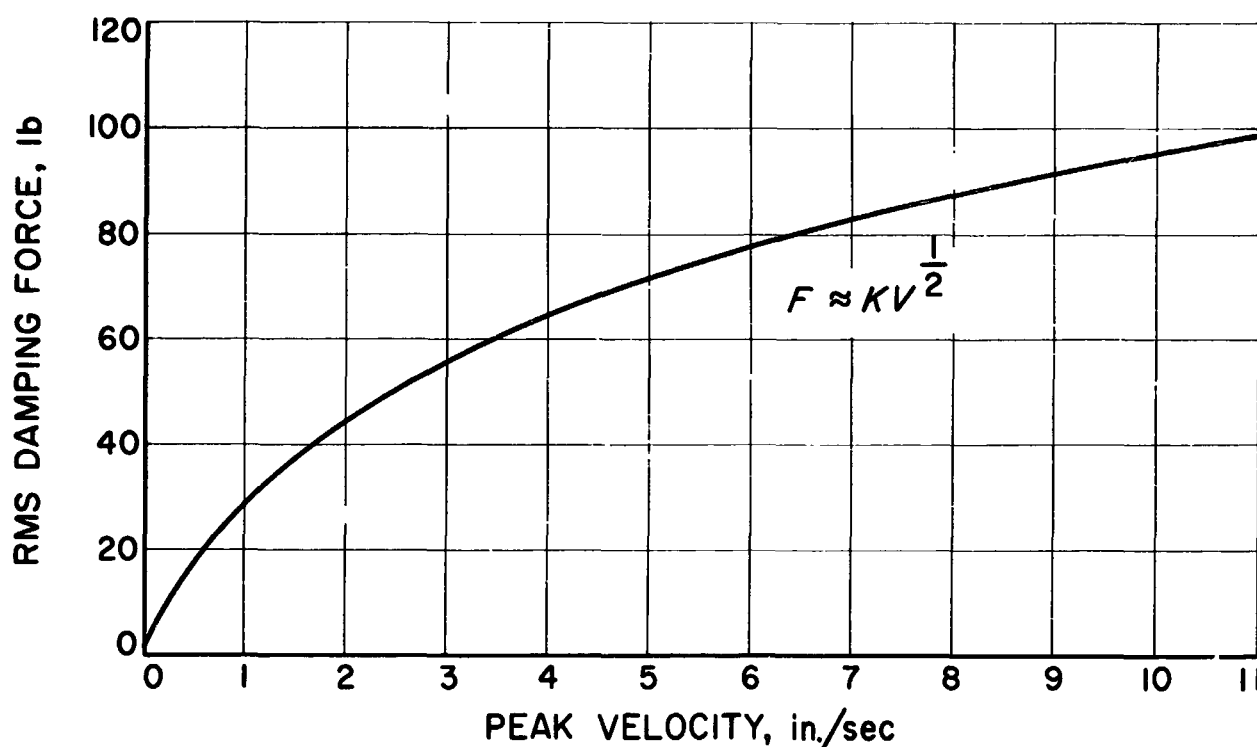


Figure 9 Force Versus Velocity for a Solar-Panel Boost Damper

Damper type-approval environmental testing included vibration, shock, centrifuge, thermal shock, thermal vacuum, and functional tests. Flight acceptance environmental testing included vibration, thermal vacuum, and functional tests.

CONCLUSIONS

The dampers described in this paper performed without difficulty throughout the spacecraft development program. Since there are no telemetry measurements that yield direct performance of the spacecraft structure, satisfactory flight performance is inferred from the proper functioning of all Mariner-IV subsystems.

This type of damper will continue to be a prime consideration for flight whenever there are requirements for a highly damped lightweight structure.

REFERENCES

1. Schmuecker, J. D.; and Wilson, J. N.: Structural and Mechanical Design of Mariner Mars. *Astronautics and Aeronautics*, Aug. 1965.
2. Gayman, M.: Development of a Point Damper for the Ranger Solar Panels, JPL TR 32-793, Sept. 1965.
3. Currie, C. C.; and Smith, B. F.: Flow Characteristics of Organopolysiloxane Fluids and Greases. *Industrial and Engineering Chemistry*, Vol. 42, No. 12, Dec. 1950.

MECHANISM FOR SPACECRAFT REFLECTANCE-DEGRADATION EXPERIMENT*

**By E. Cornish, R. K. Kissinger, and G. P. McCabe
Lockheed Missiles & Space Company**

SUMMARY

N67 16905
An instrument has been designed to expose reflective surfaces to the sun for four months in space. Solutions to design problems include a magnetic drive unit to transmit motion from an enclosed motor to the outer mechanism, a light-integrating sphere using an electronically pulsed light beam for the detection of degradation of the samples, and electronic means for repositioning samples after readout.

INTRODUCTION

An Air Force project, Advanced Solar Turbo-Electric Concept (ASTEC), proposes the use of a 40-ft-dia. mirror to concentrate solar energy to power a spacecraft. Experimental data on the degradation of ASTEC mirror materials will be obtained in a preliminary spaceflight. Samples of reflective material (1-in.-diam.) on the orbited test instrument will face the sun for a minimum of four months. The degree of degradation of the reflective surfaces will be detected by periodic comparison with an undegraded sample and will be telemetered to ground stations throughout the flight test.

DESCRIPTION OF THE MECHANISM

The mechanism constructed at LMSC for this task is composed of three principal sections together with related electronics components (figures 1 and 2). This paper

*This effort was performed under Air Force Contract Af 33(615)-1577, Aero Propulsion Laboratory, Research and Technology Division, Wright-Patterson Air Force Base, Ohio. Mr. B. L. McFadden, Jr. is the ASTEC Program Manager; Lt. P. W. Lauderback, the Project Engineer.

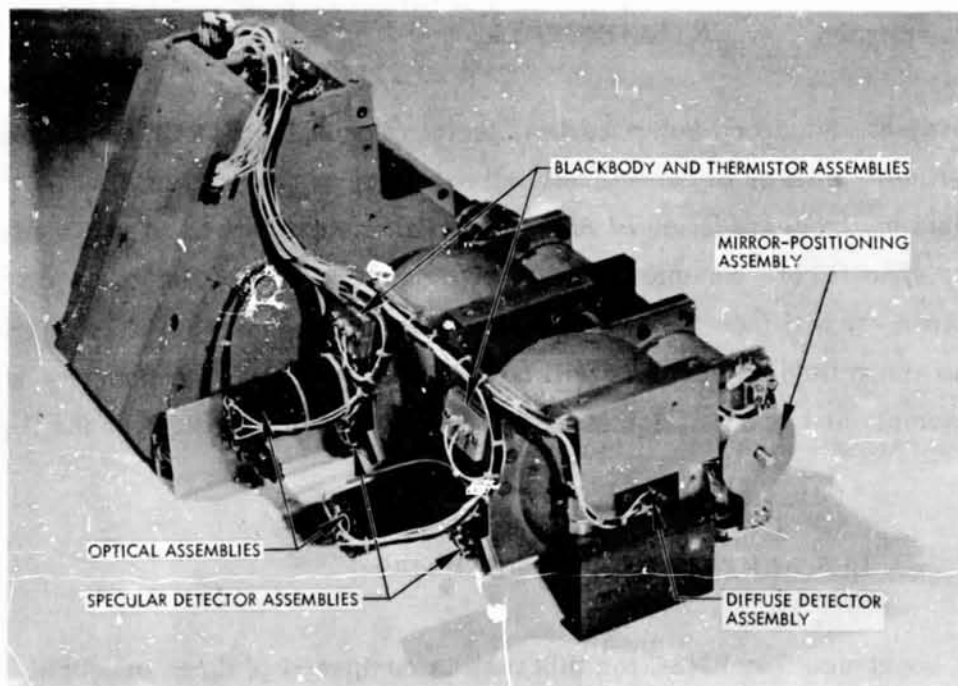
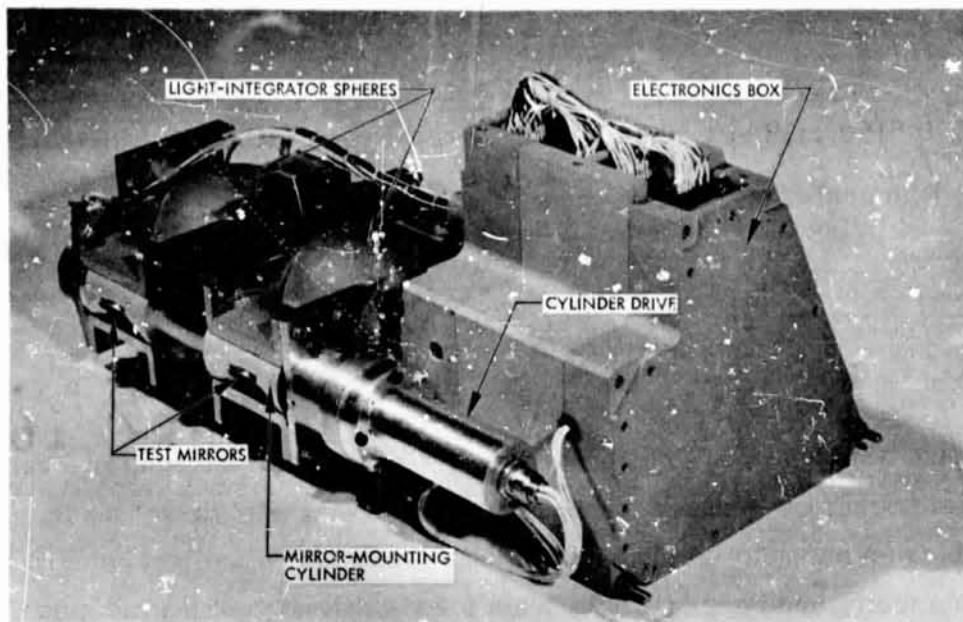
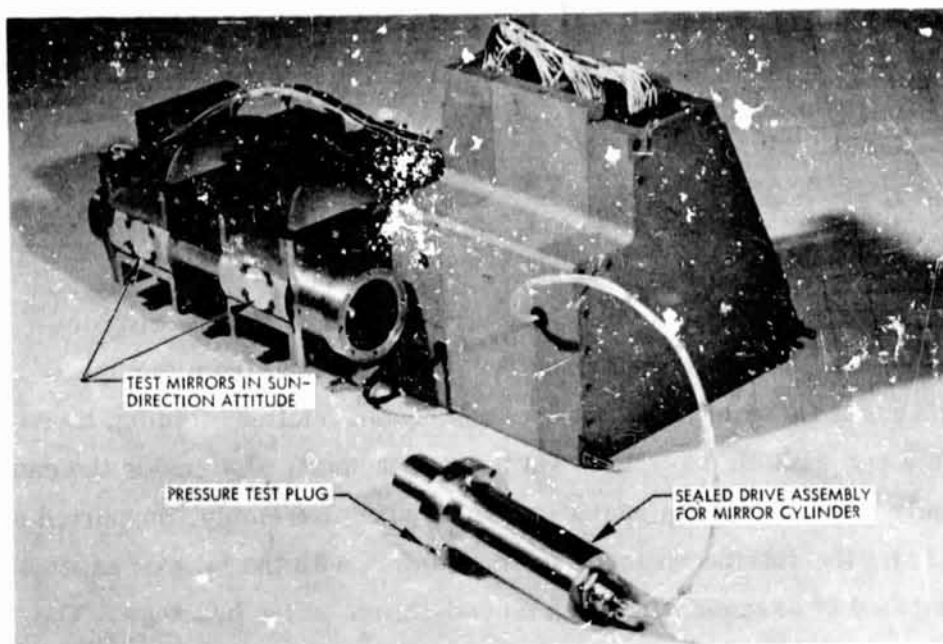
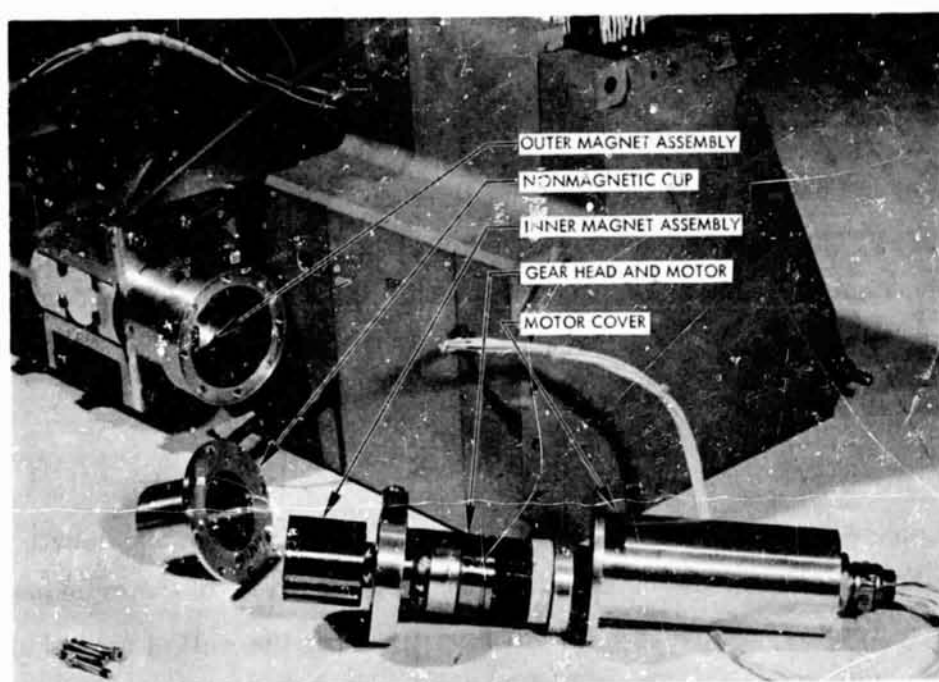


Figure 1 Mechanism for Testing Degradation of Solar Reflective Surfaces



View Showing Drive Unit Removed



View Showing Drive Unit Removed and Disassembled

Figure 2 Mechanism for Testing Degradation of Solar Reflective Surfaces

describes the enclosed motor and magnetic-drive system, the light-integrator spheres, the associated optics and detection system, and the mirror-sample positioning system.

DRIVE SYSTEM

The drive system (figure 3) rotates a cylinder on which are mounted the mirror samples. To protect the 4,000-rpm motor and 8,000:1 gear head from the space environment, which causes loss of lubricant and subsequent friction-welding, these parts are sealed in a can with air at 1 atm. On the output shaft, also inside the can, is a magnet assembly. Outside of the can is another magnet assembly, supported on the cylinder hub so that the outside magnets are concentric with the magnet assembly in the can. This method of assembly imposes no end-thrust on the bearings. The spacing between inner and outer magnets is less than 0.030 in., of which 0.007 in. is the nonmagnetic can wall. Thus, the attraction between inner and outer poles is so great that a torque of 13 in.-oz. can be induced on the cylinder hub by the drive motor. Only a small fraction of that torque is used to rotate the cylinder against the friction of the hub bearings.

The hub bearings are of epoxy-loaded with two antifriction substances - Teflon and molybdenum disulfide. The bearings are machined after being cast in place in the bearing plates. The wear in the bearings should be negligible, since the cylinder will operate for only 10 min every 2 wk, and then at only 0.5 rpm.

LIGHT INTEGRATOR SPHERE

As illustrated in figure 4, a light beam focused through a large, short-focal-length, achromatic lens falls in a 0.5-in.-diam. circle on the test mirror. As the cylinder mount for the mirror rotates, the reflected light rays traverse the wall of the sphere, enter the blackbody cavity and then into the lens opening. They then impinge on the direct or specular detector, and reflect back to the wall of the sphere. The wall of the sphere is sandblasted to provide a diffuse surface. This surface is gold plated to reflect about 97 percent of the energy between 0.6 and 2.5μ , which more than spans the range of sensitivity of the detector. If the mirror surface is degraded, some diffuse light will

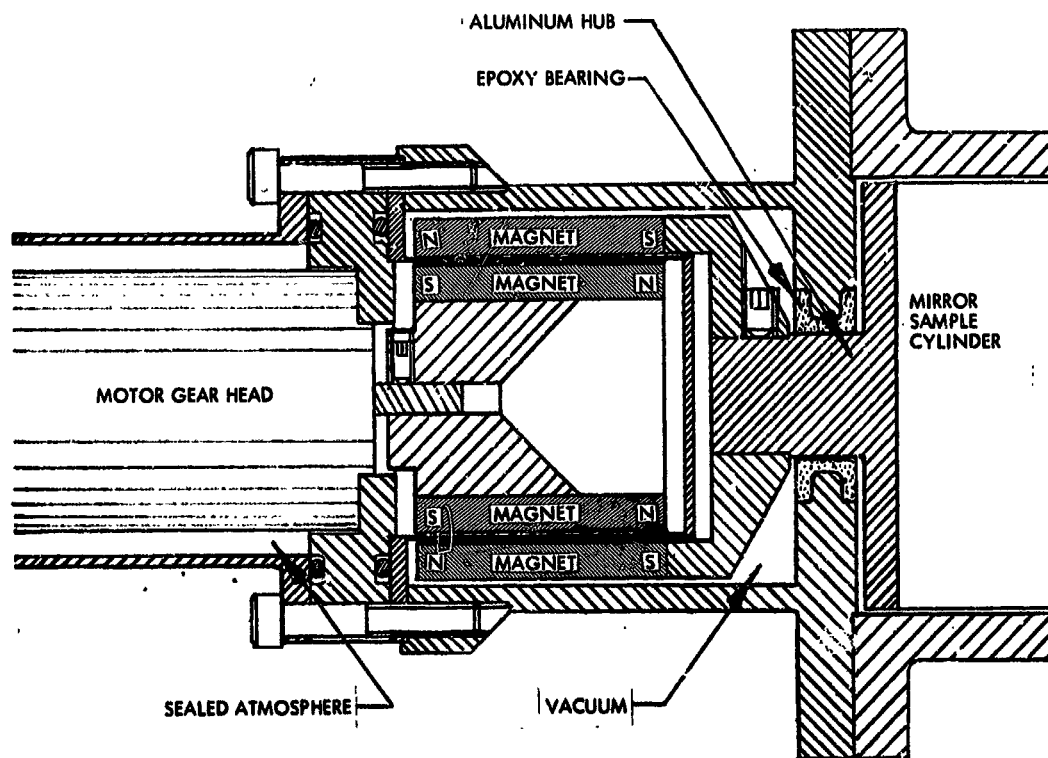


Figure 3 Drive System

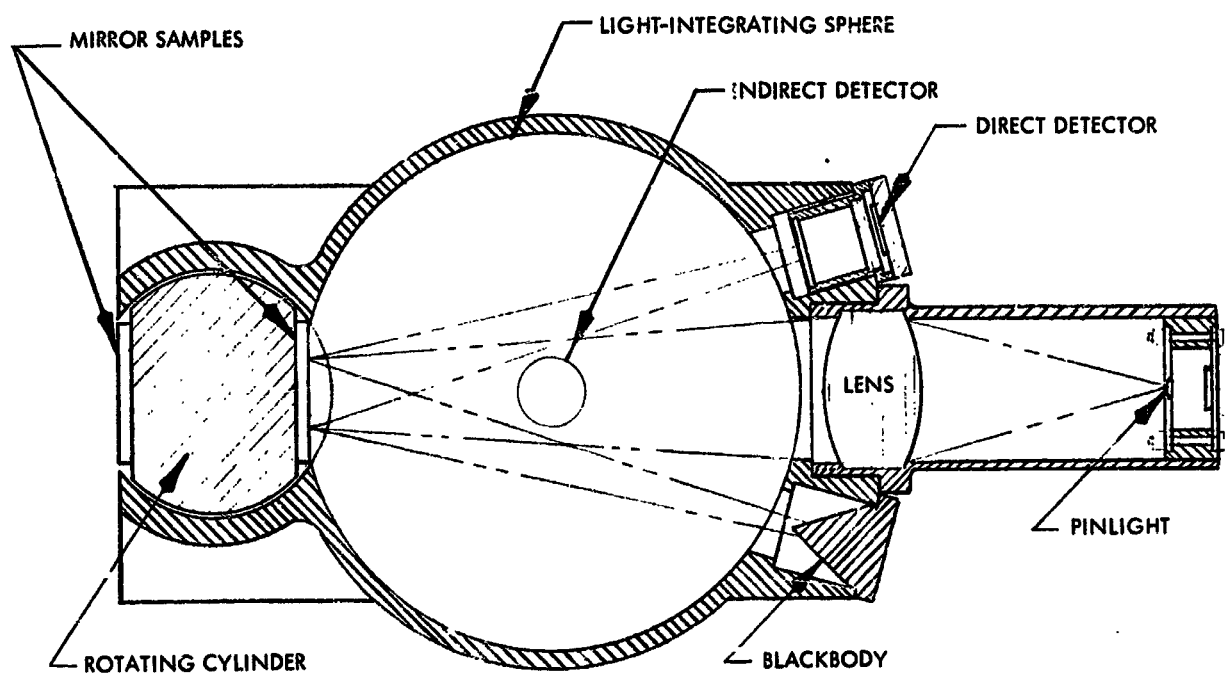


Figure 4 Light-Integrator Sphere

illuminate the sphere while the specular component of the beam is being absorbed in the blackbody hole. The indirect or diffuse detector reads the level of energy in the sphere, giving close-to-zero signal while the specular beam is in the blackbody hole, but indicating higher light intensity as the mirror degrades. The specular detector reads the intensity of the specular component when the beam falls into the specular detector hole. One mirror will be the standard undegraded sample staying inside of the sphere during exposure periods; the other mirror will be the test sample exposed to the space environment. Figure 5 shows the detector outputs for new unhazed mirror samples, demonstrating the sensitivity and repetitive accuracy of the detectors.

LIGHT PULSER

Substituting for a light-chopper, electronic modulation of a subminiature light provides a pulsed output to the two detectors that measure light intensity in the integrator sphere. A third detector uses the pulsed light to measure the angle of rotation of the cylinder on which the mirror samples are mounted. Of course, a light chopper (which exposes full light intensity and zero intensity in each cycle) could furnish a greater amount of modulated light than the electronic method (where the radiant filament cannot cool to room temperature between pulses). However, the use of a very short pulse of high voltage maximizes the electronic modulation effect and produces a quite satisfactory result. Diagrams of light-pulser output, and the response of the detector to this output, are shown in figure 6. It can be seen that the light reaches its maximum temperature instantaneously and cools off for a considerable time before the next pulse.

Electronic light modulation has cost, power-consumption, and reliability advantages when compared with mechanical light-chopping. Most important, however, it eliminates the need, as in the case of a light-chopper, for an additional drive unit, together with an enclosure for protection from the vacuum environment.

MIRROR-POSITIONING SYSTEM

At the end of the data-taking cycle, the cylinder on which the mirrors are mounted must be returned to its original position, with the test mirrors facing the sun. Since position potentiometers have rubbing contacts which are undesirable in the space environment because of possible friction welding, a frictionless method was devised. In

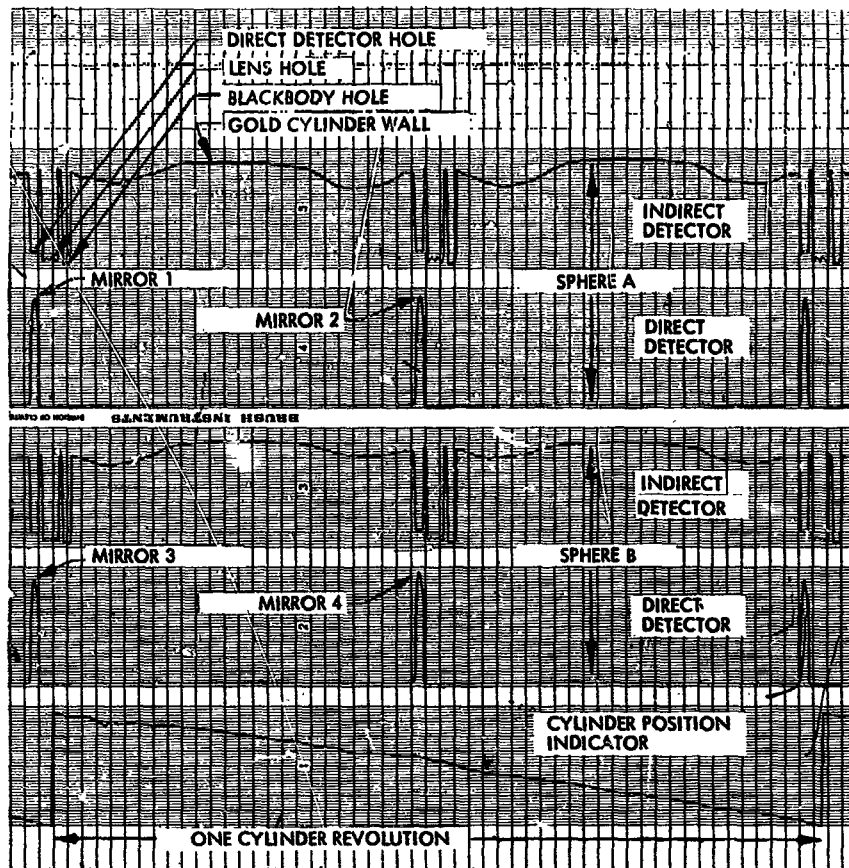


Figure 5 Detector Outputs

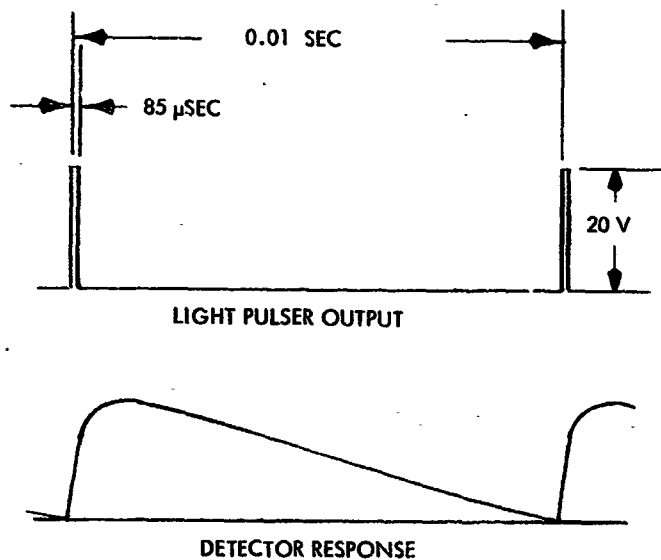


Figure 6 Light-Pulser and Detector Response

this system, circular photographic film is mounted on the mirror cylinder hub so that it revolves between two sets of light sources and detectors, as shown in figure 7.

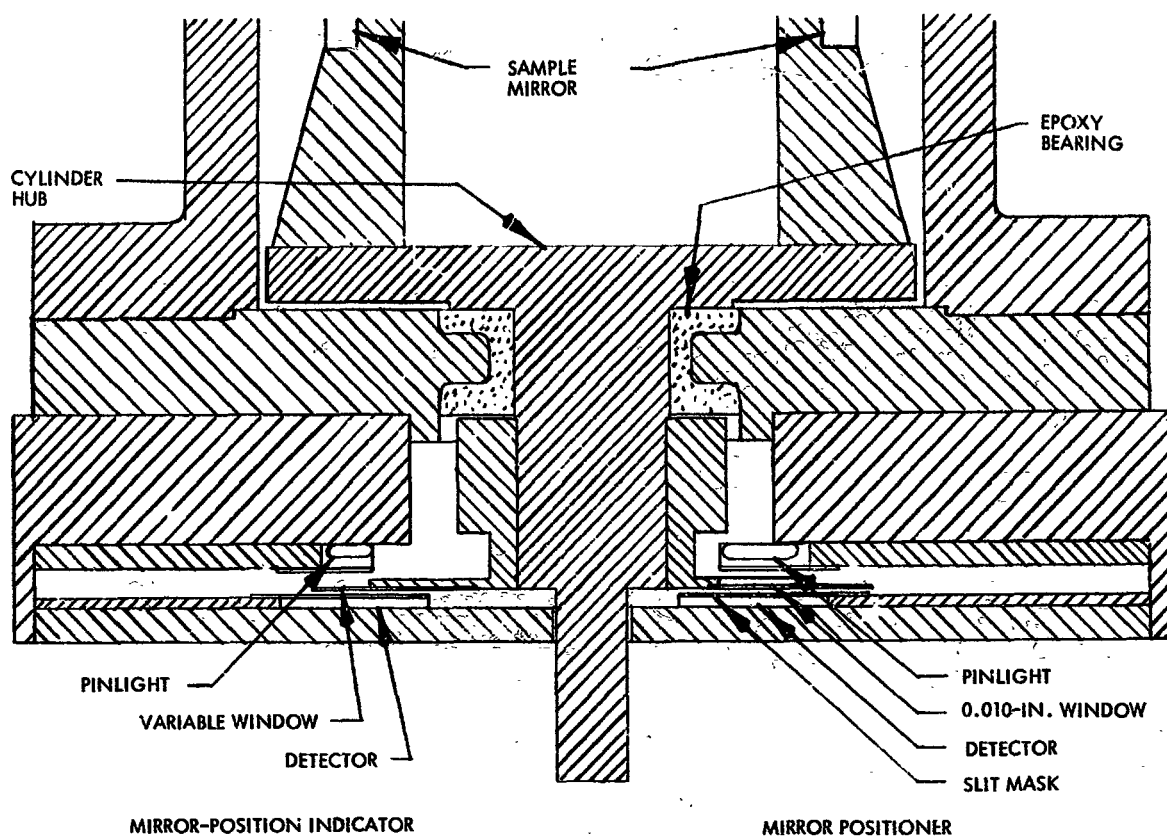


Figure 7 Mirror-Positioning System

As can be seen in figure 8, the circular film contains an annular transparency and a window 0.010-in. wide. To produce data that show the position of the cylinder at any time, an electronically pulsed light shows through the constantly increasing annular window onto its detector. From zero to 360 deg, the lighted area of the detector increases linearly. The output of the detector is amplified by an a-c amplifier; the signal is then processed by a d-c amplifier and filter circuit to render a varying position d-c voltage. The d-c voltage level at the output of the filter is a linear function of the position of the cylinder. This output voltage varies from zero to 5 v to meet the requirements for telemetering.

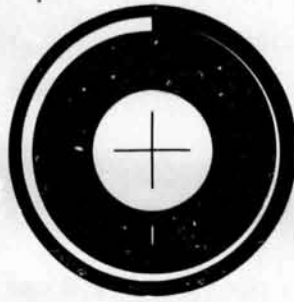


Figure 8 Window Film

To reset the exposed mirror samples so that they face the sun after a data-taking cycle, the light and detector that line up with the 0.010-in. window in the film (figure 8) are used. This light source is turned on by command from the ground station. As the cylinder continues to rotate, the transparent slit passes between the light and the detector, which results in a fast voltage rise at the detector output. This voltage is amplified and fed to a transistor switch that operates the shutoff relay to stop the cylinder drive motor. The shutoff relay and a time-delay relay supply dc to the a-c synchronous motor which brakes the motor from 4,000 rpm to zero in a fraction of a second. The shutoff relay also cuts off all power to the reflectance-degradation instrument.

TEST RESULTS

Several significant results were derived from the testing conducted under this experimental effort.

Drive

The magnetic drive was found to hold 13 in.-oz of torque before slipping. A sensitive torque meter on the mirror-mounting cylinder (with magnetic clutch removed) indicated a starting and running torque of only about 0.1 in.-oz. It has demonstrated its strength in rotating the cylinder in a smooth and stable manner.

Light-Integrator Sphere

The maximum noise level of the diffused light detector was 2 percent of the highest detector output. The highest output was obtained when a diffuse gold surface was substituted for the mirror sample.

The direct detector showed a maximum reading for a totally specular beam. When the diffuse gold surface was substituted for the mirror, its output was practically zero. Intermediate degrees of hazing of the mirror gave proportional outputs from the direct and diffuse detectors, respectively.

Light-Pulser

A subminiature lamp was pulsed at 20 v for 50 μ sec/cy at 100 cps and did not fail in 4,000 hr of operation.

Mirror-Positioning System

In many tests of the mirror-positioning system, the cylinder stopped within ± 0.5 deg of optimum position. Readout on a Brush Instrument tape showed a nearly perfect linear change from 0 deg to 360 deg, which can be calibrated to show mirror position at any time.

CONCLUSIONS

It appears that the mechanism devised for measuring the degradation of reflective materials after exposure to the space environment will operate satisfactorily for the projected 4-month flight.

The peculiar restrictions that vacuum environment imposes have been satisfactorily overcome by the use of "contactless" media. Principal examples are the use of a magnetic drive for the high-speed motor, and the use of electronically pulsed light both for positioning the cylinder upon which the mirror samples are mounted, and for the input to the photodetection device. The instrumentation developed for this experiment can detect degradation of the required order, that is, as low as a 2-percent decrease in reflectance — a distinction fine enough to rate the relative efficiency of various solar reflective materials.

**NONCONTAMINATING SEPARATION
SYSTEMS FOR SPACECRAFT
(Project ZIP)**

**By Audley B. Leaman
Lockheed Missiles & Space Company
Sunnyvale, California**

SUMMARY

N67 16906

The object of the ZIP program has been to investigate the design and feasibility of explosive separation with the goal of achieving a contaminant-free system. Various joint sections have been included in the study: self-ejecting, low-shock, high-temperature, multiple attachment, and others. Material studies have been performed to investigate the physical, temperature, and dynamic properties of various elastomers and to select the most promising candidates for utilization.

The results of these studies have established the feasibility of the ZIP system. However, the design of a separation system for a specific application will normally be a custom design based on the requirements of the specific boost vehicle and the spacecraft.

INTRODUCTION

During flight of any large missile or space vehicle, it is necessary to remove the protective shroud and detach the re-entry body, second stage, or spacecraft from the booster.

Numerous separation systems are used to perform these functions, and most of them have one feature in common — pyrotechnic or explosive material. These systems may

be generally classified into two major categories: (1) a pyromechanical system and (2) a stressed skin-separation system.

PYROMECHANICAL SYSTEMS

The pyromechanical type of system, as the name implies, uses mechanical devices activated by a means of a pyrotechnic or explosive component. Typical of such components are explosive bolts, explosive nuts, pin pullers, latches, ball-lock systems, and vee-band clamps.

These components are of the series or multiple-component type. Each component must therefore have an extremely high reliability to assure satisfactory overall system reliability, and exact timing to eliminate unacceptable tipoff angles.

As the launch vehicles employing this type of system increase in size, additional elements or more substantial structural members at attachment points are required. Both methods cause a considerable increase in the overall weight of the vehicle; furthermore, an increase in the number of elements requires an increase in component reliability to provide an equivalent system reliability.

STRESSED SKIN-SEPARATION SYSTEMS

The stressed skin-separation system utilizes the vehicle skin as the primary structural member at the interstage junction. An explosive cord is used to rupture the skin along a predetermined line. This system provides minimum weight, an air and water seal prior to separation, and maximum system reliability because of the single continuous explosive train. The explosive commonly used, known as mild detonating cord (MDC), consists of a continuous length of explosive contained in a lead tube. It resembles common resin-core solder in size and appearance. The lead tube is normally protected by a plastic sheath. The cord is available in core loadings of 1 to 20 gr/ft of explosive.

A typical cross section of the MDC type of joint is illustrated in figure 1. The joint consists of a backup ring (into which the explosive cord is inserted), an overlap ring, and the vehicle skin. When the cord is detonated, the pressure ruptures the skin as shown and accomplishes near-instantaneous separation. The detonation rate is about 25,000 ft/sec or 40 μ sec/ft.

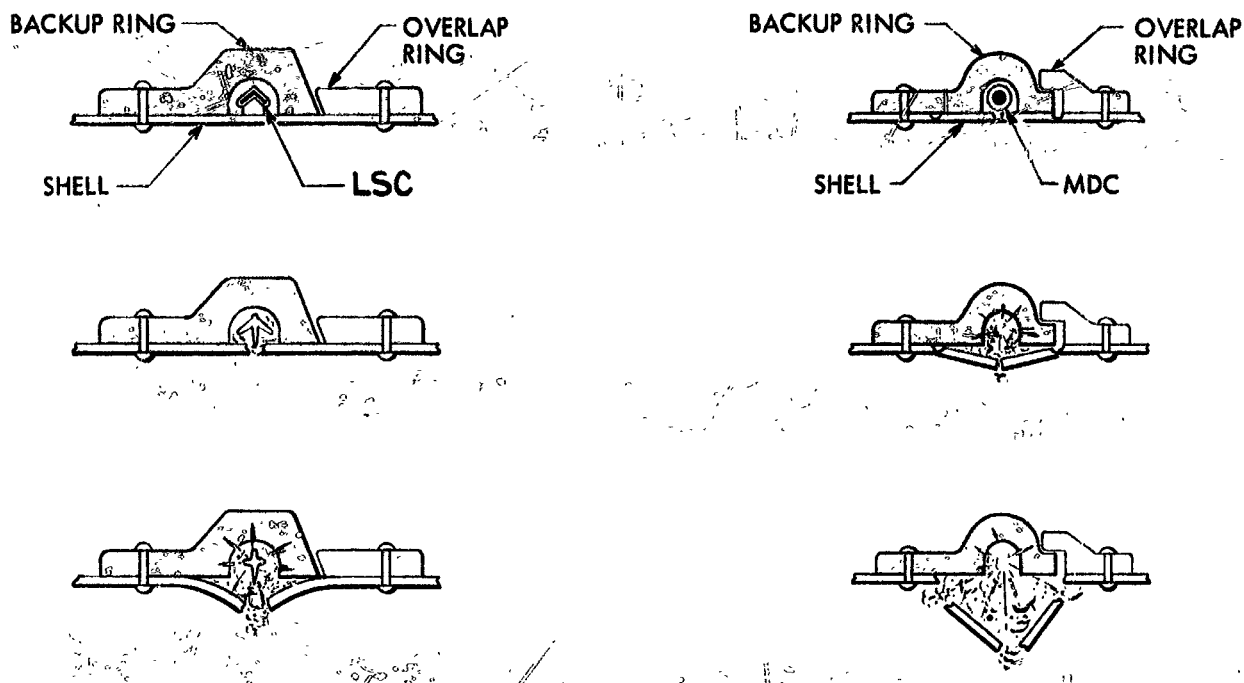


Figure 1 Separation Process in Mild Detonating Cord and Linear-Shaped Charge

This type of separation system has been used since 1957 on test and tactical vehicles developed by Lockheed Missiles & Space Company (LMSC) and for spacecraft booster separation since 1961. Failure of the system has never been reported, thus indicating an extremely high functional reliability.

PROBLEM AREAS

Certain undesirable phenomena accompany the detonation of explosives which may induce problems with regard to delicate spacecraft components. These phenomena

are as follows:

- Hot gases produce ionization and may cause shorting of electronic devices.
- The products of combustion produce solid debris which may contaminate solar cells, optical windows, and sensors.
- Fragments may puncture or otherwise damage other spacecraft components.
- The separation shock is transmitted through the spacecraft structure.

Occurrence of any one of the above phenomena can result in degradation of the performance of a mission.

DEVELOPMENT PROGRAM

Two basic approaches have been followed at LMSC to improve separation-systems performance. The first involves reducing the required quantity of explosive by charge-shaping instead of by blasting the joints apart. The second is based on containing the explosive in a tube and thereby breaking the skin without producing contaminants or fragments.

Charge Shaping

On the premise that reducing the quantity of explosives will produce less shock and contamination, four programs were undertaken at LMSC which employed a linear shaped charge (LSC) of the type shown in figure 1. The LSC is a continuous explosive cord formed into a "vee" or chevron cross-section which permits the utilization of the Monroe effect to cut rather than blast the joint apart. This cord is more efficient, and a lesser quantity of explosives is required for complete penetration. However, a significant improvement with respect to contamination or shock has not been noted. In addition, this cord, when used in small grain sizes, becomes fragile. Any damage to the jacket material causes a detonation failure and any reshaping of the cross-section results in a cutting failure. In view of the deficiencies, this approach was abandoned.

Containing the Explosive in a Tube

This approach utilizes flattened steel tubing in which the detonating cord is inserted and centered and the remaining space filled with a silicon rubber. A joint section employing this original concept (figure 2) was proved feasible. The detonation of the explosive formed the tubing into a round shape, thereby breaking the skin without any escape of contaminants or fragmentation. However, the required metal tube is heavy and awkward, and a survey of alternative materials was therefore undertaken. An elastomer being used in safety containers for in-plant handling of nitroglycerin was tested and appeared promising. The action of this elastomer on expanding, separated the metal in a manner somewhat similar to a zipper action, and the system was therefore designated as a "ZIP cord."

Figure 2 also shows a cross-section of the redesigned retainer which induces a directional force for the hydraulic action of the cord. This shape proved to be very efficient, and is the basis of a fairing ejection system now being qualified at the LMSC Santa Cruz Test Base.

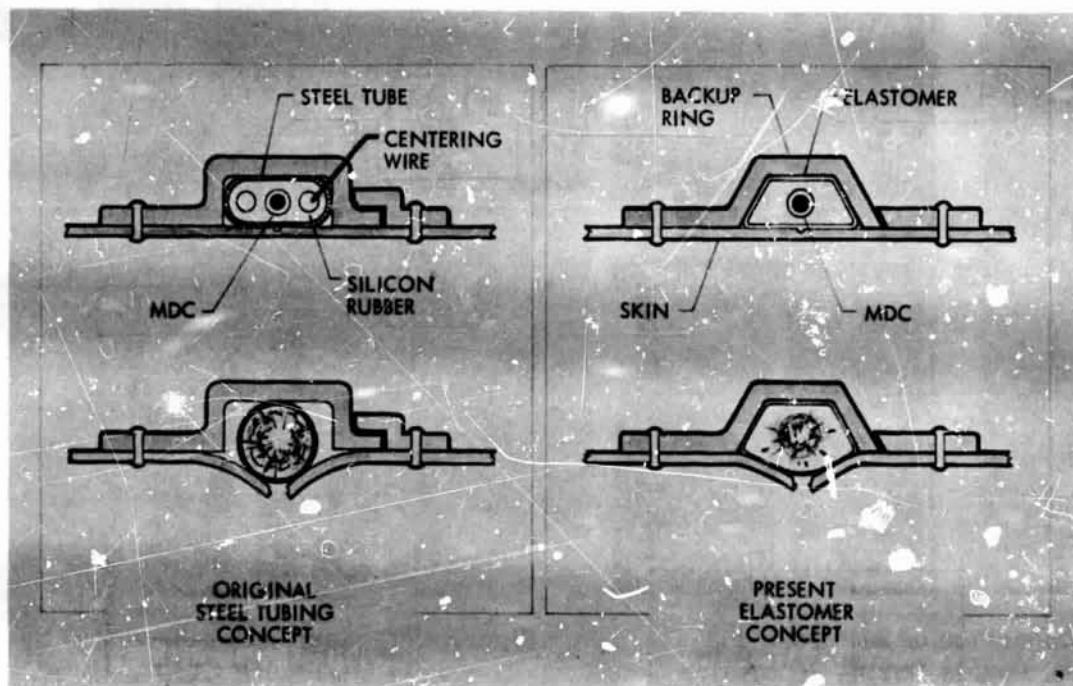


Figure 2 Original Steel Tubing Concept Versus Present Elastomer Concept

Figure 3 shows frames from a Fastax film comparing a 7-gr/ft LSC panel and a 6-gr/ft ZIP cord panel during separation. The ZIP panels contain the contaminants while LSC lets them escape. Figures 4 and 5 compare the contamination produced by the LSC panel in contrast to the clean, uncontaminated result when the ZIP cord was used. These illustrations show that the contamination due to hot gases, solid debris, and fragments has been contained.

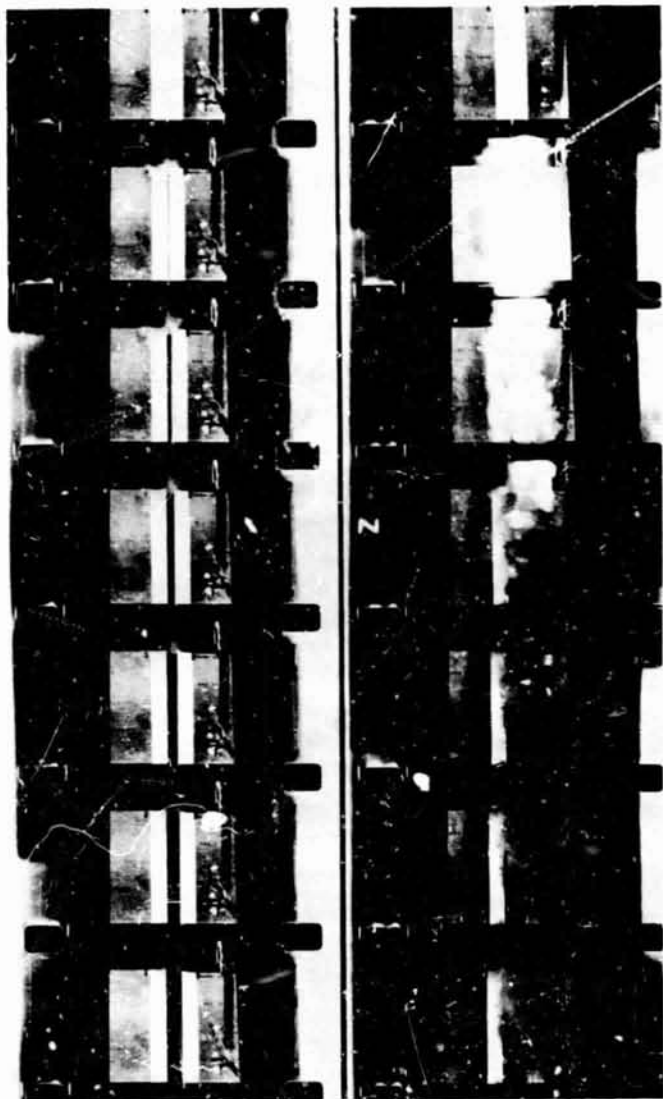


Figure 3 Comparison of ZIP Cord and LSC Panels During Separation

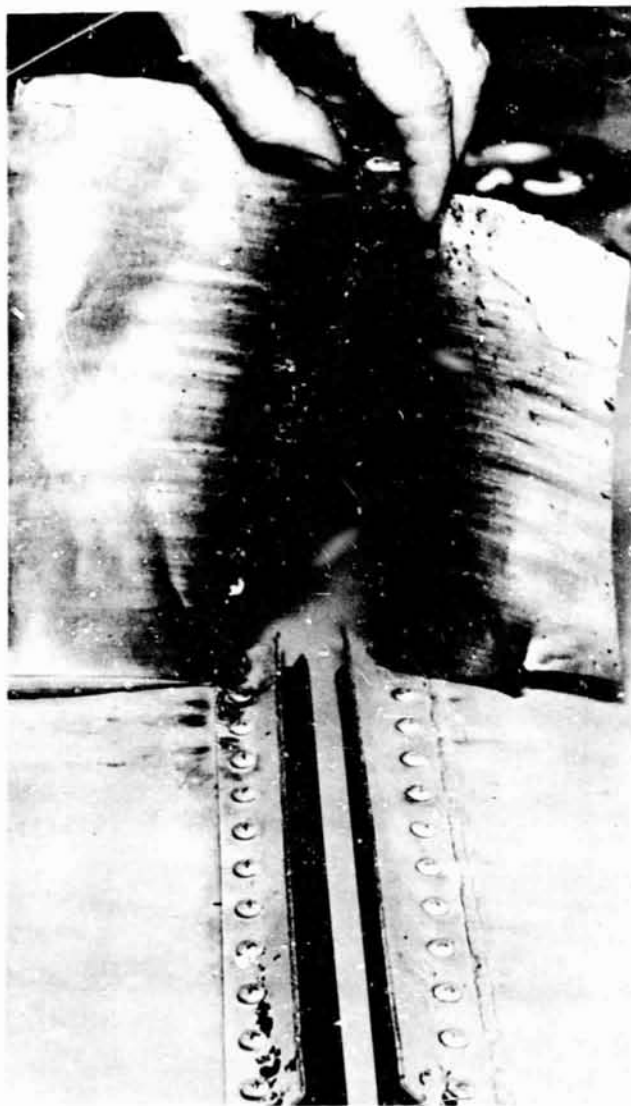


Figure 4 Contamination Produced by 7 Gr/Ft ZIP Cord



Figure 5 Absence of Contamination Following Use of 6 Gr/Ft ZIP Cord

SEPARATION SHOCK

A typical shock pattern produced by the separation is illustrated in figure 6. There is a high acceleration spike (3,000 to 4,000 g) with a 4 to 5-kc frequency, followed by damping to about 1 kc. The total time duration is about 15 to 20 ms. This type of shock does not rupture or deform structural members, but it can cause relay chatter and/or transfer. These problems can be corrected by the addition of shock mounts or redesign of components; however, their elimination normally requires additional weight and more expensive devices. Further, if the separation system can be designed to

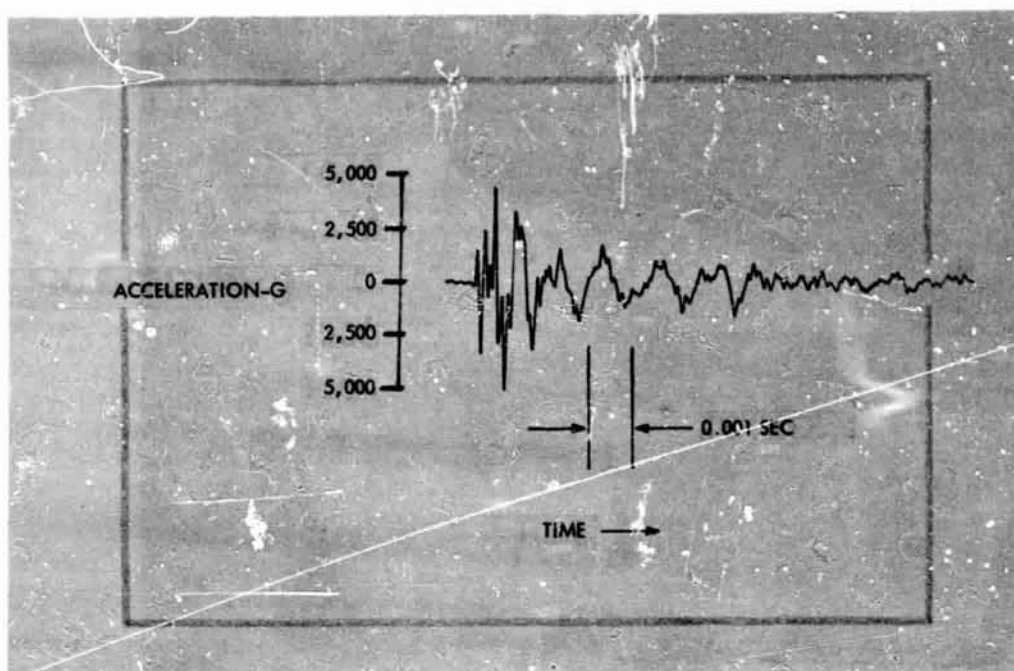


Figure 6 Typical Acceleration - Time Record for MDC Separation Joint

reduce the shock by eliminating the cause, component redesign to achieve this purpose is unnecessary.

During an investigation of a boost-vehicle program, a number of separation systems were designed and tested to provide a maximum shock reduction with maximum reliability. Joints investigated included vee-band, spring-band, and expander-tube types. The resultant decrease in shock was not sufficient to warrant a change. The disadvantages of a weight increase and/or a reduced reliability overcame the advantages of the shock reduction.

An LMSC Independent Development program conducted concurrently with the foregoing program by the LMSC Research Dynamics organization involved the investigation of shock-reduction possibility for large-structure separation systems. This program explored methods for use on future missiles and spacecraft in which vehicle diameters of 25 ft and skin thicknesses of 0.5 in. are not unreasonable. A joint design using two strands of LSC, cutting in opposite directions, was one of many tested, and resulted in reduced shock levels because of the canceling effect of the back-to-back cutting action. However, the contamination produced by the inboard cutting was unacceptable. Another

design, combining the inboard-outboard system with the contained explosive system, produced a joint, designated as the ZIP Lo-Shock design, which reduced the shock level considerably. The design and operation of this joint are shown in figure 7.

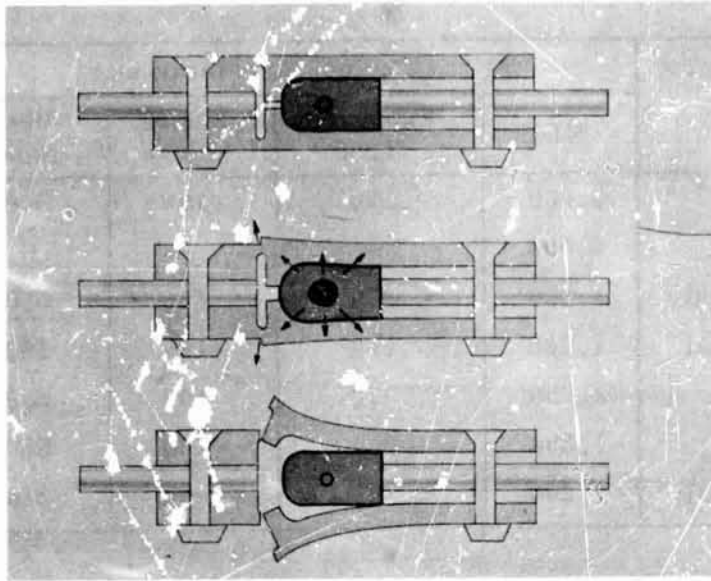


Figure 7 Low-Shock Joint Separation

Table 1 presents the shock levels produced by full-scale tests of various separation systems. The reduced values of the ZIP Lo-Shock design show it to be a feasible method for reducing shock and eliminating contaminants and ionization produced by explosive separation. In addition, the reliability and action of this joint is essentially equal to an explosive cord system.

TEMPERATURE EFFECTS

Following completion of the aforementioned program, material studies were conducted to investigate temperature effects and material dynamics. Since elastomers are temperature-sensitive, it is imperative to select materials meeting the individual temperature requirements of the system, rather than those of an all-inclusive temperature range. Presently available materials are unsatisfactory above temperature in the 300 to 350° F range. However, insulation of the joint section has proved feasible and permits the use of these materials at higher skin temperatures. At reduced temperatures, on the other hand, difficulties may be encountered because some elastomers will not expand, and others will shatter.

Table 1
FULL-SCALE TEST RESULTS

Measure- ment No.	Direction	Peak Acceleration(g)				
		MDC	Expander Tube	Spring Band	Vee Band	ZIP Cord
V3	Radial	2,000	190	190	500	200
V4	Tangential	5,000	—	—	—	290
V5	Longitudinal	1,300	220	160	550	280
V10	Longitudinal	1,200	110	180	280	650
V11	Radial	1,200	70	100	380	260
V15	Radial	1,300	260	100	550	80
V20	Longitudinal	1,200	90	50	220	500

CURRENT WORK

High-speed photographic methods have been used to investigate the action during expansion. It was determined that the joint separation takes place in 25 to 50 μ sec. The material then retracts and pulses. Figure 8 is an example of a tab release system for multiple device operation and illustrates the action of the ZIP cord when activated.

One of the latest design developments is a beryllium joint with extremely high strength that can be broken with a very low explosive charge. A technique for coating the beryllium to control fragmentation after separation has been shown to be feasible. A beryllium joint with a load-carrying capability of approximately 6,000 lb/in. was separated with 2-gr/ft explosive cord. With the advent of a separation joint using low explosively loaded cord, it becomes feasible to interconnect the ZIP cord with a confined detonating fuse (CDF). A junction has been developed which permits the design of a harness providing working sections (ZIP) and nonworking interconnects (CDF) without interrupting the explosive core. It also allows the design of a multiple-device system which is activated by a single uninterrupted explosive train, providing maximum system reliability and simultaneity.

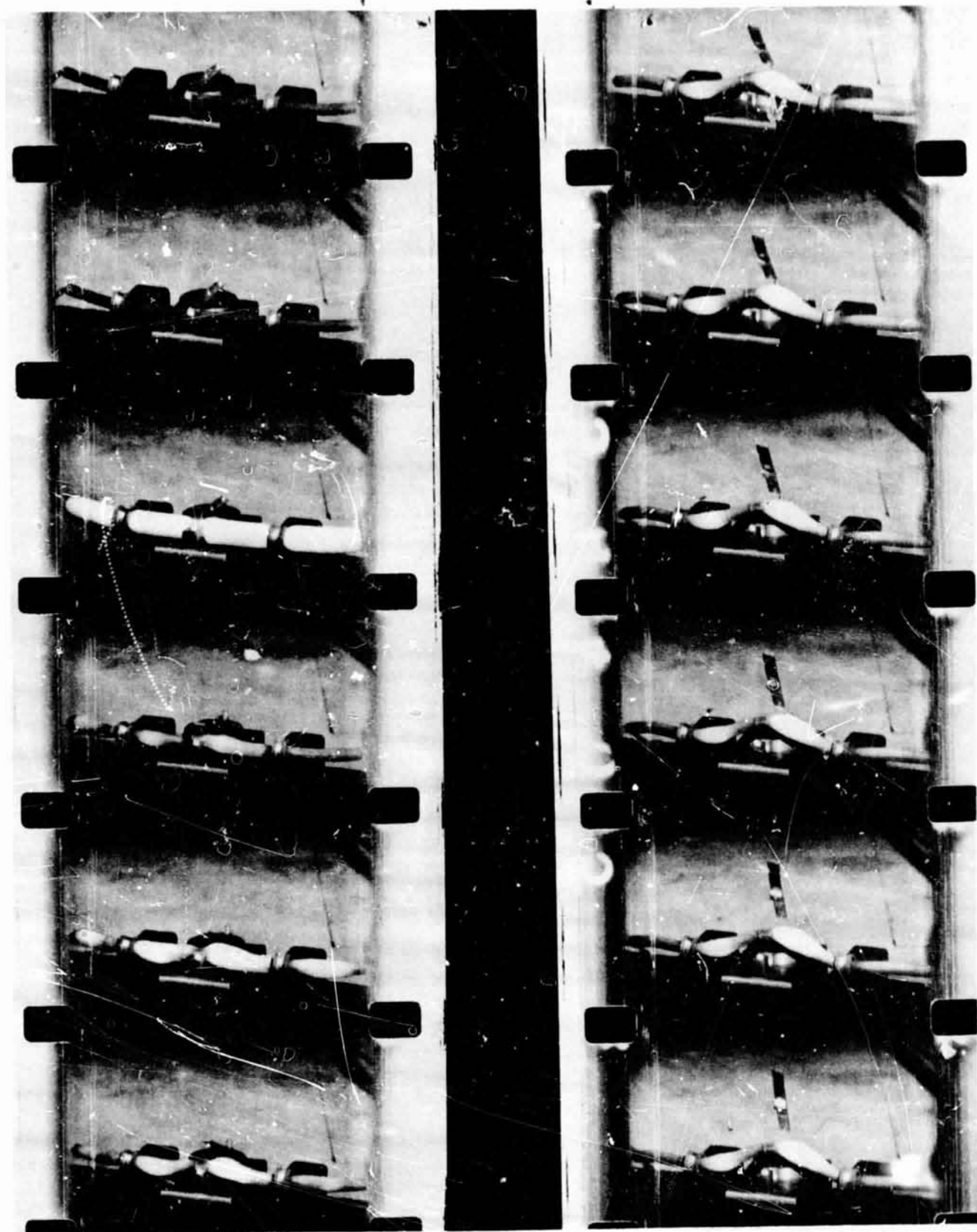


Figure 8 Tab Feasibility Test

PRECEDING PAGE BLANK NOT FILMED.

A VIBRATION ISOLATION MOUNT

By Robert E. Reed, Jr.
Ames Research Center
National Aeronautics and Space Administration

SUMMARY

N67 16907

This paper describes a vibration isolation mount for low-frequency isolation, and presents some preliminary test results. The mount described can be designed for any allowable stroke length and can provide the system with a low natural frequency. However, it is limited to an atmospheric environment and a specified load.

INTRODUCTION

One important requirement for operating dynamic or static equipment often is a limit on the amount of vibration transmitted from the surrounding structure to the equipment. For dynamic equipment, the requirement may also impose limits on vibration transmitted from the equipment to the surrounding structure. Such vibration isolation of equipment is accomplished by the proper design of the equipment-mounting system. Usually the mount is designed so that the system has no natural frequencies near the excitation frequency, and so that the first natural frequency, at least, is well below that of the excitation.

This paper discusses one particular type of isolation mount for low-frequency excitation in the neighborhood of 1 cps. The inherent difficulty with low-frequency excitation in a gravity field is in designing a mount that can support the weight of some piece of equipment and still have a natural frequency well below 1 cps. For instance, a system consisting of a linear spring, of spring constant k , supporting a mass has a natural frequency given by $\omega_n = (1/2\pi) \sqrt{g/\delta_{st}}$ where δ_{st} is the static deflection of the spring

under the force of gravity acting on the mass. For $g = 386 \text{ in./sec}^2$ and $\omega_n = 1.0$ cps, $\delta_{st} \approx 10 \text{ in.}$ However, for $\omega_n = 0.1$ cps, $\delta_{st} \approx 1000 \text{ in.}$ The spring required for $\omega_n = 0.1$ cps is obviously impractical in most cases. There are better systems, but a linear spring does demonstrate the inherent difficulty connected with low frequency.

AVAILABLE METHODS FOR LOW-FREQUENCY ISOLATION

Basically, a low-frequency isolation calls for a mount that will support the specified weight but which, for a disturbance from the equilibrium position, will provide a restoring force that is a very small fraction of the weight (i. e. , a very low spring constant). Molyneux* proposed a system of springs with a near-zero spring constant over a small range of travel. The springs are arranged so that the additional supporting force on some springs arising from a small disturbance is canceled by the other springs. Another method is a piston-cylinder arrangement in which air pressure is servo controlled to remain constant so that the piston force is constant and independent of the position of the piston.

DESCRIPTION OF MOUNT

The mount described herein provides a near-zero spring constant for virtually any length stroke while avoiding electronic servo systems, but it is limited to applications in an atmospheric environment. Basically, the mount is a piston-cylinder device in which one side of the piston is subjected to a vacuum and the other side of the piston is open to the atmosphere. The piston force, therefore, is the atmospheric pressure acting on the piston and is independent of the position of the piston. Hence, the piston provides no restoring force when it is displaced. A cross-sectional view of a typical design is shown in figure 1. The crosshatched portion is free to move with the supported mass, and the remaining part is fixed to the ground. Around the

*Molyneux, W. G.: The Design of Flexible Supports for Vibration Isolation. Royal Aircraft Establishment TN 277, Mar 1960

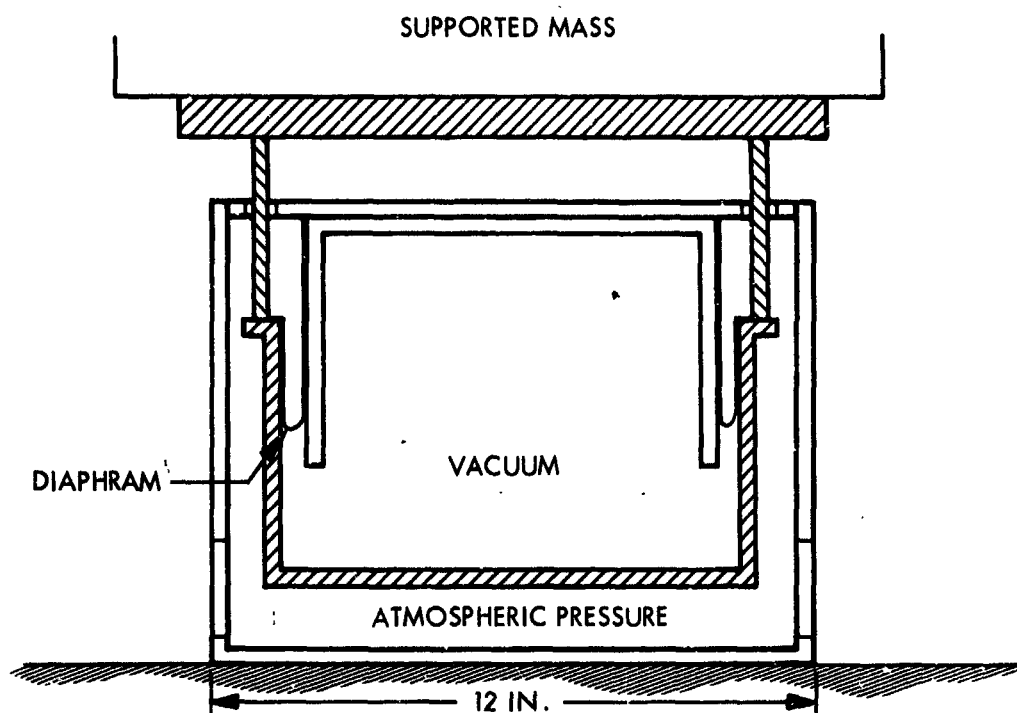


Figure 1 Typical Design

vacuum chamber a rubber-like rolling diaphragm acts as a nonsliding seal with very little resistance to motion. The model shown has an outside diameter of 12 in. and could support about 500 lb. The space beneath the vacuum chamber is exposed to the atmosphere through the holes in the outside container.

It is apparent that this mount can support only a specified weight since the atmospheric pressure is relatively constant. However, the mount can be designed to support the heaviest expected load, and balancing weights can be used to accommodate lighter loads.

The only direct connection between the supported mass and the ground is through the diaphragm. The system therefore appears to be unstable in the transverse direction; however, figure 2 shows how a lateral restoring force is created to resist any transverse motion of the piston. Conversely, it can also be concluded from figure 2 what would happen if the diaphragm were not symmetric about the vacuum chamber. The mount would seek the transverse position at which the lateral forces were balanced, and this position may not coincide with the intended center location.

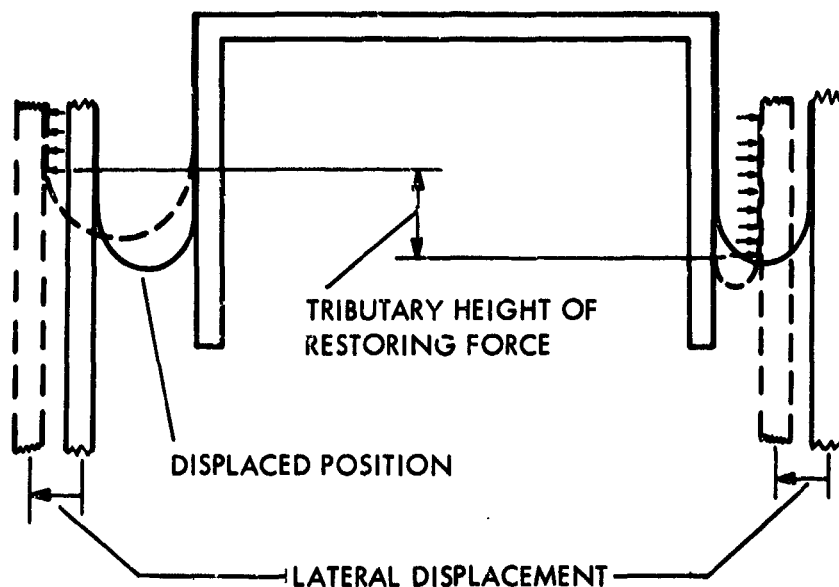


Figure 2 Transverse Restoring Forces

For any system with low stiffness, there is near-zero restoring force for certain types of motion, so the supported mass may be unstable. This mount is unstable for a rotational motion when the overturning moment due to a transverse shift in the center-of-gravity exceeds the restoring moment due to the transverse force caused by the antisymmetric change in the contact area of the rolling diaphragm against the piston for transverse or rotational motion of the piston. When the c.g. of the system is at or below the level of the mount, however, the system has a minimum energy position which is stable.

DESCRIPTION OF TEST MODEL

At present, four preliminary models have been built to test the basic operation of the mount. The dimensions and details of the model are shown in figure 3. The diaphragm was rather crudely made from a rubber sheet in the form of a conical (near-cylindrical) frustum with a covering over the small end (figure 4). The diaphragm was cemented to the inner piston and then stretched onto the outer flange and cemented. All parts except the diaphragm were made of steel, although aluminum parts could be used to give a lighter mount. Each model weighed about 60 lb, with the movable parts weighing about 35 lb per mount. The maximum allowable

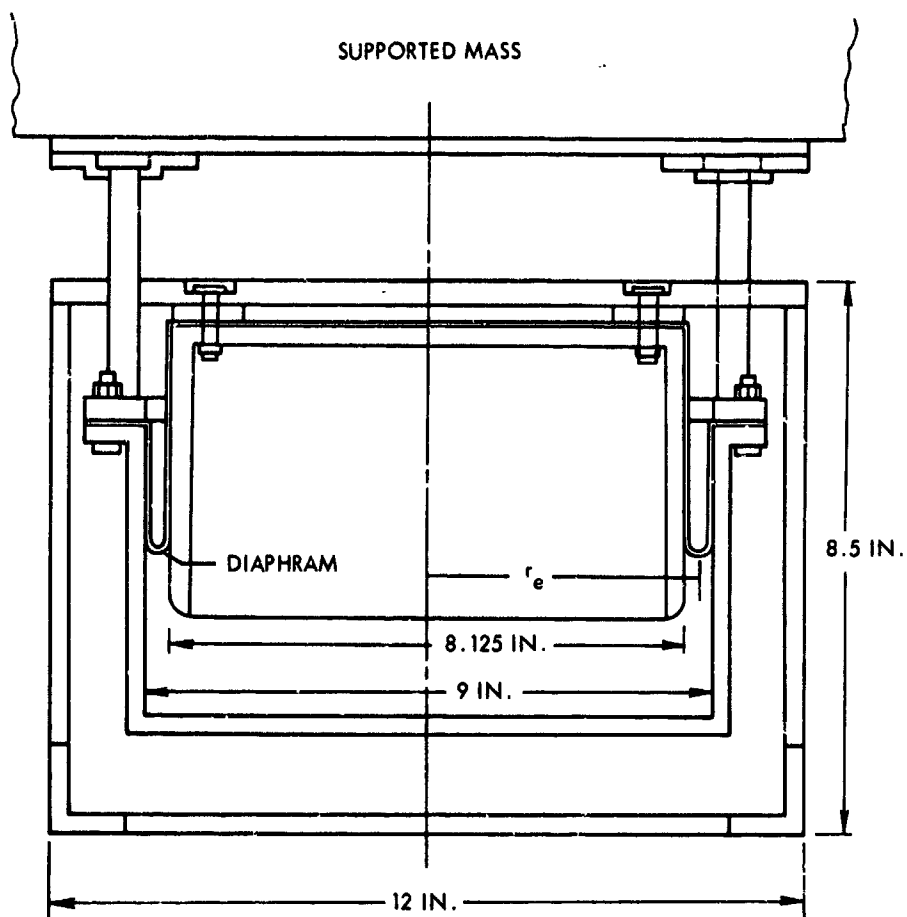


Figure 3 Test Model

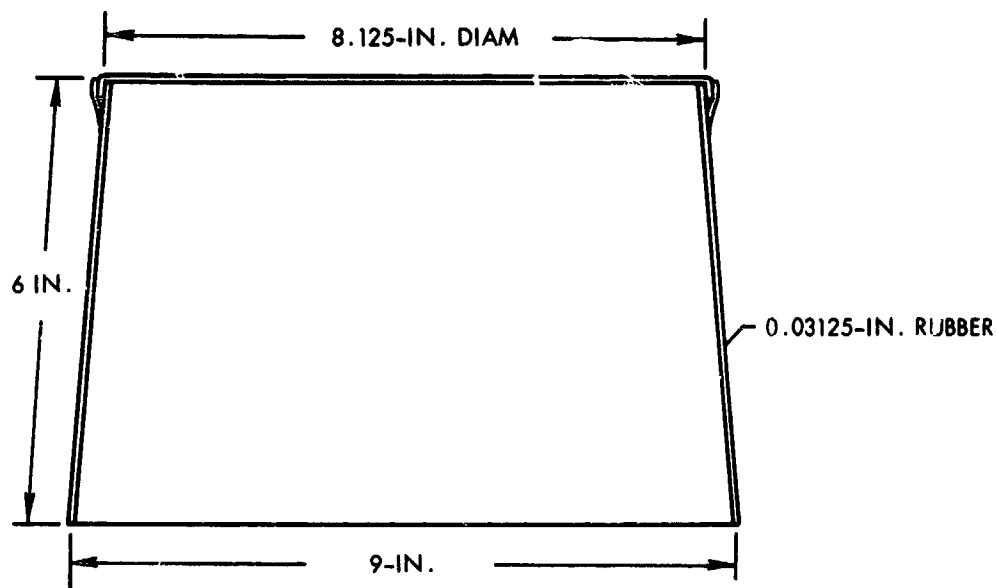


Figure 4 Sealing Diaphragm

stroke was arbitrarily set at approximately 3 in. As shown in figure 3, the stroke is stopped at each end by metal-to-metal contact before the diaphragm is straightened out. This prevents the diaphragm from having to carry any of the weight of the supported mass.

A free-body diagram shows that the effective area of the piston is a circle with a radius equal to the distance from the axis to the center of the toroidal section of the diaphragm (denoted by r_e in figure 3). The effective piston area for the model is 57.5 sq in. which gives a lifting force of 846 lb at standard atmospheric pressure.

TEST RESULTS

The mounts were first tested using a 3,000 lb seismic block. The four mounts supported the block at the bottom corners. Because of the spacing of the mounts, the block was able to rotate with almost vertical motion of the mounts. As the block rotated, the shift of its c.g. caused an overturning moment that increased the rotation. This unstable motion can be prevented by either adding horizontal sliding springs to give a restoring moment, or allowing the seismic block to move only vertically. This stability problem does not arise if the c.g. of the system is below the mounts; therefore, a test was conducted with an 850-lb load suspended below the mount.

The diaphragms were found to be unsymmetrical to the point where the mounts would not center themselves properly. This created a problem because a small lateral motion or rotation will cause the movable parts to rub against the fixed surfaces. Commercially available molded diaphragms should eliminate this problem.

Some leakage was present in the system. Coating the metal parts helped considerably, but a vacuum pump was run continuously while the mount was operated, because the leakage began to decrease the lifting force in a matter of a few minutes without the pump. Regardless of these problems, it was felt that the mount had possible applications and a more refined model is being considered for more accurate tests.

The natural frequency of these models was measured to be about 0.17 cps. The system appears to have relatively high damping (about 10 percent of critical damping), but it should be remembered that the maximum damping force ($c\dot{x}_{\max}$) for critical damping is only about 7 lb for a displacement of 1 in.

CONCLUSIONS

This vibration isolation mount offers a system with a natural frequency substantially below 1 cps. It can be designed to allow practically any length stroke. The mount avoids any electronic servo systems and is economical to build. It does, however, require the presence of an atmosphere and can support only a single specified load. Preliminary tests indicate that some care must be taken in making the diaphragms to insure that they are symmetrical. As for any low-frequency system, some thought must be given to how the weight is to be supported to avoid unstable motion.

PRECEDING PAGE BLANK NOT FILMED.

GEMINI/AGENA DOCKING MECHANISM

By P. H. Meyer
McDonnell Aircraft Corporation
St. Louis, Missouri

SUMMARY

N67 16908

The Gemini/Agena docking mechanisms utilize simple mechanical elements to provide a capability for initial engagement between two orbiting vehicles. The docking mechanisms then rigidize the attachment in a manner suitable for subsequent maneuver with the Agena propulsion system. Finally, the mechanisms provide a capability for disengaging and repeating the entire docking cycle. The mechanical elements used are found in daily terrestrial applications.

INTRODUCTION

The basic design requirement for the Gemini/Agena docking mechanisms was constrained by the calendar time available from design concept to test hardware. Maximum utilization was made of simple mechanisms and reliance on past hardware, design, fabrication, and operational experience. In-process design reviews emphasized the concept of avoiding need for development improvements by reason of simplicity. During the development of the Gemini/Agena docking mechanisms, tests were conducted on shock-attenuation, latch, and rigidizing mechanisms, and on normal as well as emergency disengagement provisions.

MECHANISM DESIGN AND FUNCTION

The principal parts of the docking mechanisms and the docking maneuvers are pictured in figure 1. This illustration shows the docking adapter (a cylindrical structure rigidly mounted to the Agena), the docking cone with its indexing vee-slot, and the indexing bar to enter the docking cone vee-slot mounted near the forward end of Gemini.

Portions of the shock-attenuation system capable of absorbing initial impact and part of the latch hooks and latch receptacles used for initial engagement of the two vehicles are also pictured.

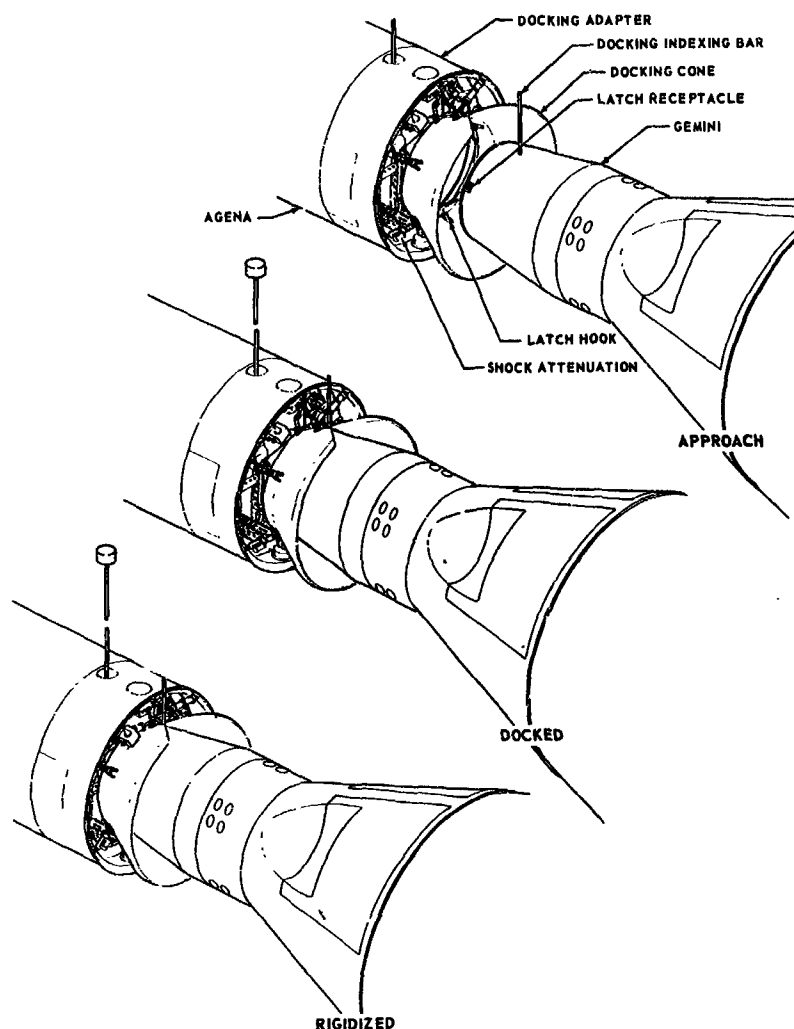


Figure 1 Gemini/Agna Docking and Rigidized Maneuvers

Static conditions and the relative movement of the docking cone and the spacecraft as they progress from docked to rigidized maneuvers are shown in figure 1. Roll misalignment is corrected by the docking indexing bar in the vee-slot of the docking zone. Spacecraft attitude-maneuvering may also be used after one or more latches have engaged. The docking indexing bar is a pyrotechnic device installed flush with the spacecraft mold line. The bar is extended before docking, and then jettisoned at completion of the docking maneuver. The docking and bar functions are electrically initiated and controlled by the Gemini crew.

SHOCK-ATTENUATION MECHANISMS

The shock-attenuation system (figure 2) supports the docking cone on the docking adapter with a set of seven viscous dampers, four of which are spring-loaded to the extended position. This effectively provides limited free motion in three axes. The principal energy absorption is in the compression direction and is accomplished by simple orificing. The extension rebound is also damped but only for the purpose of limiting velocity to that which avoids loss of contact after initial impact.

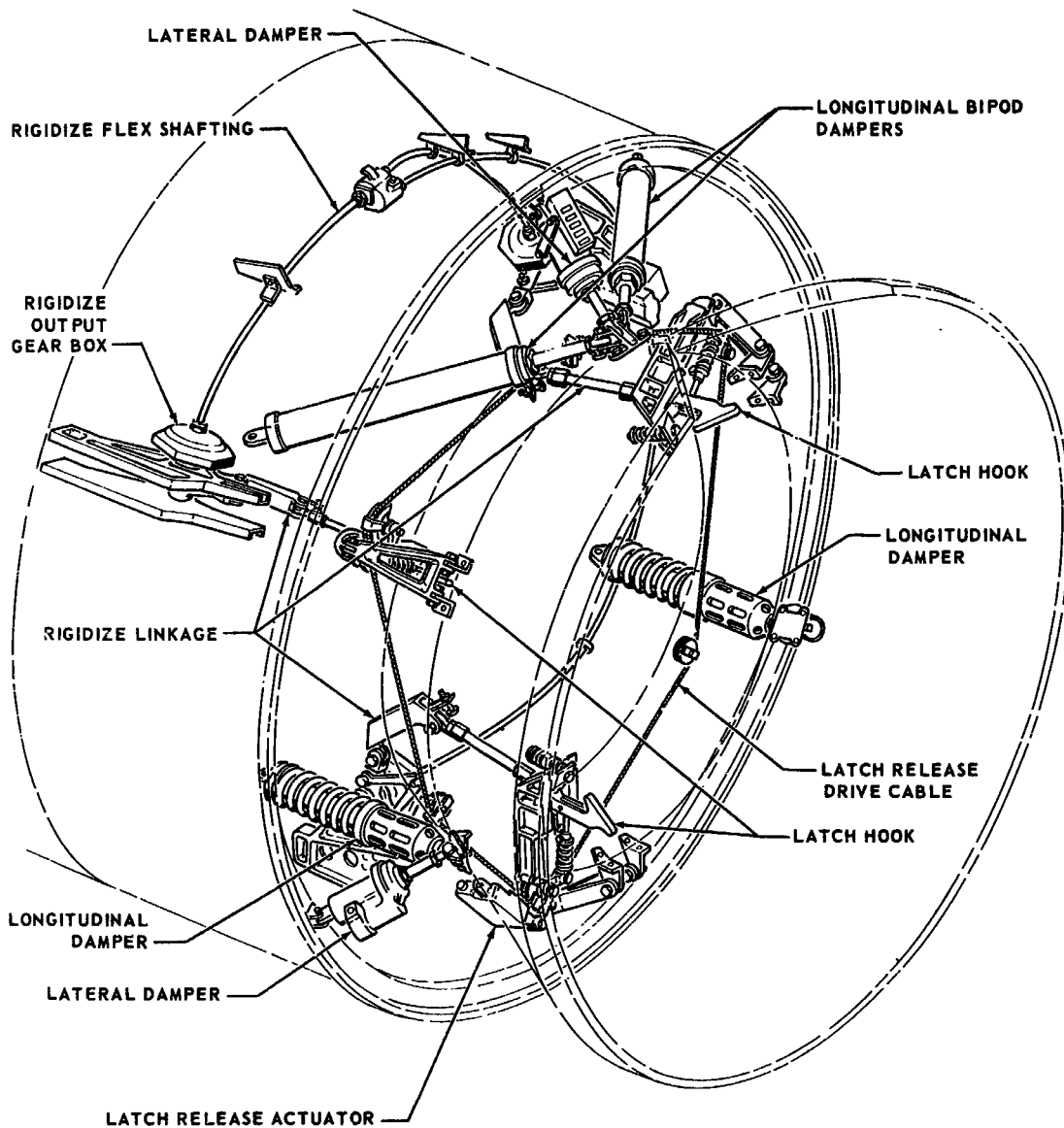


Figure 2 Gemini/Agna Docking Mechanism

The docking cone has three attach points symmetrically located around its circumference for the shock-attenuation attachments. The two points on either side of the docking-cone V provide for attachment of one longitudinal and one lateral damper. At the third docking-cone attach point, the longitudinal damping load provisions needed to be in a bipod arrangement because equipment in the docking adapter prevented installation of the single longitudinal damper. The lateral damper at this third point is identical to the other two.

Initial engagement of Gemini to Agena is accomplished by three spring-loaded latch hooks located 120 deg apart circumferentially at the bottom of the docking cone. The latch hooks mate with similarly located latch receptacles on the spacecraft nose. The docking cone shape and motion on its damper/spring suspension system compensate for both offset and angular misalignments.

LATCH MECHANISM

In a typical latch arrangement (figure 3), the latch hook proper is pivoted with its cam surface extending inside the docking cone. The entry of the latch receptacle depresses the latch hook against its spring cartridge until the receptacle passes, then the latch hook re-extends to engage the receptacle. Relative motion between the latch hook and the follower operates a toggle switch mounted on each latch hook and connected by spring cartridges to the follower.

The follower straddles the latch hook and is pivoted to rotate independently of the latch; when the latch hook is retracted, the follower moves with it due to the mechanical attachment through switch and spring cartridges. When the latch hook extends to engage the latch receptacle, the follower cannot extend with the latch hook because the end of the follower bears on the forward end of the latch receptacle at a point flush with the spacecraft mold line. This restraint of the follower causes the differential motion to operate the electrical switch which signals that the spacecraft are engaged.

When all three latches are engaged, thus operating all three switches, the electrical circuit is closed to start the rigidize cycle. In this engaged position, the spacecraft nose is not firmly bottomed in the docking cone. The rigidize load is applied at the

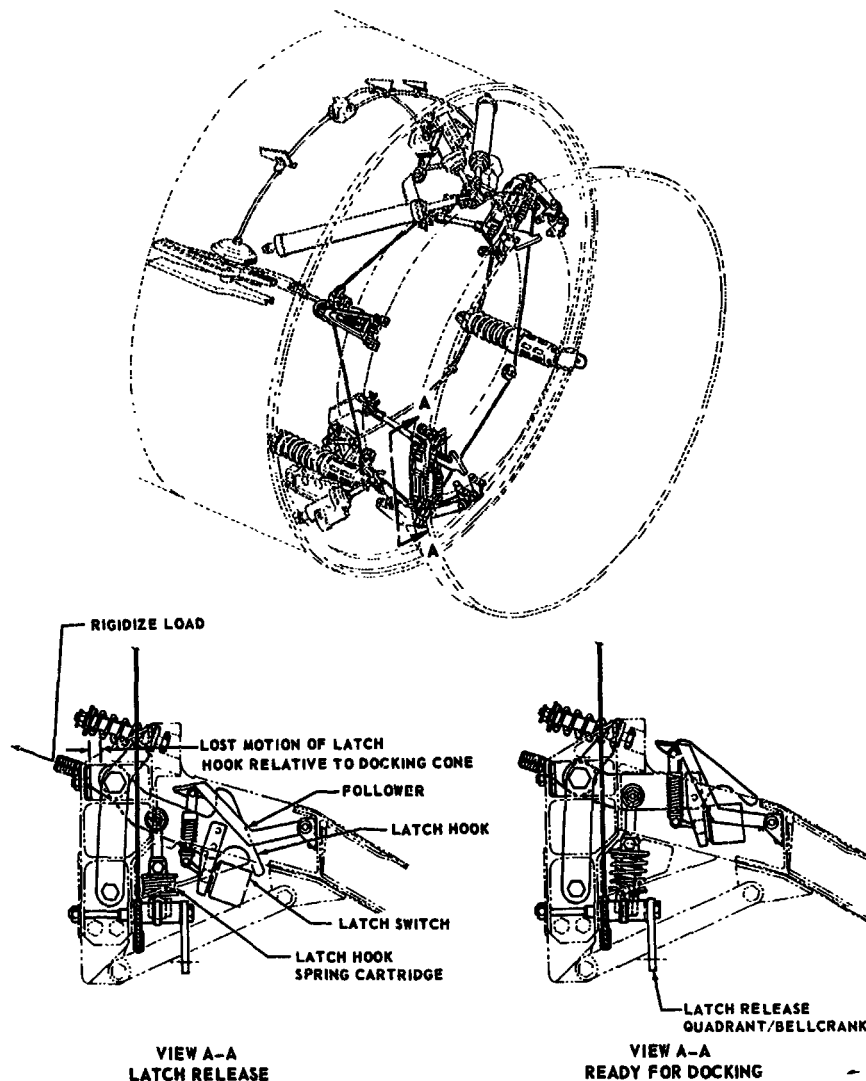


Figure 3 Latch Mechanism

latch-hook pivot point and thus pulls the latch hooks toward the bottom of the docking cone; the docking cone remains initially fixed because of the extension springs on the longitudinal dampers. When the spacecraft has bottomed-out in the docking cone, the rigidize mechanism continues to pull spacecraft and docking cone together against the spring load of the longitudinal dampers.

The mechanism to rigidize the docking cone consists of three identical sets of over-center linkages driven by gear boxes through flex shafting from an electric motor. These linkages retract the docking cone by pulling on the three latch-hook pivot points to bring hardpoints on the docking cone to bear on hardpoints in the docking adapter.

RIGIDIZING MECHANISM

The rigidizing linkage (figure 4), occupies two positions. The bell crank on the output gear box travels approximately 140 deg to the over-center position of the links, and also actuates electrical switches at each end of the travel to provide signals for both the rigidized and the unrigidized condition. The rigging of this linkage is accomplished through permanently installed strain gages on each of the tension links. The specific Gemini intended to fly with a specific Agena is utilized to be the "tool" for torquing the tension link to a specified preload as read from the strain gages. A known and closely controlled preload is required to take bending loads between docking adapter and spacecraft when maneuvering with the Agena propulsion system. Too great a preload may overload or stall the linkage drive motor.

The rigidizing motor (figure 4), is geared to two output shafts having a 2 to 1 speed relationship. The low-speed output operates a direct drive through flexible shafting to one of the rigidize gear boxes. The high-speed output drives an H-gear box which also has two output shafts and reduces the speed to drive the remaining two gear boxes used for rigidizing. The gear reduction from motor to output drive arm is approximately 3500 to 1.

In the development program on full-scale hardware, overall mechanical efficiencies were not as high as anticipated and, therefore, the drive motor torque was increased. Since this increased output was demonstrated to be adequate for all loading conditions, concern over single-point failures dictated a further component evaluation to establish that all parts of the system up to the output gear-box bell crank be capable of taking a load equivalent to 100 percent of the motor output at 100 percent efficiency. This assumes that the worst condition would exist if the entire motor output is exerted on one of the three linkage branches with the other two having a zero-resisting load. Every component of the system was statically torqued to failure; the results showed the flex shaft loaded in the "unwrap" direction to be the weakest link, but still equal to 117 percent of the single-point ultimate load failure criteria.

Disengagement of Gemini from Agena is a switching function accomplished by the Gemini crew. The method for reversal from a rigidized to a docked condition is clearly indicated. At this point, the latch release mechanism (figure 2) is activated

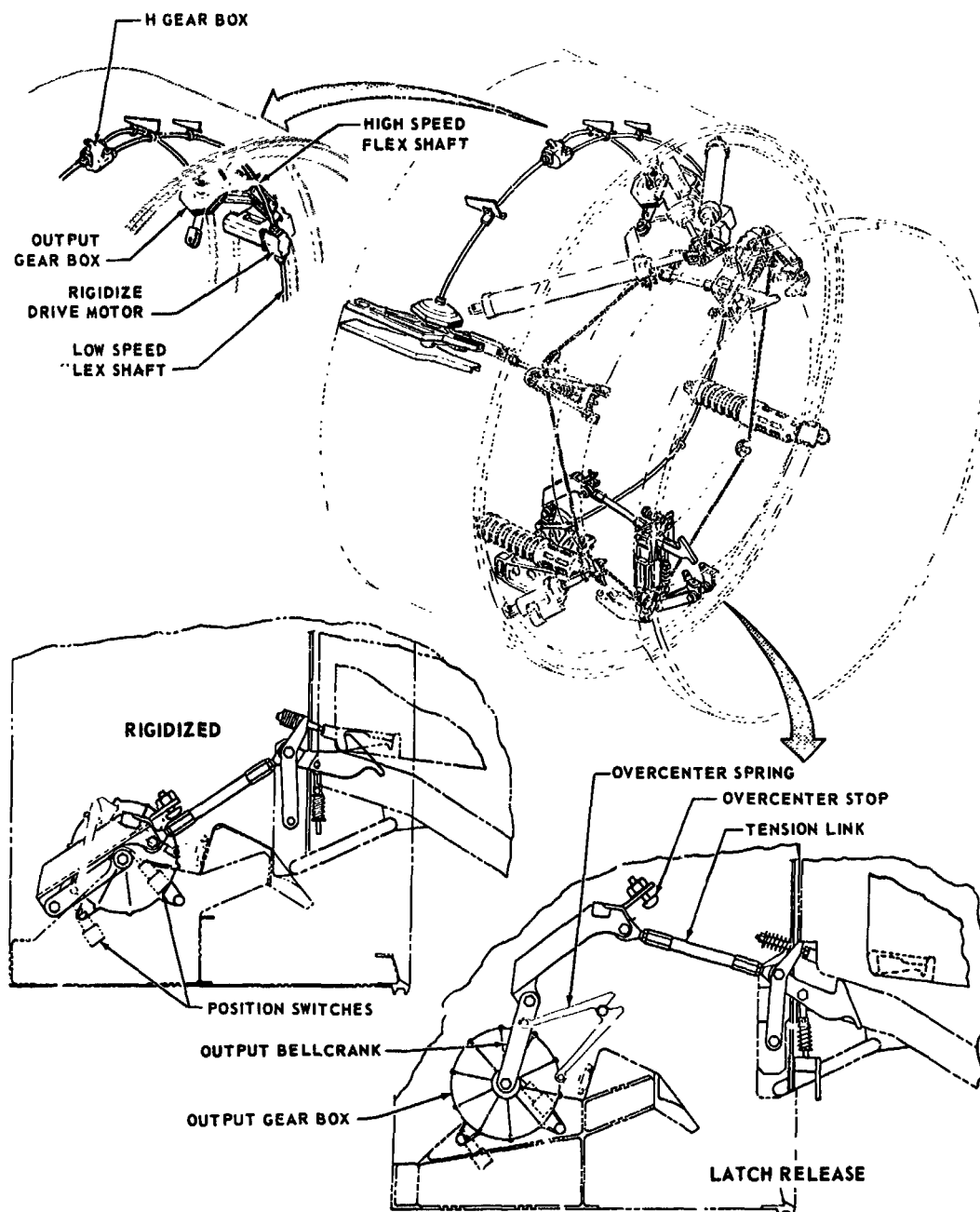


Figure 4 Rigidizing Mechanism

for the first time. This mechanism is mounted on the docking cone and is powered by an electric motor-driven screw jack which drives a "run-around" cable system. At each of the three latch points, the cable is attached to a quadrant/bell crank. Mounted on each bell crank is the latch-hook spring cartridge which, as the bell crank rotates, acts as a tension link to retract the docking-cone latch hooks from the spacecraft latch

receptacles, thus leaving the spacecraft free to back out of the docking cone. Power to the latch-release screwjack is applied at the start of the unrigidize cycle. After the Gemini is completely withdrawn, the power is reversed to reposition the latch-release mechanism in readiness for a repetition of the docking maneuver.

Mechanical reset of latch hooks is due to a spring-loaded lever-operated switch bearing on the spacecraft when it is approaching the bottom of the docking cone. The latch-release actuator includes a slip clutch, permitting the motor to run when the screwjack is either stalled or at the end of its stroke. This feature makes possible power application at the start of the unrigidize cycle when the preload on the latch hook does stall the screwjack; also, at the end of the unrigidize cycle, the screwjack drives to its mechanical stops until the spacecraft is gone, ensuring that full travel of the latch hooks has disengaged the spacecraft. Development testing of the slip clutch demonstrated a less than 15 percent decrease in load pickup capability after 10 consecutive minutes of slippage.

In the event of mechanism failure, emergency disengagement is accomplished by jettison of the latch receptacles on the spacecraft. This is the function of a pyrotechnic actuator which retracts the pin that provides the structural attachment of latch receptacle to spacecraft. No separation force is applied; the crew must back out of the docking cone after latch receptacle jettison. Further docking maneuvers are, of course, impossible.

Evaluation of all mechanisms was performed on a full-scale specimen of representative production hardware. Maximum mission duty cycles were exceeded with operational performance in terms of load capability and operating speed measured before and after. The specimen was soaked at high altitude for 5 days, then checked for performance; while maintaining altitude, the chamber was cooled, the specimen soaked at 65°F, and again operated. Following this, the chamber temperature was raised to 160°F, and the specimen stabilized while maintaining altitude for additional cycles. Operational testing showed no degradation of the mechanisms.

Final evaluation was accomplished on full-scale dynamic tests (figure 5) with both simulated vehicles having proper weight and mass distribution, and with actual hardware for the complete target docking adapter and the forward spacecraft sections.

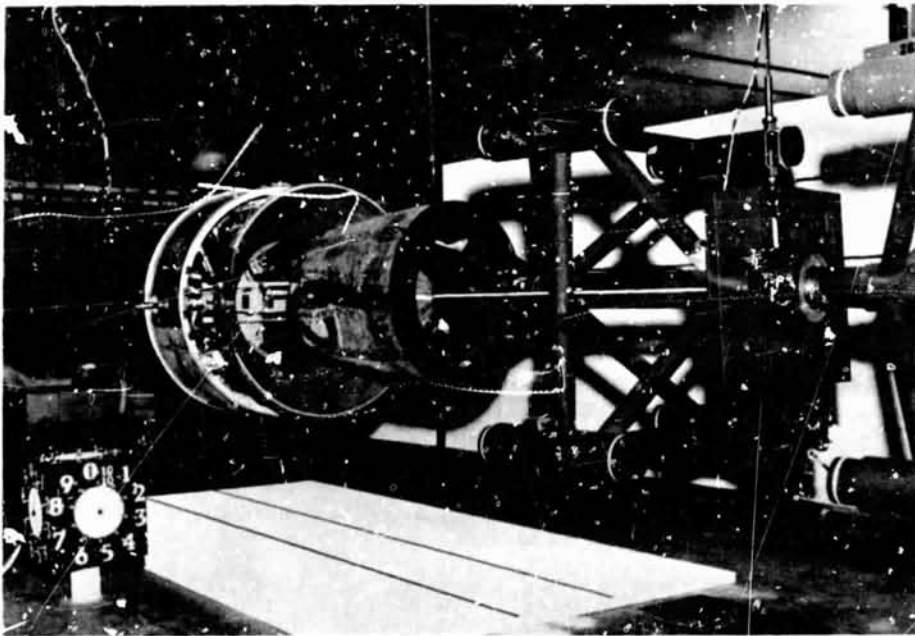
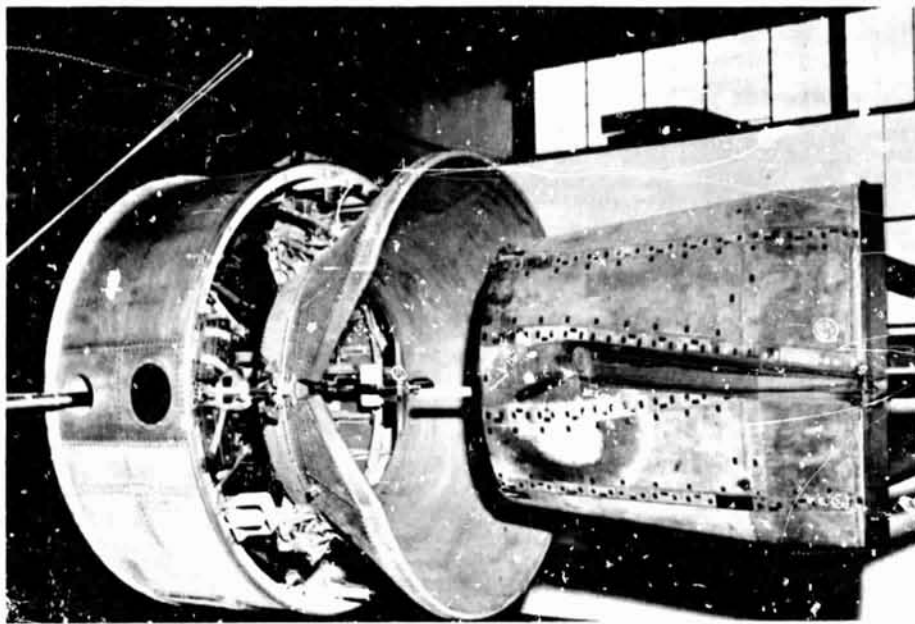


Figure 5 Dynamic Test

In the dynamic tests, ceiling heights having adequate strength limited the pendulum length to 56 ft and, therefore, did not permit testing at large separation distances. Outdoor testing could not be performed because of potential draft disturbances. The pendulum angle, under 1-g conditions, gave an ultimate velocity of 1.75 fps at approximately 20 in. of separation. During 22 impact test runs there were no failures and no cases of exceeding design loads. It was predicted that 12 of the 22 runs would accomplish successful engagement of one or more latches based on previous quarter-scale dynamic tests; 10 of the 12 predictions were correct. In the two cases of failure to latch, less than 10 lb of equivalent attitude thrust did engage latches.

DRAG MAKE-UP SENSOR FOR LOW-ALTITUDE SATELLITES

By William R. Davis
Lockheed Missiles & Space Company

SUMMARY

N67 16909

Satellite environments ordinarily impose many constraints on a system designer. On the other hand, it is sometimes possible for a designer to use the environment to his advantage. The drag make-up sensor described in this paper is a case in point. Characteristics of the satellite environment were exploited to simplify greatly the instrumentation needed to measure, and compensate for, satellite air-drag force. A photoelectric pickup is used to detect the position of an untethered ball that floats loosely in a "cage" within the vehicle. A thruster on the vehicle, controlled by a ball-cage position signal, keeps the cage (and vehicle) centered on the ball and thus in a drag-free trajectory. (The ball is shielded from the air stream by the vehicle.) Hardware for a flight test is described.

INTRODUCTION

The environment in which a system operates usually imposes constraints on the designer and frequently leads to a complicated design. Occasionally, however, the designer can use the environment to his advantage to produce a simpler design. A significant environmental condition in many satellites, for instance, is the almost total lack of sensible weight or net force (due to either gravity or acceleration). It seems straightforward, then, to try to use this fact in a system for air-drag compensation in low-altitude satellites. This is suggested in spite of the existence of numerous on-the-shelf accelerometers, because the accelerations to be measured and countered are in the region from about 10^{-8} to 10^{-6} g, without any requirement for handling accelerations in excess of 10^{-5} g.

SENSOR DESIGN

The idea of using a proof mass within a satellite to achieve a zero-drag trajectory has been suggested by several people working in this field. The most complete treatment is that of Lange (ref. 1). The proposed systems have been complex, inasmuch as they were part of long-term experiments to make very precise measurements. These systems typically require reducing perturbing forces to the order of 10^{-12} g. More simplified missions, such as reducing (but not necessarily completely eliminating) orbit decay of low-altitude satellites, require decreasing the net (air drag) deceleration to about 10^{-8} g.

A simple error analysis showed that, for a vehicle with an attitude control system that keeps one vehicle axis aligned (nominally) along the velocity vector (i.e., in the direction of the drag force), it is not necessary to require the vehicle to "follow" and not touch the ball (proof mass) in a direction transverse to the direction of the drag force. This result led to the design and study of a sensor and system in which only the position of a ball along the vehicle roll axis (i.e., that axis aligned with the drag force) is monitored and controlled. In this scheme, the ball is allowed to contact the side walls of a tubular cage. Displacement along the cage axis is measured by a phototransistor, and this information is used to control thrust on the vehicle and prevent the ball from contacting either end of the cage. Figure 1 shows a functional sketch of this concept. Figures 2 and 3 show the flyable ball and cage hardware.

To utilize only the simplest detection means, i.e., position, the system requirement for rate information to provide a damped control of ball-cage position was solved by deriving a synthetic rate signal electronically. The use of derived states in control systems is a standard technique. Recent work of Luenberger (ref. 2) presents useful general results and applications. The particular method of deriving rate in this system was suggested by the work of Leonard (ref. 3) on long-life control systems.

The electronics employed use standard solid state components (figure 4). These include, in addition to the phototransistors, a pair of light-emitting diodes, about two dozen transistors, and associated resistors and capacitors.

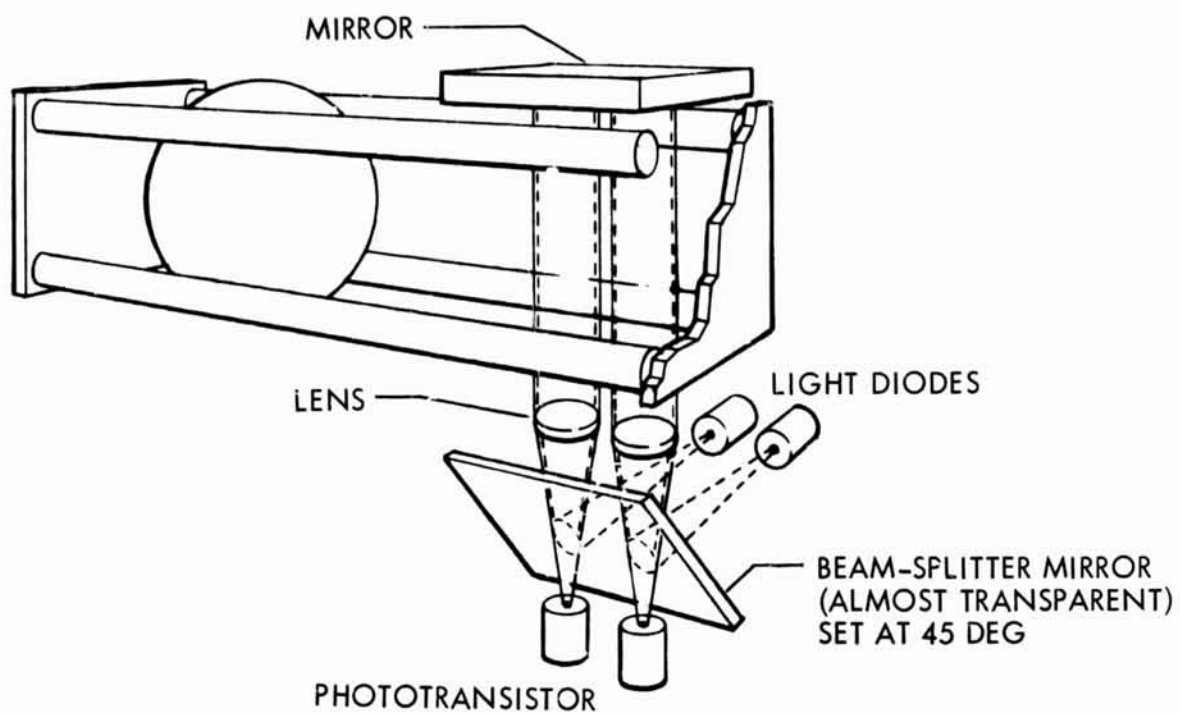


Figure 1 Ball-in-Cage Mechanization

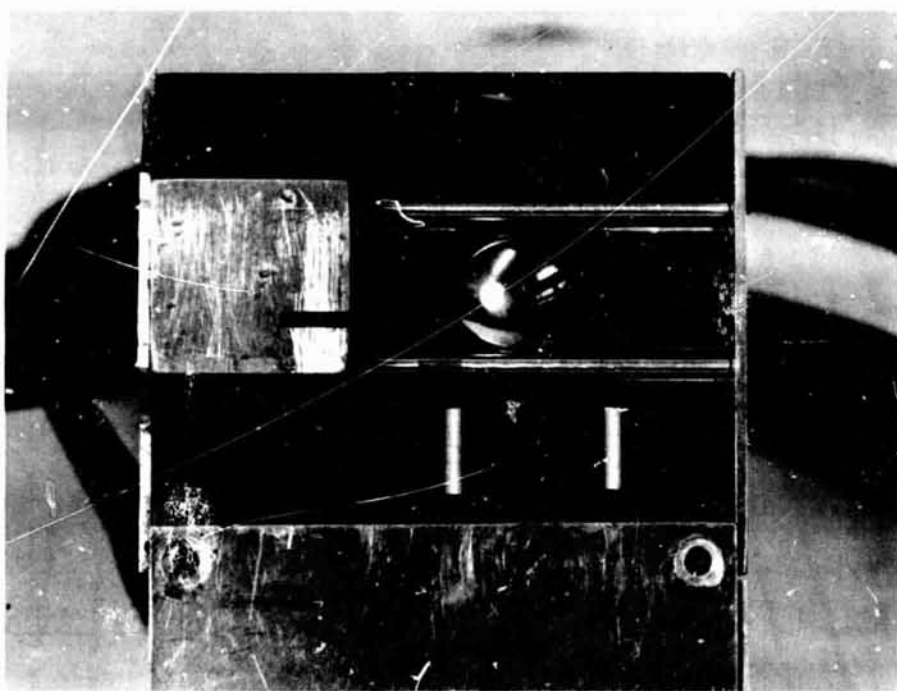


Figure 2 Position Sensor

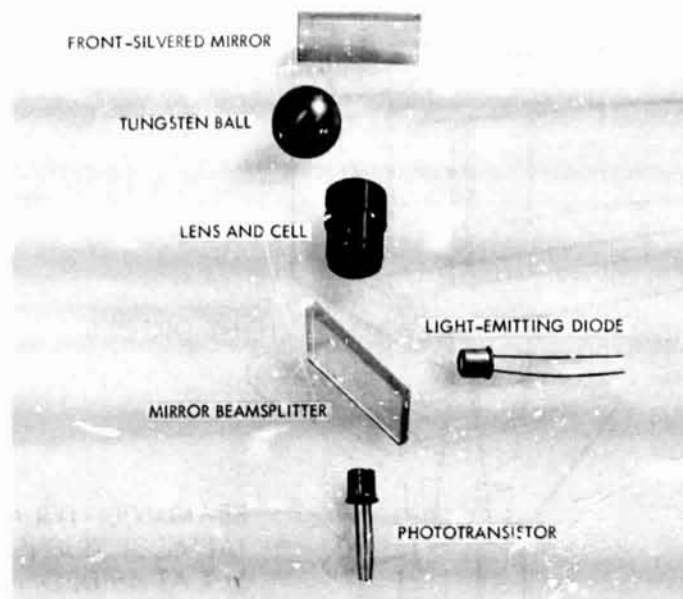


Figure 3 Position Sensor Optical Components

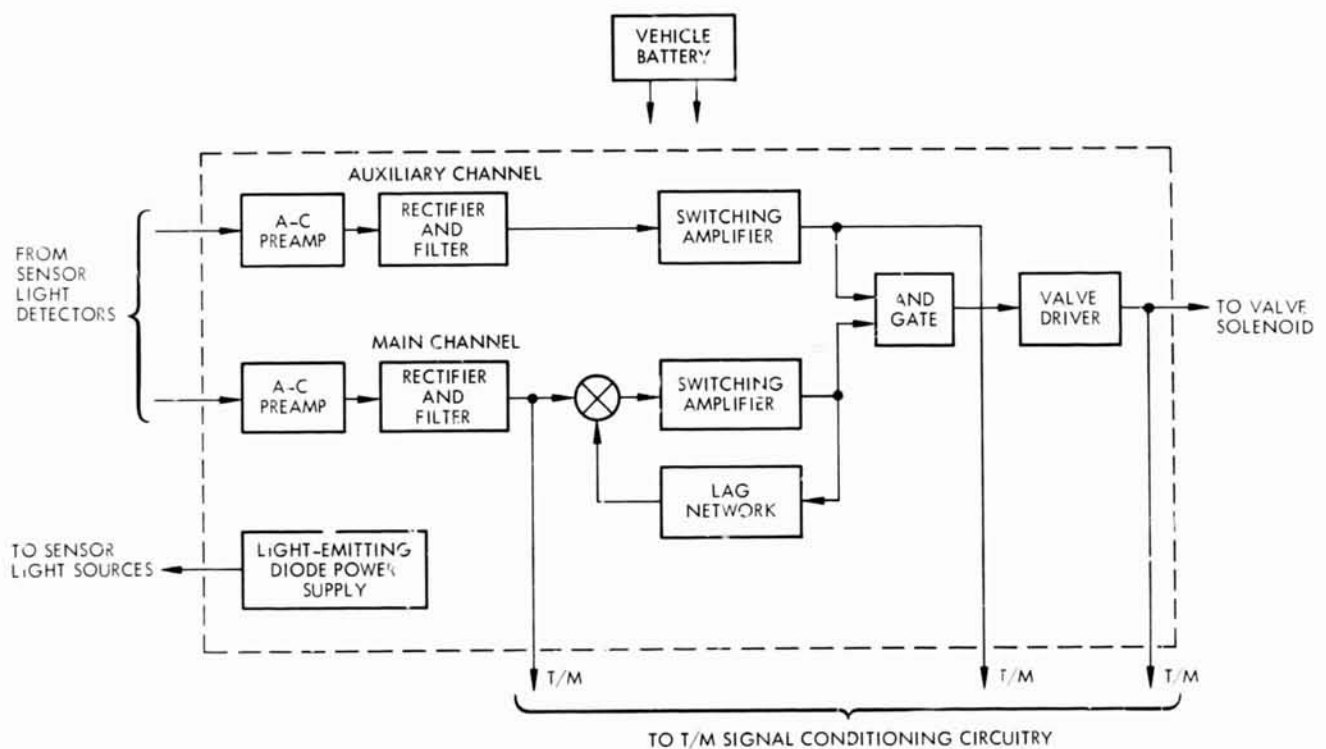


Figure 4 Electronic Package - Block Diagram

For thrust, the system uses standard Agena attitude-control jets modified to operate at a low thrust of about 0.10 lb. Figure 5 shows all components of the system.

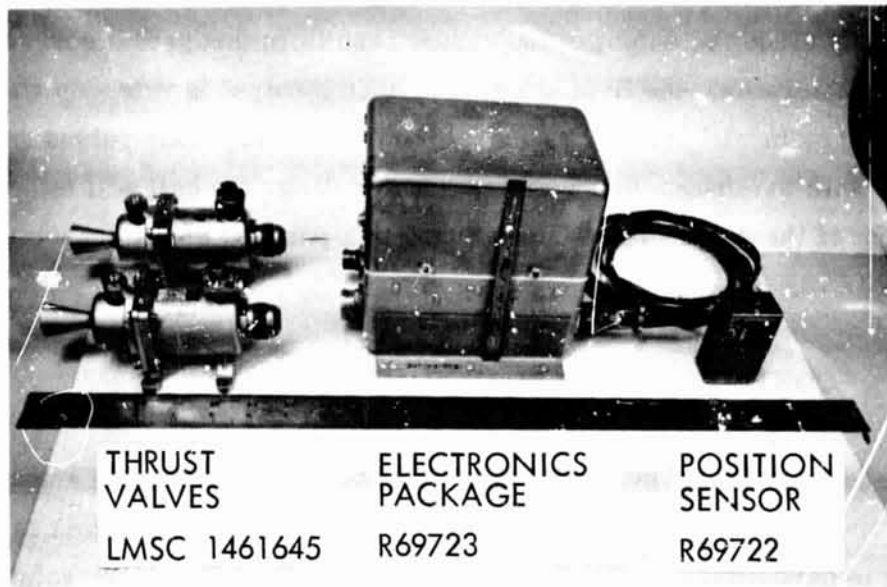


Figure 5 Drag Make-up System

THEORY OF OPERATION

The operation of the system is simple and straightforward. The overall control scheme utilizes the fact that active thrust need only be provided in one direction, i.e., in opposition to the drag. In the absence of control thrust, therefore, the ball tends to accelerate toward the front of the cage. The light from the two light-emitting diodes is collimated and caused to cross the cage in a transverse direction and fall upon phototransistors. The two beams are identified as main and auxiliary.

The main beam is positioned so that, as the ball moves rearward (under thrust), the beam is gradually occulted by the ball. In this process, the signal from the phototransistor decreases to zero. As the ball continues rearward, the beam is again uncovered (but from the wrong side). Since it is not desirable to thrust in aid to drag, the signal is deactivated in this region by the auxiliary beam, which is also uncovered as the ball starts to uncover the main beam to the rear. By this technique, the form of the main sensor is kept simple, in that it does not have to distinguish the "sense" of ball displacement.

As the ball moves forward, the signal increases, calling for more thrust. This is accomplished by switching the thruster completely on whenever the switch input threshold is exceeded. The signal into the switch consists of the output of the light sensor plus a rate signal derived from passively integrating the switch output by means of a lag circuit. Since the output of the switch results in thrust that corresponds to (i.e., produces) acceleration, the first integral of switch output is rate. In steady-state operation, this system will produce a series of constant magnitude pulses whose duty cycle increases with the drag. Hence, for a greater drag, the ball will offset more toward the front of the cage. The system thus has a position offset proportional to the external force.

CONTROL SYSTEM PERFORMANCE

The ideal procedure for any design synthesis is to operate the system in the actual situation and adjust the parameters to achieve optimum performance. But this is not always possible. It is particularly difficult in the present problem since the solution utilizes the near-zero-g environment of the satellite. However, because the control is along one axis only, a good simulation can be performed in the laboratory.

By suspending a ball on a bifilar torsion pendulum (figure 6) time-constants and effective forces corresponding to those expected in orbit were generated. In this simulation, torque on the pendulum corresponds to force on the vehicle. The torque was produced by two mechanisms: torsion in the bifilar suspension, and magnetic torque on a magnet resulting from the earth's magnetic field and the field produced by two Helmholtz coils in the test fixture. By sending an appropriate bias current through the coils, the noncontrol torque on the pendulum was matched to the air drag force. To simulate the varying air drag of an eccentric orbit, the bias current was slowly varied in a preprogrammed fashion.

Control torque was produced by sending a control current through the coils. This current was produced by the sensor placed in the path of the suspended ball. Circumferential motion of the ball in the simulation thus corresponds to axial motion of the ball relative to the case in orbit.

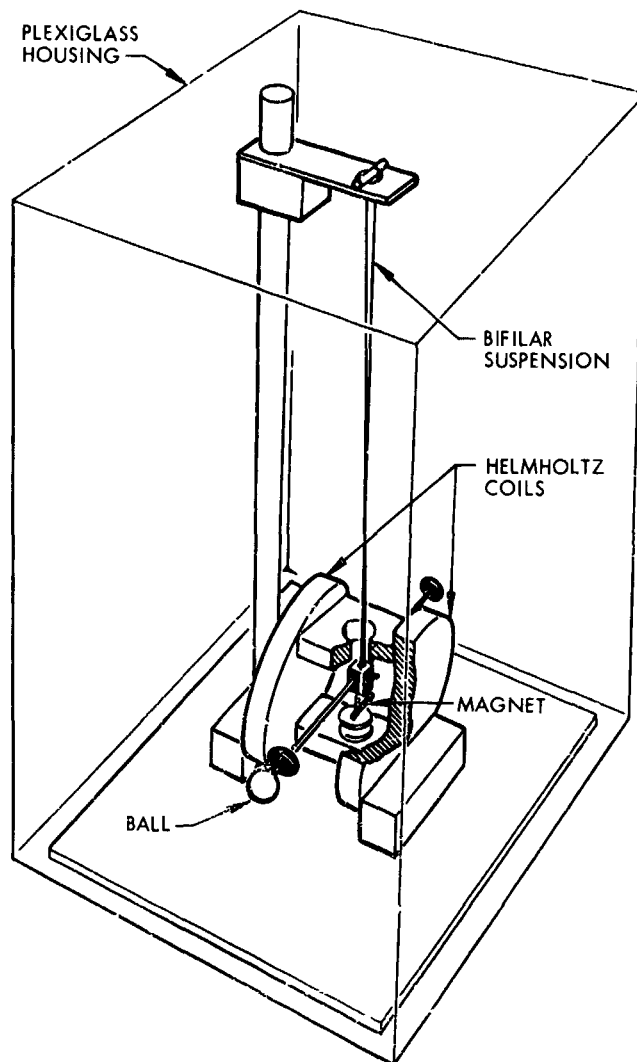


Figure 6 Laboratory Test Fixture

With this scheme it was possible to incorporate actual system time constants and components in a real-time, closed-loop simulation. Only the gas jets were not used. Acquisition and damping were evaluated for various system parameters, such as integration time constant, cage dimension, switching amplifier hysteresis and minimum on-time, ball size, and light beam aperture under various external environments – especially the extremes in drag force from apogee to perigee. Figure 7 shows a series of acquisition runs at various drag levels for various apertures. Typically, the system acquires from an extreme ball displacement in less than one minute. Although it can operate up to 100-percent duty cycle, it is typically set so that a 30-percent duty cycle will counter the perigee drag force.

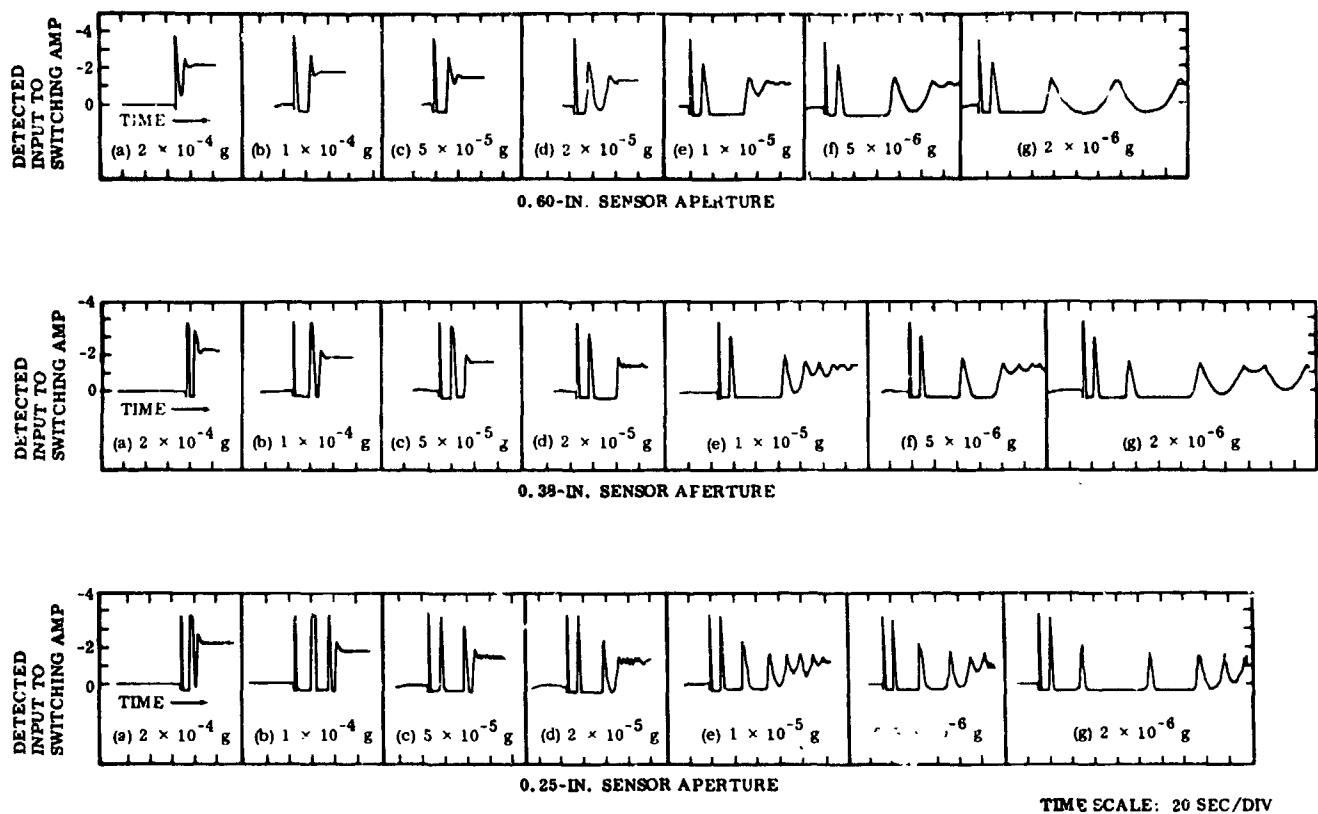


Figure 7 Acquisition Behavior

Performance optimization through the simulation has resulted in the following parameter selection:

- | | | | |
|----------------------------------|------------|--|--------------|
| ● Ball size | 0.50 in. | ● Switching amplifier minimum on-time | 0.06 sec |
| ● Cage length | 1.55 in. | ● Thrust level (2 jets at 0.1 lb each) | 0.2 lb |
| ● Light beam aperture | 0.28 in. | ● Minimum impulse | 0.012 lb/sec |
| ● Lag network time constant | 0.55 sec | ● Switching line to back of cage | 0.8 in. |
| ● Switching amplifier hysteresis | 10 percent | ● Dynamic range | 300 to 1 |

DRAG MAKE-UP PERFORMANCE

The preceding description relates to the details of the scheme for keeping the cage ends from hitting the ball, which was the main criterion in the total design synthesis. To assess the device as an accelerometer, it is necessary to look at the total system performance. Table 1 shows the results of an error analysis that included the most significant errors and perturbations. Although some of the sources affect the system in an impulsive manner rather than as a steady force, the effects have been interpreted in terms of an equivalent steady (i.e., constant) specific force.

From Table 1, it can be seen that angle-of-attack and thrust misalignment produce the significant transverse forces, whereas the vehicle attitude oscillations produce the significant longitudinal forces. Although the transverse forces are about 20 times larger than the longitudinal forces, they result in ephemeris perturbations of the same order of magnitude. This is due to the different way the two types of errors propagate. The result is quite interesting since it indicates that, from an error sensitivity standpoint, the system is well balanced.

The absolute magnitude of the RSS in-track disturbing force is about 0.15 percent of the drag force. The drag cancellation to this accuracy should therefore be achievable with this system. Since the first three forces in Table 1 depend upon the drag force, the system would operate at higher altitude with the same accuracy until the error from vehicle self-gravity dominated. This could be reduced considerably by proper location of the proof mass. With such accuracy, the system more than meets the design objective, namely, to provide a system for drag cancellation to an accuracy better than 1 percent.

Table 1
ERROR ANALYSIS RESULTS

Error Source	Magnitude and Direction Relative to Drag Force (g)		Comment
	Along	Transverse	
Drag	3×10^{-6}		125 (nm)
End Wall Hit	0	7.5×10^{-7}	(System malfunction)
Side Wall Contact			
Thrust Misalignment	9×10^{-10}	6×10^{-8}	$\mu = 1/4 \quad \alpha = 1 \text{ deg}$
Angle of Attack	6×10^{-10}	6×10^{-8}	$\mu = 1/4 \quad \alpha = 1 \text{ deg}$
Vehicle Attitude (Limit Cycle, Oscillation)	1.6×10^{-9}	0	1-deg peak 1,000-sec period
Vehicle Self-Gravity	1.4×10^{-9}	—	—
Vehicle Stray Fields (Magnetic)	10^{-14}	—	—

REFERENCES

1. Lange, B. O.: The Control and Use of Drag Free Satellites. Stanford University (Ph.D. thesis). Sudaer 194, June 1964.
2. Luenberger, D. G.: Observing the State of a Linear System, IEEE Trans. on Military Elec. Mil 3 no. 2, Apr. 1964.
3. Leonard, B. S.: Analysis and Modification of the Derived Rate System for Long-Life Attitude Control of Space Vehicles, Lockheed Missiles & Space Company, LMSC-577639, Oct. 1964.

ACKNOWLEDGMENTS

The author wishes to acknowledge the major contribution of J. K. Matsunaga, who served as project engineer on the sensor development, and the efforts of D. R. Payne, R. L. McKenzie, M. E. Stickney, and R. P. Sherwood, who contributed to the program throughout the development.

SPACECRAFT HYDRAULIC TIMERS*

By Harland D. Trimble
Jet Propulsion Laboratory
California Institute of Technology

SUMMARY

N67 16910

Spacecraft hydraulic timers provide triggering for certain celestial events without using command or sequencing capability and also provide mechanical redundancy for electrical functions. Hydraulic timers developed and tested at the Jet Propulsion Laboratory (JPL) were flown successfully on the flights of Ranger VI, VII, VIII, and IX, and on Mariner IV. This discussion centers on problems encountered by JPL as these timers passed from the initial design stage through development and flight test.

INTRODUCTION

The primary objective of the Ranger VI, VII, VIII, and IX spacecraft was to photograph the surface of the moon and to transmit the pictures back to Earth with a high degree of resolution. The Ranger-VI flight was successful in that the spacecraft completed its flight. However, the television system did not function as planned, and no pictures were transmitted to Earth. Rangers VII, VIII, and IX were completely successful. Mariner IV was intended to gather scientific data during its 229-day flight to Mars and to return TV pictures of the Martian surface. It, too, was successful, returning over 23 million scientific measurements and the first detailed pictures ever taken of the Martian surface.

*This paper presents the results of one phase of research conducted at the Jet Propulsion Laboratory, California Institute of Technology, under Contract NAS7-100, sponsored by the National Aeronautics and Space Administration.

As the Ranger and Mariner spacecraft functioned automatically, the commands used were (1) to provide information to the spacecraft, (2) to override preprogrammed events if desired, and (3) to back up automatic functions if necessary. Mechanical timers were flown on all these spacecraft to provide triggering for certain events without using command or sequencing capability and to provide mechanical redundancy for electrical functions. The Ranger and Mariner timers, although similar to those flown on the Pioneer IV spacecraft, were required to be highly reliable, with emphasis on simplicity and noninterference with the operation of spacecraft prime functions. The timers were to be initiated by means of spacecraft-booster separation and to be compatible with all spacecraft subsystems.

The Ranger hydraulic timers were required to perform the following functional commands:

- Backup pyrotechnic systems arming at separation + 2.5 ± 0.5 min
- Backup power increase television camera subsystem at separation + 17 ± 2.0 min
- Initiate television telemetry turn-on at separation + 30 ± 2.0 min
- Backup solar panel deployment at separation + 45 ± 2.0 min
- Backup sun acquisition at separation + 60 ± 2.0 min

The Mariner hydraulic timers were required to perform the following functional commands:

- Initiate the GSE Safe at separation + 25 ± 20 sec
- Initiate pyrotechnic "B" arm at separation + 30 ± 20 sec
- Initiate data encoder at separation + 180 ± 80 sec
- Initiate solar panel deployment at separation + 160 ± 80 sec

DESIGN PRINCIPLE

A photograph (figure 1) shows the assembled Mariner timer, which — like the Ranger timer — utilizes a spring-loaded piston to force silicone oil through a capillary tube. As shown in the diagram of the Ranger timer (figure 2), the purpose of the check valve (1) is to allow rapid re-choking. The beryllium copper bellows (2) compensates for

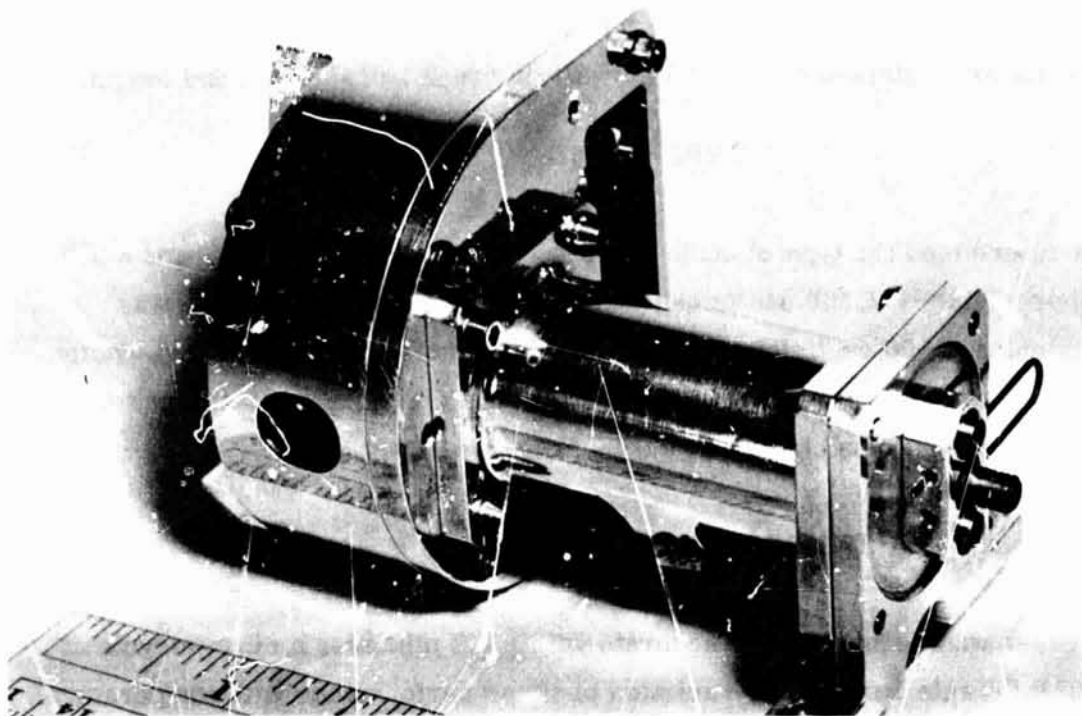


Figure 1 Assembled Mariner Hydraulic Timer

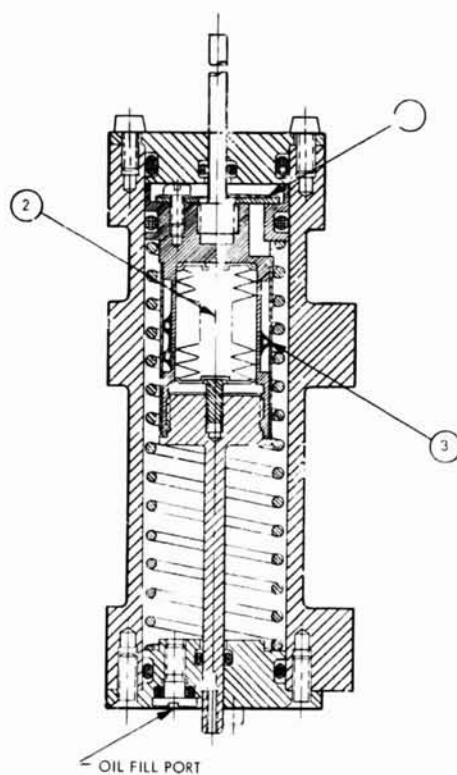


Figure 2 Cutaway of Ranger Timer Assembly

changes in the effective cylinder volume as the piston travels through its stroke and the oil changes volume due to temperature changes. Dimensions of the Ranger timer capillary tube (3) are: diameter, 0.050 in.; wall thickness, 0.006 in.; and length, 3 in.

TYPE OF OIL

Experiments determined the type of oil to be used in the hydraulic timers, and a silicone oil of approximately 2,500 centistokes viscosity was selected. Timing was adjusted by thinning 2,500 centistoke oil with silicone oil of 100 centistokes viscosity. The oil was added to the timers under vacuum to ensure that no air was trapped in the fluid. Double seals were used to ensure that leakage would not occur.

TEMPERATURE DEPENDENCE

The Ranger timer was required to be accurate within ± 2 min over a 60-min cycle at a constant 70°F. Table 1 shows the variation of timer performance with temperature. The devices flown were sufficiently accurate for the job, and the emphasis throughout the development phase was on establishing reliability.

Table 1

NORMAL ACTUATION TIMES AND TOLERANCES
FOR SPACECRAFT HYDRAULIC TIMERS

Type of Timer	Nominal Actuation Time (Min)	Tolerances At		
		70°F High-Temperature Time (Min)	150°F High-Temperature Time (Min)	-300°F Low-Temperature Time (Min)
SFA-BU	2.5	± 1.5	± 1	± 4
RP-BU	17.0	± 5	± 8	± 30
RCA-TO	30.0	± 7	± 15	± 55
A3-BU	45.0	± 10	± 20	± 90
A4-BU	60.0	± 20	± 30	± 130

Elaborate temperature-compensation systems were not included in either the Ranger or Mariner timers because of the desire to keep the mechanisms as simple as possible. The Ranger timer was thermally isolated from the spacecraft structure to minimize timer temperature extremes. External surfaces were fabricated of polished aluminum. A thermal shield consisting of 30 layers of aluminized Mylar was fitted over the timer in order to further minimize temperature variations due to sun or shade differences in the earth-orbital phase of the flight. Figure 3 shows the Ranger timer complete with thermal shield mounted on the spacecraft.

The Mariner timer external surfaces were also fabricated of polished aluminum. However, this timer did not require an individual thermal shield, since it was located behind the spacecraft main lower thermal shield. Accuracy was less critical with the Mariner timer, since it was designed to operate within ± 80 sec over a cycle of 160 sec.

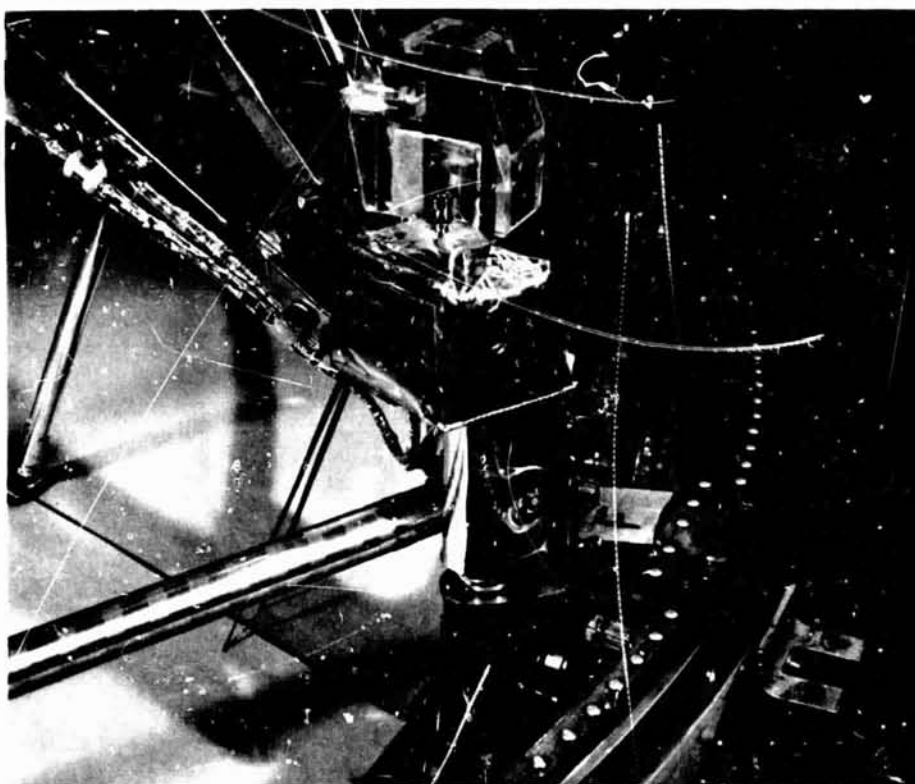


Figure 3 Ranger Timer Complete With Thermal Shield

MECHANICAL AND ELECTRICAL DESIGN

The Mariner timer incorporated several improvements resulting from experience with the Ranger timer. The Ranger timer, for example, had to be removed from the spacecraft for recocking and it was necessary to change the O-ring seals every time the timer was opened for filling. This became a nuisance because of the many refillings necessary to obtain the proper oil viscosity. Provision was therefore made for recocking of the Mariner timer on the spacecraft. The Mariner timer also made use of an improved fill port which allowed oil changing without seal damage.

Both the Ranger and Mariner timers drove electrical switches. The switch end of the Ranger timer, with the housing removed, is shown in figure 4. The switch was sealed in an airtight enclosure to eliminate possible problems due to the vacuum environment.

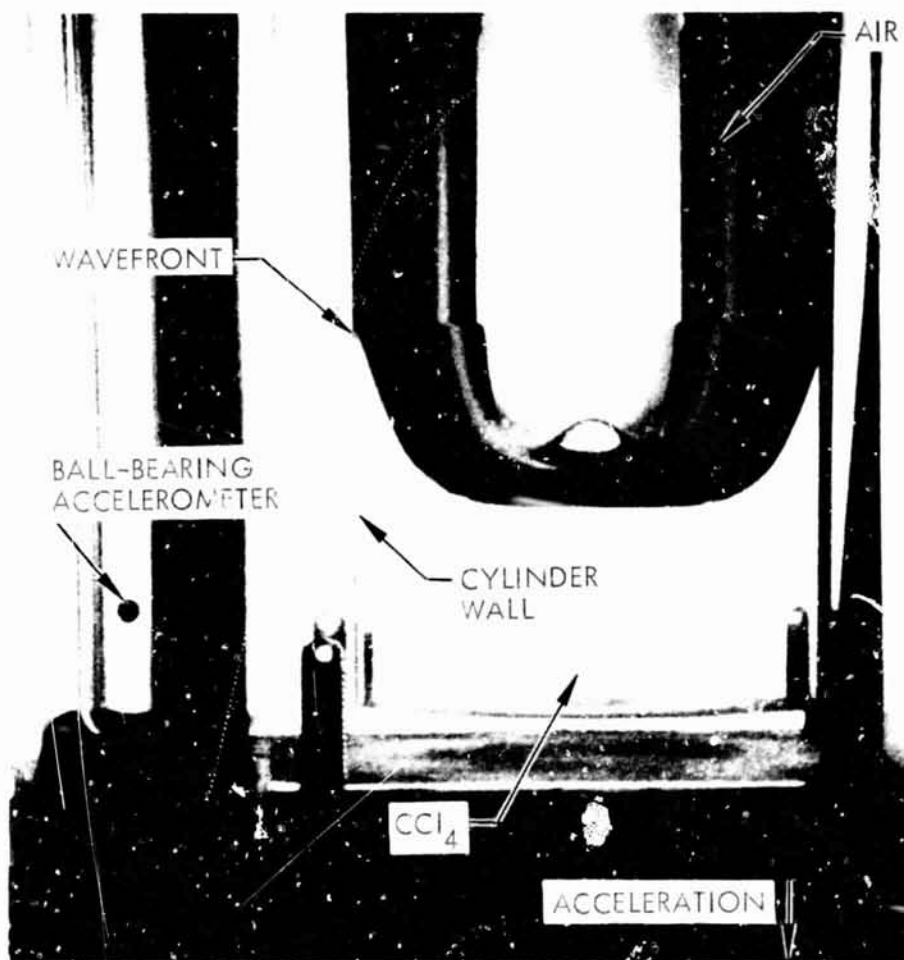


Figure 4 Switch-End of Ranger Timer With Housing Removed

The Ranger switch was a rotary device with double, fixed contacts for each single wiper contact; all contacts were silverplated. Sealing was accomplished with O-rings, and a hermetically sealed electrical connector was used.

The Mariner switch was made up of four carefully screened, hermetically sealed micro-switches which were purchased as complete units. The flight Ranger unit, including the timer and switch assembly, weighed 0.98 lb. The Mariner unit weighed 0.6 lb.

QUALIFICATION TESTING

Some design deficiencies were uncovered during preliminary testing of the Ranger timer prototype assemblies. Mounting the unit to the spacecraft was difficult because of the weight of the timer and the isolated mounting location. The original bracket was a welded heat-treated unit. Welds broke repeatedly during shake because of deflection of the assembly during resonance. The problem was solved by removing the weld in the critical area and allowing the bracket to flex.

During vibration the internal cable harness broke at resonant frequencies where soldered to the switch contacts. This problem was solved by securing the harness more firmly.

During testing of the type-approval unit, it was found that the timer error over a 60-min cycle was increasing. This was found to be due to an uneven load on the shaft of the timer which, during vibration, caused a permanent set in the shaft, allowing it to drag against the housing. A small support arm was installed between the first and second command motors to relieve the unbalance condition causing this problem. A requirement of always storing the timers in the cocked position was specified.

Another problem appeared after a little over 12 mo of assembled life. The O-rings were degrading and required replacing. A 12-mo maximum shelf life requirement was imposed, and all units reaching that shelf life were reworked and requalified. In addition, a 30-day check was run on each assembly.

In order to qualify as flight assemblies, the switches were required to pass the time-cycle test after flight acceptance environmental testing before delivery.

- Vacuum leak check of the switch cabinet and hydraulic timer for oil or pressure loss
- Wide-band vibration in three planes; test-switch contact chatter monitored during test
- Vacuum temperature tests with two profiles representing lowest and highest possible temperatures
- Operational life tests on the electrical switch assembly to verify reliability of operation

The Mariner timers had relatively few problems during testing, due to the incorporation of Ranger experience during development of the Mariner timer. Mariner tests were similar to the Ranger tests but at levels calculated to simulate the Mariner environment.

FLIGHT RESULTS

There were no flight anomalies detected in any of the Ranger or Mariner timers.

SOLAR CELL GRAVITY-STABILIZATION BOOMS

By Bodwell D. Osborne
Lockheed Missiles & Space Company

SUMMARY

N67 16911

For certain scientific measurements in space, a stable platform is not only desirable but essential. Such a platform, to meet today's needs, must also be equipped with a power plant.

This paper presents a scheme for combining a spacecraft gravity-stabilization boom with a solar-cell array, examines some of the relevant problems, and proposes a method for testing the mechanism in an underwater environment, where zero-gravity conditions can be approximated.

INTRODUCTION

If an engineer were to take 2,000 solar cells, each 24 in. long, and arrange them in 500 sections of 4 cells each around a central hollow core, string them on a conducting wire, deploy them 1,000 ft into space, and pull them end-to-end, he would have a uniquely combined electrical-power and attitude-control system. He would also probably be faced with considerable skepticism from his fellow engineers.

Nevertheless, such a device may well prove practicable for an Earth-orbiting satellite (although lengths of 100 to 300 ft would possibly suffice in such instance). The proposed combination of attitude control and power systems reduces the number of deployable systems, lessens thermal bending (which is of some concern in long booms),

positions the cells beyond the shadow areas, and eliminates the need for Sun-aligning servo systems.

Many spacecraft stabilization systems — both active and passive — have been devised. The type considered here is a passive gravity system employing very long booms (figure 1) that act on the same principle as the balancing pole used by a tightrope acrobat.

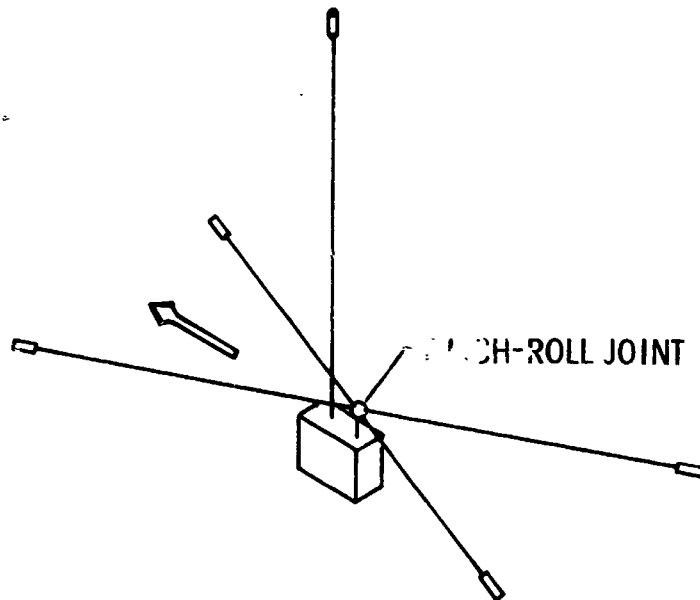


Figure 1 Passive-Gravity-Gradient Stabilization System

The solar cell is an effective and proven means for obtaining spacecraft power. Its one irrevocable requirement is that it must look at the Sun. The solar cell array must therefore project beyond the shadow of the platform's many accoutrements. A common way of meeting this requirement is shown in figure 2. Extending the solar array still further from the shadow area, (e.g., 100 ft or more) provides about the same extension as the gravity-stabilization boom and therefore leads to a design combining the two systems.

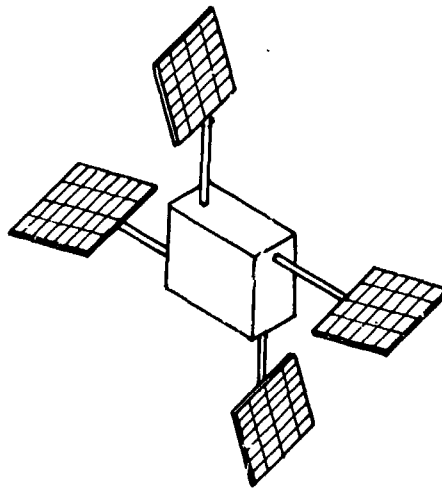


Figure 2 Passive Multiple Solar-Array System

Some recent developments reinforce this concept. The Westinghouse Corporation, as an example, has developed, under Air Force sponsorship,* a solar cell in lengths up to 30 in. which lends itself excellently to a long, slender configuration. Some major satellite programs (among them, Transit, NRL, ATS, and the Medium-Altitude Communications Satellite) have placed considerable emphasis on developing a variety of configurations for stabilization booms and a variety of dampers. In each of these instances, the solar array systems were separate. Further, at a recent symposium,** every program report indicated flight operational problems related to stowage and deployment, thermal bending and whipping of booms resulting from rapid thermal changes when traveling in and out of the Earth's shadow, and shadowing of the solar array by vehicle equipments.

The combining of stabilization booms and solar arrays could alleviate these problems. The technology could be adapted to all configurations of spacecraft stabilization booms and therefore should be of value to any company that is performing, or will perform, stabilization development.

*Flight Accessories Laboratory, Wright-Patterson Air Force Base, Ohio

**National Aeronautics and Space Administration Symposium on Passive-Gravity-Gradient Stabilization, Ames Research Center, May 10-11, 1965

ELECTRICAL CHARACTERISTICS OF BOOMS

The level of power output that can be anticipated from booms of 100-ft and 1,000-ft lengths is indicated by the following data:

- Average effectiveness of a four-cell module (based on an effectiveness of 1 for a normally illuminated cell) 1.25
- Output of a 24-in. module* (0.43 v; 1.75 amp) 0.75 w
- Output of 100-ft boom (22 v; 1.68 amp) 37 w
- Output of 1,000-ft boom (200 v; 1.60 amp) 320 w
- Energy rate of three 100-ft booms (diode and AWG No. 18 wire losses included) 1,400 w-hr/day
- Energy rate of three 1,000-ft booms (diode and AWG No. 18 wire losses included) 12,000 w-hr/day

The above values are averages over a period of a year. They take into account a temperature of 115°F and exposure to sunlight during 63 percent of that period. The peak electromotive force is not indicated. It would be about 50 v for a 100-ft boom system. (A 1,000-ft boom system probably would require 10 parallel, connected 100-ft sections, even though the foregoing power output summary assumes a series string.) The power listed is for a tri-boom system, since three booms represent a minimum assembly required to neutralize pitch, roll, and yaw disturbances.

Figure 3 illustrates such a system with the damper boom divided in the center, i.e., two 90-ft and two 45-ft booms. The solar array depicted has a capability of limited two-axis Sun alignment, which will somewhat perturb the satellite attitude.

*Based on tabular data submitted to the author by Westinghouse Electric Corporation for 1- by 30.5-cm cells, Nos. u470-2, u525-2, u544-1, and u544-2

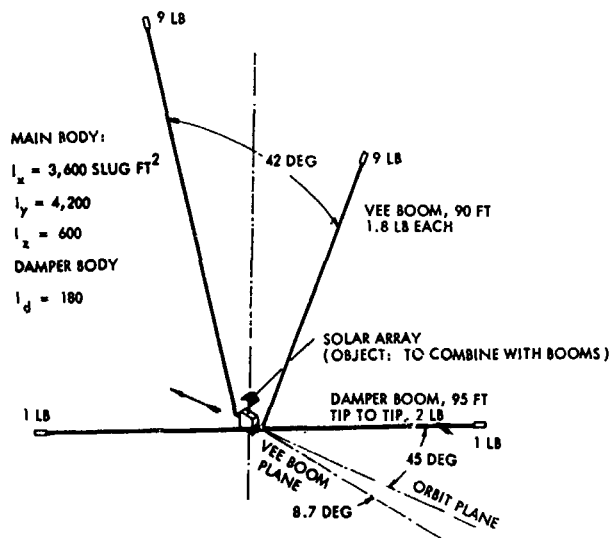


Figure 3 Computed Configuration Using a Passive System, Vee-Boom Design

A single-module assembly is illustrated in figure 4. There are relatively few details. The assembly consists of the following components:

- 4 Westinghouse dendritic solar cells, 1-cm wide by 30- to 60-cm long by 10 mil thick; blue, gridded, N on P or a radiation-resistant drift-field cell of similar dimensions
- 1 vertebra – a hollow aluminum or beryllium-copper structural conductor, silver plated at the mating ends
- 1 viscoelastic spring – a coil spring, coated with polyurethane to retard unfurling time
- 6 spring clips – polyurethane-coated connection links between vertebra and cell
- 1 insulating cross – phenolic, to prevent shorting the series circuitry
- 20 shock snubbers – elastomeric honeycomb vibration-damping sections
- 8 end caps – plastic, to provide sliding support to the cell ends and lateral constraints so as to permit thermal excursions in axial directions only (figure 5)

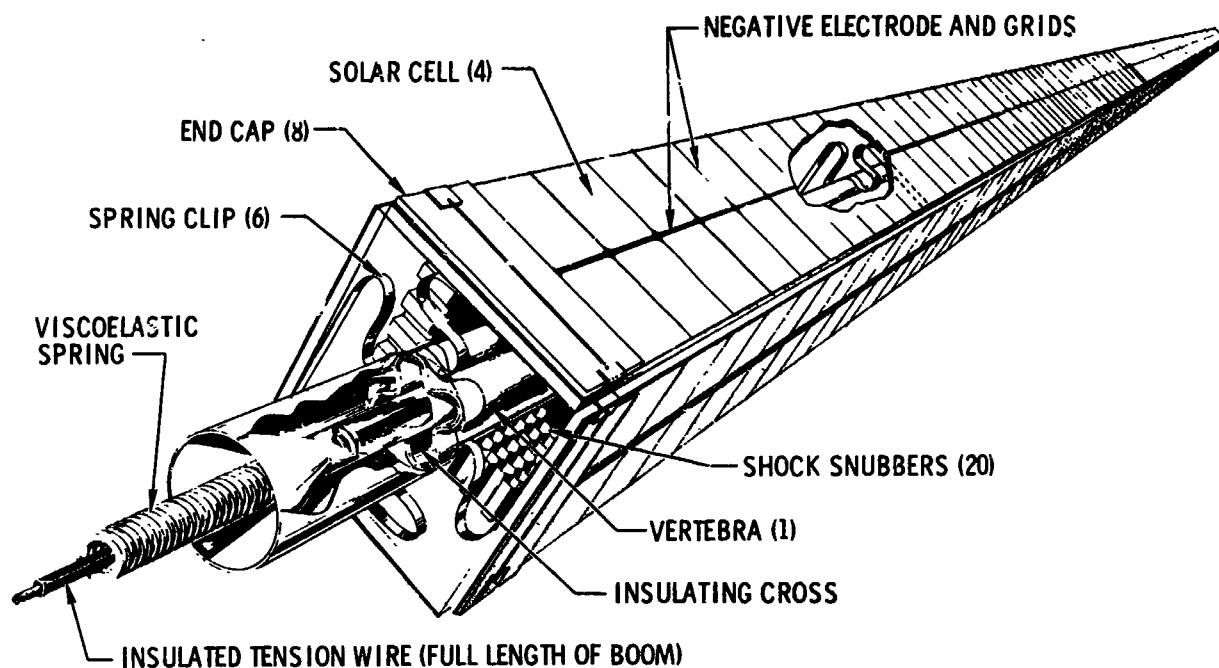


Figure 4 Module Assembly

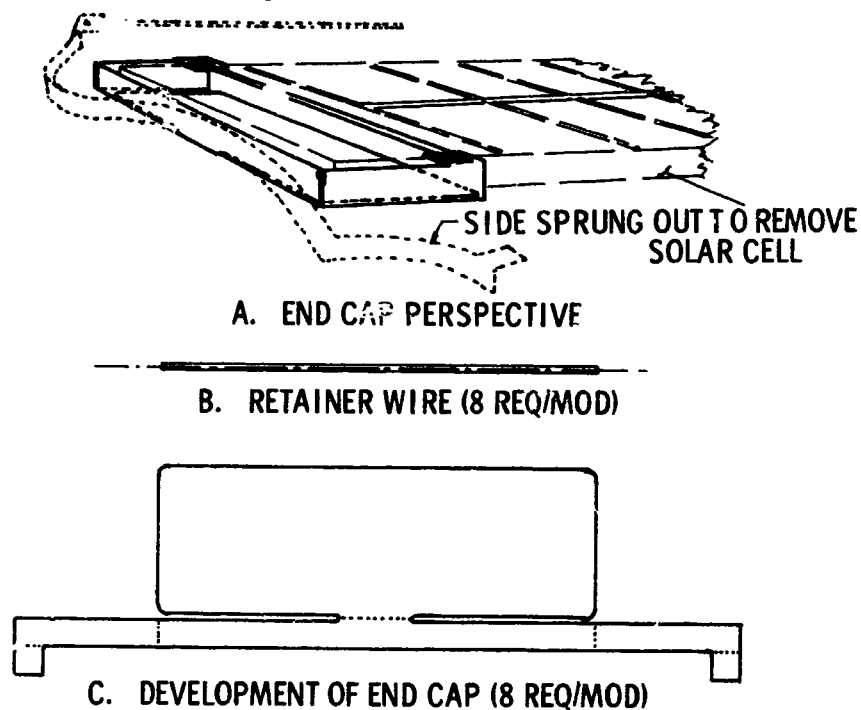


Figure 5 End Cap Detail

SYSTEM ASSEMBLY

The system assembly comprises the following components:

- 1 insulated tension wire - braided copper, about AWG No. 18, running the full length of the boom and serving a dual purpose as rigidizer and conductor for electrons
- 1 winch and supporting structure - fastened to boom damping system
- End mass - assemblage weighing approximately 9 lb, covered with solar cells and housing a compression spring to which tension wire is attached

Each module is threaded on the tension wire, folded about the coil spring, packed into a firm package, and secured in place with a single squib-activated pin puller. The tension wire is locked mechanically and electrically onto the drum of a small winch. The winch motor is controlled by ground command (figure 6).

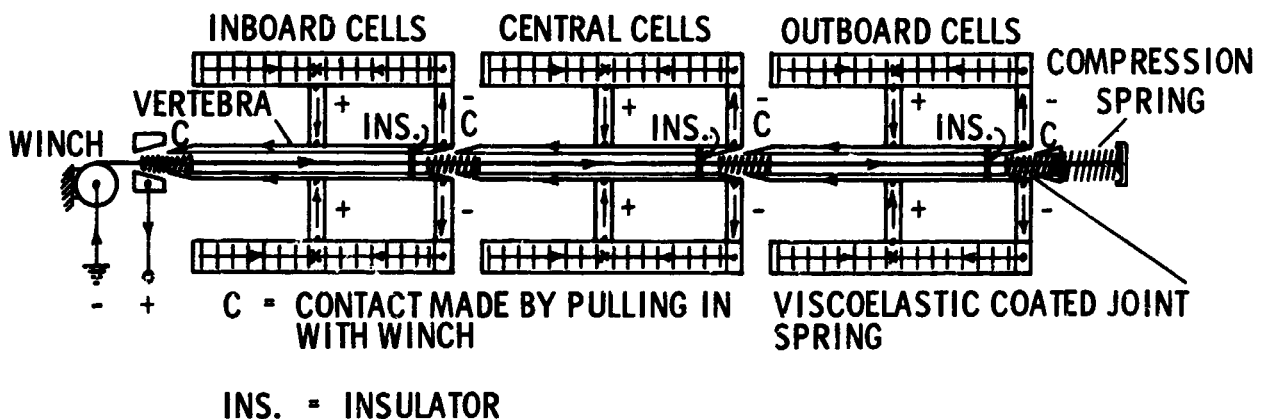
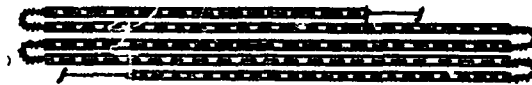


Figure 6 Electrical Detail

SYSTEM OPERATION

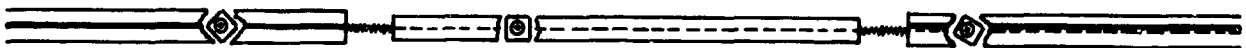
After the vehicle has been de-spun and stabilized, or "captured," the pin puller pyrotechnic material is fired on command, activating the pin puller and releasing the package cover. Figure 7 diagrams the sequence of operation.



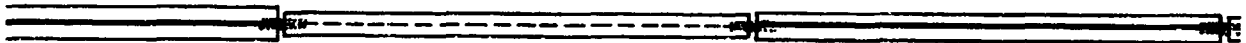
A. FOLDED



B. UNFOLDED (MONITORED)



C. OPENED



D. WINCHED TOGETHER

Figure 7 Operation Sequence

The end mass, being the last element packed, will be the first ejected. Since it will experience the least number of restraining forces, it will lead off the procession by slowly unfurling outward, hinging about its coil spring. The viscoelastic coating will slow down the process to prevent the springs from unfolding too rapidly and cracking the coils. When all the modules have sequentially deployed themselves, they should be axially aligned. The precise point at which this condition is attained

cannot be determined positively without a monitor. (However, a TV camera is not recommended, and certainly not a closed circuit, because its power requirement would be charged against the power-boom system.) The time required for the cells to open into the box formation is independent of the deployment sequence. In figure 7, C and D can be interchanged or considered to be performing simultaneously.

Assuming that alignment has been attained, the ground station sends in a command to the winch motor, which begins winching in the slack tension wire, drawing the modules together, and forcing them into the conical seats provided at the ends of each vertebra. At a predetermined tension value, the winch will lock itself and open the motor circuit. The compression spring in the end mass prevents the boom from buckling under an overload and guarantees a prestressed boom.

VERTEBRA

The central core of the vertebra can be seen in cross section in figure 8.

The core could be formed by rolling a round external tube onto an annular tube and soldering the two together. The cross-arms provide excellent transverse loading in the stowed position, and save about 9 percent overall stowage volume on a strength-to-weight comparison with a round tube. There is a sufficient thickness of metal in the vertebra to provide good thermal conduction, and enough surface to provide good electrical conduction. One end is fitted with a conical plug or male connection, the other with a mating conical socket or female section which is insulated from the main body (see figure 8). Since the complete vertebra is hollow, it will permit the passage of the tension wire.

No attempt has been made to control twisting of the modules relative to each other; since output is based on average value, a random rotational orientation will not alter the output.

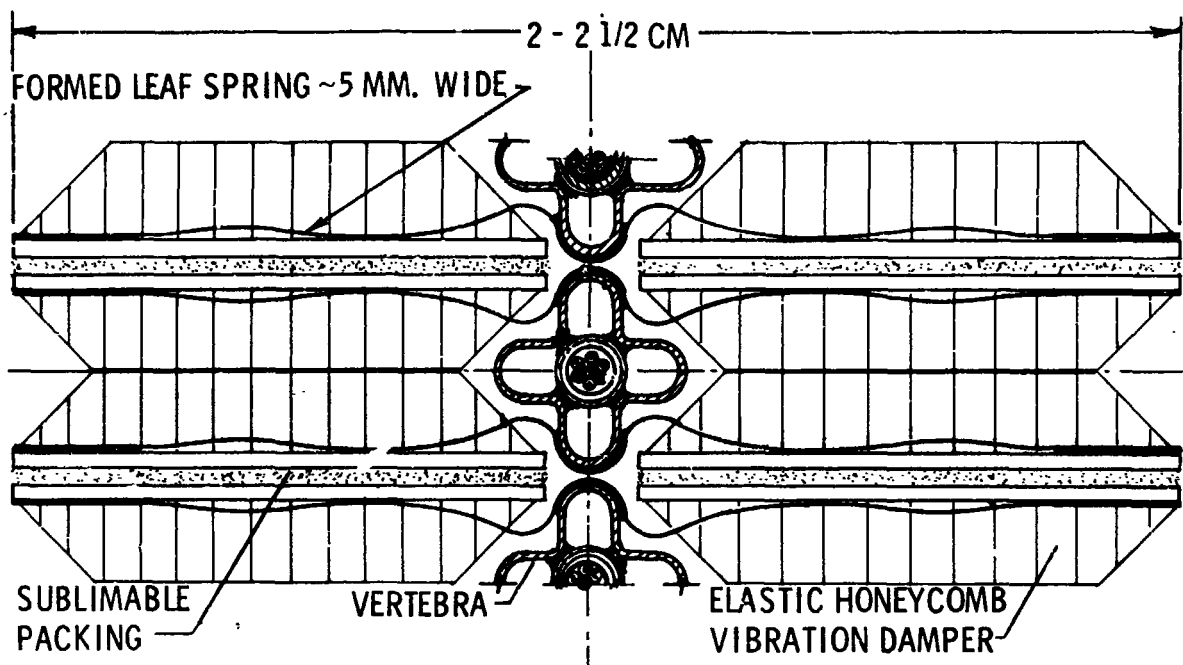


Figure 8 Module - Section Showing Folded Position for Stowing

MECHANICAL BENDING

The extremely minute extent of the bending forces that bear upon an orbiting satellite is difficult to appreciate. In the motion picture of the Gemini IV capsule, Major White's glove appeared to maneuver out through the hatch. However, it was the capsule doing the maneuvering and not the glove, which is probably still in orbit. In other views, ribbons were seen to be dangling from the capsule with almost complete immobility.

At 555 km altitude, the atmosphere contains, at a solar maximum, a concentration of some 70 million assorted particles/cc - 4 quadrillion times less than that prevailing at sea level. These particles, (molecules), however, can cause an aerodynamic loading of 1.5×10^{-4} ft-lb. When the Sun shines upon the boom, the photon flow amounts to negligible 0.03×10^{-4} ft-lb. The gravity-gradient moment amounts to about 24×10^{-4} ft-lb, or roughly 0.5 in.-oz, an amount which the design can readily handle.

THERMAL BENDING

Another difficult concept is that of a tiny rod, bathed in the vast expanse of solar radiation, suffering significant bending owing to the sunny (white) sides expanding and the shady (black) sides contracting. If the temperature of the two sides of the boom can be kept equal, the boom will not experience thermal bending.

One method of maintaining a zero thermal gradient would be to screen the boom from the direct rays of the Sun; however, this would require that the screen travel alongside and completely circumvent the boom without being a part of it. Another possible solution would be to "box in" the boom, which would induce a constant ambient temperature. Here again, the box should not touch the boom.

The next logical solution could be to surround the boom (with solar cells, for instance) using a central support moving perpendicular to the axis of the boom without imparting extraneous forces to the boom. The heat conducted to the boom through the support must be small enough to be lost in the thermal noise. This is comparable, in effect, to building a greenhouse and using one of its excellent characteristics (ambient control) to advantage (figure 9).

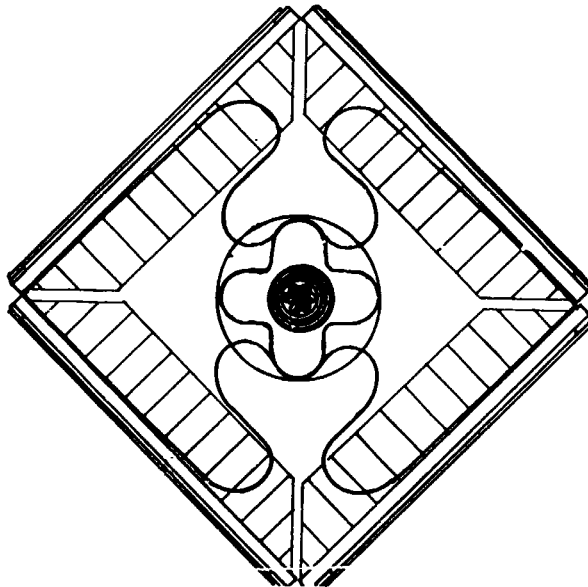


Figure 9 Module - Section Showing Active Position of Cells After Deployment

The price exacted for gaining an even heat is higher temperatures. The cells will probably experience a maximum temperature of about 115° to 120° F, a loss of some 12 percent in power from that of room temperature.

SIMULATED ZERO-G TESTING

Before one of these systems is flown, an operational test should be performed — one that simulates the nearest environmental conditions. The major unknown factor is the path of deployment, which brings up the following questions:

- Will each module unfurl in sequence, or will one be displaced in turn by one more aggressive?
- Will the slight residual motion of the satellite after capture cause the boom to suffer a catastrophic buckle?
- Will the wires "hang up?"

None of these questions can be positively answered without an operational test in a zero-g environment.

From an engineering standpoint, water comes closer to providing a practical workable zero-g fluid than any other medium. The model must be designed with an overall specific gravity of one. This, of course, requires the selection of materials very different from those planned for flight. The springs and wires, however, should probably be the same as those planned for use in flight, which requires that their negative buoyancies be compensated for by positive buoyancy inherent in materials selected for the mock vertebra and solar cells. A good, relatively inexpensive source of such materials is wood chemically impregnated to seal out moisture, or gas-entrained plastics. The method envisioned is to set up a flight package mockup under water in a large test tank, such as the Lockheed Underwater Missile Facility (LUMF) used for testing models at LMSC, and to film a number of underwater deployment sequences. Time factors will not be accurately simulated, but ratios of times and sequences will be simulated.

Water thermal currents, if induced in the proper direction, might offer a perturbation equivalent to satellite residual motion after capture, which would subject the boom to an appropriate bending moment for the test.

CONCLUSIONS

It appears that the combination of the power and stabilization systems promises a step toward greater success of experiments conducted from space platforms. Testing the required mechanisms in an underwater environment that simulates the zero-g condition of space will, hopefully, confirm the mechanical feasibility of such a scheme.

PRECEDING PAGE BLANK NOT FILMED.

ANALYSIS OF AEROSPACE IMPACT PROBLEMS

By D. Hayes, C. Cawood, and T. Kertesz
University of Santa Clara

SUMMARY

N67 16912

This paper describes a graphical technique for analyzing the behavior of objects during and after impact. The technique is illustrated by the presentation and experimental verification of an analysis of a particular system. Single impacts with various initial conditions are examined. The analysis is then extended to cover the case of repeated impacts of the same objects. Degeneration of system motion to either a pure central or a pure sliding impact mode is confirmed by both theoretical and experimental results. The existence of a critical angle, which determines the degenerate mode, is established.

INTRODUCTION

Graphical analysis of impact may be applied to numerous engineering problems involving relatively low velocities and noncentral impact conditions. It is particularly useful in obtaining predictions of velocity vectors during and after impact, as in orbital docking maneuvers and grazing incidence of soft landing payloads on the lunar surface. Impact problems encountered in the design of payload release mechanisms can also be readily handled. Although the impacts considered are of a nondestructive magnitude, the velocity vectors are significantly affected by tangential friction impulses as well as by the impulses usually considered normal.

The technique used for analyzing these impacts is based on an analysis of the general, two-body impact problem developed by E. G. Routh (ref. 1) at the turn of the century. As an example of this method, the impact of a steel ball on an infinitely rigid wall is examined. The experimental results obtained from this example are compared with those calculated from the theory for various initial impact angles.

The conditions examined include noncentral single and multiple impacts and the influence of the coefficients of elastic restitution and friction on the resulting velocity vectors and angular rotations. For the case of multiple impacts the existence of a critical initial impact angle is established analytically and verified by experimental results. This angle determines which of the two modes of degeneracy the motion of the system will acquire.

SYMBOLS

e	coefficient of restitution
$-I_F$	tangential friction impulse
I_N	normal impulse
$I_{N,C}$	normal impulse for zero compression velocity
m	mass of ball
$()_n$	initial value for nth impact
$()'_n$	a value during and after nth impact
R	radius of ball
u	tangential velocity component
V	total velocity of impacting ball
v	normal velocity component
θ	angle of incident impact
θ_c	critical angle defining system degenerate mode state
μ	coefficient of friction
ω	angular velocity of ball

EXPERIMENTAL SYSTEM

A simple experimental apparatus was devised to permit the qualitative study of initial and multiple impacts of a solid steel ball on a massive steel surface. The system, as shown in figure 1, consisted of a 2.0-in.-diameter steel ball suspended by a 76-in. glass-fiber cord so as to just clear the floor plate.

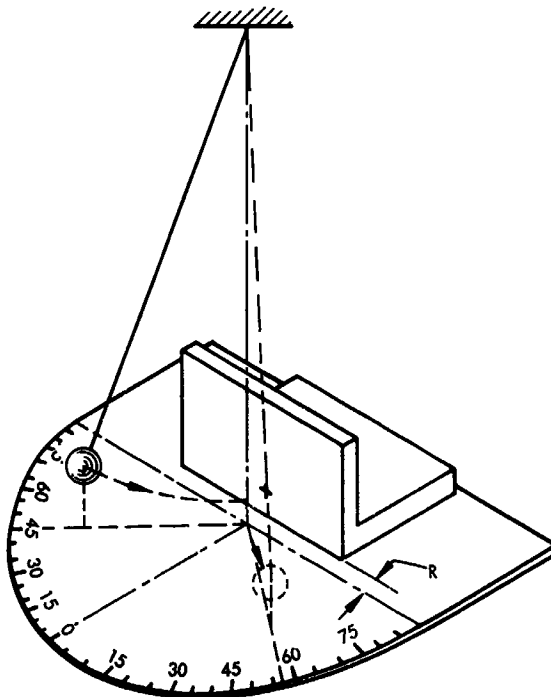


Figure 1 Experimental Setup

A protractor scale drawn on the floor plate allowed angle measurements to be made within ± 3 deg. A heavy steel angle plate, located 1.0 in. from the protractor scale center with the contact face parallel to the protractor base line, provided a suitably rigid impact surface.

All experiments were performed by carefully releasing the ball from a point above the protractor scale arc with zero-angular velocity. This provided a reasonably uniform impact velocity (44 in./sec) for all initial impact angles.

Angles were measured from the normal to the impact surface by placing the pivotal angle-bars under the path of the ball.

The use of a glass-fiber cord provided a torsion-free pendulum suspension, which allowed the ball to freely acquire angular velocity during impact. This angular velocity was also retained without dissipation; therefore, it could be considered as an initial condition for the next impact in the multiple-impact cases. Typical system behavior is shown in figure 2.

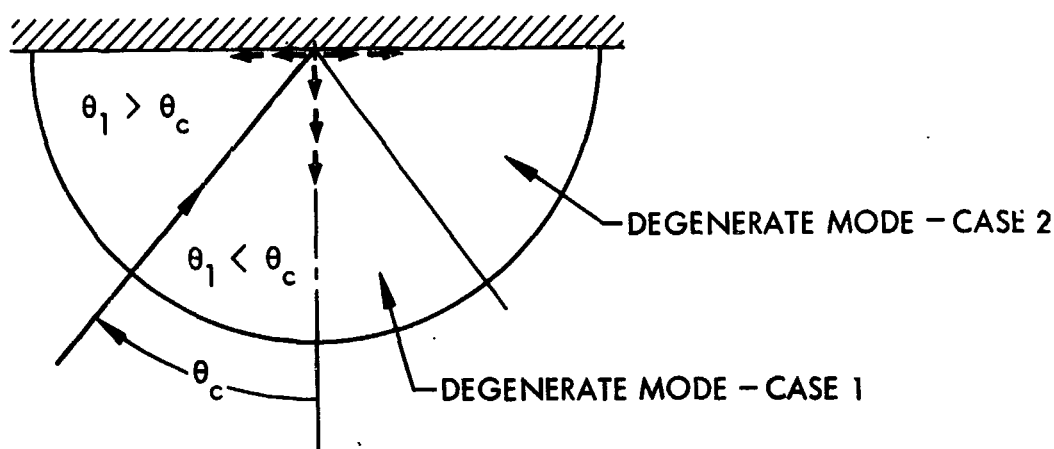


Figure 2 Critical Angle - Mode Diagram

ROUTH ANALYSIS-IMPACT EQUATIONS

The Routh analysis of impact assumes that the bodies are rigid and that elasticity is limited to a small region at the impact point. Application of the conservation of momentum equations leads to the definition of a normal impulse I_N and, as a result of friction, to a tangential impulse I_F . Details of this analysis are available in refs. 2, 3, and 4. From the Routh analysis, equations for these impulses are developed and shown to result in straight lines on an impulse diagram. For the particular system examined, these lines are parallel to the I_F and I_N axes, respectively, as shown in figure 3.

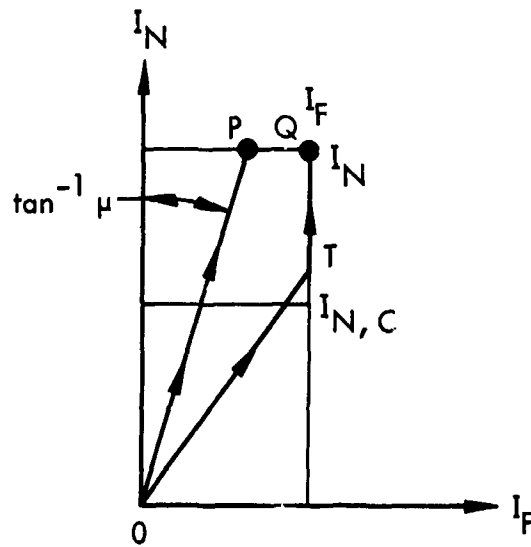


Figure 3 Routh Impulse Diagram

System behavior is studied by tracing the path of a representative point starting at the origin and proceeding at an angle equal to the arctangent of the friction ($\tan^{-1} \mu$) toward the limiting value lines $I_{N,C}$, I_N , and I_F . The $I_{N,C}$ line represents the point of maximum compression of the ball, i.e., zero-compression velocity. The I_N line, located at $I_N = I_{N,C} (1 + e)$, represents the added normal impulse due to elastic restitution and is the line at which system contact ceases. The I_F line represents the value of tangential impulse required to reduce the sliding velocity to zero. Two distinct modes of behavior are shown on the diagram in figure 3.

Case 1, as noted by path OTQ, reaches the maximum value of I_F at point T. This implies that the ball ceases to slide and attains pure rolling during contact. No further friction impulse develops, and the representative point moves to the point Q on the $I_{N,C} (1 + e)$ line at final contact.

Case 2 is shown by path OP and represents the condition of sliding throughout the time of contact. Note that, although I_F has continued to increase during contact, it has not reached the value required to reduce the sliding velocity to zero.

For simplicity, the assumption is made that the friction coefficient μ is constant and, therefore, the final values of impulse are those shown at points Q and P.

Single Impact

The diagram in figure 4 defines the system state before and after a single impact. Use of the Routh method yields the following impulse values and final state equations for the two cases discussed above.

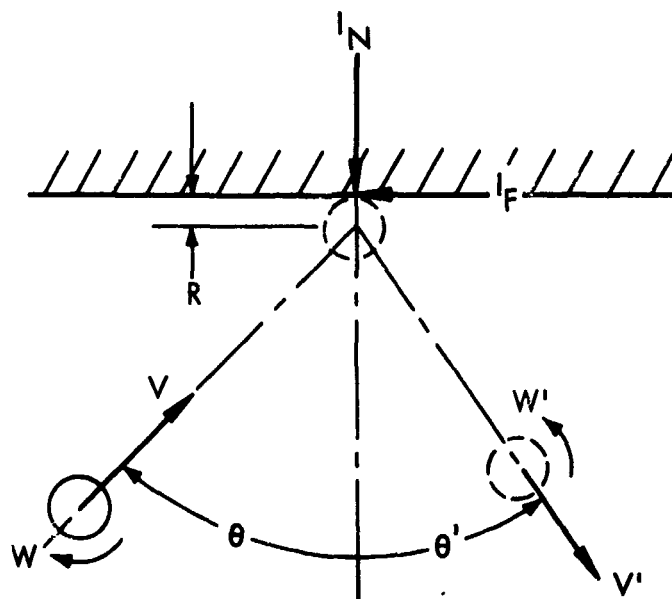


Figure 4 Diagram of Impact

● Case 1 - Pure Rolling Attained

$$I_N = m V \cos \theta_1 (1 + e) \quad (1)$$

$$I_F = \frac{2}{7} m V \sin \theta_1 \quad (2)$$

$$v_1' = -ev_1 \quad (3)$$

$$u_1' = \frac{5}{7} u_1 \quad (4)$$

$$\omega_1' = -\frac{5}{7} \frac{u_1}{R} \quad (5)$$

$$\theta_1' = \tan^{-1} \left[-\frac{5}{7e} \tan \theta_1 \right] \quad (6)$$

Note that when $e = \frac{5}{7}$ the angle of rebound will equal the angle of incidence.

● Case 2 - Sliding Throughout Contact

$$I_N = m V \cos \theta_1 (1 + e) \quad (7)$$

$$I_F = m V \cos \theta_1 (1 + e) \mu \quad (8)$$

$$v_1' = -e v_1 \quad (9)$$

$$u_1' = u_1 - v_1 (1 + e) \mu \quad (10)$$

$$\omega_1' = -\frac{5}{2} \frac{v_1}{R} (1 + e) \mu \quad (11)$$

$$\theta_1' = \tan^{-1} \left[\frac{(1 + e)}{e} \mu - \frac{\tan \theta_1}{e} \right] \quad (12)$$

In this case the angle of rebound will equal the angle of incidence if

$$\tan \theta_1 = \mu \frac{(1 + e)}{(1 - e)}.$$

Multiple Impact

The final values of the first impact may be used as initial conditions for a second impact. In this case a value of angular velocity must be considered in addition to the normal and tangential velocity components. This procedure is continued to the n th rebound, and constraints are defined for the system behavior of Case 1 and Case 2. This eventually leads to a definition of the system degenerate modes. Note that the tangential impulse shown in figure 4 reverses direction for each successive impact. The general expressions for normal and tangential impact for the n th rebound in terms of velocity components are:

$$I_N = m v_n (1 + e) \quad (13)$$

$$I_F = (-1)^{n-1} \frac{2m}{7} \left[u_n + \omega_n R \right] \quad (14)$$

These values are now used to obtain results for the two modes of system behavior.

● Case 1 - Pure Rolling Attained n th Rebound

Assume that pure rolling is attained in each successive impact, which requires that $\omega_n \equiv \frac{u_n}{R}$. The following final values in terms of initial angle and velocity components for the n th rebound ($n \geq 1$) are obtained:

$$v_n' = -e^n v_1 \quad (15)$$

$$u_n' = (-1)^{n-1} \frac{5}{7} \left(\frac{3}{7} \right)^{n-1} u_1 \quad (16)$$

$$\omega_n' = (-1)^n \frac{5}{7} \left(\frac{3}{7} \right)^{n-1} \frac{u_1}{R} \quad (17)$$

$$\theta_n' = \tan^{-1} \left[(-1)^n \frac{5}{7e} \left(\frac{3}{7e} \right)^{n-1} \tan \theta_1 \right] \quad (18)$$

Equation (18) implies that θ_n' approaches zero as n becomes large. From the assumption that pure rolling is always reached on the impulse diagram, however, a constraint exists which implies that $I_F < \mu I_N$ for all values of n . In terms of system constraints this becomes

$$\theta_1' < \tan^{-1} \frac{49}{20} \mu e (1 + e) \quad (19)$$

As long as this constraint is met, convergence of θ_n' to zero will always occur in a pure rolling mode.

- Case 2 – Sliding Throughout n th Rebound

Recall that for the single impact case, $I_F = \mu I_N$. Using this definition of I_F , the final values of velocities and angles for the n th rebound ($n \geq 1$) are as follows:

$$v_n' = -e^n v_1 \quad (20)$$

$$u_n' = (-1)^{n-1} \left[u_1 - \mu v_1 \frac{(1+e)}{(1-e)} (1 - e^n) \right] \quad (21)$$

$$\omega_n' = -\frac{5}{2} \mu \frac{v_1}{R} \left[1 - (-e)^n \right] \quad (22)$$

$$\theta_n' = \tan^{-1} \left\{ (-1)^n \left[\frac{\tan \theta_1}{e^n} - \frac{\mu(1+e)}{e^n(1-e)} (1 - e^n) \right] \right\} \quad (23)$$

To satisfy the requirement that sliding occurs for all successive impacts, I_F must be greater than μI_N , where I_F and I_N are determined by use of the general expressions in equations (13) and (14). The least value that will satisfy this inequality is given by

$$\theta_1 > \tan^{-1} \left[\frac{7}{2} \mu (1 + e) \right] \quad (24)$$

This is the corner value of the initial impact diagram and implies that θ_1 less than the above value will result in rolling contact for the initial rebound.

Equation (23) implies that the degenerate mode in this case is represented by θ_n' approaching 90 deg, provided that the sliding mode is maintained. The constraint to maintain the sliding mode is obtained from equation (23) by requiring that

$$\theta_1 > \tan^{-1} \left[\mu \frac{(1 + e)}{(1 - e)} \right] \quad (25)$$

Critical Angle

The critical angle of θ_1 is the least value for which the angle of rebound will be greater than the angle of incidence. This suggests that a certain value of the initial impact angle will define the boundary between the two degenerate mode states of the system. The system behavior for initial angles between those defined by equations (19) and (25), although always resulting in $|\theta_n| < |\theta_{n-1}|$, alternates between rolling and sliding until θ_n becomes sufficiently small to meet the requirements of pure rolling as defined by equation (19). Therefore the critical angle can be defined as

$$\theta_c = \tan^{-1} \left[\mu \frac{(1 + e)}{(1 - e)} \right] \quad (26)$$

Computed Values and Experimental Results

Values of the friction coefficient for steel-on-steel were obtained by measuring the drag of the ball with a Chatillon force gage and comparing it to values given in the Mechanical Engineers' Handbook (ref.5). The coefficient of restitution for normal impact was obtained by observing the average decay of the normal rebound amplitude during five cycles.

The values obtained for use in the computations were $\mu = 0.1$ and $e = 0.8$. These values were assumed to be constant throughout the duration of the impact.

Values of I_N and I_F were computed for five initial angles using the relations defined by equations (13) and (14). An impulse diagram was then constructed for each initial angle as shown in figure 5. Since the quantity $m V$ appears in all terms of the impulse

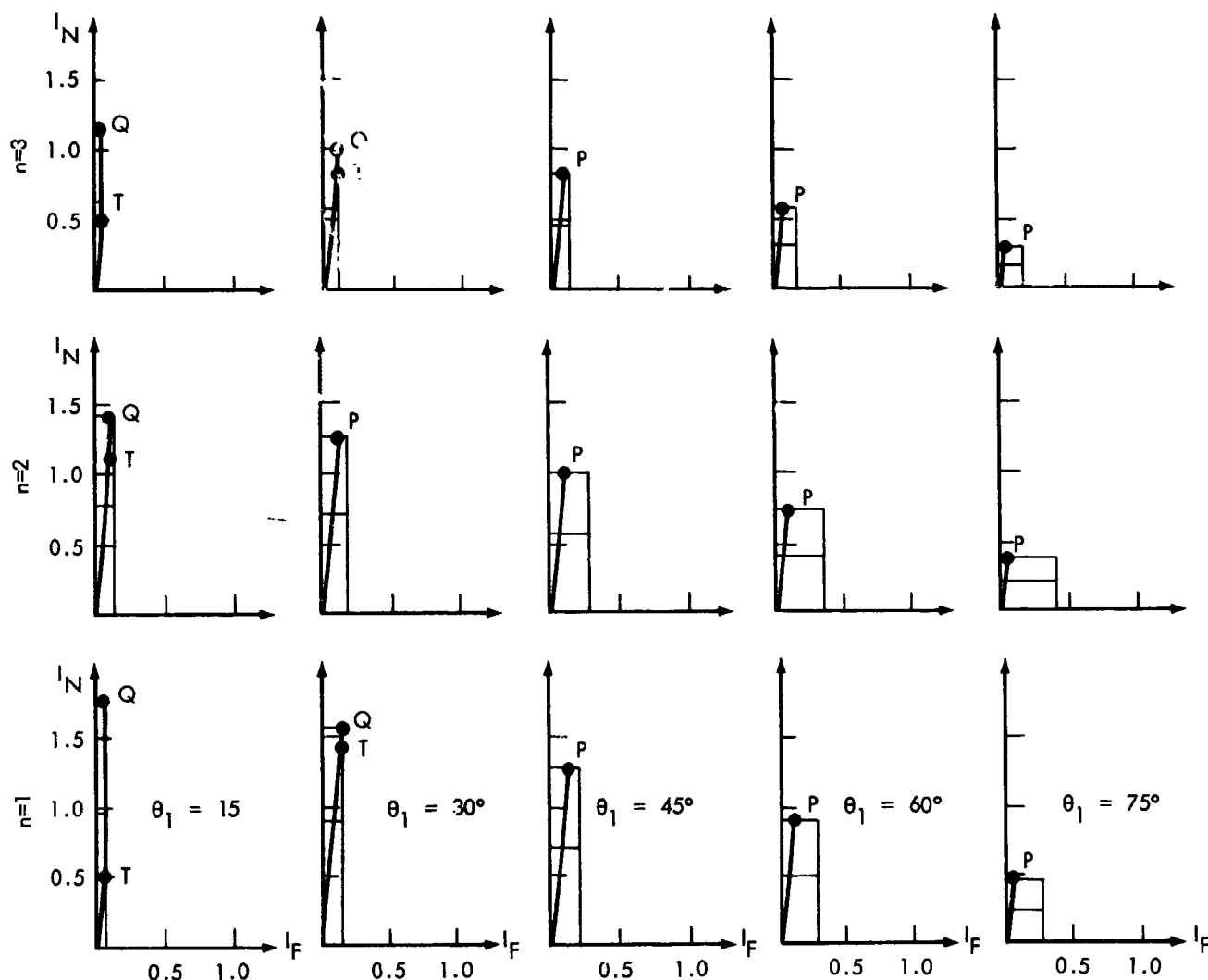


Figure 5 Routh Impulse Diagrams, Steel-on-Steel

equations, it can be considered as a scale factor and may be normalized out. The path of the representative point was then established for each initial angle to determine whether a rolling or sliding mode of system behavior existed at the time of loss of contact. With the mode established, the final values of velocity, rotation, and angle were determined using the appropriate relations from equations (3) through (12). The computations were then continued using the above values as initial conditions to establish a set of I_N , I_F values for the second set of impact diagrams. This procedure was again used to obtain a third set of impulse diagrams. Rebound angles for the first three impacts resulting from each of the five initial angles are shown in table 1.

Table 1

REBOUND ANGLES

Initial angle (deg)	θ_1' (deg)		θ_2' (deg)		θ_3' (deg)	
	C*	E**	C	E	C	E
15	-13.5	-13.8	7.6	7.2	- 2.8	- 2.2
30	-27.3	-28.3	26.4	26.4	-15.5	-20.0
45	-45.1	-49.8	45.2	54.4	-45.3	-58.0
60	-62.7	-63.2	65.6	72.4	-68.4	-74.6
75	-77.3	-78.2	79.5	81.0	-81.2	-81.8

*Calculated

**Experimental

Figure 5 shows that the steel ball will reach a condition of pure rolling during impact for each of the three successive impacts when the initial angle is 15 deg. When the initial angle is 30 deg, however, the pure rolling condition is reached only during the first and third impacts, whereas sliding throughout the contact occurs for the second impact, as shown in figure 5. For the remaining initial angles, sliding occurs throughout the duration of each successive impact.

Good agreement between the computed and the measured values of the rebound angles was obtained. In addition, the predicted values of the critical angle and the required angle for an equal rebound agreed closely with the experimental results. The value of the critical angle obtained from equation (26) is verified by the 45 deg impulse diagram results, which are the first to show divergence of the rebound angles toward 90 deg. Also, it can be observed that the exact value of θ_c is that initial angle for which the first rebound angle equals the initial incident angle ($\omega_1 = 0$). This result is verified by the first rebound angle of -45.7 deg resulting from a 45.0-deg angle of incidence.

Thus, a critical angle is shown to exist. Initial angles less than this value degenerate to a normal impact mode with zero angular velocity. Initial angles greater than this critical value diverge to a pure sliding mode at $\theta_n = 90$ deg, with a residual angular velocity as defined by equations (22) and (23).

CONCLUSIONS

In evaluating any method of analysis the engineer generally asks two questions:

- How well does it predict the natural phenomenon?
- How difficult is it to perform?

At the outset of this analysis, the implicit question was: can the behavior of a body, impacting in the presence of dissipative forces, be determined by the use of some simple tools without recourse to higher mathematics? It has been shown that an affirmative answer can be given to this question. A designer can find the final degenerate state an impacting body will reach once it has dissipated all the kinetic energy in either the normal or tangential velocity component. It has been shown that the mode a body relaxes into is solely a function of its material properties and the initial state of motion.

The method developed by E. J. Routh more than 60 years ago for a simple impact can be altered to enable the designer to predict, in one step, the final state that will exist after a series of impacts. It was also shown that if knowledge of the intermediate states is desired, the necessary calculations can be performed with ease.

The experiments indicated that, while the method is simple, care must be used in its application. The material constants — friction and restitution — must be well defined. Moreover, these experiments have shown that good agreement between theory and practice will result only when secondary effects caused by high friction, body distortion, etc., are minimal.

REFERENCES

1. Routh, E. J.: The Elementary Part of Dynamics of a System of Rigid Bodies. The MacMillan Co., 1905.
2. Timoshenko, S. and Young, D. H.: Advanced Dynamics. McGraw-Hill, 1948.
3. Herzl, G. G.: General Solution of the Rigid Body Impact Problem, AIAA J., vol 2, no. 1, May, 1964.
4. Goldsmith, W.: Impact — The Theory and Physical Behavior of Colliding Solids. Edward Arnold Publishers Ltd., London, 1960.
5. Marks, L. S., ed.: Mechanical Engineers' Handbook, sixth ed., McGraw-Hill, 1958.

COMPRESSION-SPRING SEPARATION MECHANISMS

By T. G. Harrington
Lockheed Missiles & Space Company

SUMMARY

N67 16913

The use of compression-spring mechanisms in the separation of spacecraft and shrouds is discussed. Guidelines are laid down whereby the separation restraints can be used to determine the necessity, or lack thereof, of closely guiding the spring. Experience (design, analysis, and flight) is cited to show what can be accomplished by proper design of the mechanisms.

INTRODUCTION

The separation of spacecraft components, which occur in every flight, represents crucial and major events that must be successfully executed to fulfill mission requirements. Separation systems vary as widely in physical and functional properties as the performance requirements which they must satisfy; however, most systems use helical compression springs as an energy source. This paper summarizes the principal design characteristics of separation mechanisms and empirical data obtained from actual separations in space.

RESTRAINT COEFFICIENT

Spacecraft mission requirements generally define sufficiently the degree of sophistication which must be incorporated in the design of the ejection mechanism. The simplest ejection mechanism — the free spring — can be used successfully in some applications. However, as the restraints imposed on the separation event become more restrictive, a point is reached when the spring must be guided. To help define this point, it is useful

to compute the restraint coefficient c_r , which is proportional to the ratio of translational to rotational energy of the system:

$$c_r = \frac{20 M V_r^2}{I \omega_r^2}$$

where

- c_r = restraint coefficient
- M = mass of ejected body, slug
- V_r = required separation velocity, ft/sec
- I = moment of inertia of ejected body, slug-ft²
- ω_r = tip-off restraint, deg/sec

The numerical constant in the formula (20) was chosen so that the critical value of c_r would be 1, i.e., for values smaller than 1, simple free springs can be used, and for values larger than 1 the spring should be guided. It is important to understand that this coefficient is presented only as a guide for determining the type of spring mechanism to be used; the final selection depends on a detailed analysis of each individual case.

In the case of payloads, both the separation velocity and the tip-off rate restraints are generally defined. However, in the case of over-the-nose shrouds, i.e., one piece shrouds which must be separated forward over the payload, the allowable tip-off rate must be determined by analysis, through use of the required ejection velocity and allowable shroud-separation envelope. Listed below are the values of c_r , computed by using the restraints and mass properties of some representative shrouds and spacecraft:

<u>Mission</u>	<u>c_r</u>	<u>Separation Mechanism</u>
Mariner C Shroud	6.36	Guided
DME-A Spacecraft	5.48	Guided
Mariner C Spacecraft	2.70	Guided
Ranger Spacecraft	1.44	Guided
Alouette Spacecraft	0.15	Free spring

The springs used in all of these applications are of helical design with closed and ground ends and the mechanisms are close-tolerance guided systems such as shown in figures 1 and 2. The exception was the Alouette in which a single large diameter file spring was employed because of the lenient tip-off restraint.

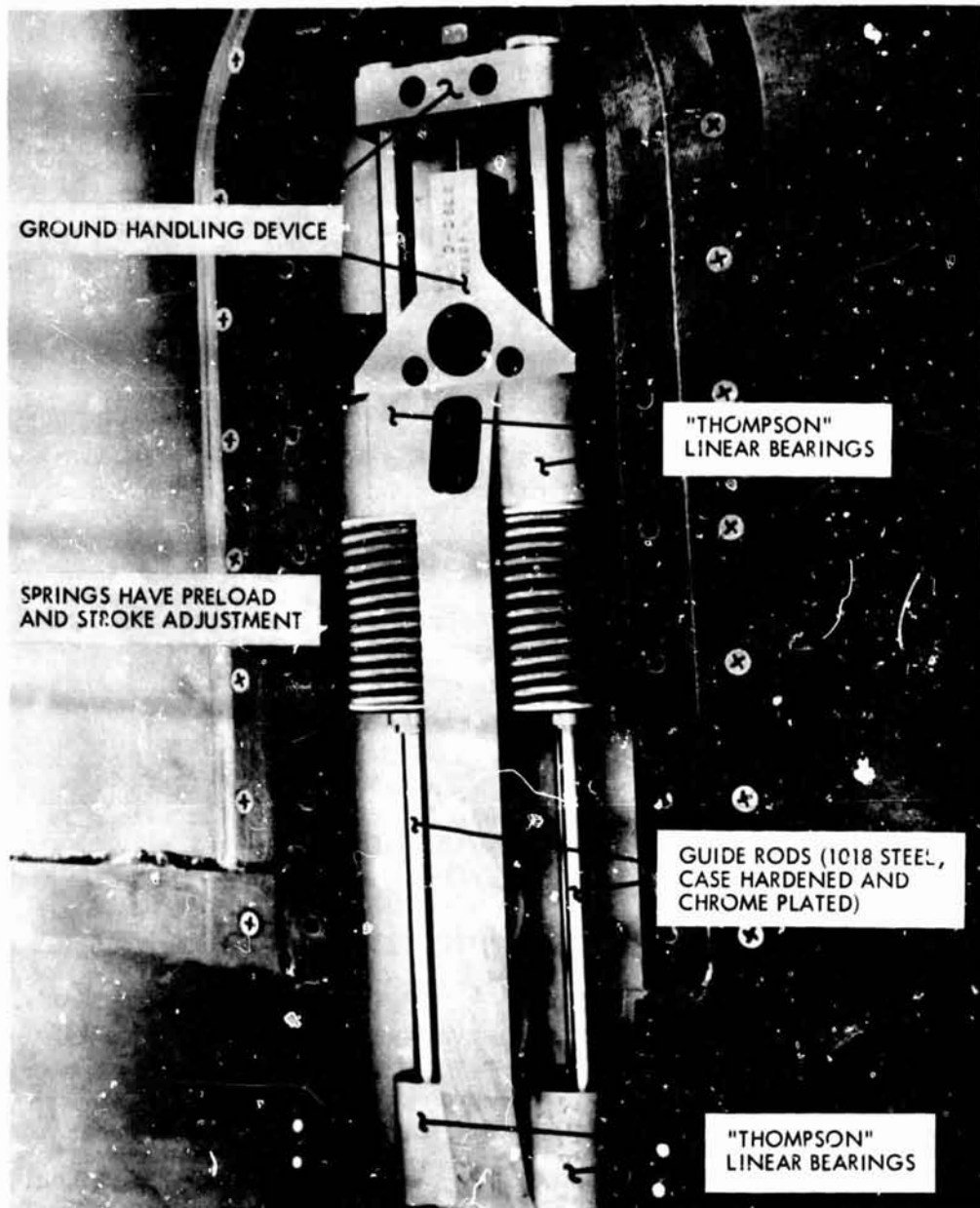


Figure 1 Compression-Spring Separation Mechanism

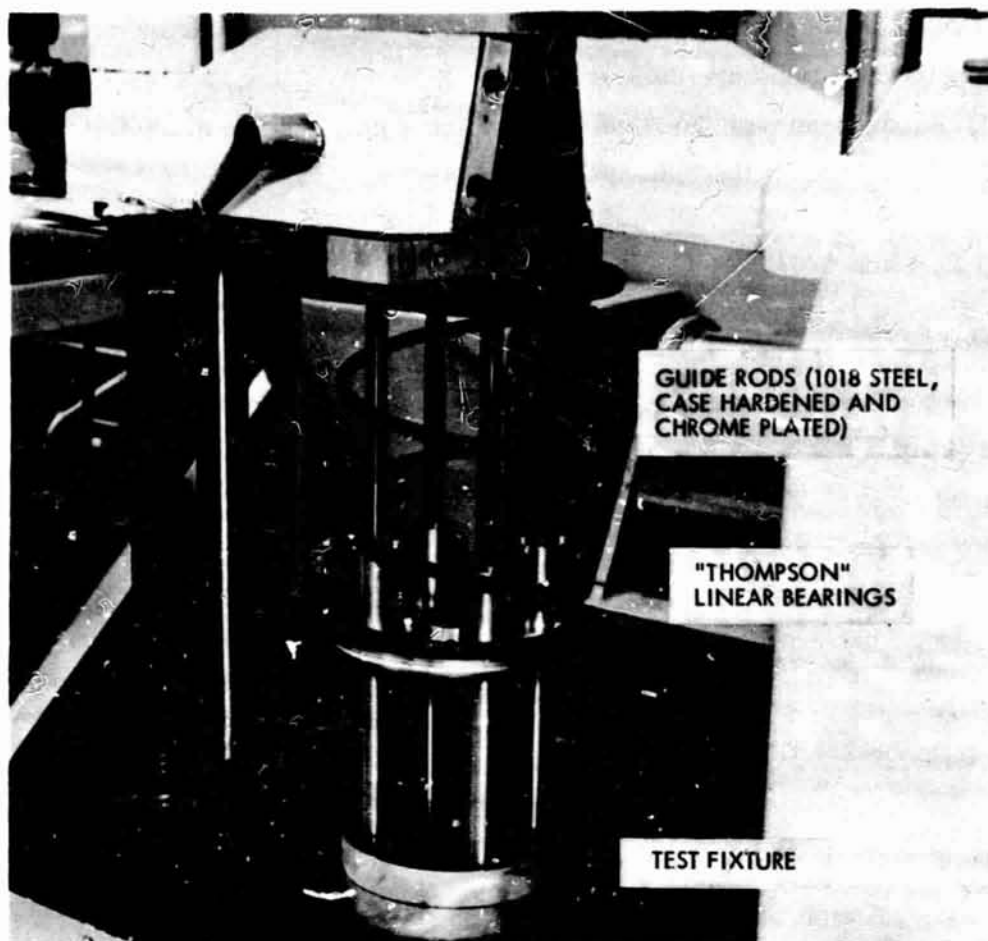


Figure 2 Compression-Spring Separation Mechanism

SEPARATION MECHANISM FOR MARINER C SHROUD

The design of ejection systems is probably most interesting and challenging when applied to unguided over-the-nose shrouds. In this application, it is the spring mechanisms which ultimately define the separation envelope of the shroud.

The shroud employed in the Mariner C flight (the Mars probe) can be used to great advantage in a discussion of this type of system. The basic performance requirement of the separation was that it be separated in a manner that would avoid collision with the payload. The separation velocity was set at 8 ft/sec, due to an unrelated trajectory constraint. In the light of this information, together with data on the envelopes of the shroud and spacecraft, the tip-off rate constraint was determined and the

restraint coefficient c_r was computed as 6.36 as previously indicated. The severity of this constraint can be more easily visualized in terms of clearances. The critical clearance items were the aft plane of the shroud and the tip of the spacecraft solar panels which meant that the shroud aft plane could not experience more than 4.4 in. (the static clearance) of transverse motion in the 100 in. of separation distance required to clear the panels. In other words, the shroud aft plane had to be ejected along a line displaced not more than 2.5 deg. from the intended direction.

To satisfy the requirement it was necessary to design a system that would induce a minimum of transverse velocity into the shroud aft ring. This was accomplished by using the compression spring mechanism shown in figure 1. The mechanisms were mounted in the aft end of the shroud so that the guide rods transmitted the spring force to the adapter interface ring. Upon release of the vee-band (used to hold the shroud during ascent) the springs then accelerated the shroud to approximately 90 in./sec in 4.5 in. of separation. The object of using close-tolerance guide rods and bushings was to minimize any play in the system that would result in the shroud moving transversely with respect to the adapter center line, i.e., unless the mechanism plungers actually slid on the interface ring.

Analysis and tests have shown that slippage does not occur because the shear forces developed at the plunger tips are less than the friction potential assuming an interface with a coefficient of friction of 0.4. This lack of slippage is helpful in that

(1) the shroud aft plane has no transverse velocity at the time of spring extension, and (2) the rotational rates introduced are less because the instantaneous center of rotation lies in the separation plane and the resistance to torques, i.e., the rotary inertia of the shroud, is therefore increased by Md^2 (the inertia transfer term). Use of this approach is probably the most important single thing that can be done to reduce the tip-off rate for, in many cases, the transfer term increases the inertia by over 100 percent and thereby reduces the tip-off rate by over 50 percent, assuming the torques to be the same.

There are, however, some mechanism and systems parameters which do introduce velocities of the aft plane, notably spring misalignment and vehicle rotational rate.

In the case of spring misalignment, the effect is obvious in that the shroud separates — along the line defined by the angle of misalignment and the aft plane thereby acquires a transverse velocity which is the component of the separation velocity, as computed using the sine of the misalignment angle. In the Mariner shroud, this effect was minimized by controlling the misalignment to ± 0.25 deg. Usually, little can be done about the vehicle pitch rate and this effect therefore must simply be accepted as it occurs.

LABORATORY AND FLIGHT TEST PERFORMANCE

The Mariner shroud, to date, has undergone but one flight test, in which it operated satisfactorily. The ejection system, however, performed successfully in 34 laboratory separations in the Mariner program and, just recently completed 8 additional tests in the Lunar Orbiter program, which employs this shroud with minor modifications. The actual shroud aft plane separation envelope as determined by test and analysis is shown in figure 3. The illustration shows that the transverse motion of the shroud aft plane is 2.0 in. at 100 in. of separation, due to the separation mechanism alone.

The system in the ranger spacecraft underwent 9 tests in which the tip-off rate in the worst-on-worst case (arithmetic, as distinguished from statistical addition on individual effects) was predicted to be 2.5 deg/sec. The system was flown 9 times and always performed satisfactorily as shown by post-separation data.

Separation tests were run on the Mariner D spacecraft system and it was determined that the extreme tip-off rate would be 1.4 deg/sec. It was further shown that the major cause of the tip-off rate was the relatively large (1.125 in.) c.g. offset. The effect of the offset can be eliminated completely by the proper setting of the spring preload and stroke, and it was shown that the tip-off rate can be held below 1 deg/sec. even in the worst-on-worst case.

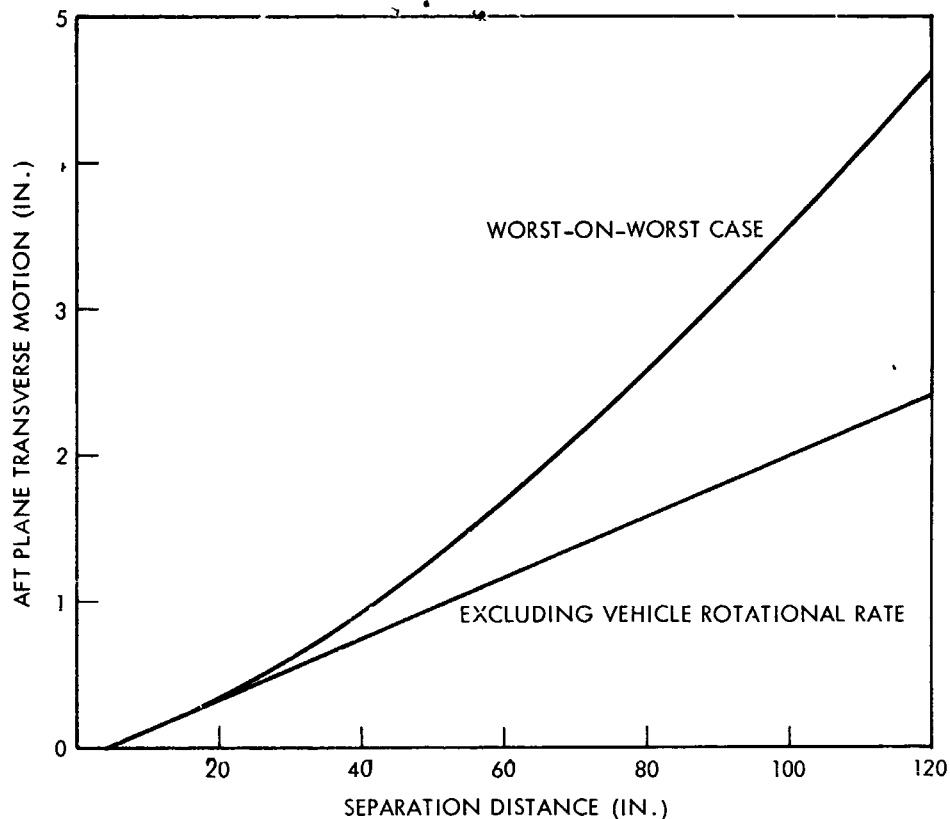


Figure 3 Separation Envelope of the Mariner C Shroud

The four tests of the actual Alouette flight-item ejection spring showed a tip-off rate of less than 7 deg/sec, which is very low for the free spring mounting. The spacecraft experienced rates up to 28 deg/sec during the extension of the spring, but this value always decreased considerably before spring extension. The flight of the spacecraft last year showed that the system functioned as intended.

The DME-A spacecraft used an ejection spring exactly like that of the Alouette. Because of the tight constraint on tip-off rate, however, it was installed in the mechanism shown in figure 2. The six separation tests of the actual flight hardware showed the tip-off rate to be less than 2 deg/sec whereas postflight data from the spacecraft have shown that the measured rate was less than 3 deg/sec. It does not appear likely that a closer correlation can be achieved.

It has been shown that the separation restraints can be used to determine the advisability of utilizing guided mechanisms. The use of mechanisms such as those discussed herein can reduce significantly the separation misalignment. Their performance can be analytically assessed, thus reducing the cost of testing.

MARINER-IV SCIENCE PLATFORM STRUCTURE AND ACTUATOR
DESIGN, DEVELOPMENT AND PERFORMANCE*

By G. Coyle and E. Floyd
Jet Propulsion Laboratory
California Institute of Technology

SUMMARY

N67 16914

This report describes the Mariner-IV scan platform and actuator, and the problems encountered in its development. Equipment test results and flight experience are summarized to support the discussion of design adequacy. The scan structure and actuator design are considered to be a reasonable solution within the framework of schedule, structural efficiency, interface definition, and, most important, desired functional objectives. The design techniques and problem areas described are considered to be useful data for application to future spacecraft programs.

INTRODUCTION

The Mariner-IV spacecraft has successfully completed its 229-day trip to Mars. The objectives of the Mariner mission were to obtain scientific data in interplanetary space and near Mars, close-up TV pictures of the Mars surface, and atmospheric data. In all respects, these objectives have been achieved.

The planetary science and acquisition sensors consisted of a TV, ultraviolet photometer, wide-angle Mars sensor, and narrow-angle Mars sensor. Total weight of the platform-mounted sensors was 11.5 lb. All sensors were to be mounted to provide

*This paper presents the results of one phase of research conducted at the Jet Propulsion Laboratory, California Institute of Technology, under Contract NAS7-100, sponsored by the National Aeronautics and Space Administration.

parallel optical axes. Location of the integrated package was to be such as to provide an unobstructed field of view of the planet near the region of closest approach. The thermal environment had to be compatible with vacuum operating temperature extremes of 0° to 100° F and minimum storage temperature of -50° F.

FUNCTIONAL DESCRIPTION

Science Platform. The objective of the science platform subsystem (figure 1) was to provide a gimbaled support structure capable of satisfying the pointing requirements for the experiments, structural and thermal compatibility, alignment accuracies, and spacecraft system interaction requirements.

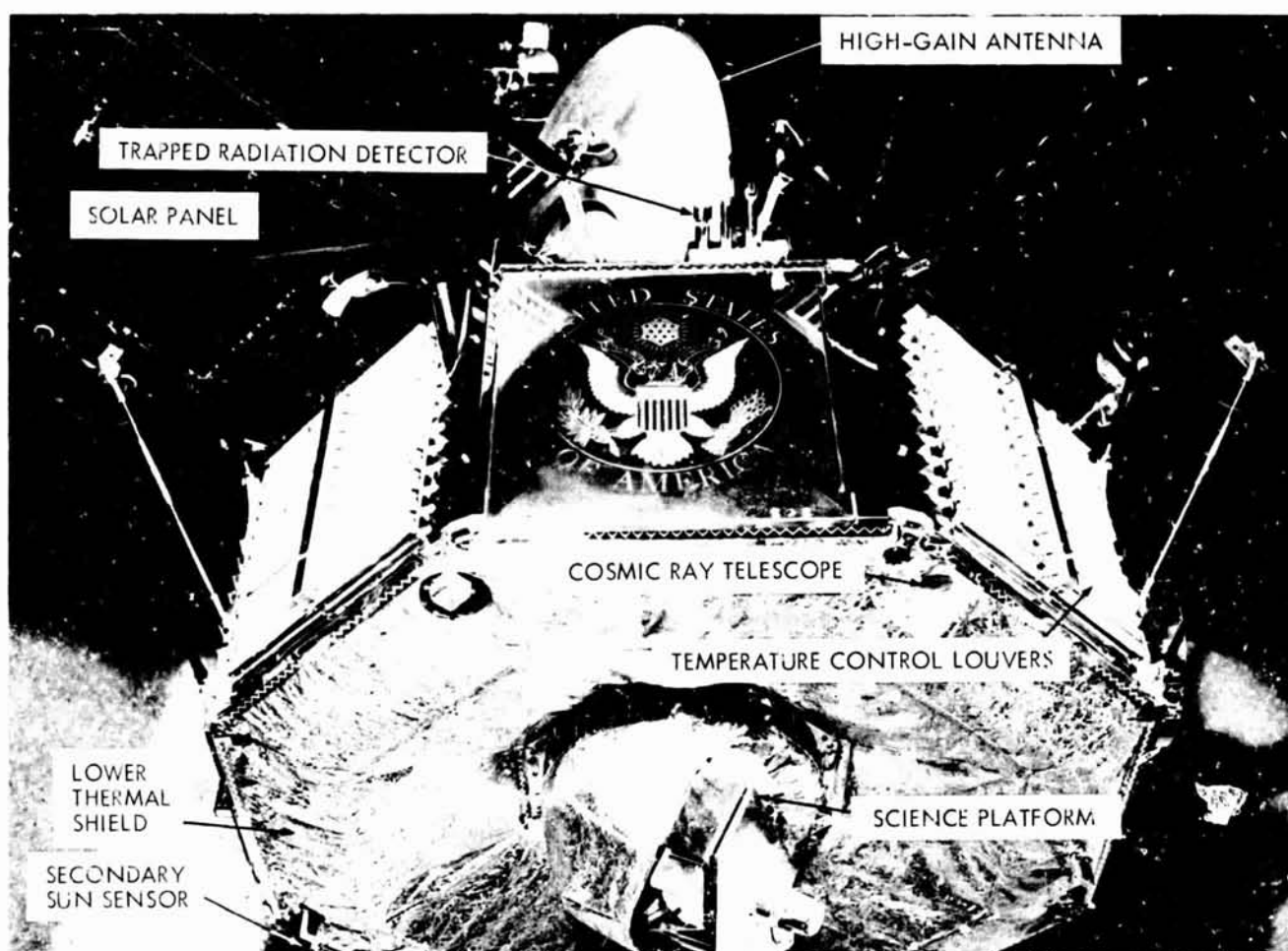


Figure 1 Mariner-IV Spacecraft

To provide the necessary field of view and be compatible with basic bus structure requirement, the science package was mounted at the bottom of the central cavity of the basic octagon. The pointing direction was chosen to be 120 deg from the sun, with the 180-deg scan axis parallel to the spacecraft Z axis.

Scan Actuator. The scan actuator consisted of a 2-w, 26-v, 400-cps, split-phase motor and reduction gear train, providing an angular output speed of 0.5 deg/sec. A slip clutch limited the output torque to 40 in. -lb.

Science Cover. The function of the deployable science cover was to provide: structural support and articulation, protection for the sensor optics from stray sunlight and micro-meteorite damage during cruise, and a light source array, powered from the ground umbilical, to check proper operation of the science and acquisition sensors during systems and on-pad tests.

DEVELOPMENT

Science Platform

Restrictions on the required field of view and scan freedom dictated a cantilevered tube (figure 2) mounted in bearings. A machined, two-piece aluminum instrument mount was riveted to the over-hung portion of the tube, and scan motion was introduced through a splined drive link located on the inboard end. Relative location of the scan actuator and drive link was based on consideration for cable harness routing to the science instruments. A brief description of the science platform components is as follows:

- Support Shaft. The 3.00-in. -diameter scan tube with 0.060-in. -thick walls, has a first mode bending frequency of approximately 80 cps and tube strength sufficient to provide a reasonable safety margin, assuming a lateral load of 50 g rms. Torsion loads were supported through a single pyrotechnic pin-puller latch located immediately below the lower bearing mounted to the spacecraft structure. A check on the effect of latch stiffness and tube size on torsional frequency modes demonstrated a first mode torsional resonance of 150 cps.

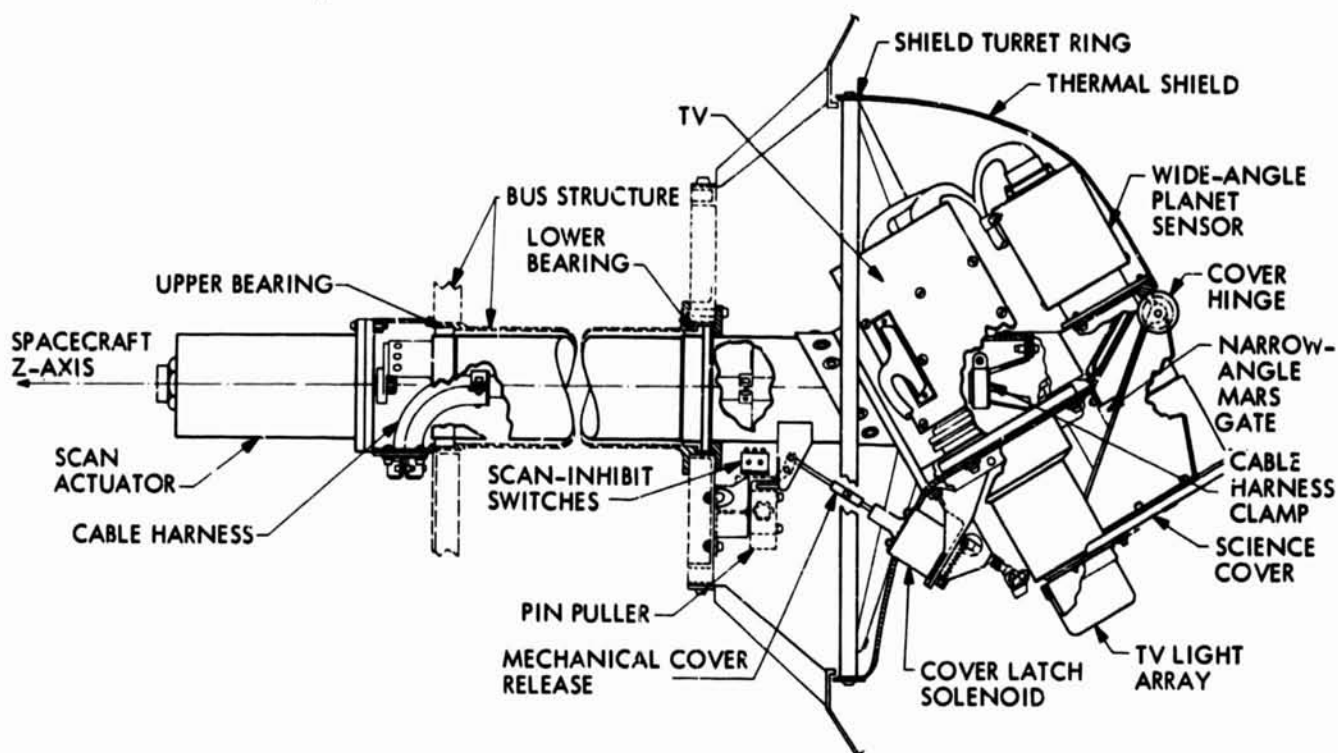


Figure 2 Section View of Science Platform

- **Instrument Mount.** The platform support structure was machined in one piece with all bulkhead mounting planes parallel to ensure critical alignment between instruments.
- **Scan Bearings.** The bearings selected for use on the scan platform were of the sleeve liner type with Teflon-filled asbestos used as a liner material. Diametral bearing clearance was 0.002 in. , based on anticipated temperature gradients across the joint and consideration for the resultant nonlinear response of the system to vibration input. Axial loads were removed through the flanged lower bearing which had an end play of 0.0005 to 0.0015 in.
- **Thermal Environment.** As a result of the poor thermal conduction path through the scan bearings, radiation transfer had to be relied upon almost entirely. The 1-ft length of scan tube through the center of the bus and the support structure on the bus were black-anodized. All external surfaces on the science platform were polished aluminum or gold-plated to reduce heat loss. The entire instrument package was enclosed in an insulated turret shell that rotated

with the platform. With the science packages painted black and open directly to the interior of the bus, radiation transfer was accomplished. The resultant configuration assembled on a flight spacecraft is shown in figure 3.

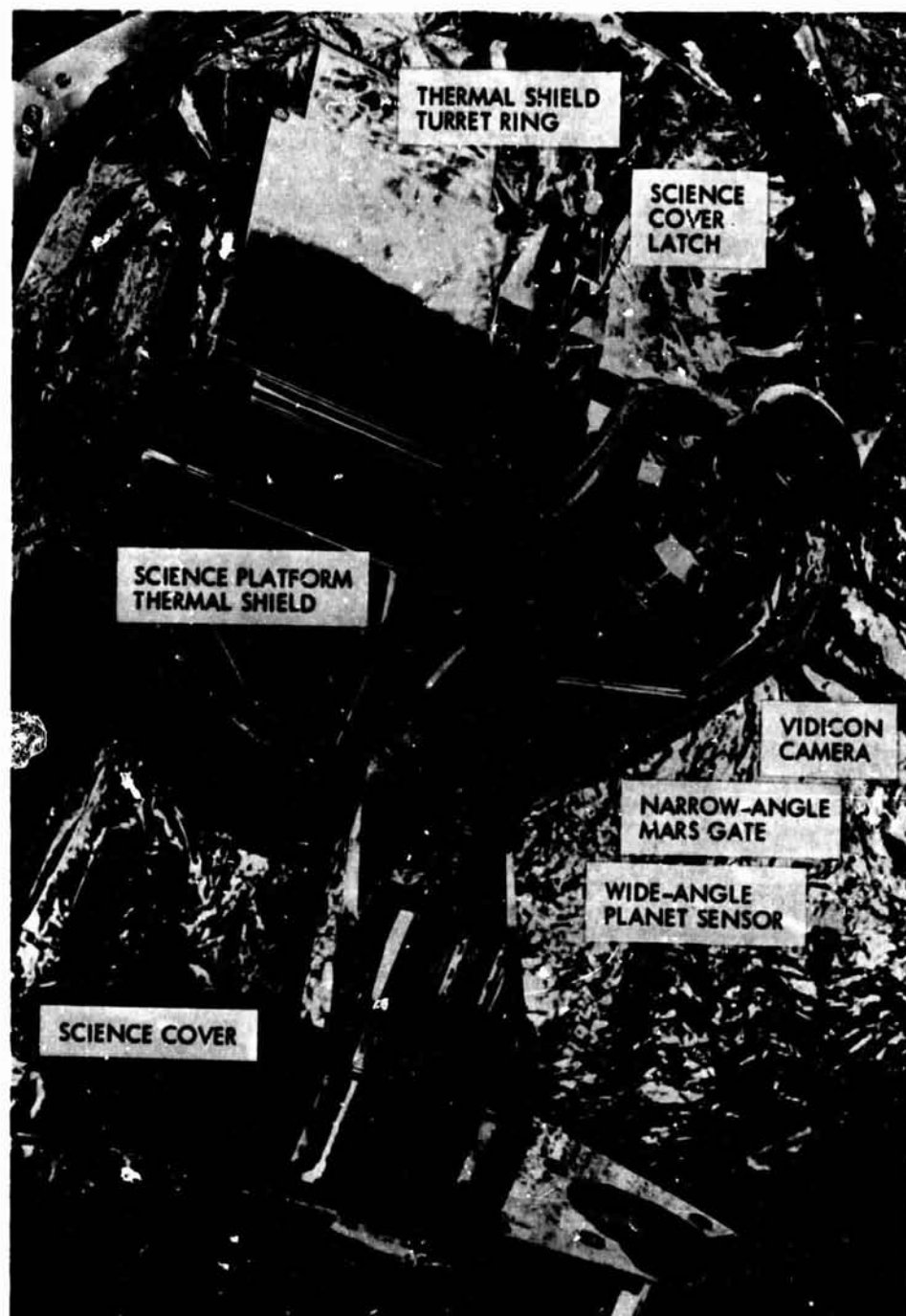


Figure 3 Platform With Turret Shield

Scan Actuator

A method of routing the cables down the scan platform tube was devised which required that the scan actuator be relocated from inside the support tube to the top of the primary structure. The cylindrical actuator assembly, with cover removed, is shown in figure 4. A brief description of the scan actuator components is as follows:

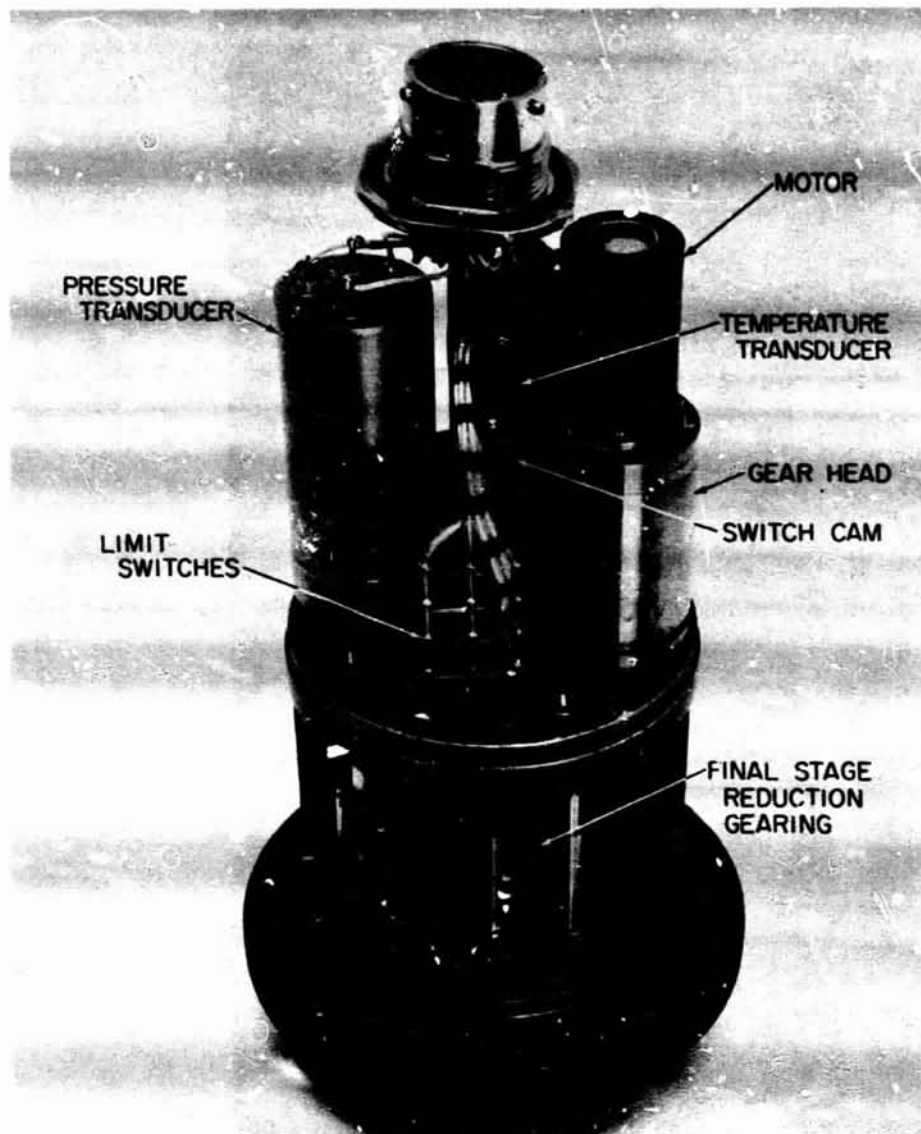


Figure 4 Scan Actuator

- Scan Motor and Drive. The scan actuator consisted of a 400-cps, 26-v, 8000-rpm synchronous motor and reduction gear train, providing an angular output speed of 0.5 deg/sec. The first stage of reduction (980 to 1) was achieved in a gear-head attached to the motor. An additional 98 to 1 reduction was achieved external to the motor gear-head, using a magnesium housing and standard gearing techniques.
- Gears. Prior to the fabrication of the scan actuator, a series of tests indicated that anodized 2024 aluminum gears running on electroless, nickel-plated, 303, stainless steel gears without lubrication was a favorable combination. As an added safety factor the aluminum gears in the aluminum-stainless-steel running combination were further protected by electrofilm dry lubricant.
- Bearings and Seals. Except for the output shaft bushing, phenolic separator, Class 7, ball bearings were used in the actuator. Each bearing and separator was vacuum-impregnated with F-50 silicone oil. To prevent Brinelling during vibration, the lower end of the output shaft was supported in a Teflon compound bushing rather than by a ball bearing.

The output shaft was pressure-sealed by two Viton quadrings spaced 0.050 in. apart. When coated with F-50 silicone oil, the Viton quadrings, with the void between filled with oil, provide a labyrinth-type seal. The gear housing cover around the glass header electrical connector and separation plane was sealed with Viton O-rings. The actuator assembly was pressurized to 30 psia with dry air, which replenishes the oxide coatings on components as it is removed by wear, thus preventing cold welding.

- Scan Reversal Interface. The required actuator scan angle was ± 90 -deg from a center position. A set of cam-operated microswitches pulse the scan logic system at each limit, reversing the direction of the scan. For redundancy each limit incorporated two hermetically sealed microswitches.
- Telemetry Outputs. An angular scan position indication was provided by coupling a single-turn potentiometer to the output shaft through a stage of anti-backlash gearing. To provide engineering pressure and temperature environment information, transducers were installed internal to the scan actuator.

In addition to the conventional environmental tests, a life test was conducted on the scan actuator by driving a science platform subjected to a vacuum of 10^{-6} mm Hg. Life testing was also conducted with the pressure plug removed to simulate the eventuality of pressure loss during flight. Since the vacuum chamber cannot reach the low pressure of the space environment, the actuator was heated to 130°F to speed lubricant evaporation. No malfunctions were noted during the 80-day test.

Science Cover

Optics details for the TV and wide-angle sensor were finalized very late in the program. To meet the hardware delivery schedule, therefore, a basic cover assembly mounting plate, designed to accommodate various configurations, would change only as required to attach each instrument. The final configuration of the science cover is shown in figure 5. A brief description of the cover components is as follows:

- Cover Plate. Lightweight, low heat loss, and, most important, bending stiffness such that boost loads would not be amplified through the cover into the optics assemblies were the basic requirements for the cover plate. A bonded aluminum honeycomb sandwich structure satisfies these criteria.

A 3/16-in. hex honeycomb core of 0.0007-in. -thick aluminum alloy was used for the plate. The cover sheets were 0.004-in. -thick aluminum alloy bonded to the core, using Metal-bond 406 adhesive and cured in temperature cycles up to 350°F. Epon 913 adhesive was used for fill-in insert locations and around the edge of the plate.

- Hinge Hardware. The hinge bearings (No. 10-32 threaded shank monoball rod ends) were a stock item except for substitution of A-286 corrosion resistant steel because of nonmagnetic considerations. The monoball liner consisted of a fiberglass-Teflon weave. A bearing run-in procedure was utilized to ensure low friction with a 3 in.-oz maximum breakaway torque being reasonably achieved.

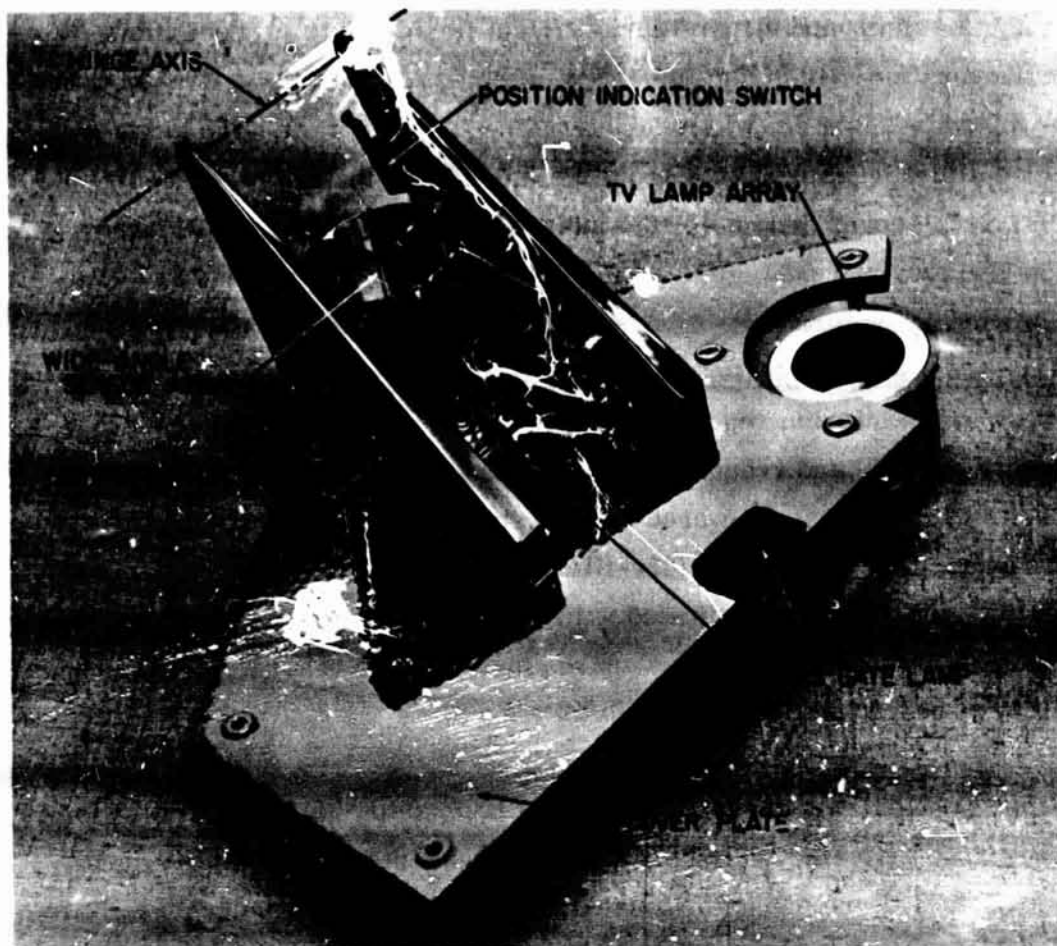


Figure 5 Science Cover Assembly

Clock springs of 0.016-in. Elgiloy nonmagnetic spring material were used to provide the cover opening force. Molybdenum disulfide drylube was deposited on the spring material to guarantee a resistance to cold-welding when the spring was preloaded. Since in-flight actuation was zero-g, the spring preload needed only to overcome bearing friction and cable resistance. However, ground testing requirements gave a considerable margin to this value, resulting in a specified spring torque of 24 in.-oz per spring in the latched position.

- Lens Cover Assembly. In general, the individual lens cover housings consisted of a 0.020-in.-thick, double-walled aluminum shell similar to the TV cover assembly. Double-filament bulbs were mounted in Teflon inserts with blocking diodes and terminal boards mounted on the back side of the inner shell. In the case of the TV cup, a Viton bumper was attached to provide the required

stray-light shielding, and still retain sufficient flexibility to prevent transmission of vibration loads from the cover to the optics assembly. The housing used for the wide-angle planet sensor was similar, except for lamp location and the use of quadrant baffles to sequence the areas illuminated. To complete the science cover assembly, the individual lens covers were attached to the cover plate, and the pigtail wiring was routed to a terminal board on the hinge leg.

- Cover Latch and Latch Actuator. The importance of reliability of actuation to the success of the mission required the cover latch and actuator to be as fool-proof, overdesigned, and redundant as possible. The latch itself consisted of simple over-center linkage powered by dual stainless springs coated with dry-film lubricant. Link pivots were dry-film coated stainless shafts in aluminum housings with side clearance adjusted with Teflon washers. The springs, when in the on-center position, generated approximately 13 lb of force with the required over-center motion set at 2 lb to trigger.

A push-type solenoid was chosen for primary latch actuation because it satisfied the performance criteria, had inherent long vacuum-storage capability, and was compatible with the capacitor discharge power supply. A solenoid utilizes a much simplified reliability test program as compared to a single-shot pyrotechnic device. The solenoid was capable of 3.8-lb force at 20 v and 5.8-lb force at the rated 26-v capacitor charge voltage for a required 0.090-in. stroke, or approximately three times the required latch actuation force.

In case of failure in an element of the solenoid circuit, a mechanical backup was provided as an unrelated secondary release. The mechanization chosen consisted of a spring-loaded lanyard plunger which is automatically tripped when the scan platform is rotated. The resultant configuration (figure 6) allows nearly complete redundancy.

In addition to the conventional environmental and performance tests, one spare solenoid and one complete assembly were subjected to a temperature-vacuum life test (although not considered a qualification test) with the chamber environment held at 130° F and

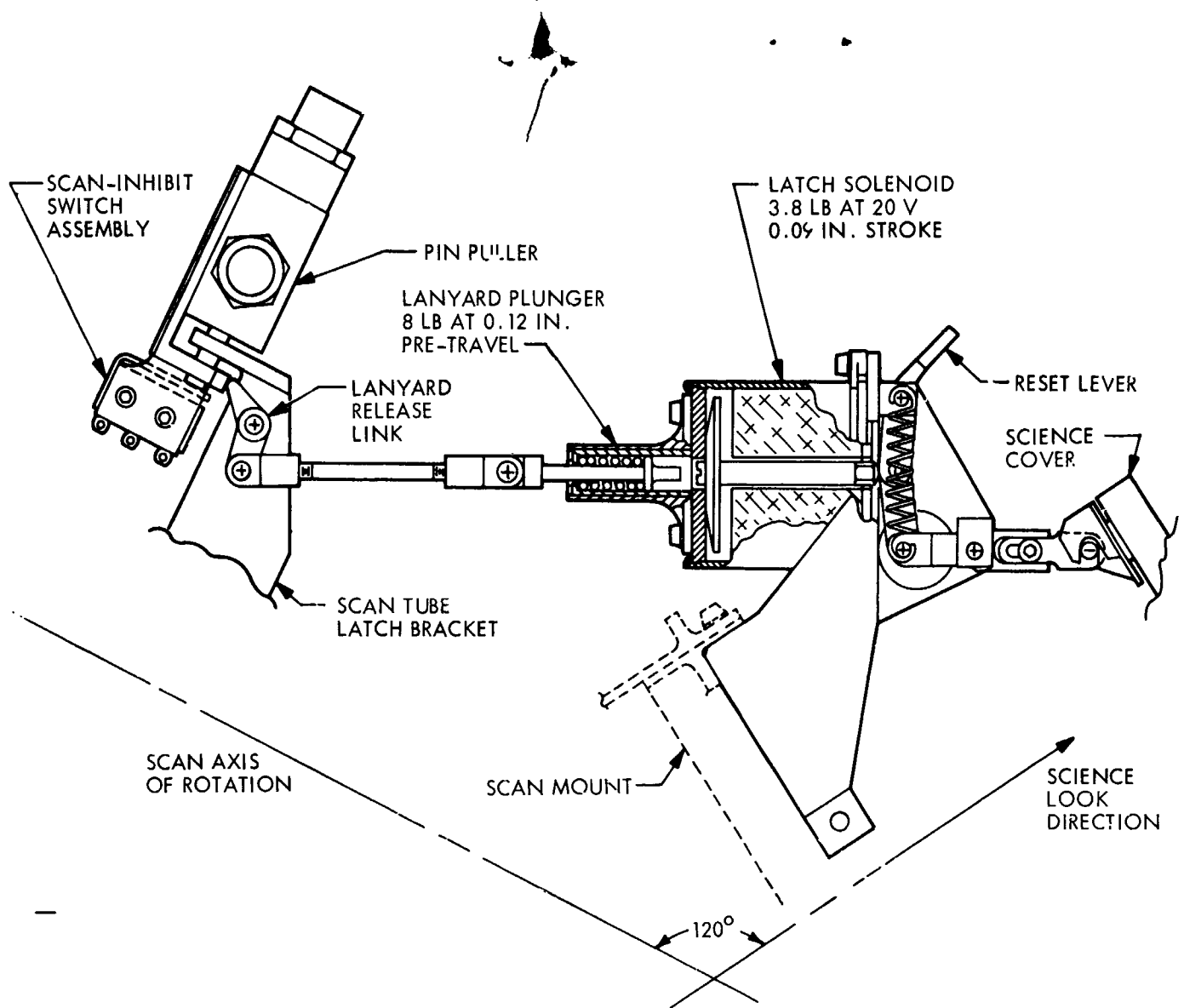


Figure 6 Cover Latch and Lanyard Assembly

approximately 10^{-6} mm Hg. The solenoid was cycled once a day against a plunger pre-load with an end-of-stroke indicator to verify actuation. The science cover assembly with a separate solenoid and latch was under vacuum for time periods varying from 15 to 30 days and then actuated. At the completion of the 180-day test cycle, no failures were noted.

INTEGRATED SYSTEM TESTING

Complete systems tests were conducted with the platform, actuator, and science cover installed on the flight spacecraft and subjected to operational tests to determine functional

adequacy. Simulated flight sequences were performed to determine if the following basic design goals were achieved: proper operation of the actuator using the flight instruments and providing proper scan motion, and capability of the science cover and latch assembly to perform their proper functions of actuation when using flight pyrotechnic power supplies and instrument calibration by means of the cover lamp array.

FLIGHT EXPERIENCE

Mariner IV has completed its mission with all scan platform and actuator hardware having operated properly. Immediately following injection, the scan-inhibit switch verified proper actuation of the pinpuller. At launch plus 75 days commands were sent to actuate the science cover and exercise the scan system. Ten full scan cycles, or 2 hr of scan operation, were run with all elements operating properly. Verification of cover deployment was received, and readings on scan-actuator pressure indicated a 0.7 psi pressure loss since prelaunch checkout. Plots of scan platform position versus time indicated smooth operation with a measured scan speed of 0.505 deg/sec.

At Mars encounter (launch plus 229 days), the scan system was again operated for approximately 2 hr without measurable change in performance. Although the science cover had been deployed previously, telemetry indication verified that solenoid current had been applied properly. The operating temperature of the TV was measured as 21° F during encounter, which was well within the allowable range, and verified the adequacy of the thermal environment. The use of standard O-ring sealing techniques on the actuator output shaft was also proven adequate, based on the measured 0.7 psi temperature-corrected pressure loss at launch plus 75 days and a quite acceptable 2.9-psi pressure loss from the original 29.5 psi fill pressure as measured at launch plus 229 days. Operation with such a leak rate could have been accomplished for a considerably longer period of time with high confidence in the unit's reliability.

NONMAGNETIC EXPLOSIVE-ACTUATED INDEXING DEVICE

By John P. Bauernschub, Jr.
Goddard Space Flight Center
National Aeronautics and Space Administration

SUMMARY

N67 16915

A nonmagnetic, explosive-actuated, indexing device was developed for a magnetometer experiment flown on the Pioneer-VI Spacecraft. Conventional indexing devices were not suitable for use in instruments designed to measure low-intensity magnetic fields.

This device features an arrangement by which new explosive-piston actuators are cycled into position to provide 11 independent operations. The pistons actuate a bistable escapement which permits precisely 180-deg rotation of the magnetometer sensor.

Although the device was designed for a specific purpose, it is basically a nonmagnetic stepping motor. It can be modified for other stepping increments, and more operations can be provided.

INTRODUCTION

Development of a nonmagnetic indexing device was required so that the magnetometer experiment aboard the Pioneer spacecraft could be calibrated during flight. A calibration technique, in which the magnetometer sensor is rotated 180 deg, determines the drift in the sensor. The magnetometers for these missions were designed to measure spatial magnetic fields between the orbits of Venus and Mars. The intensity of the magnetic field in this region is below 10 γ ; thus, it was essential to minimize the

permanent field of the instrument and measure the drift in the magnetometer. Permanent magnetic fields are minimized by using only nonmagnetic materials.

A novel feature of this device is the method by which repeated operations are obtained with explosive piston actuators. Normally, such devices are used for one-shot operations because, by their very nature, they can be detonated only once, and are not retractable. However, this design overcomes these limitations with a sequential firing arrangement and automatic replacement of spent actuators. This paper describes the mechanical and electrical functions of the design which evolved, and the unique problems encountered. It concludes with an evaluation of the objectives achieved and suggests other applications for this device.

OBJECTIVE

The prime objective of this program was to develop a nonmagnetic device capable of repeatedly indexing, on command, the magnetometer sensor to precisely 180 deg. The requirements essential to achieving this were:

- Permanent magnetic field of the mechanism must be less than 0.25 γ at 0.5 in.
- 180 deg \pm 15 min rotation within 15 sec after receipt of earth command
- Minimum of 10 cycles
- Power allotment - less than 1 watt
- Weight allotment - 0.75 lb

A numerical reliability goal was not defined; however, failsafe and redundant techniques were to be used where feasible.

DESIGN PRINCIPLE

The problem of selecting an approach was reasonably well resolved in that the conventional electrical stepping motors and solenoid actuators were not suitable because of

their inherent magnetic fields. Effort was therefore concentrated on adapting spring-powered devices, which resulted in the explosive-piston actuated, bistable, escapement concept.

DESCRIPTION OF MECHANISM

The device, shown in figure 1 with the fiberglass cover removed, is mounted on the end of a boom. The principal feature of the design is an indexing apparatus that includes a magnetometer sensor and a sensor ratchet which are fastened to a shaft that rotates in a housing. A spring attached to the housing and the sensor ratchet exerts a torque, forcing the rotating assembly against one of the two rotating arms. The two positions on the shaft, located 180 deg from each other, are stable. This design configuration acts as a logical (decision-making) element since, for any position of the rotating assembly, spring torque is exerted in the direction of the nearest ratchet arm.

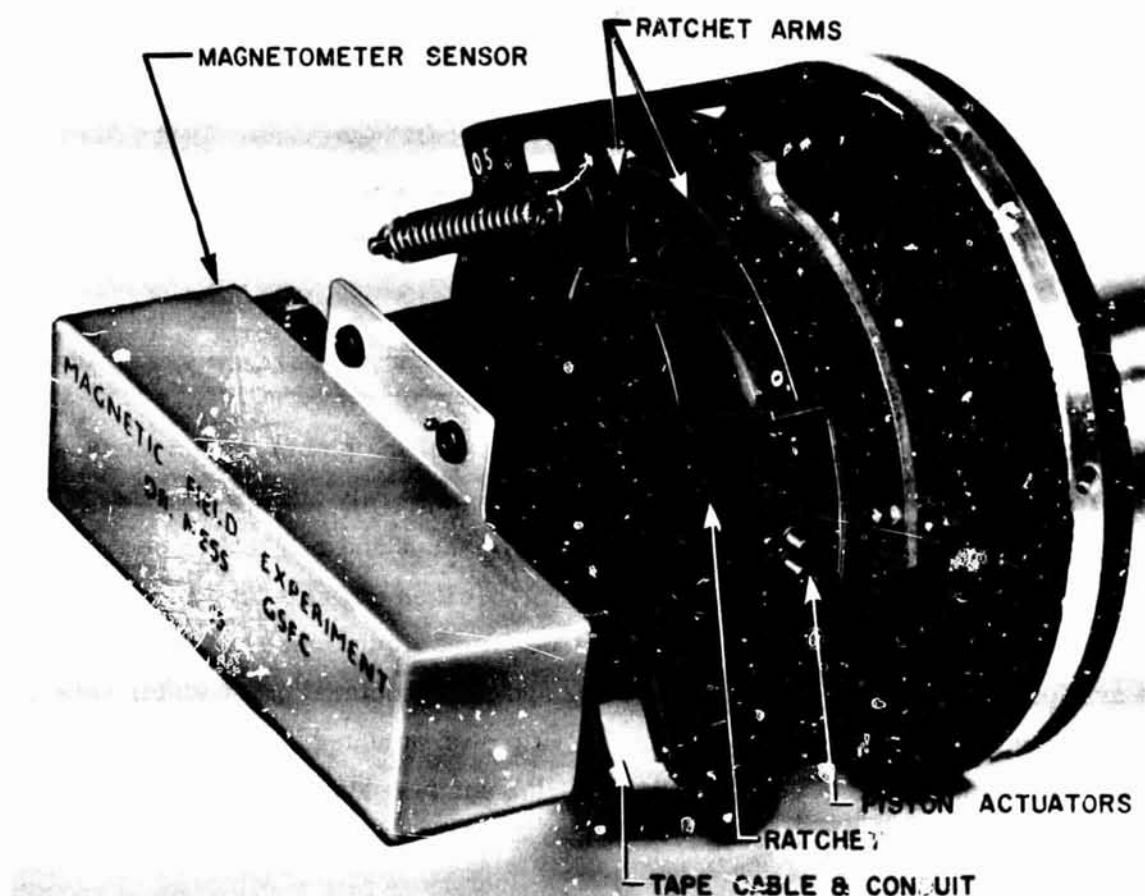


Figure 1 Fluxgate Magnetometer Indexing Device

The sensor ratchet arm is secured to a piston ratchet arm which has two piston-impact surfaces positioned 180 deg from each other. Eleven pairs (one of each pair for redundancy) of piston actuators (figure 1) protrude from a piston actuator housing. Attached to this housing is a printed-circuit commutator (figure 2) to which the piston wires are connected. This is the movable portion of the commutator, and its direction of rotation is opposite that of the magnetometer sensor. The brush portion of the commutator is rigidly attached to the annular support structure.

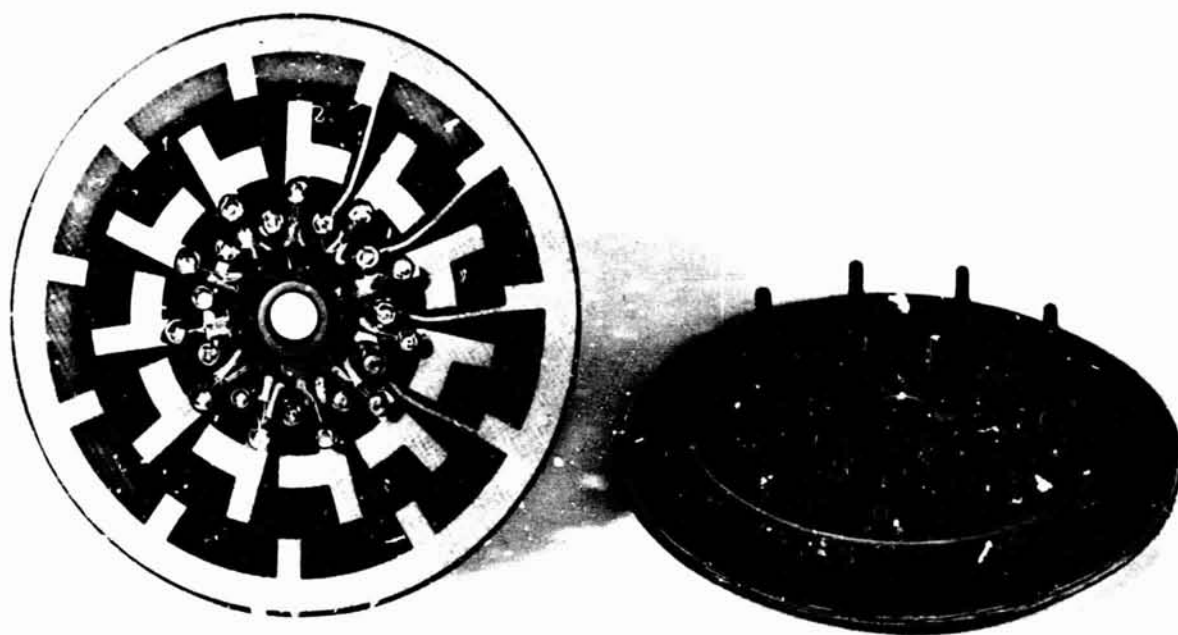


Figure 2 Commutator and Piston Actuator Housing

The force of detonation extends a piston $1/8$ in. against one of the piston impact surfaces on the piston ratchet arm. The piston ratchet arm pivots outwardly and carries the sensor ratchet arm with it. The ratchet, along with main shaft and magnetic sensor, disengages the sensor ratchet arm and rotates 180 deg. It then engages the opposite side of the ratchet arm, coming to rest in its other position. Simultaneously, the piston ratchet arm permits the piston actuator housing and its associated commutator section to rotate 15 deg. In this manner, another pair of piston actuators are positioned under the opposite piston surface, and are available for another detonation command.

Lubrication

To avoid the friction and cold-weld problems associated with the hard vacuum of space, shafts were made of aluminum, and then hardcoated and precision-ground to provide a hard oxide surface. Molybdenum disulfide was then bonded to the surfaces. An aluminum thrust washer, which supports the rotating parts under a constant, centrifugal acceleration of 12 g imposed by the spinning spacecraft, was fabricated and treated in the same manner. The main-shaft bushings and the piston actuator housing, which rotates on the main shaft, were fabricated from Delrin*.

Electrical Functions

In the ordnance circuit, the following sequence of events occurs on receipt of an indexing command. The experiment electronic system is energized, and the command to index is sent from the ground station to the spacecraft. Upon receipt of this command, the spacecraft sends a pulse to the magnetometer electronic system. This activates a circuit that charges a 100 μ f capacitor to 12 v in 10 sec. The capacitor is then electronically switched to the commutator brushes, which direct the power to the proper piston actuators. The discharge burns the bridge wires, detonating the piston actuators. A 27-ohm resistor in the magnetometer electronic system effectively shunts the firing terminals of the piston actuators. This eliminates the possibility of a charge remaining in the circuit, which could fire the next set of actuators when they move into position.

The commutator provides circuitry for firing the proper piston actuators and prevents the accidental firing of pistons in the reserve position. Each pair of piston actuators is wired in parallel to terminals on the commutator. One terminal of each pair of piston actuators is electrically connected to the commutator ground circuit. The other common terminal of each pair connects to an individual printed circuit pad. This pad is shaped so that it intercepts two tracks of brushes.

*Delrin—trade name for a product manufactured by E. I. Du Pont de Nemours & Co., Inc.

Sixteen pairs of brushes, attached to the commutator brush support (figure 3), are used in pairs for redundancy and will be considered as a single brush. Ten brushes, attached to a common printed circuit which is the electrical ground, wipe the inside track. Their purpose is to short out all actuators that are not in the firing position. The brushes contact the individual pads on the commutator (figure 2). The pads are long enough to maintain contact with one set of brushes for two steps.

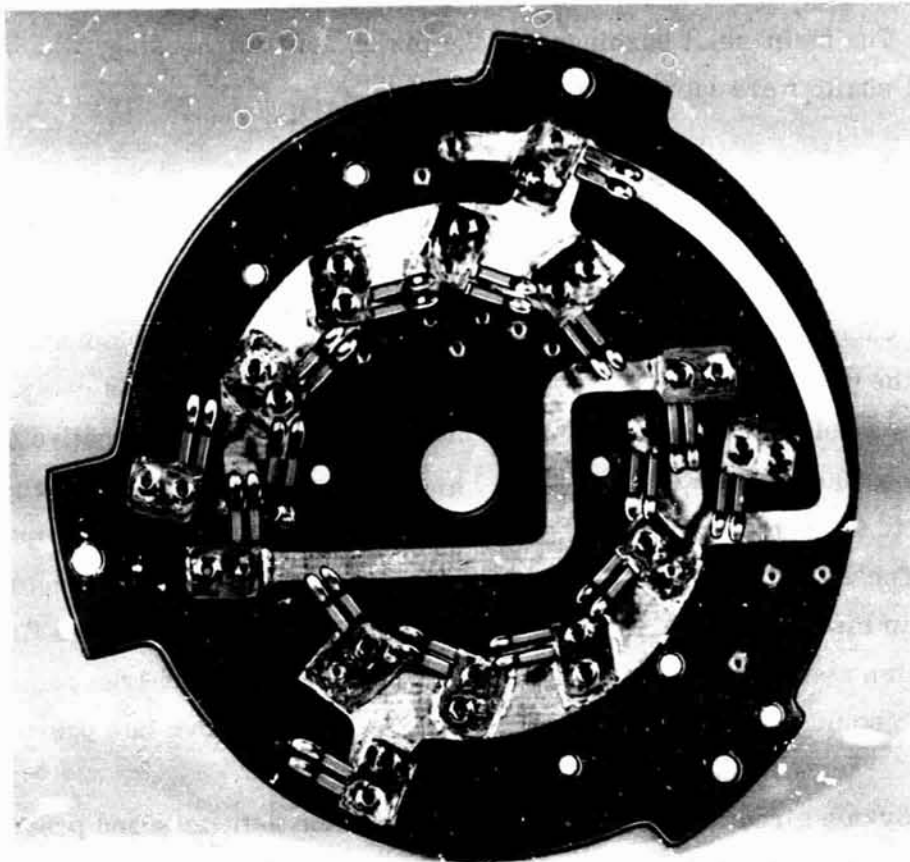


Figure 3 Commutator Brushes

Two brushes on the second commutator track, mounted 180 deg apart, contact the individual pads and direct firing impulses to the piston actuators. Although they are wired together and, therefore, energized simultaneously, it is the position of the commutator that determines which pistons are fired.

The third commutator track is for direct sensing of the side which is in the firing position. This information is transmitted to earth. Two brushes, positioned 180 deg apart, contact grounded pads in this track and complete a circuit. The pattern on the commutator allows only one circuit to be closed at a time.

The fourth commutator track is ground. This track is an annulus conductor to which two brushes, positioned 180 deg apart for redundancy, make contact. The ground terminals of all the piston actuators and the pads for determining the actuator housing position are connected to the annulus conductor. A printed circuit connects the two brushes for the outside track with the ten brushes that contact the inside track.

A miniature electrical connector is located on the opposite side of the commutator brush support (figure 4). When a plug is inserted in this connector, it prevents accidental firing by shorting the actuator circuit.

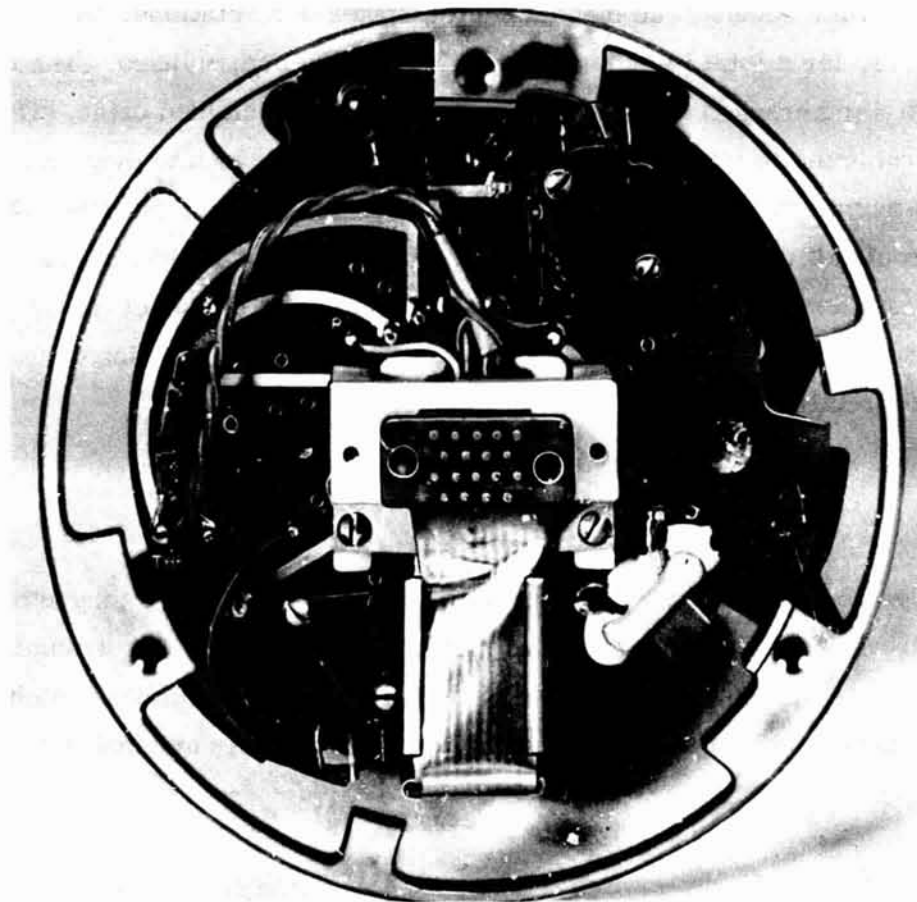


Figure 4 Commutator Brush Support

Fluxgate Position Indicator

Two nonmagnetic snap switches, used to determine if the fluxgate magnetometer is in the 0 or 180 deg position, are attached to the commutator brush support (figure 4). A pin extends from the main shaft, parallel to but displaced 0.093 in. from the shaft axis. As the shaft and pin rotate, the pin displaces the switch arms, which actuate the switch. The fluxgate is on the opposite end of the shaft; therefore, the switches indicate its position. The switch closes a circuit in the experiment electronic system, which transmits this information through the spacecraft telemetry system to earth.

Magnetometer Sensor Circuit

Weak signals are obtained directly from the fluxgate magnetometer; therefore, a commutator cannot be used because there are seven electrical connections and conventional wiring is too cumbersome because the magnetometer makes 5.5 rotations. A tape cable with five layers, for a total thickness of 0.007 in., therefore, is used. The cable is copper-bonded Mylar arranged to provide a seven-conductor shielded cable. One end of the cable terminates in a printed-circuit connector that plugs into the magnetometer sensor. To permit the desired rotation, the cable is coiled in a housing beneath the sensor. It is routed through a U-shaped conduit out and over the indexing mechanism, and terminates in an interface connector which is mounted on the center of the brush support board on the side opposite the brushes. All wires from the indexing device that mate with external circuitry are routed through this connector.

DEVELOPMENT PROBLEMS

When the device was first attached to the spacecraft boom and tested, the magnetometer rotated 360 deg instead of 180 deg. High-speed movies clearly showed the dynamic coupling between the ratchet arms and twisting of the boom when the rotating ratchet arm hit the stop. This motion caused the ratchet arms to return to their original position,

and the magnetometer continued rotating through 360 deg until it returned to its initial position of 0 deg. In this position, however, the resulting forces from the impact held the ratchet arms in position. This situation was corrected by increasing the off-center spring tension and by installing an additional spring to hold the ratchet arms in the 180-deg position.

Two interesting problems occurred with materials selected for this device. In both cases, materials which are normally nonmagnetic were found to be magnetic. In one instance the Elgiloy power spring had oxidized due to a heat treatment, resulting in a slightly magnetic oxide coating. In the other, the position-indicating snap-switch cases and the seals through which the piston actuator electrical leads passed were made of a glass-filled plastic resin that was found to be magnetic. Investigation revealed that the magnetic condition was a function of the fiber length; shortening the glass fibers corrected the condition.

ALTERNATIVE CONFIGURATIONS

There are various methods for obtaining the same mechanical output; e.g., the dual ratchet arms could be replaced with a single ratchet arm and gear-train coupling. Such a device, utilizing a planetary gear system, has been built. The bistable escapement was selected for this application principally because it provides an additional fail-safe feature. This feature ensures proper sensor alignment because it can latch only in the 0 to 180 deg positions.

OTHER APPLICATIONS

Other applications for this device include an X-ray camera for sounding-rocket experiments. In this type of camera, each frame has its own filter, and these frames must be positioned accurately for calibration. This device could also be used as a non-magnetic command programmer in which each step of the commutator initiates a different event.

CONCLUSION

The program described in this report substantiates the feasibility of the selected approach; relatively few problems were encountered, and these were satisfactorily resolved. The indexing is positive; the sensor rotates 180 deg, ± 10 min within 12 sec after receipt of command, and only on command. The permanent magnetic field of the model is less than the required 0.25 γ and the power consumption is much less than 1 watt.

The device was first flown on the Pioneer-VI spacecraft, which was launched 16 December 1965. It was first actuated on 23 December 1965, and it has been actuated four times since then. It will be flown again on another Pioneer spacecraft later this summer.

LOW-TEMPERATURE EFFECTS ON MATERIALS FOR AEROSPACE MECHANISMS

By Warren E. Henry
Lockheed Missiles & Space Company

SUMMARY

N67 16916

A knowledge of the effects of low temperatures on materials is becoming increasingly vital to the conduct of scientific and technical tasks involved in space exploration and related ventures. Advantages of low-temperature technology are: (1) the avoidance of mechanical or other failures in spacecraft which are normally subjected to low temperatures, (2) the greater sensitivity and increased resistance to fatigue of devices under low-temperature conditions, with improved performance compared to that possible at higher temperatures, and (3) the special unique properties evidenced by certain materials under low-temperature conditions. This study encompasses the cataloging, evaluation, and correlation of properties. Suggestions and examples of applications of cryogenic materials are given, including superconducting gyroscopes, high-sensitivity indicators, and high-reliability aerospace mechanisms.

INTRODUCTION

Aerospace mechanisms, involving moving parts in aerospace vehicles as well as rigid body motions in space, depend vitally on the following properties of the materials from which they are fabricated:

- Mechanical
- Thermal
- Electrical
- Magnetic

These properties are often temperature-dependent (refs. 1-4). This characteristic must therefore be recognized, understood, and used in the design of aerospace mechanisms (ref. 5), since they are normally subjected to very low temperatures in the space environment (e.g., approaching absolute zero). Ensuring best performance in space demands an appreciation of the properties of aerospace materials at both high and low temperatures; there is often a correlation between high-temperature properties and low-temperature properties.

Aerospace mechanism instrumentation can be enhanced by taking advantage of low-temperature properties of materials, such as high magnetic intensities with rare earths and high magnetic fields in large volumes for radiation shielding of sensitive components of aerospace mechanisms. Further, many propellants for aerospace mechanisms must be kept at low temperatures.

Special magnetothermal properties of materials at low temperatures can be used for temperature control at the surfaces of aerospace vehicles, thus protecting the mechanisms that are subjected to wide variations of temperature. It must be remembered that the aerospace mechanisms loop may include man — a particularly fragile "mechanism."

The reliability of aerospace mechanisms can depend on temperature; many mechanical and other failures are directly traceable to temperature effects. Involved here are fatigue, flutter, frequency considerations, etc.

Low temperature technologies can be used for special mechanisms, such as superconducting gyroscopes for guidance and stabilization and superconducting galvanometers and bolometers for supersensitive sensor applications. Finally, an understanding of low-temperature effects can lead to increased understanding of the electronic structure of the atom, thus laying the foundation for further application to new and improved aerospace mechanisms.

In general, the effectiveness, reliability, and usefulness of aerospace mechanisms depend on the properties of materials and systems, and on the controlled changes that can be effected in such properties. These properties, in turn, can be highly temperature-dependent. If, for example, A represents behavior of an aerospace mechanism, P represents a pertinent physical property, and T represents the absolute temperature, the following relations can be expressed

$$dA = \sum_{n=1}^N \left(\frac{\partial A}{\partial P_n} \right)_T dP_n \quad (1)$$

$$dP_n = \left(\frac{\partial P_n}{\partial T} \right)_{P_1 \dots P_{n-1}; P_{n+1} \dots P_N} dT \quad (2)$$

where

dA = Total infinitesimal change in the aerospace mechanism behavior

dP_n = Total change caused by temperature of nth physical property

N = Number of physical properties involved (both known and unknown)

n = Index number of physical property

Thus,

$$dA = \sum_{n=1}^N \left(\frac{\partial A}{\partial P_n} \right)_T \left(\frac{\partial P_n}{\partial T} \right)_{P_1 \dots P_{n-1}; P_{n+1} \dots P_N} dT \quad (3)$$

TEMPERATURE-DEPENDENCE OF PHYSICAL PROPERTIES OF MATERIALS

The successful, optimum operation of aerospace mechanisms is dependent upon the properties of material and upon changes in such properties. (See equation 1.) The general change in physical properties is given by equation (2). The chief physical properties applicable here fall under the four categories previously mentioned.

Temperature-Dependence of Mechanical Properties at Low Temperatures

Significant aspects of the effects of temperature on mechanical properties are as follows:

- Elastic Constants. The elastic constants of simple metals have been calculated from quantum mechanics and first principles by Löwdin for absolute zero. Some theoretical work has been done on the temperature-dependence of elastic constants. Experimental work has been done by Overton (ref. 2) and others on some metals and insulators at low temperatures, and there are examples of several types of changes with temperature of the C_{11} , C_{12} , and C_{44} elastic stiffness constants at low temperatures. This fact must be borne in mind when an aerospace mechanism depends on the value of the elastic constants of materials, for there are sometimes large as well as discontinuous changes in the stress-strain relationships at low temperatures.
- Tensile Strength. At low temperatures, the yield stress can change. For some materials, such as certain stainless steels, the tensile strength fortunately increases with low temperatures. However, for each material used, the changes with temperature must be studied and tested at low temperatures, such as in 302 and 310 stainless steel at 25°K and 303 at 21°K. It is necessary to take into account the effect of cycling at low temperatures. The plastic flow is usually less pronounced at low temperatures but should be tested on new materials to be used in aerospace mechanisms.
- Damping. The internal friction at a given flexing frequency leading to damping or heating is temperature-dependent. Alpha brass is an example of a material subject to this effect.

Thermal Properties at Low Temperatures

Many thermal properties change at low temperatures. Following are some examples:

- Specific Heat. In metals, specific heat changes rapidly as temperatures fall below the Debye temperature, varying as the cube of the

absolute temperature. This specific heat is significant for aerospace mechanisms where heat dissipation and temperature control are involved.

- Thermal Conductivity. The heat-conducting capacity is a function of temperature at low temperatures. As the temperature is lowered, most alloys decrease in thermal conductivity. On the other hand, elementary pure metals, such as copper and aluminum, reach a peak in thermal conductivity at low temperatures. The degree of this thermal conductivity determines the ease with which equilibrium can be obtained and retained in aerospace mechanisms.

Electrical Properties

Metals usually increase in electrical conductivity as the temperature decreases, and the conductivity becomes infinite, in many cases, at a superconducting transition. This circumstance makes possible many applications to aerospace mechanisms. Semiconductors and insulators, however, show a decreased electrical conductivity as the temperature is lowered.

Magnetic Properties

Magnetic properties can be categorized as diamagnetic and paramagnetic. Diamagnetism arises from the orbital motion of electrons around atoms and through molecules, which occurs in all substances. Diamagnetism, except for superconductivity, is small and temperature-independent.

Opposed to diamagnetism is paramagnetism. Strong paramagnetism arises from unpaired electrons in the unfilled shell, or from itinerant electrons in an electron energy band. Strong paramagnetism is temperature-dependent; magnetic susceptibility increases as temperature is lowered. As the temperature lowers, paramagnetic material becomes either ferromagnetic, ferrimagnetic, antiferromagnetic, or metamagnetic. For example, anhydrous chromium trichloride becomes ferromagnetic at

16°K whereas certain alloys of manganese, antimony, and chromium are metamagnetic, i.e., ferromagnetic at room temperature and antiferromagnetic at lower temperatures. It is necessary to study the magnetic characteristics of materials for aerospace mechanisms at low temperature in order to obtain the suitable, reliable characteristics for design of aerospace mechanisms. General studies are necessary in order to learn how to modify the ferromagnetic properties or the superconductive properties of materials to be used in the future.

DEPENDENCE OF AEROSPACE MECHANISMS ELEMENTS ON PHYSICAL PROPERTIES

Examination of aerospace mechanisms reveals that capabilities and performance are closely related to the physical properties of materials. A few examples warrant consideration.

Elastic Constants

One example of the importance of elastic constants is the way in which they enter into calculations (or determination) of flutter speed, since the flexure-torsion is involved. The selection of materials, as well as the size and shape of members, should be based on the values of the elastic constants. The stress-strain characteristics are important for all mechanisms where stresses are applied or where distortions (e.g., elongation) are important. Also, the force constants determine important vibration or other frequency characteristics.

Damping

Partial or full critical damping is essential in guaranteeing the safety and reliability of aerospace mechanisms. Parasitic (mechanical) oscillations can set up even with small applied forces. At low temperatures, internal friction must be high enough to counter any tendency of the mechanism to oscillate at a characteristic frequency. An easily demonstrated example is a lead bell operated at low temperatures.

Fatigue

Obviously, parts that are flexed, or otherwise mechanically cycled, must be fatigue-proof beyond the extent to which cycling occurs. Ground test failure rates on aerospace mechanisms are disconcertingly high (ref. 6).

Tensile Strength

This consideration is obviously important for any component of a mechanism that must be able to support (by a healthy margin) the forces contended with under all possible conditions of operation. Tensile-strength deficiencies are likely to result in catastrophic failures.

Magnetization and Magnetic Susceptibility

Many parts of mechanisms (e.g., motors, timers, dampers, and controllers) are dependent on the intensity of magnetization of a component, remanence of a part, and susceptibility and coercivity of a material.

Miscellaneous Properties

Examples of other relevant properties are hardness, particularly for gimbals; size and shape-restricted tolerances for close fitting or precision aligned members; and radiation transmission characteristics for infrared radiation.

DEPENDENCE OF AEROSPACE MECHANISMS ON TEMPERATURE

In accordance with equation (3), it is possible to examine the direct temperature dependence of the behavior of an aerospace mechanism.

Flutter Speed

If A is a behavior such as flutter speed (ref. 7), the calculations are based on internal friction (or structural damping), elastic constants, and the c.g. The temperature-dependence of this calculated value is balanced off by the temperature of the damping. Redesign is carried out until this balancing is obtained, and can include an additional automatic damping based on a magnetic-damping increase as the temperature decreases.

Fatigue

There are cases of increase of reliability against fatigue fracture of brass as the temperature decreases. This was shown by Long and Simon (ref. 1) in connection with the design of moving parts at liquid hydrogen and liquid helium temperatures. In other words, if A is the behavior in terms of reliability or running time before failure, P_i the property of fatigue resistance, and T the absolute temperature, then, in accordance with equation (3),

$$\left(\frac{\partial A}{\partial P_i} \right)_T > 0$$

$$\left(\frac{\partial P_i}{\partial T} \right)_{P_2 \text{ --- } P_N} < 0$$

and, therefore

$$\frac{dA}{dT} < 0$$

which indicates that the time of use of the mechanism is increased by lowering the temperature.

The situation with certain steels is just the opposite. Here

$$\left(\frac{\partial A}{\partial P}\right)_T > 0$$

$$\left(\frac{\partial P}{\partial T}\right) > 0$$

so that

$$\frac{dA}{dT} > 0$$

and a decrease in temperature brings about a decrease in reliability and in operating time.

Stability at Low Temperature

Among the threats to stability is a change in elastic constants. In this case, A represents the behavior tending toward stability, and the effect of temperature on the stability through changes in damping is the question presented.

- A lead bell, for example, has a sonorous ring at liquid-nitrogen temperatures and yields a thud at room temperatures. If P is internal friction,

$$\left(\frac{\partial A}{\partial P_i}\right)_T > 0$$

$$\left(\frac{\partial P_i}{\partial T}\right)_{P_1 \dots P_i - 1 ; P_{n+1} \dots P_N} > 0$$

then $(dA)/dT > 0$, and the stability due to damping decreases with decreasing temperature.

- Considering magnetic damping at low temperatures, a magnetized member is moved with respect to an electric current. Here, if P_i represents magnetic susceptibility

$$\left(\frac{\partial A}{\partial P_i}\right)_T > 0$$

but

$$\left(\frac{\partial P_i}{\partial T}\right) < 0$$

therefore

$$\frac{dA}{dT} < 0$$

and the stability can be increased by lowering the temperature of the normal magnetic material.

- Considering eddy current damping, P_i is taken as electrical conductivity.

$$\left(\frac{\partial A}{\partial P_i}\right)_T > 0$$

$$\left(\frac{\partial P_i}{\partial T}\right) < 0 \quad (\text{for a metal})$$

$$\frac{dA}{dT} < 0$$

so that a decrease in temperature gives an increase in stability from damping.

Stress-Strain at Low Temperature

Let A represent the behavior against yield under stress. If P_i is the tensile strength

$$\left(\frac{\partial A}{\partial P_i} \right)_T > 0$$

Now for stainless steel 302

$$\left(\frac{\partial P_i}{\partial T} \right) < 0 \text{ and } \frac{dA}{dT} < 0$$

and decrease in temperatures at low temperatures leads to increased resistance to yield stresses.

Some discontinuities have been noted in stress-strain curves at low temperatures for stainless steel 302 and 303. Whenever there is a low-temperature phase transistion, the pertinent properties can change markedly.

Surfaces and Lubricants

Smoothness of operation can depend on the relative hardness of rubbing surfaces.

Characteristics of the lubricant are also important. If the temperature is lowered, the lubricant can become too viscous and finally glassy. Animal fat has proved to be a good lubricant at low temperatures.

Magnetohydrodynamic Propulsion

Let A represent propulsion behavior or effectiveness. If P_i is the intensity of magnetization of the active component,

$$\left(\frac{\partial A}{\partial P_i} \right)_T > 0$$

$$\left(\frac{\partial P_i}{\partial T}\right) < 0$$

thus

$$\frac{dA}{dT} < 0$$

and the propulsion is more effective the lower the temperature.

Maintaining Relative Tolerances

If two members fit each other to within close tolerances, temperature is important. If A is now a difference tolerance such as 0.0005 in., separation between two concentric cylinders,

$$\left| \left(\frac{\partial A}{\partial P_i}\right)_T - \left(\frac{\partial A}{\partial P'_i}\right)_T \right|$$

must be bounded and

$$\frac{dA}{dT}$$

must be limited, which means that

$$\left(\frac{\partial P_i}{\partial T}\right) \text{ and } \left(\frac{\partial P'_i}{\partial T}\right)$$

must be bounded. Another case in which bounds must be put on the expansion and contraction is the case of the change of the frequency of components, as in the instance of a rotor affected by a change in the moment of inertia.

SPECIAL APPLICATIONS OF LOW TEMPERATURES

Many low-temperature phenomena can be used in connection with aerospace mechanisms. Examples of current uses are low-temperature fuel gages, fuel pumps, and coolants for sensors and control devices. Many of these are subject to improvement. Following are examples of future uses of low-temperature technology in aerospace mechanisms design:

- The superconducting gyroscope based on the expulsion of magnetic flux from a shaped superconductor and thus suspending a suitable fast-speed rotor for a gyroscope.
- The superconductive galvanometer based on a reduction of the resistive component of the galvanometer coil impedance to zero. This hypersensitive instrument will be useful in high-sensitivity aerospace mechanisms.

CONCLUSIONS

The aerospace mechanism is unavoidably subject to low temperatures. Aerospace mechanism behavior is related quantitatively to physical properties of component materials and their physical arrangement. The four categories of properties — mechanical, thermal, electrical, and magnetic — can vary markedly with temperature. Finally, direct dependencies of aerospace mechanisms behavior on temperature have been outlined and illustrated, establishing the importance of low-temperature effects on materials for aerospace mechanisms.

REFERENCES

1. Long, H. M.; and Simon, F. E.: *Nature*, vol. 172, 1953, p. 581.
2. Overton, W. C.; and Gaffney, J.: *Phys. Rev.*, vol. 98, 1955, p. 969.
3. Collins, S. C.; Ezekiel, F. D.; Sepp, O. W.; and Rizika, J. W.: *Proc. Am. Soc. Testing Materials*, vol. 74, 1956, pp. 1-13.
4. Henry, W. E.: *High Magnetic Fields*, M.I.T.-Wiley Presses, Cambridge and New York, 1962, p. 552.

REFERENCES (continued)

5. Henry, W. E.: Proc. Lockheed Research and Engineering Symposium for Lockheed Management, Chapter 8, Palo Alto, Calif., May 23-24, 1963.
6. Space and Aeronautics, Jan. 1964, p. 92.
7. Missin, E.: J. Roy. Aeronaut. Soc., vol. 68, 1964, p. 357.

HIGH-IMPACT-RESISTANT MECHANISMS*

By James L. Adams
Jet Propulsion Laboratory
California Institute of Technology

SUMMARY

N67 16917

Investigations performed at the Jet Propulsion Laboratory indicated that a large variety of complex and efficient spacecraft mechanisms can be built to survive impacts on the order of 10,000 g from several hundred fps. Problems associated with ruggedizing such mechanisms are discussed in this paper, and a variety of related design techniques and methods are presented. Several specific mechanisms designed to survive a range of shock environments are described. Results from investigations conducted by other organizations confirm the conclusions arising from the JPL studies.

INTRODUCTION

Unmanned explorations of planets and their satellites must eventually include the landing of scientific payloads. The ability of landed equipment to survive influences the selection of landing modes and the probability of mission success. Spacecraft capable of such landings require mechanisms to accomplish various functions associated with erecting and articulating the spacecraft and performing scientific experiments. Various representative mechanisms and related components are being developed at the Jet Propulsion Laboratory (JPL). Some of the findings of the JPL investigations are discussed in this paper.

*This paper presents the results of one phase of research conducted at the Jet Propulsion Laboratory, California Institute of Technology, under Contract NAS7-100, sponsored by the National Aeronautics and Space Administration.

DESIGN PHILOSOPHY

Impact levels investigated at JPL include those extending up to 10,000-g peak acceleration with energies corresponding to pre-impact velocities up to 500 fps. This range covers impacts likely to result from unsophisticated retro-braking or untrimmed aerodynamic entries. The Ranger seismometer capsule, for example, was to impact at approximately 200 fps. The payload was covered with 7 in. of balsa wood to absorb the kinetic energy. The resulting impact acceleration at the payload would have been on the order of 2,500 g.

In approaching problems in ruggedizing equipment capable of surviving impacts of this order, JPL emphasizes stiffness in order to minimize excessive deflection. Energy absorption and acceleration-limiting material and equipment is applied to the payload as a unit rather than to components of the payload. This approach is logical for impacts of 2,000 to 10,000 g since deceleration strokes range from 0.7 in. (an average of 10,000 g from 200 fps) to 23 in. (an average of 2,000 g from 500 fps). Local use of crushable structure or shock mounting is useful to attenuate sharp peaks on the shock pulse, but rather difficult to use for attenuating average shock levels. About 5 in. of crushable structure would be necessary to halve the deceleration levels on a component in a payload exposed to a rectangular 10,000-g pulse from 500 fps.

Experience shows that mechanism ruggedization for high impact is quite straightforward. All parts must be sufficiently sturdy to survive the impact, and all bearing points must be adequately sized. Balance must be controlled to avoid unwanted torques. After preliminary sizing through the use of simple, analytical techniques, the development of ruggedized mechanisms proceeds on a cut-and-try basis. Although improved analytical design techniques are being pursued at JPL, the program at this time is largely experimental in nature. Analytical techniques such as wave theory and shock spectrum analysis have not been generally used because of the geometrical complexities

involved. The intent of the JPL effort has been to demonstrate feasibility and search for problems, rather than optimize.

TESTING

The Jet Propulsion Laboratory utilizes a 50-ft drop tower, a bungee-powered shock machine, and 3-, 6-, and 22-in.-diameter air guns for performing impact tests. The drop tower is used for tests up to 50 fps, the shock machine up to 200 fps, and the air guns up to 500 fps. The majority of the mechanism testing has been done on the shock machine, shown in figure 1. This machine utilizes two 20-ft strands of 3/4-in. bungee cord for energy. At 80-percent elongation, this cord stores sufficient energy to accelerate a 10-lb load (test specimen plus carriage) to 200 fps. This machine consists of a specimen carriage which rides on a pair of I-beam guide rails, an impact block, a cocking mechanism, and a release device. Various velocities can be achieved by varying the release point.

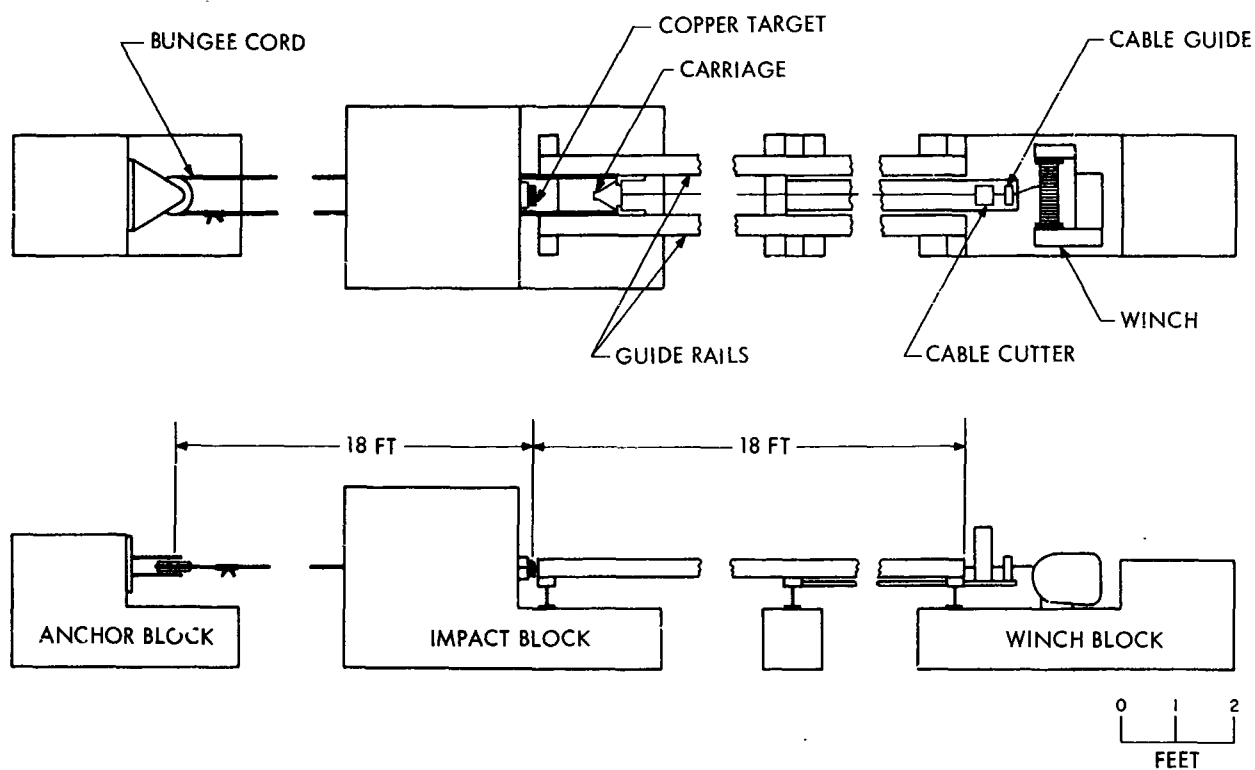


Figure 1 Jet Propulsion Laboratory Horizontal Shock Machine

Shocks are obtained by impacting a penetrating tool on the nose of the carriage against various target materials attached to the impact block. Typically, flat-nosed tools are impacted against annealed copper targets. Such a test from 200 fps might produce a rectangular pulse with an average amplitude of 10,000 g, a rise time of 0.1 ms, and a duration of 0.6 ms.

Mechanisms to be tested are either bolted directly to the test carriage or held in a rigid fixture. An accelerometer is mounted on the carriage or on the specimen to record the impact shock. Accelerometer data as well as strain gage data and other electrical signals are transmitted from the carriage by means of trailing wires. Tubing and cables can also be attached to the carriage to provide electrical power and compressed gases to the specimen if needed. Specimens are typically tested in all principal distinguishable directions. An axially symmetrical device (e.g., a turbine) would be tested axially and radially. A more complex mechanism might be tested in six different directions. If damage is not cumulative, specimens are tested at increasing impact levels until failure occurs or until the target level is reached.

RUGGEDIZED MECHANISMS

One of the more difficult problems in ruggedizing mechanisms for high-impact survival is that of providing adequate bearing area to prevent damage. This is especially true if rotating element bearings are used, as they often are in space. Many mechanical spacecraft functions are powered by small electric motors utilizing rotating-element bearings. Tests performed at JPL on rolling-element bearings under impact indicate that it is impractical to expect standard bearings to support objects such as motor rotors at g levels on the order of 10,000. Design approaches for supporting bearings that will not transmit impact loads through the rolling elements therefore have been investigated.

Figure 2 is an exploded view of a motor which has been ruggedized. This is a synchronous high-torque (1.1 in.-oz at 8 000 rpm) motor (Gaylord Rives No. B344 size 13) which has been modified by supporting the bearings in six-degree-of-freedom spring mounts. The rotor and the housing have been reworked so that clearances are small (typically, 0.005 in. axially, and 0.001 in. radially).

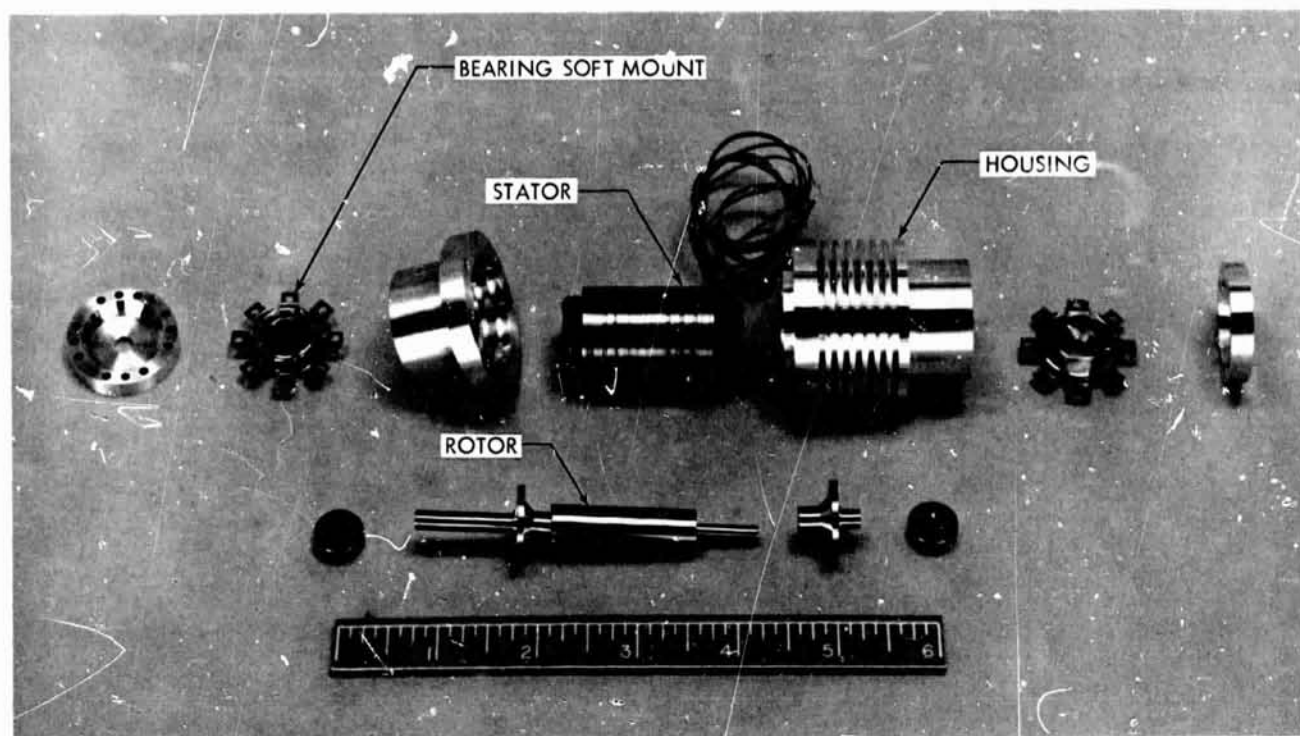


Figure 2 Ruggedized Electric Motor

During impact, the springs deflect sufficiently to prevent bearing loads from becoming damaging. The major loads are absorbed by bottoming between the rotating mass and the housing. Similar modified motors have survived repeated impacts of 10,000 g from 200 fps in all principal directions.

Figure 3 shows a prototype air turbine which was fabricated and tested. This device was built to test the spring-mounted bearing approach with a relatively large (8 oz) mass rotating at high speed during impact. The turbine was rotated at approximately 30,000 rpm with compressed air before, during, and after impact. The unit was impacted axially and radially at 10,000 g from 165 fps. Although the rotating speed changed slightly during impact, the device regained its pre-impact rotating speed and operated successfully for a 2-hr period before shut-down. Examination did not reveal any significant bearing damage, and damage to the turbine and housing was small.

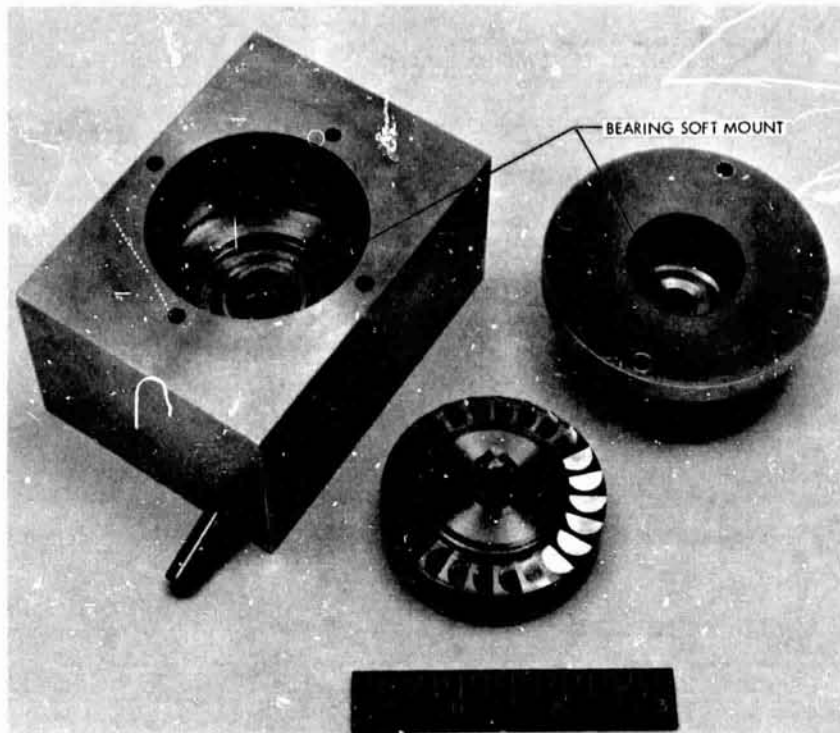


Figure 3 High-Impact Air Turbine

Figure 4 shows a spring-operated rotary gas valve developed in conjunction with a ruggedized scientific instrument effort. This device is a three-position valve used to interconnect several gas lines in various combinations. The valve is powered by a "spirator" spring which stores sufficient energy for 45 cycles. The unit, which weighs 0.5 lb and can be triggered by a small solenoid, has successfully withstood impacts of 5,000 g from velocities in excess of 100 fps. Although it has not been tested at 10,000 g, the valve should survive such impact levels with no major problems.

Figure 5 shows a pressure regulator developed for low flow rates and stability under high impact. Many pressure regulators are inadequate under impact because they utilize a large mass and a spring to achieve the proper dynamic characteristics. This regulator utilizes diaphragms as both the pressure sensor and springs. For use in space, the back of the diaphragms must be covered with sealed chambers so that the output is insensitive to ambient pressure.

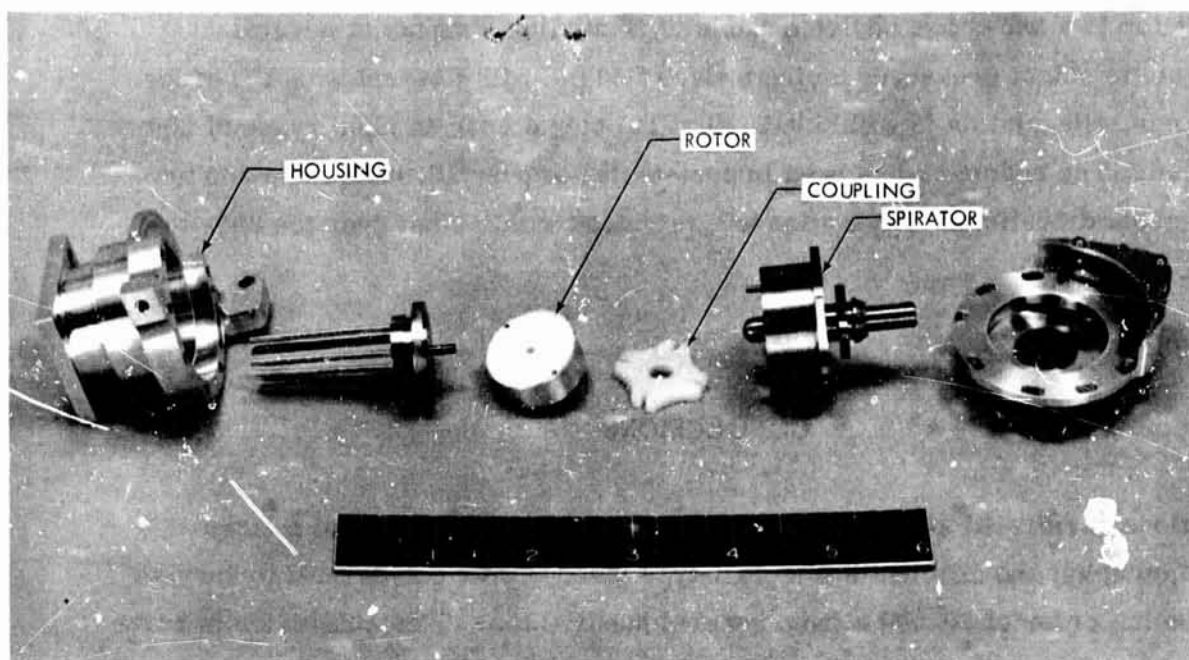


Figure 4 Rotary Gas Valve

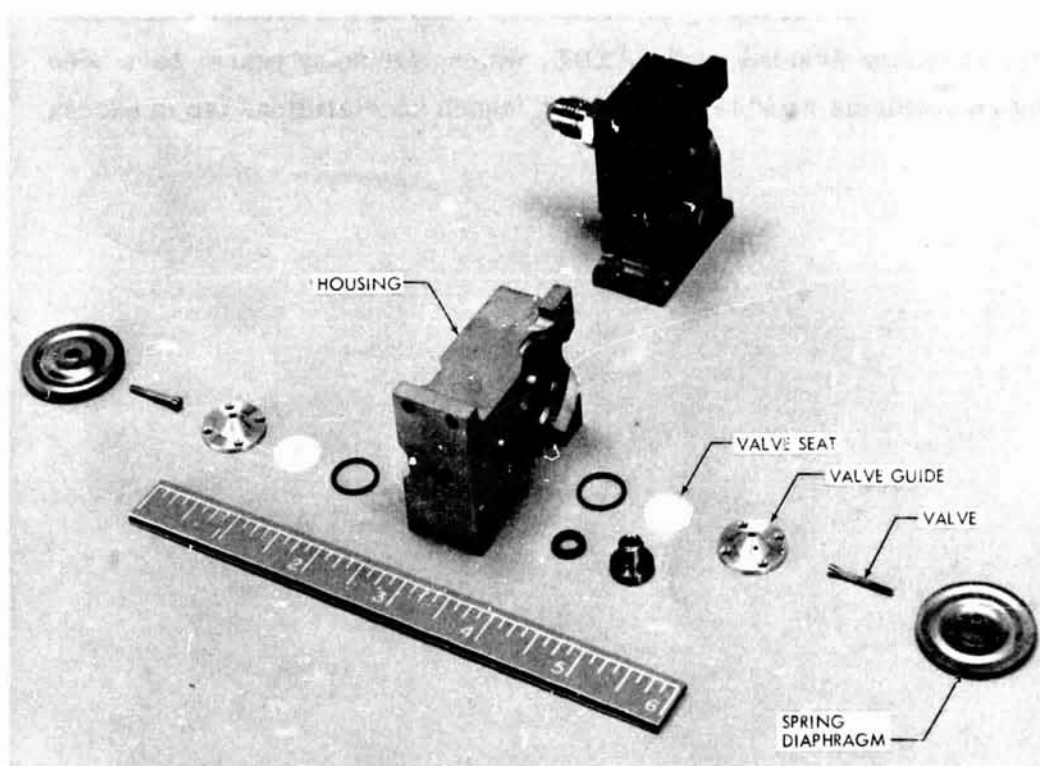


Figure 5 High-Impact Pressure Regulator

The regulator is a two-stage device capable of regulating a supply at several thousand psi to output pressures on the order of 60 psi with flow rates on the order of 50 ml/min. Regulation is within 0.5 psi at the output over an input range of 200 to 1,500 psi. The regulator has been impact-tested at over 10,000 g from 200 fps in all principal directions. Regulation has remained within 1 psi over the 200- to 1,500-psi input range.

CONCLUSIONS

Investigations performed at the Jet Propulsion Laboratory indicate that a large variety of complex and efficient spacecraft-type mechanisms can be built to survive impacts on the order of 10,000 g from several hundred fps. This conclusion is borne out by work performed by other organizations, such as the Philco - Aeronutronic Division, which developed a mechanical facsimile system for possible hard landing from a Ranger spacecraft, and ordnance laboratories, such as the Diamond Ordnance Fuze Laboratory, Picatinny Arsenal, and CARDE, which, for many years, have been developing fuzing mechanisms capable of surviving launch accelerations far in excess of 10,000 g.

A PYROTECHNIC SHOCK ISOLATION MECHANISM

By A. I. Ikola
Lockheed Missiles & Space Company

SUMMARY

N67 16918

The detonation of explosives in pyrotechnic devices produces several sources of shock excitation. This shock, which may be considered as measurable and unmeasurable excitation, can cause equipment failures. Solution of a pyrotechnic shock problem therefore calls for consideration of testing, analysis, equipment modification, and shock isolation. A shock mount that has proved simple to use and extremely effective in protecting equipment is discussed in relation to problems generally present when using shock mounts. Test results demonstrating the performance of the shock mount are also presented.

INTRODUCTION

Pyrotechnic shock is generated by such devices as Primacord, jet cord, squib valves, pin pullers, strap cutters, bolts, and nuts. These devices are used in missiles and spacecraft to perform such functions as staging, nose-fairing separation, valve operation, antenna erection, and satellite ejection.

High reliability, low weight, and a long shelf life are advantages that make these devices applicable to many designs. A disadvantage, however, is that they use propellants or explosives which have rapid burning rates that produce high shock input to the vehicle structure.

The immediate effect of a detonation occurs within the first few microseconds when stresses are produced in the structure in the vicinity of the pyrotechnic device. The

stress waves are quickly transmitted throughout the structure so that, as they are attenuated, the original impulse energy in the detonation is converted into vibrational energy in the structure. This latter effect occurs after approximately 500 μ sec of the detonation.

A second source of shock occurs when the detonation forces rapidly fracture vehicle structure, bolts, or nuts during a stage- or nose-fairing separation. This fracturing of metal is followed by a third source of shock which occurs when the expanding gases from the detonation, or the release of stored tension or compression forces, produce rapid structural distortions near the pyrotechnic device. The combination of these shock sources (and probably several additional sources) produces what is considered the pyrotechnic shock environment.

PYROTECHNIC SHOCK ENVIRONMENT

Description of a pyrotechnic shock environment requires definition of conditions that are considered unmeasurable (or measurable only by highly specialized laboratory techniques) as well as conditions that are measurable by ordinary instrumentation techniques.

Unmeasured Shock

This shock is in the form of stress waves and is characterized by a "jump" or discontinuity in the parameters of the materials. In most isotropic structural materials, shock waves will develop during propagation of compression waves above the yield point of the material. Shock waves will not form, however, nor be maintained, during propagation of tensile stress, no matter how great that stress. A shock wave induced by a pyrotechnic separation device can cause a jump in pressure in the detonation area to several hundred atmospheres in a few nanoseconds. Unmeasured shock, of which the above example constitutes only one type, can cause damage to equipment and vehicle structure.

Measured Shock

This category can be defined as a high-amplitude, complex vibration transient which decays from a maximum amplitude to 10 percent amplitude in approximately 10 ms. The general characteristics of the complex vibration transient are peak amplitudes of approximately 4,000 g, with a predominant frequency of approximately 5,000 cps. Simultaneously present with the high-frequency vibration are the several lower-amplitude and lower-frequency components necessary to complete the complex vibration transient. Although this shock activity level is present within 5 to 10 in. of the device, shocks of lower amplitude are present throughout the vehicle.

PYROTECHNIC SHOCK MEASUREMENT

An extensive shock-measuring program was performed at Lockheed Missiles & Space Company (LMSC), using a flight-quality vehicle. Measurements were made throughout the vehicle with piezoelectric transducers mounted on one-in. cubes of aluminum to sense the shock produced by the pyrotechnic separation of the vehicle from the booster. The data was recorded on a magnetic tape system with a frequency capability up to 10,000 cps. Data reduction consisted of both oscillograms and shock-spectrum analysis.

In general, test results indicated that oscillogram transients and shock-spectrum frequency distribution remained essentially the same, with a significant reduction occurring in the amplitude of the shock as the distance from the shock source increased. Figure 1 shows a typical shock spectrum and oscillogram at 5 in. from the shock source. Figure 2 shows the shock amplitude reduction with increasing distance from the shock source.

APPROACHING A PYROTECHNIC SHOCK PROBLEM

When confronted with a pyrotechnic shock problem, LMSC generally applies four methods of approach, as follows:

- Testing
- Analysis
- Equipment modifications
- Shock isolation

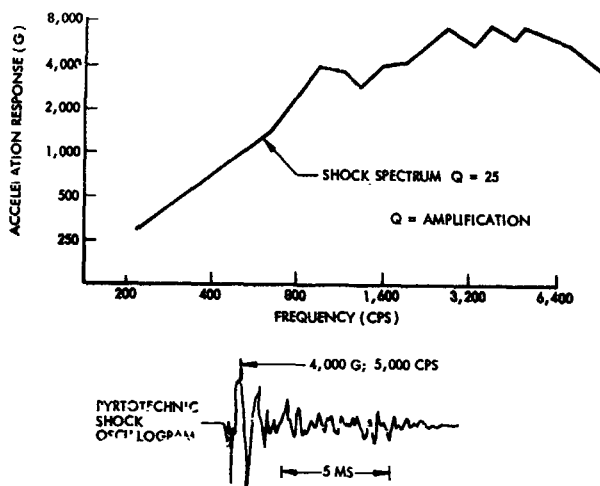


Figure 1 Shock Environment

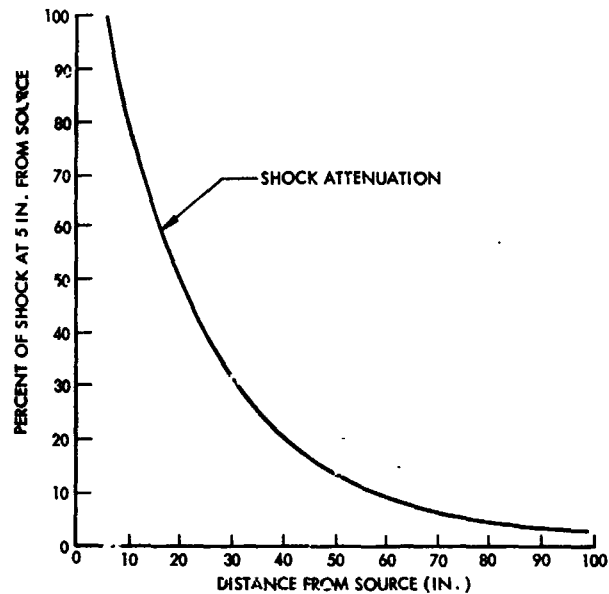


Figure 2 Shock Attenuation

Testing

Testing is the only accepted method at LMSC for obtaining flight qualification of equipment. It is essential that such testing be realistic in order to prevent unnecessary equipment damage or to preclude a false sense of flight confidence. A testing facility developed at LMSC has proved to be a realistic simulation of a pyrotechnic shock environment. The basic requirements for the facility are as follows:

- The pyrotechnic shock environment must be generated by a pyrotechnic source.
- The test facility fixture must be similar to the flight vehicle structure.

Drop- and pendulum-type impulse testers are not used because they produce severe overtests in the lower frequencies and are difficult to control to the desired test spectrum. The rigid test fixtures and the nonpyrotechnic shock source also discourage their use. Such problems as schedules, test costs, and the complexity of research experiments often prevent testing and, as a result, require that alternate methods of obtaining confidence be found.

Analysis

Stress-wave propagation in solids is very difficult to analyze because of the nonlinear stress-strain relationship of materials during plastic behavior above the yield point. High-speed computers employed to handle numerical techniques have yielded solutions to the one-dimensional wave-propagation problem. Experimentally, techniques have been developed to gather data to establish stress wave parameter relationships (Hugoniot curves), to obtain damage threshold levels, to establish data about damage mechanism and strain rate effects, and to verify the solutions obtained by the analysts. Various workers have recently attempted to obtain a solution to the two-dimensional problems, however, data of real value to the design engineer are not readily available.

Shock-spectrum analysis is used to compare the severity of the measured portion of the pyrotechnic shock environment with equipment specification vibration and mechanical shock tests. This analysis usually shows the pyrotechnic shock to be significantly more severe near the explosive device. As the distance from the shock source increases, the damage potential of the vibration environment (20 to 2,000 cps) eventually exceeds the indicated damage potential in the pyrotechnic shock environment. This technique is suggested only as a means of showing the inadequacy of the typical mechanical shock and vibration tests as a means of substitution for the effects of the pyrotechnic shock. Figures 3 and 4 show a comparison of typical mechanical shock, vibration, and pyrotechnic shock (vibration) environments.

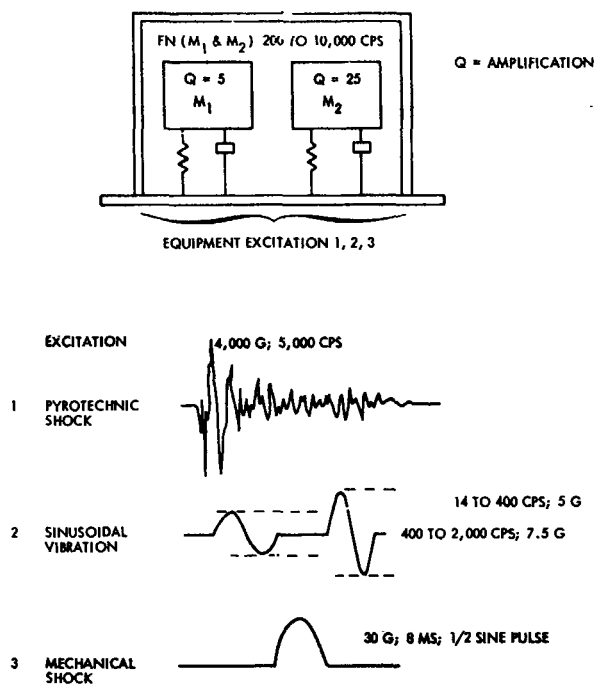


Figure 3 Equipment Excitation

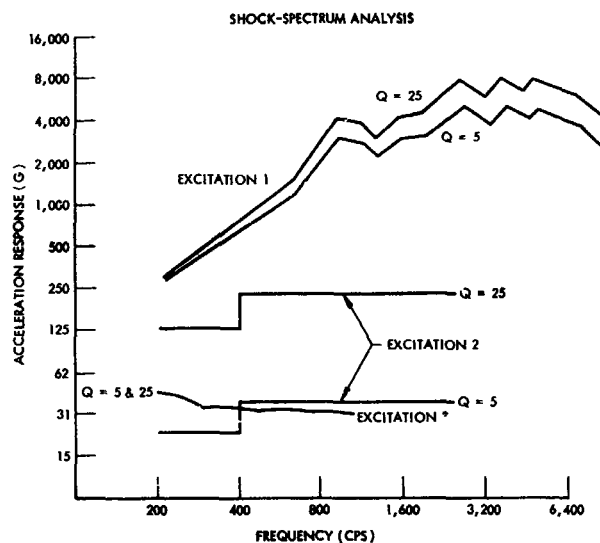


Figure 4 Response Comparison

Equipment Modification

Sometimes, the only practical means of solving a shock problem is by modifying the equipment. The following are some typical modifications:

- Placing relay circuits in an energized rather than de-energized state during shock to decrease the tendency for relay chattering or transferring
- Increasing command-circuit time constants to prevent activation from control circuits that display short-duration chattering and transfer characteristics
- Using timers to unlatch relays suspected of accidental latching during the shock event

Equipment modifications, although adding considerable flight confidence, are not considered as a method of equipment qualification unless the modified equipment is subsequently shock-tested.

Shock Isolation

An effective method of improving equipment performance during a shock event is shock isolation by means of shock mounting. It is, however, only a means of improving equipment confidence unless the mount, in combination with the equipment, is shock-tested.

POTENTIAL SHOCK-MOUNTING PROBLEMS

Commercially available shock mounts will generally do an excellent job of isolating equipment. There are several considerations, however, in addition to shock isolation itself. Among these are the following:

- Installation space
- Weight
- Heat dissipation
- Equipment alignment
- Universal application

Vehicle Structural Vibrations

Vehicle structural vibrations, which range from a few cycles a second to more than 10,000 cps, have been analyzed and incorporated into qualification test specifications for all equipment. Figure 5 shows a vehicle flight-vibration spectrum and vibration qualification levels.

Equipment installation frequencies that coincide with structural frequencies will usually cause equipment flight vibrations in excess of qualification levels. Before installing shock mounts on equipment that has previously been qualified when hard-mounted to a structure, it is necessary that several calculations be made to determine the installation frequency. When these calculations indicate frequencies close to dangerous flight vibrations, shaker tests or pull tests must be used. Figure 4 shows that shock-mounted equipment frequencies between 100 and 300 cps are desirable for use with the vibration environment profile shown.

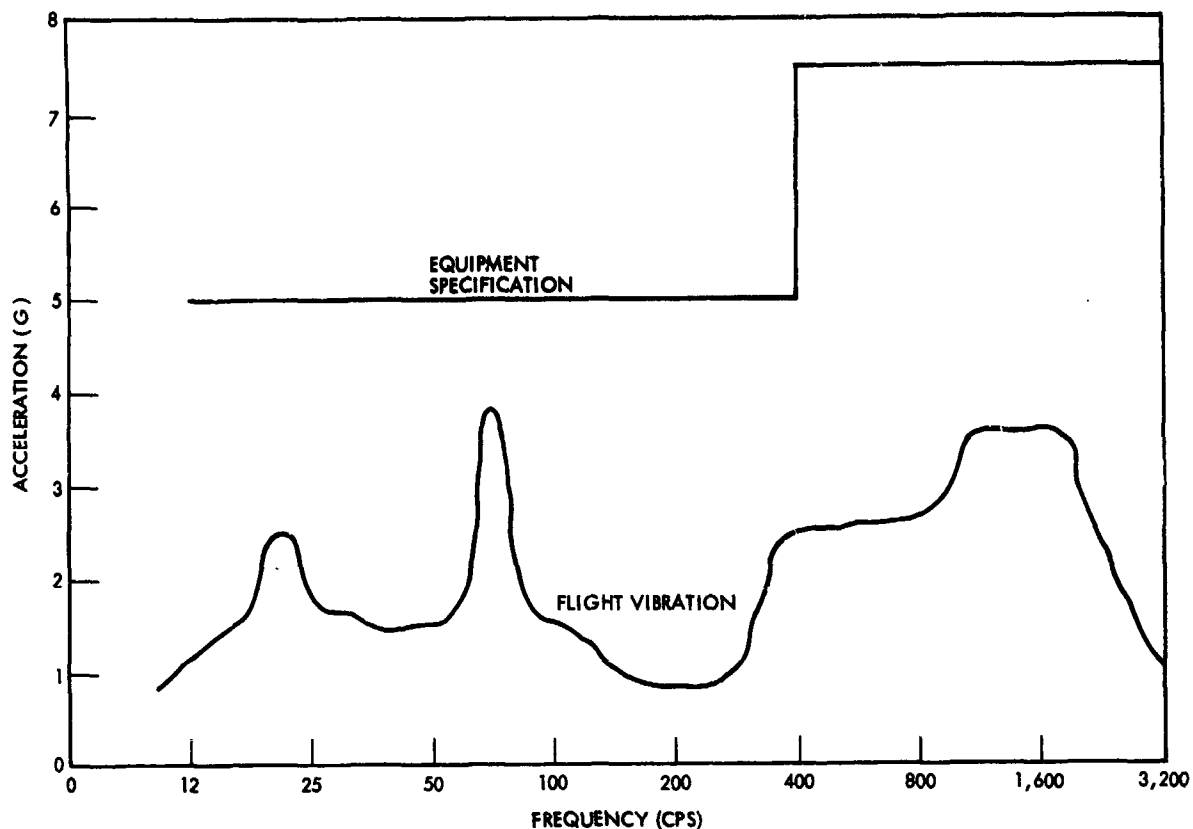


Figure 5 Equipment Specification Vibration and Flight Vibration

Installation Space

Discovery of a shock-sensitive component often entails the installation of a shock mount where adequate space is not available. Shock mounts should therefore be as small as possible, requiring little additional installation space.

Weight

The major objection to the extensive use of shock mounts is the resulting increase in spacecraft weight. Wherever possible, therefore, equipments are qualified for flight without shock mounts.

Heat Dissipation or Absorption

The amount of heat dissipated or absorbed by equipment must be controlled so that operating temperature limits do not exceed qualification levels. A shock mount, when used on high-heat-producing equipment, adds to the thermal problem by acting as an insulator. Shock mounts, therefore, are to be avoided in these cases except where equipment is scheduled to operate for short periods only. A moderate amount of equipment-produced heat may be dissipated by the use of flexible conducting straps between the equipment and the vehicle structure. Such straps are only feasible, however, for equipment that produces a limited amount of heat.

Alignment

Alignment of equipment containing optical or tracking systems is difficult when combined with a requirement for shock mounting. These equipments are costly, often one of a kind, and require maximum shock protection without being subjected to the abuse of testing. The shock mount must maintain accurate dimensional stability once aligned while simultaneously providing the maximum possible shock reduction.

Universal Application

Although less important than performance, universal application is of considerable importance from a cost-reduction standpoint. Each installation should therefore require a minimum of modification to equipment and to the vehicle, as well as a minimum of analysis and testing prior to use.

LMSC PYROTECHNIC SHOCK MOUNT

The type of shock-mount technique generally used at LMSC for equipment protection is shown in Figure 6.

The mount configuration consists of two silicone rubber washers and a length of plastic shrink tubing. The washers isolate the equipment-package mounting flange from the

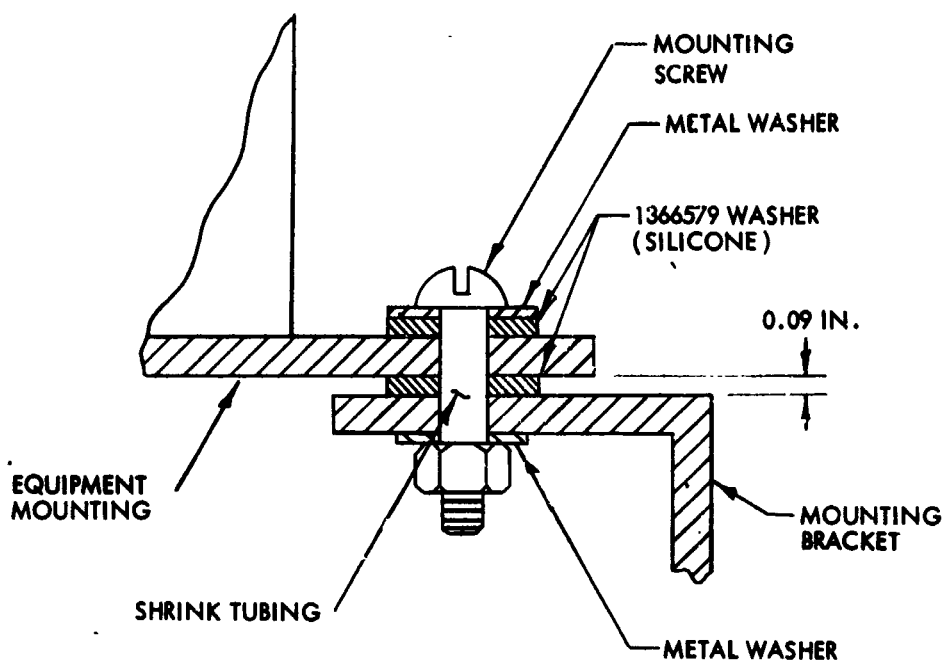


Figure 6 Shock Isolation Mount

vehicle structure. The shrink tubing placed around the mounting bolt completes the isolation of the equipment from the vehicle structure. The washers are semirigid, being in the 50 to 60 durometer range. The installation is completed by using a gage to control the compression of the washers from an initial 0.125-in. to a 0.090-in. thickness.

This configuration, in addition to providing good shock isolation, has well satisfied requirements relative to structural vibrations, space limitations, weight, equipment alignment, and universal application.

Heat dissipation requirements, when not excessive, are solved by using conducting straps similar to those used with standard mount systems. Vehicle structural vibrations have not presented any significant problems, since the weight and installation configuration of most equipment produces installation frequencies between 100 and 200 cps. This frequency is ideal for separating equipment vibration from major vehicle structural vibration while simultaneously acting as a typical vibration isolator for the higher-frequency vehicle vibrations. Considering the vibrations generated during the pyrotechnic shock (Figure 1), it also is reasonable to predict substantial reductions of the measured

pyrotechnic shock. To return to the unmeasured portion of the pyrotechnic shock environment (i.e., stress waves in the structure) it is theorized that the shock reaching the equipment will be significantly attenuated by the impedance mismatch between the vehicle structure and the rubber mounts.

SHOCK-MOUNT PERFORMANCE

Although the concept of the simplified LMSC shock mount seemed practical the mounts were subjected to pyrotechnic shock tests before being accepted for vehicle use. The equipment tested was a small package containing several relays that controlled functions in the vehicle guidance system. Two tests were performed – one with and one without shock mounts. The equipment was instrumented with vibration transducers to measure the shock during both tests. In addition, instrumentation was placed on the facility to ensure that shock generated during both tests were equal.

The equipment was activated in its functional mode and all control circuits were monitored by an oscillograph capable of detecting chatter or transfer in the order of 400 μ sec. The performance of the shock mounts was then evaluated in terms of the reduction in the measured shock and in terms of improved equipment operating performance, which includes the unmeasured shock.

The results from the measured portion of the spectrum are shown in figure 7 as a reduction of the shock-spectrum response and also as a reduction of the peak amplitude of the transient vibration. The results in both forms of data analysis clearly indicate substantial attenuation of the shock environment.

The results of the functional portion of the test program are more significant than the shock-spectrum reduction, since improved functional performance is the only justification for the use of shock mounts. Figure 8 shows an oscillograph record of the relay chatter and transfer characteristics when tested with and without shock mounts installed on the equipment package.

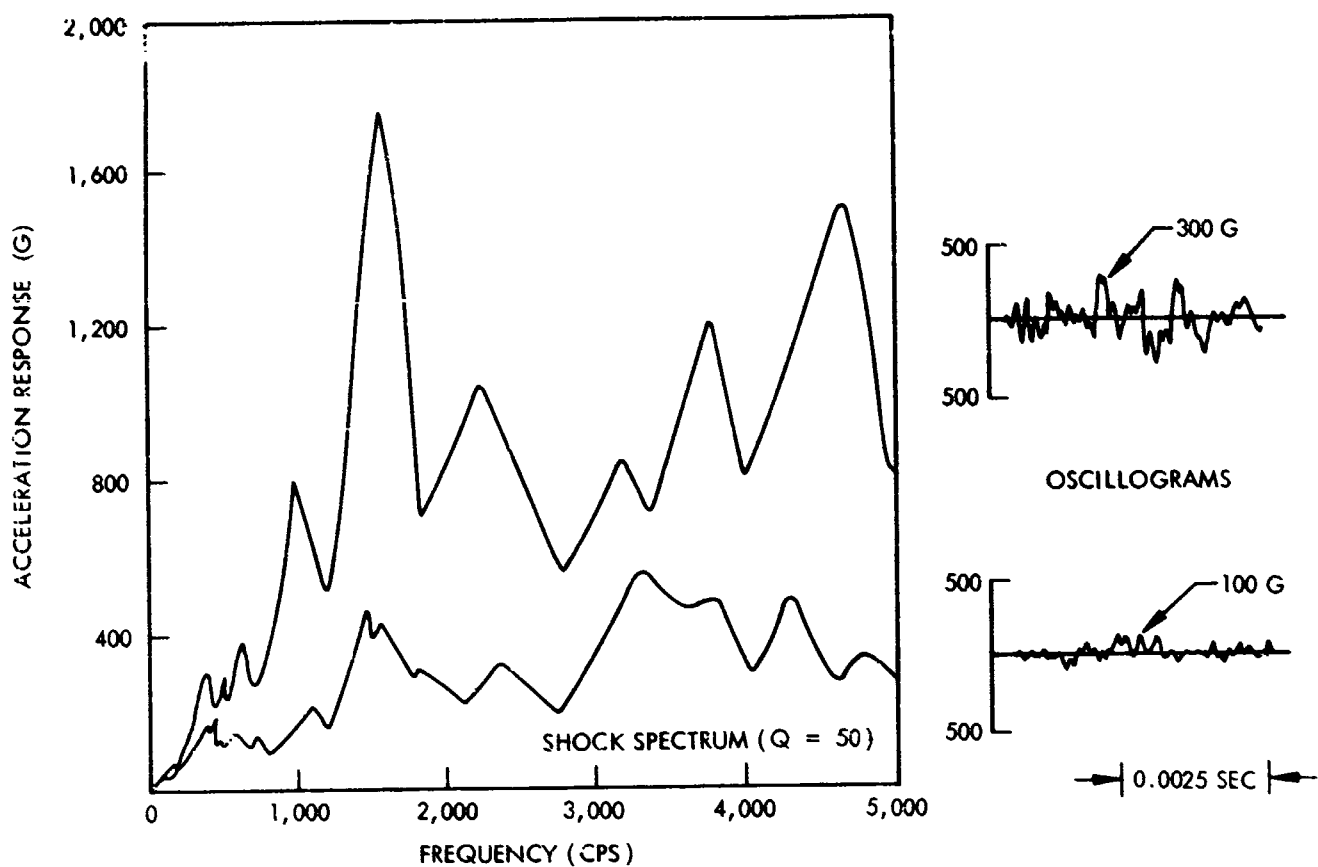
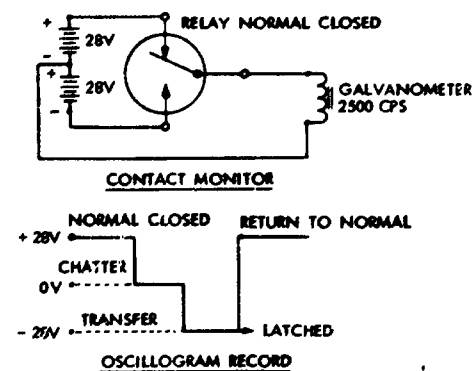
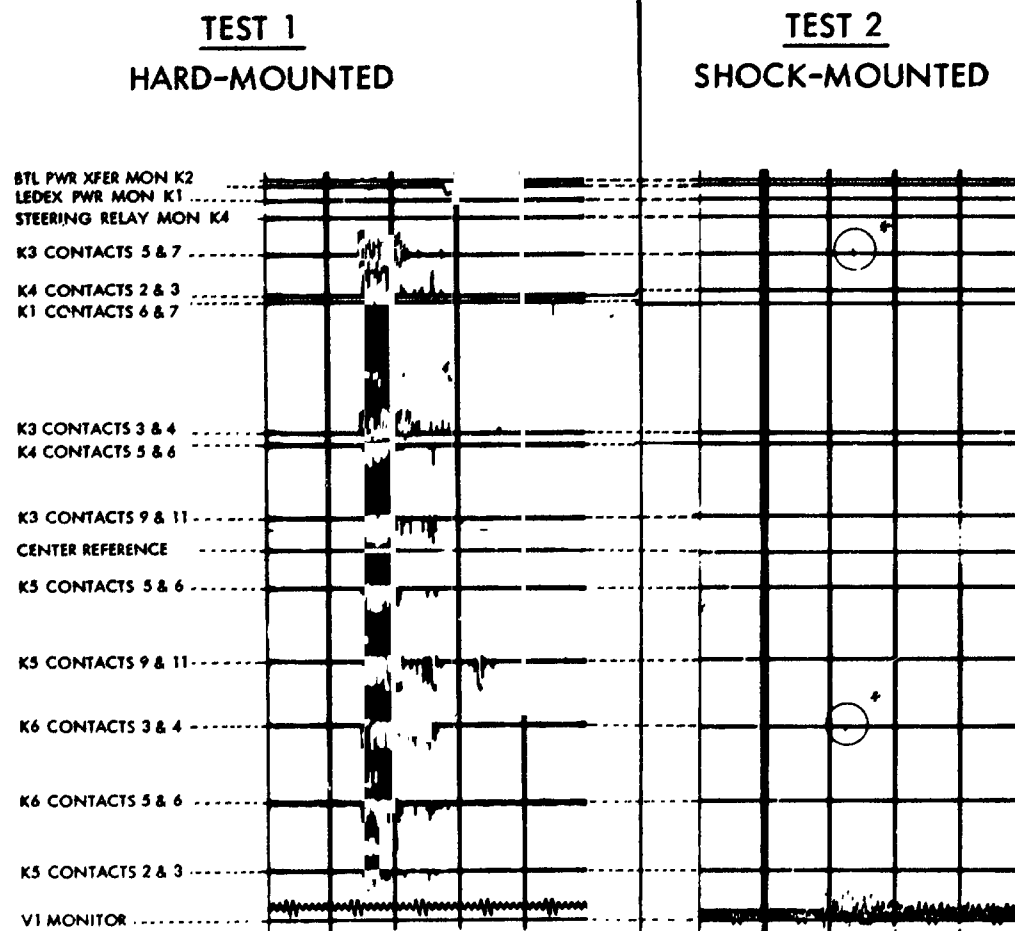


Figure 7 Typical Box With and Without Shock Mounts



RELAY OPERATION			
RELAY	CONTACTS	SHOCK MOUNTS	
		BEFORE	AFTER
K1	1 & 7	OK	OK
K2	1 & 2	CHATTER	OK
K3	5 & 7 3 & 4	CHATTER CHATTER TRANSFER	OK OK OK
K4	1 - 2 & 3 5 & 6 9 & 11	CHATTER CHATTER CHATTER CHATTER	OK OK OK OK
K5	5 & 6 9 & 11 2 & 3	CHATTER TRANSFER CHATTER CHATTER	OK OK OK OK
K6	2 & 4 3 & 6	CHATTER TRANSFER CHATTER TRANSFER	OK OK OK OK

Figure 8 Test Results - Guidance System Control Box

CONCLUSIONS

The shock mount represents an excellent method for protecting equipment against the effect of a pyrotechnic event and thereby improving its performance. Equipment modification has also proved useful. However, LMSC experience in this area has indicated that testing is the only positive method of assuring equipment flight qualification.

Analysis is helpful in comparing the severity of a pyrotechnic shock with that caused by other dynamic environments although the suitability of analysis for the solution of present equipment shock problems is still beyond the state of the art.

ACKNOWLEDGMENT

The author wishes to thank Mr. R.O. Doverspire for his contribution and discussion on stress waves during the preparation of this paper.

CONICAL PIVOT BEARINGS FOR SPACE APPLICATIONS*

By George G. Herzl
University of Santa Clara

SUMMARY

N67 16919

Literally millions of terrestrial precision instruments make use of conical pivot bearings because of their compactness and low friction (either with or without lubrication). Such bearings have inherent tolerance to the space environment, and they can be designed to withstand the high impact accelerations associated with vehicle launch and other events. Their advantages make them admirably suited to mechanisms used in spacecraft. This paper presents some analyses of conical pivot bearing characteristics and performance, in addition to criteria for minimal torque design. It also supplies formulas for calculating optimum bearing dimensions.

INTRODUCTION

Although there has been considerable experience gained in the design and production of conical pivot bearings over the years, further analytic work is needed. Actually, there has been very little such analysis since the early 1930's, in spite of the rapidly changing environments in which instruments are used and the ever-higher performance demands.

The advent of spacecraft instrumentation, with its low operating loads, opens up a whole new field of application for conical pivot bearings. Such bearings show particular promise for mechanisms used in the passive (or near-passive) long-life

* Based in part on a previously published article by G. G. Herzl, "How to Design for Minimum Torque in Conical Pivot Bearings," Machine Design, 9 Dec 1965, pp. 146-152.

satellite systems that are currently being emphasized. One appropriate application would be in a damper for a gravity-stabilized spacecraft, where extremely low torque is essential to proper system functioning.

The friction torque of conical pivot bearings is comparable to that of hypothetical journal bearings having shaft diameters of the order of a few thousands of an inch, yet conical pivot bearings can be used in instruments capable of withstanding impact accelerations as high as 1,000 g.

The two materials generally used in a conical bearing — synthetic sapphire for the bearing and steel for the shaft — have proved their suitability for aerospace mechanisms. They performed well in radiation and hard-vacuum experiments where other common bearing materials failed (ref. 1). One of the Ranger I spaceflight experiments was the friction-testing of various combinations of materials. During the entire experiment, the sapphire and steel combination maintained a consistently low coefficient of sliding friction.*

In the analysis of pivot bearings, the fundamental considerations for determining contact pressure between pivot and bearing are the position of the pivot (i.e., horizontal or vertical in analogy to terrestrial applications) and the location of the contact between pivot and bearing (i.e., in the spherical bearing region or on the sloping sides).

Friction torque depends on geometry of the pivot and bearing, amount and direction of applied load, material properties, and various environmental factors. The crucial part of the design analysis, with respect to minimal friction characteristics of conical pivot bearings, is the determination of the smallest possible pivot tip radius consistent with the requirement that under all possible operating conditions the tip material will undergo only elastic, and not permanent, deformation.

*Data for synthetic sapphire sliding against 440C stainless steel indicate a reduced coefficient of sliding friction, $\mu = 0.07$, compared with $\mu = 0.12$ to 0.15 for laboratory vacuum tests. No significant change in coefficient was observed during the Ranger I experiment (ref. 2).

SYMBOLS

A	= Angle between bearing axis and vertical (deg)
a	= Radius of circular contact area (in.)
B	= Angle between bearing axis and shaft (deg)
C	= Angle defined in figure 1 (deg)
c	= Major semiaxis of elliptical contact area (in.)
D	= Angle between external load L and perpendicular to bearing axis (deg)
d	= Minor semiaxis of elliptical contact area (in.)
E	= Modulus of elasticity (psi)
e	= Angle between centerline and tangent of bearing (deg)
K	= Quantity defined in equation (10) (psi)
L	= Total external load (lb)
P	= Normal bearing load (lb)
R	= Radius (in.)
R'	= Minor radius of curvature (in.)
R''	= Major radius of curvature (in.)
r	= Radius (thousands of an inch)
T	= Torque (lb-in.)
t	= Torque (mg-cm)
w	= Width of bearing in a plane perpendicular to axis of symmetry (in.)
y	= Combined deformation of pivot and bearing at contact (in.)
z	= Distance between apex and contact point projected to bearing centerline (in.)
α	= Dimensionless parameter from figure 4
β	= Dimensionless parameter from figure 4
δ	= Parameter defined in equation (9) (deg)
ϵ	= Half-cone angle of bearing (deg)
θ	= Quantity defined in equation (11) (deg)
λ	= Dimensionless quantity from figure 4
μ	= Coefficient of sliding friction
ν	= Poisson's ratio
ϕ	= Angle between planes containing minor principal radii of curvature of bearing and pivot (deg)
σ	= Contact pressure (psi)
ψ	= Angle of pivot roll on bearing from central position to nearest point of slippage (deg)

Subscripts

- b = Bearing
f = Friction
g = Quantity (gm)
h = Horizontal shaft
L = Total external load
m = Quantity (thousandths of an in.)
p = Pivot
v = Vertical shaft
0 = Point at which the spherical region joins the conical region

CONTACT LOADS

Contact load of a conical pivot bearing depends on load direction and on position of the pivot axis. This paper will consider only the positions for which friction torque is maximal (or horizontal) and minimal (or vertical) (ref. 3).

Horizontal Shaft

In this case, the stable pivot position at rest is in the direction of the total external load, which includes gravitational, centrifugal, and electromagnetic forces. It is the coplanar configuration (figure 1) in which angles C_1 , C_2 , and C_L are equal, and angle $D = 0$; the axes of the pivot and the bearing are parallel; and angle $A = 90$ deg if the total external load is due only to gravity.

An external torque applied to the pivot causes it to move up the side of the bearing until the friction is insufficient to prevent slippage. The traversed angle ψ (figure 2) depends on the coefficient of friction between pivot and bearing at the point of contact where slippage occurs. By equating the corresponding components of the external force and the friction force just before slippage occurs,

$$\psi = \tan^{-1} \frac{\mu}{\cos e} \quad (1)$$

Summation of forces vertically in figure 2, and consideration of equation (1), yields

$$P = 0.5 L (\cos^2 e + \mu^2)^{-1/2} \quad (2)$$

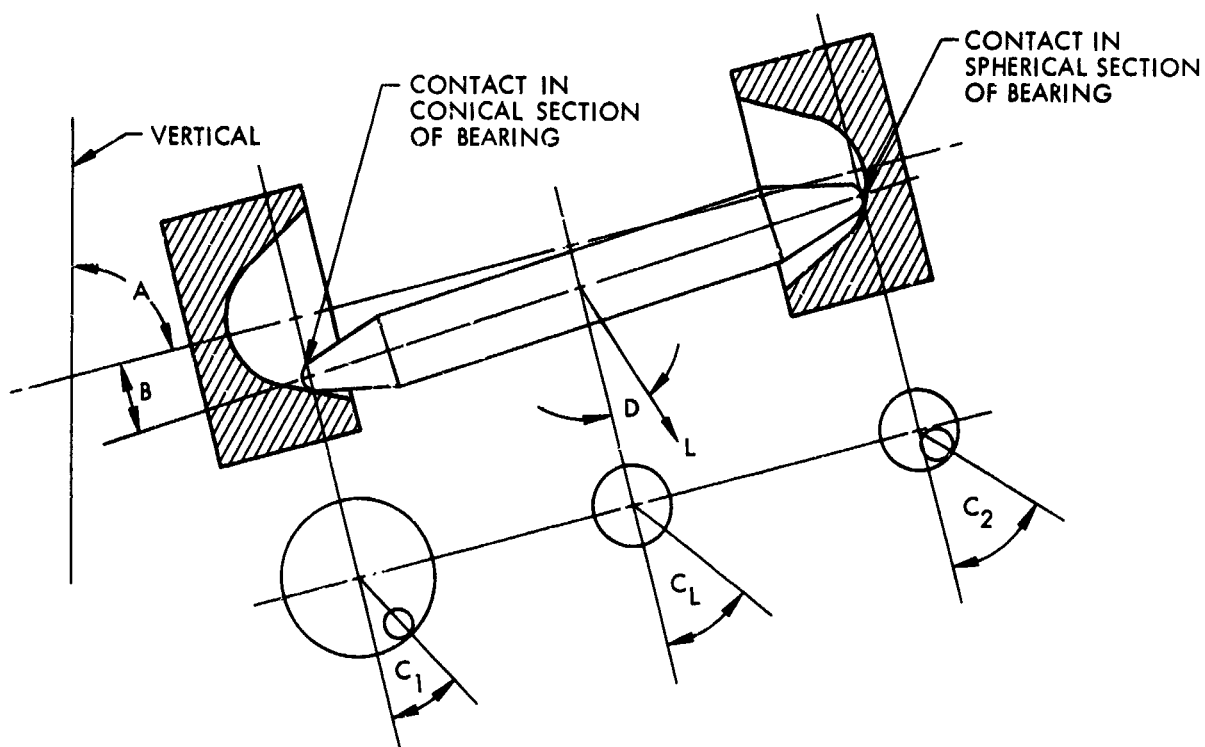


Figure 1 Pivot Bearing System - General Configuration

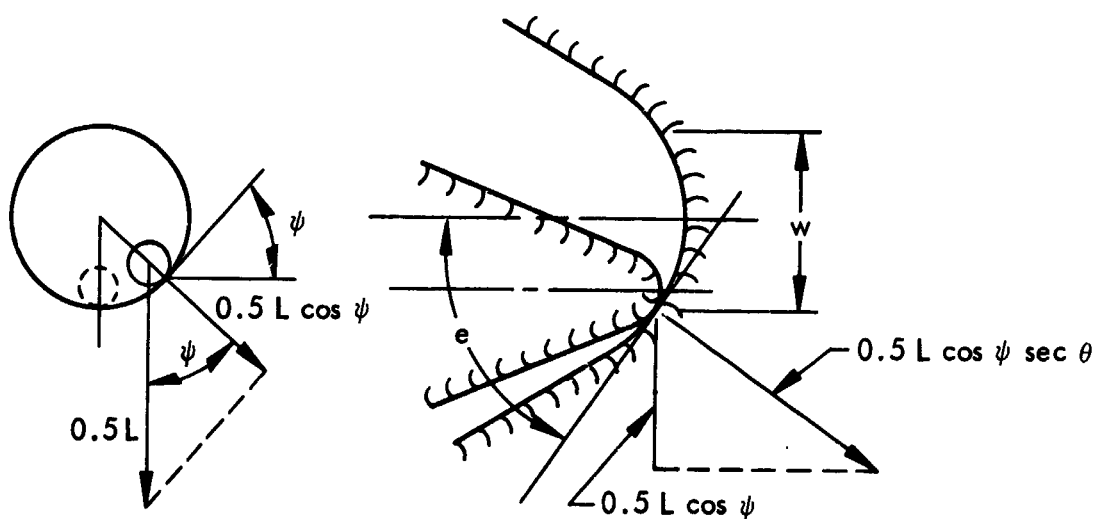


Figure 2 Horizontal Shaft Configuration - Sectional View

The plot of equation (2) in figure 3 indicates that the bearing load increases significantly if contact between the pivot and bearing is near the bearing apex. Conversely, when contact is in the conical section of the bearing, where $e = \epsilon$, the bearing load has a constant value of

$$P = 0.5 L (\cos^2 \epsilon + \mu^2)^{-1/2} \quad (3)$$

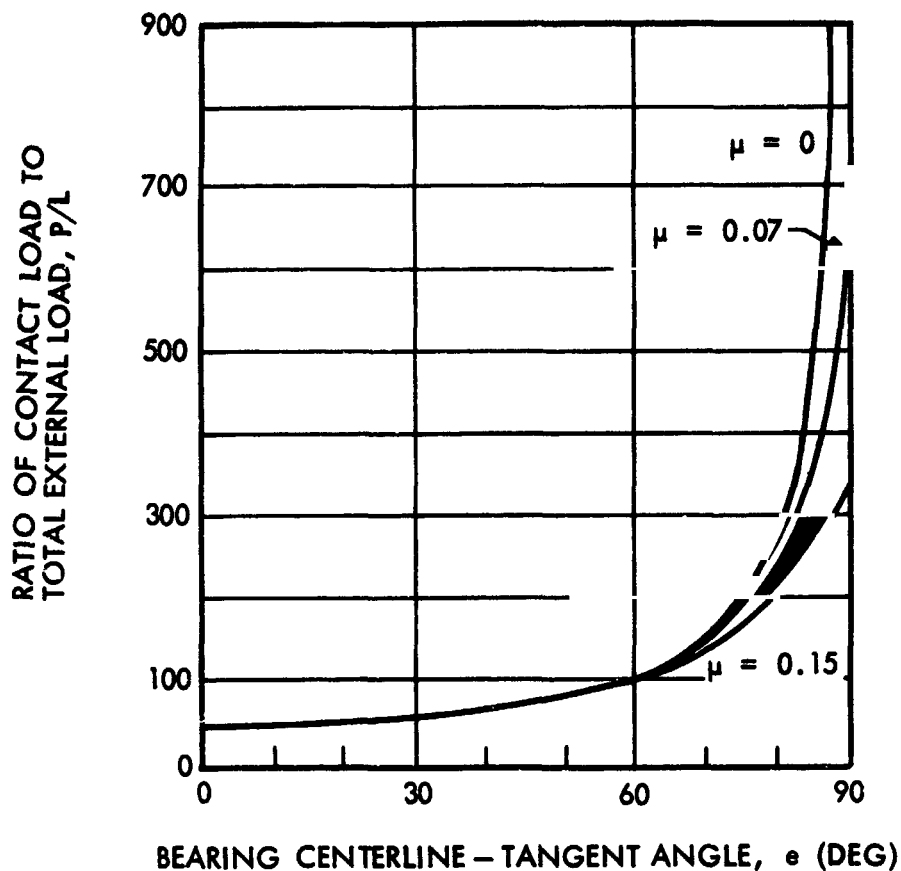


Figure 3 Ratio of Contact Load to Total External Load Versus Angle Between Centerline and Tangent to Bearing

The contact load on each horizontal bearing is less than the total load since the half-cone angle of conical pivot bearings is, in practice, always less than 60 deg.

Vertical Shaft

In this case, contact is in the apex of one of the two bearings and angle D (figure 1) is either +90 or -90 deg. The load on one bearing when the shaft is vertical is equal to the total external load

$$L = P \quad (4)$$

Equation (4) is valid only when the bearing and shaft axes are parallel (e.g., in compasses where the moving element containing the bearing is suspended on a shaft with a conical pivot). Conversely, a shaft is in unstable equilibrium when one end is supported by a bearing and the other end leans against the upper bearing. This induces second-order factors in equation (4); however, these factors can be neglected in practical calculations.

CONTACT PRESSURE AND AREA

The inherent low-friction characteristic of pivot bearings is mainly due to the small tip radius capable of supporting the load without permanent deformation under all operating conditions.

Common practice in many instrument applications is to make the tip as sharp as possible and let deformations resulting from load increase the tip radius. This method is inexpensive since it does not require shaping of the tip or design calculations. Deformation of the tip, however, results in an irregular (as opposed to spherical) shape, and bearing friction is neither minimal nor uniform. Both of these frictional considerations are important in high-performance instruments which operate at low torque levels, and often at very slow speeds where small jerks are not permissible. Another disadvantage is that the irregular shape of the tip enhances the formation of wear debris that can clog a lubricated bearing when it is positioned with the concave side up, or when the system operates in a weightless environment.

Optimal operational and frictional characteristics are obtained from spherical pivot tips with a minimum radius that deforms only elastically under operational loads. The contact pressure should be less than the allowable contact pressure for minimum tip radius. The ultimate operational pressure depends on properties of the mating materials and the pivot cone angle. Uncertainty of the magnitude of the worst dynamic loads requires a factor of safety to determine the allowable contact pressure. Several investigators have reported on allowable loads for pivots (refs. 4, 5, and 6). A conservative value (based on Stott's measurements and on a limited number of loading experiments) for ultimate pressure is 1.6×10^6 psi.

The following general assumptions, in addition to those usually made in conventional bearing design, apply to the method of determining minimum allowable pivot tip radius presented here:

- Pivot tip and bearing apex are spherical.
- Pivot tip radius is smaller than bearing apex radius.
- Cone angle of bearing is larger than cone angle of pivot.
- All deformations occur near point of contact; pivot and bearing are considered to be rigid bodies elsewhere.
- Materials of pivot and bearing are isotropic and homogeneous.
- Frictional forces acting in a plane perpendicular to the normal bearing load are neglected.
- The modulus of elasticity of the pivot tip material is $E_p = 3 \times 10^7$ psi and Poisson's ratio of $\nu = 0.3$ (typical of the various steels used for pivots).
- Bearing is made of sapphire (ref. 7) or a similar (hexagonal) crystalized aluminum (Al_2O_3) with $E_b = 5 \times 10^7$ psi and a hardness of 9 on the Mohr scale. Specific gravity is 3.95 to 4.10, and melting point is over $2,000^\circ C$. In absence of published data on Poisson's ratio for sapphire, assume $\nu = 0.2$ (same as for hard glass). (Poisson's ratio has only minor influence on the results of the calculations.)
- Maximum compression stress is the dominant design factor, so the developed formulas consider neither maximum shear nor tensile stress. Experiments show this assumption to be generally justified, but it should be verified for each application.

From Hertz's theory (ref. 8) for the general case of two bodies in contact (refs. 9 and 10)

$$\sigma_{\max} = 0.478 \frac{P}{cd} \quad (5)$$

where

$$c = \alpha \left(\frac{P \delta}{K} \right)^{1/3} ; \quad d = \beta \left(\frac{P \delta}{K} \right)^{1/3} ; \quad y = \lambda \left(\frac{P^2}{K^2 \delta} \right)^{1/3} \quad (6,7,8)$$

$$\delta = \frac{4}{1/R'_p + 1/R''_p - 1/R'_b - 1/R''_b} \quad (9)$$

$$K = \frac{8}{3} \frac{1}{(1 - \nu_p^2)/E_p + (1 - \nu_b^2)/E_b} \quad (10)$$

Values of α , β , λ , as functions of θ , are shown in figure 4, where

$$\theta = \arccos \frac{\delta}{4} \left[\left(\frac{1}{R'_p} - \frac{1}{R''_p} \right)^2 + \left(\frac{1}{R'_b} - \frac{1}{R''_b} \right)^2 - 2 \left(\frac{1}{R'_p} - \frac{1}{R''_p} \right) \right. \\ \left. \times \left(\frac{1}{R'_b} - \frac{1}{R''_b} \right) \cos 2\phi \right]^{1/2} \quad (11)$$

The point of contact between the pivot and the bearing is either in the spherical region of the bearing when $z < z_0$, or in the conical region when $z > z_0$ (figure 5). The value of z depends on the total end play of the system.

Contact in Spherical Region

The problem can be idealized by considering contact of the convex side of a sphere with the concave side of a larger sphere. Substituting the principal curvatures and angle from figure 5 into equations (9) and (11),

$$\delta = \frac{2}{r_p^{-1} - r_b^{-1}} \text{ and } \theta = 90 \text{ deg}$$

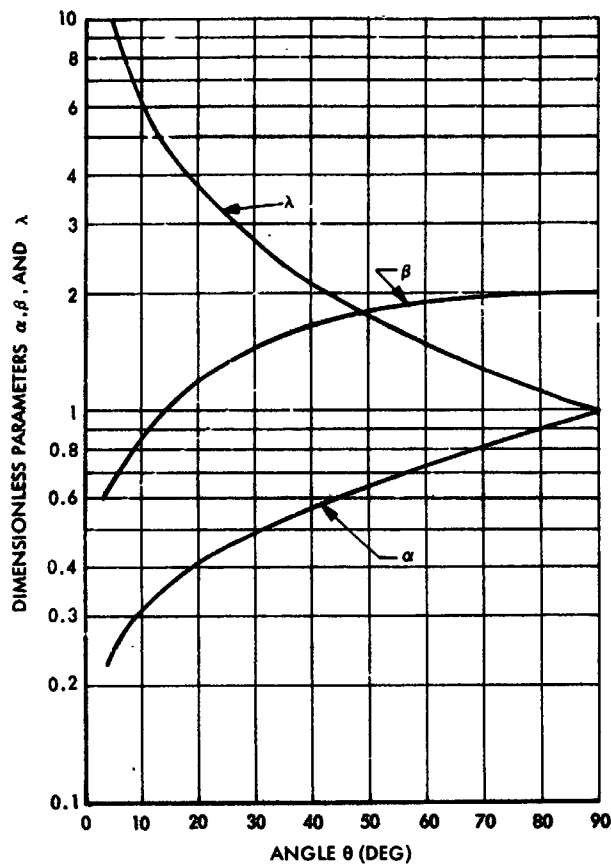


Figure 4 Dimensionless Relationships for α , β , and λ as Functions of Angle

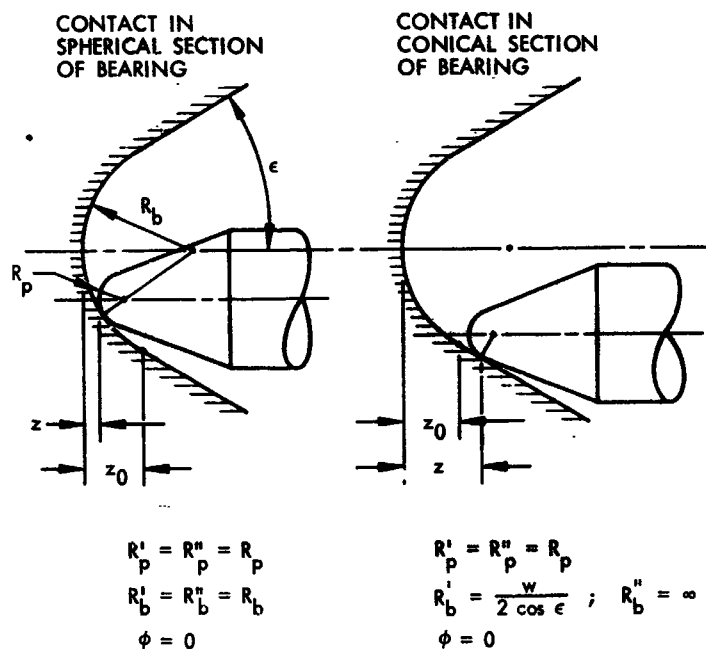


Figure 5 Pivot-Bearing System — Cross Section

From figure 4, $\alpha = \beta = 1.0$ and $\lambda = 2.0$. Substituting these values into equations (5), (6), (7), and (8) yields

$$a = c = d = 1.26 K^{1/3} (R_p^{-1} - R_b^{-1})^{-1/3} P^{1/3} \quad (12)$$

$$y = 1.589 K^{-2/3} (R_p^{-1} - R_b^{-1})^{1/3} P^{2/3} \quad (13)$$

$$\sigma_{\max} = 0.301 K^{2/3} (R_p^{-1} - R_b^{-1})^{2/3} P^{1/3} \quad (14)$$

The contact area is a circle. as is to be expected.

To obtain equations more suitable for practical calculations, substitute into equations (12), (13), and (14) the representative pivot and bearing material constants

$$a_m = 0.0438 (r_p^{-1} - r_b^{-1})^{-1/3} P_g^{1/3} \quad (15)$$

$$y_m = 1.89 \times 10^{-3} (r_p^{-1} - r_b^{-1})^{1/3} P_g^{2/3} \quad (16)$$

$$\sigma_{\max} = 0.556 \times 10^6 (r_p^{-1} - r_b^{-1})^{2/3} P_g^{1/3} \quad (17)$$

Hence, the quantity $(r_p^{-1} - r_b^{-1})$ is called the contact curvature.

Equation (17) is represented in figure 6. Two principal ways of using figure 6 are illustrated by the following examples:

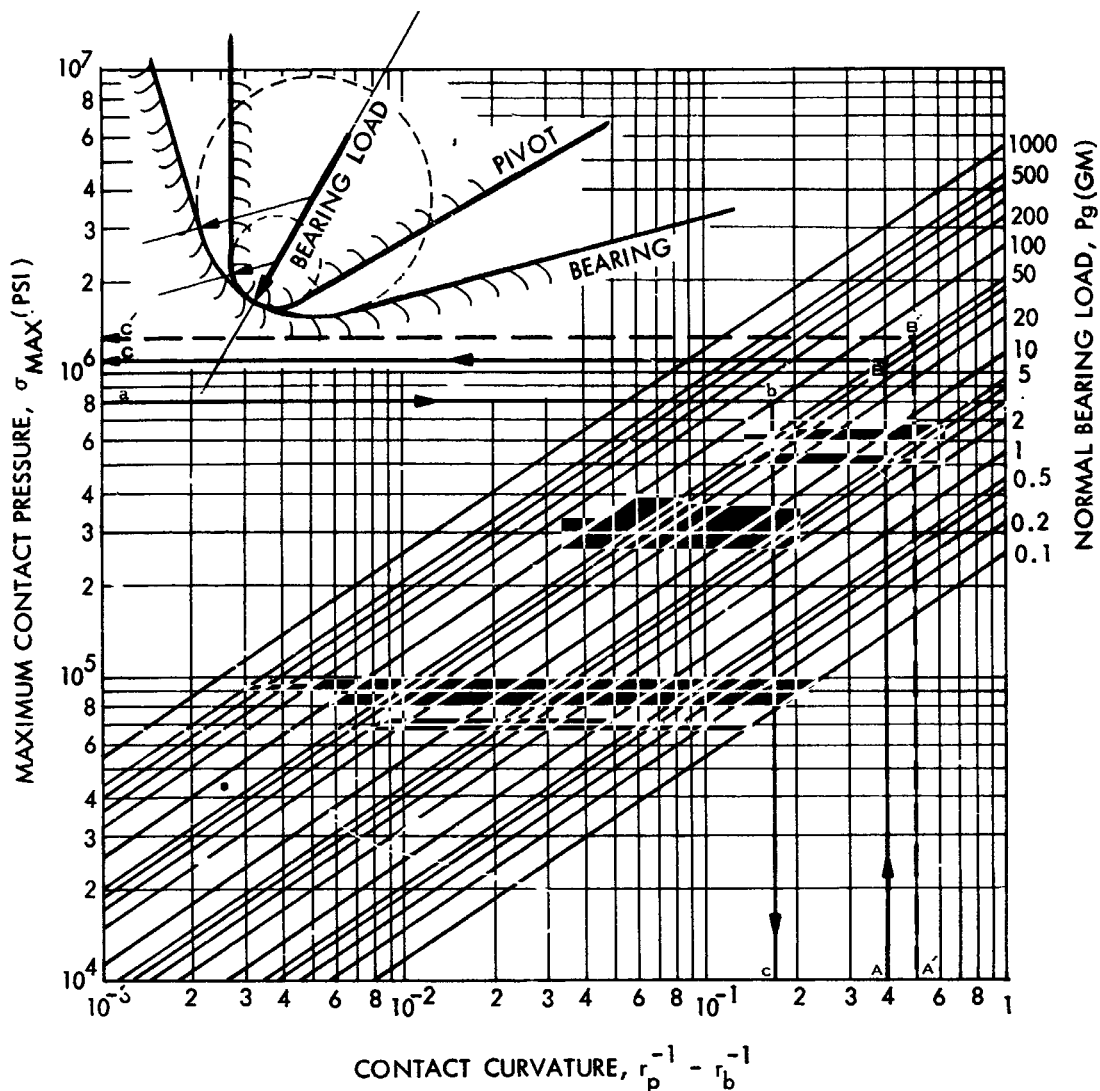


Figure 6 Maximum Contact Pressure Versus Contact Curvature for Contact in Spherical Section of Bearing

- **Example 1.** Determine the maximum contact pressure for a vertical pivot tip of 0.002-in. radius and a 0.010-in. bearing apex radius, when bearing load is 50 gm.

Solution. The contact curvature is equal to $1/2 - 1/10 = 4 \times 10^{-1}$. Draw a vertical line from the value of contact curvature to the 50-gm diagonal load line. Then, follow a horizontal line to the ordinate. The resulting contact pressure is 1.1×10^6 psi. The influence of the bearing apex radius on the resulting contact pressure is evident from the diagram. If the bearing apex

radius were equal to infinity (corresponding to a flat surface), the contact curvature would be equal to $5 \times 10^{-1} \text{ (in.} \times 10^{-3})^{-1}$ and the resulting contact pressure would be $1.3 \times 10^6 \text{ psi}$.

- **Example 2.** Determine the minimum tip radius of a conical pivot having 60-deg cone angle when subjected to a 100-gm vertical load.

Solution. The ultimate contact pressure (contact pressure at which slight traces of permanent deformation occur) for a hardened steel pivot with a 60-deg cone angle is $1.6 \times 10^6 \text{ psi}$. With a safety factor of 2, to account for possible uncertainties of the amount of load, material imperfection, and tolerances, the value of permissible contact pressure is $8 \times 10^5 \text{ psi}$. Proceed from ordinate to the diagonal line corresponding to the 100-gm load. The contact curvature is found vertically below. For a bearing with an apex radius of 0.010 in., the minimum tip radius that will not undergo permanent deformation is equal to 0.0038 in.

A comparison of results with the most comprehensive published work on pivot bearings, by Stott (ref. 6), and the published diagrams by Warring (ref. 11), indicates that the stresses calculated by equation (17) are conservative. This is chiefly due to consideration of the elasticity of the bearing material in this analysis.

The relationship between the radius of the contact surface (between pivot and bearing) and the contact curvature, described by equation (15), is shown in figure 7. Radii of contact surfaces for Examples 1 and 2 are $a = 0.22 \times 10^{-3} \text{ in.}$ and $a = 0.35 \times 10^{-3} \text{ in.}$, respectively.

Contact in Conical Region

When contact of the pivot is in the conical section of the bearing, the problem can be idealized as the contact of the convex side of a sphere with the concave side of a cone. Substitution of the principal curvatures and angle into equations (9) and (11) yields

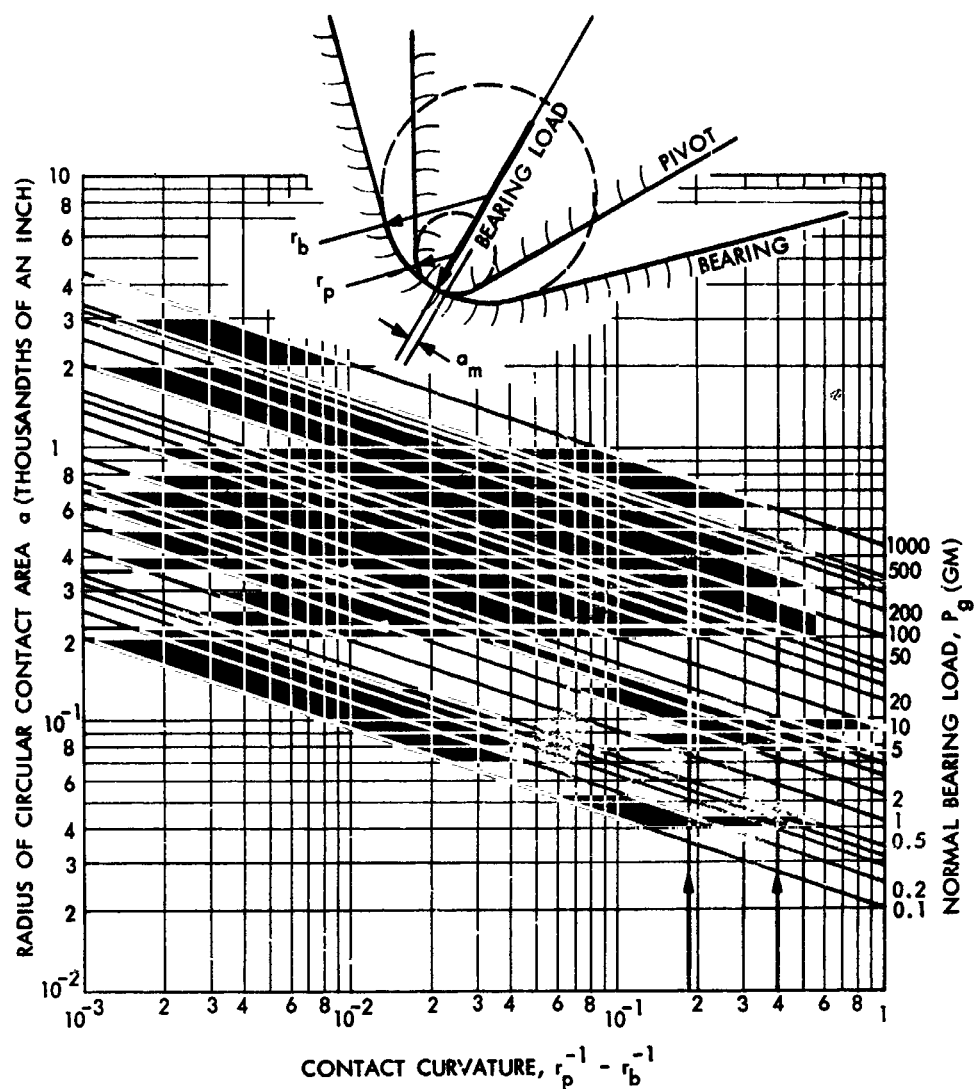


Figure 7 Radius of Contact Surface Versus Contact Curvature for Contact in Spherical Section of Bearing

$$\delta = \frac{2 R_p}{1 - \frac{R_p}{w} \cos \epsilon} \quad (18)$$

and the dimensionless relation

$$\theta = \arccos \frac{1}{\frac{w}{R_p} \sec \epsilon - 1} = \arccos \frac{1}{\frac{w_m}{r_p} \sec \epsilon - 1} \quad (19)$$

For practical bearings with contact in conical region, equations (5) and (8) can be rewritten as follows:

$$\delta_m = \frac{2 r_p}{1 - \frac{r_p}{w_m} \cos \epsilon} \quad (20)$$

$$c_m = 3.475 \times 10^{-2} \alpha (P_g \delta_m)^{1/3} \quad (21)$$

$$d_m = 3.475 \times 10^{-2} \beta (P_g \delta_m)^{1/3} \quad (22)$$

$$y_m = 1.205 \times 10^{-3} \lambda P_g^{2/3} \delta_m^{-1/3} \quad (23)$$

$$\sigma_{\max} = 1.062 \times 10^3 P_g c_m^{-1} d_m^{-1} \quad (24)$$

The use of equations (19) through (24) is illustrated in the following example:

- Example. Determine the maximum contact pressure and the semiaxes of the contact ellipse for a pair of horizontal pivot tips, each with an 0.002-in. radius, when subjected to a total external load of 50 gm. Angle $\epsilon = 30$ deg, and the width of the bearing at the point of contact is 0.020 in.

Solution. The contact load on each bearing is, from equation (2), $P_g = 28.6$ gm. Equations (19) and (20) yield $\delta_m = 4.38$ (in. $\times 10^{-3}$) and $\theta = 84$ deg 29 min. The corresponding values from figure 4 are $\beta = 0.94$ and $\alpha = 1.06$. From equations (21) and (22), $d_m = 0.165 \times 10^{-3}$ in. and $c_m = 0.186 \times 10^{-3}$ in. Equation (24) yields the maximum contact pressure, $\sigma_{\max} = 0.99 \times 10^6$ psi.

CALCULATION OF FRICTION TORQUE

Horizontal Configuration

The friction torque necessary to maintain the rotation of a horizontal shaft suspended on two bearings is expressed in terms of friction radius R_f (figure 8):

$$T_{fh} = 2 P \mu R_f \quad (25)$$

Substituting the value of P from equation (2) in this expression, considering that $R_f = R_p \cos e$, and changing the units, then

$$t_{fh} = 2.54 \mu r_p L_g \left[1 + \left(\frac{\mu}{\cos e} \right)^2 \right]^{-1/2} \quad (26)$$

When contact is in the conical region of the bearings,

$$e = \epsilon$$

and

$$\left[1 + \left(\frac{\mu}{\cos \epsilon} \right)^2 \right]^{-1/2} \approx 1$$

therefore

$$t_{fh} \approx 2.54 \mu r_p L_g \quad (27)$$

For example, if a horizontal shaft ($L_g = 100$ gm, $\epsilon = 30$ deg, $r_p = 3.8$ (in. $\times 10^{-3}$), $r_b = 10$ (in. $\times 10^{-3}$) is suspended on two conical bearings, and if the coefficient of friction $\mu = 0.12$, then the friction torque $t_{fh} = 115$ mg-cm.

Friction torque is significantly higher when contact is near the apex of the bearing because the bearing load and the corresponding minimum pivot radius become large, as indicated in figure 3.

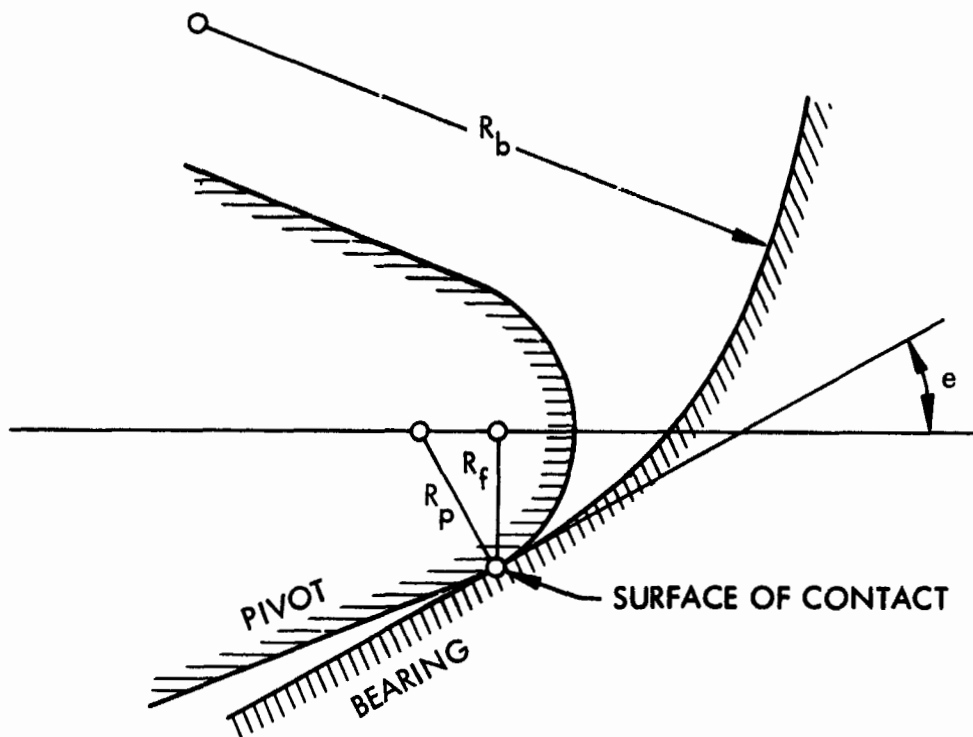


Figure 8 Friction Radius R_f of Conical Pivot Bearing

Vertical Configuration

The relationship between contact pressure and the distance from the center of pressure for a given diameter of contact is given by Hertz as

$$\sigma = 1.5 \frac{P}{\pi a^2} \left(1 - \frac{r}{a}\right)^{1/2} \quad (28)$$

Consideration of couples of elementary areas of the surface of contact and corresponding pressures and integration over the entire area yields for total friction torque (ref. 6)

$$T_{fv} = 0.589 L \mu a \quad (29)$$

Where total external load L was substituted for bearing load P , Stott has shown that equation (29) is accurate to second-order quantities for actual contact surfaces. For practical calculations

$$t_{fv} = 1.496 L_g \mu a_m \quad (30)$$

The value of a_m may be obtained from figure 7, or from equation (15).

Substitution of equations (4) and (15) into equation (30) yields:

$$t_{fv} = 6.55 \times 10^{-2} L_g^{4/3} \mu \left(r_p^{-1} - r_b^{-1}\right)^{-1/3} \quad (31)$$

This expression indicates that if the pivot and bearing are only elastically deformed, frictional torque is proportional to the 4/3 power of load. Carson reports that, for increasing loads producing small permanent deformations, friction torque is proportional to the 3/2 power of load (ref. 12). In practice, however, the difference in calculated friction, using the exponents 4/3 and 3/2, is small when the supported element weighs less than 5 gm.

When the pivots have large areas of contact resulting from wear and overload, friction is linearly proportional to load. However, pivots having permanent deformation do not have optimal frictional characteristics and are therefore beyond the scope of this analysis. References 13 and 14 provide further details of operation under these circumstances.

CONFIGURATION COMPARISON

A summary of the characteristics of various conical pivot configurations, and a summary of their performance, is given in the table that follows:

Table 1
COMPARISON OF PIVOT BEARING CONFIGURATIONS

Aspect	Horizontal Configuration		Vertical Configuration
	Contact in Spherical Region	Contact in Conical Region	
Contact Load	Less than total external load, except when end play is very small. See equation (2) and figure 3.	In practice, always less than total external load. Depends on cone angle. See equation (3) and figure 3.	Equal to total external load. See equation (4).
Contact Area	Circular outline. Radius proportional to cube root of bearing load and inversely proportional to cube root of contact curvature. See equation (15) and figure 7.	Elliptical outline. Semiaxes proportional to cube root of product of bearing load and pivot-tip radius. Smaller when contact is near spherical region. See equations (19-22).	Circular outline. Radius proportional to cube root of bearing load and inversely proportional to cube root of contact curvature. See equation (15) and figure 7.
Total Penetration	Proportional to $2/3$ power of bearing load and cube root of contact curvature. See equation (16).	Proportional to $2/3$ power of bearing load and inversely proportional to cube root of tip radius. Small near spherical region. See equations (19), (20), and (23).	Proportional to $2/3$ power of bearing load and cube root of contact curvature. See equation (16).
Maximum Contact Pressure	Proportional to cube root of bearing load and $2/3$ power of contact curvature. See equation (17) and figure 6.	Proportional to bearing load and inversely proportional to contact area. Less near spherical region. See equations (19-24).	Proportional to cube root of bearing load and $2/3$ power of contact curvature. See equation (17) and figure 6.
Friction Torque	Proportional to total external load, pivot tip radius, and coefficient of friction. Increases significantly when end play is very small. See equation (26).	Proportional to total external load, pivot tip radius, and coefficient of friction. Less when contact is near spherical region. See equation (27).	Proportional to $2/3$ power of total external load and coefficient of friction and inversely proportional to cube root of contact curvature. See equations (30) or (31) and figure 7.

CONCLUSIONS

Conical pivot bearings offer a simple technique for achieving a predictable alignment within a small space and for providing extremely low friction. These advantages and their inherent tolerance for the space environment make them good candidates for use in aerospace mechanisms. The designer should find them of particular merit where specifications include moderate loads and low friction torque.

REFERENCES

1. Lockheed Missiles & Space Company: Space Materials Handbook. Second ed., MI-TDR-64-40, 1954.
2. California Institute of Technology, Jet Propulsion Laboratory: Friction Measurements on a Low Earth Satellite. TR-32-402, 1963.
3. Lawson, A. C.: Design Factors for Jewel Bearing Systems. Machine Design, Apr. 1954.
4. Thomas, H. R.; and Hoersch, W. A.: Stresses Due to the Pressure of One Elastic Solid Upon Another. University of Illinois Bulletin 212, July 1930.
5. Wilson, W. M.; Moore, R. L.; and Thomas, F. P.: University of Illinois Bulletin 242, Feb. 1932.
6. Stott, V.: An Investigation of Problems Relating to the Use of Pivots and Jewels in Instruments and Meters. Nat. Phys. Lab., Collected Researches (London). vol. 24, 1931.
7. Norton, F. H.: Refractories. McGraw-Hill, 1949.
8. Hertz, H.: Gesammelte Werke. Vol. 1, 1895.
9. Whittmore, H. L.; and Petrenko, S. N.: Friction and Carrying Capacity of Ball and Roller Bearings. Bureau of Standards Tech. Paper 201, 1921.
10. Roark, R. J.: Formulas for Stress and Strain. McGraw-Hill, 1954.
11. Warring, R. H.: Calculating Frictional Losses in Jewel Bearing Movement. Design News, Apr. 1957.
12. Carson, R. W.: Merit Factor for Measuring Serviceability of Electrical Indicating Instrument. Instruments, vol. 7, Oct. 1934.
13. Goss: Mechanical Factor of Merit With Respect to Electrical Instruments. General Electric Review, vol. 36, 1933.
14. Edgumbe and Ockenden: Industrial Electrical Measuring Instruments. Pitman, 1933, p. 44.

COMPRESSION SPRINGS AT ELEVATED TEMPERATURES

By M. J. Siegel
University of Southern California

SUMMARY

N67 16920

The behavior of compression springs is affected by increased temperatures. The most significant factors affecting springs are a loss of load and length (relaxation), and a change in the modulus of rigidity. Relaxation will reduce preset loads or change the location of supported components whereas a change in the modulus of rigidity will alter the spring rate. Both factors must be taken into account when designing compression springs. Curves and equations are presented (for music wire, 18-8 stainless steel, 17-7 PH, and Inconel-X) which can aid in the design of compression springs for use at elevated temperatures.

INTRODUCTION

A spring is a mechanism element used primarily to provide elastic deflection under load and to perform the following functions:

- (1) Control motion (e.g., keeping a follower in contact with its cam)
- (2) Supply or measure forces (e.g., maintaining the pressure setting in a safety-relief valve)
- (3) Absorb energy (e.g., absorbing shock in docking mechanisms; damping vibration)
- (4) Store energy (e.g., ejection mechanisms in satellites)

The devices in the foregoing categories (1) and (2) use fixed-deflection springs. In category (1), the spring is constrained to move between fixed limits; in category (2), it is compressed at the time of assembly and remains in that fixed position during

most (or at least part) of its use. The devices in categories (3) and (4) use springs that are generally free to deflect in proportion to the energy absorbed or stored. Except for limits placed on the springs to prevent overload, they are unrestrained.

SYMBOLS

a	constant for a given material
D	mean spring diameter (in.)
d	wire diameter (in.)
G	modulus of rigidity (psi)
K	constant for a given material
L	relaxation
m	constant for a given material
N	number of active turns
n	constant for a given material
P	load (lb)
R	spring rate
τ	longtime shear stress
S_o	initial shear stress (psi)
S_s	stress
T	absolute temperature ($^{\circ}$ Rankine)
t	temperature ($^{\circ}$ F)
Δ	spring deflection (in.)
ϵ	strain
Subscripts	
o	initial
s	shear

COMPRESSION SPRINGS

The most common type of spring is the cylindrical, helical, compression spring. Its primary stress is a shear stress caused by a torsional moment when the spring is

axially loaded. This stress can be expressed as follows:

$$S_s = \frac{8PD}{\pi d^3} \quad (1)$$

The deflection, due to load P , is

$$\Delta = \frac{8PD^3N}{Gd^4} \quad (2)$$

From equation (2) we obtain the spring rate

$$R = \frac{Gd^4}{8D^3N} \quad (3)$$

Equation (2) can be plotted as shown in figure 1. The spring rate is the slope of the $P - \Delta$ curve when the relationship is linear, which is the case for elastic materials that obey Hooke's Law. For a given load P , the energy in the spring is equal to the area under the $P - \Delta$ curve shown in figure 1.

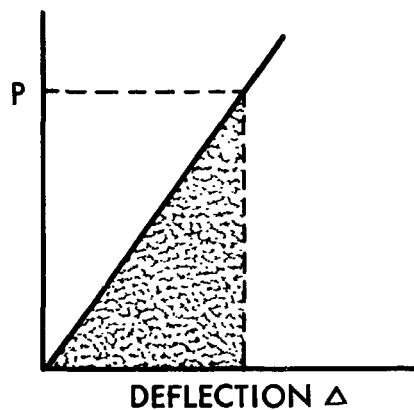


Figure 1 Load Versus Deflection

Equations (1), (2), and (3) assume the spring to be completely elastic. Equations (2) and (3) are based on the modulus of rigidity G .

INFLUENCE OF TEMPERATURE

When a spring is subjected to a change in temperature, equations (1), (2), and (3) are not sufficient to predict the spring behavior. Temperature changes may result in the following effects:

- Change in value of the modulus of rigidity G
- Creep (loss of dimension) or relaxation (loss of load)
- Change in shear yield stress

Modulus of Rigidity at Elevated Temperatures

The modulus of rigidity for several materials is plotted against temperature in figure 2. For simplicity, these curves have been linearized over the temperature

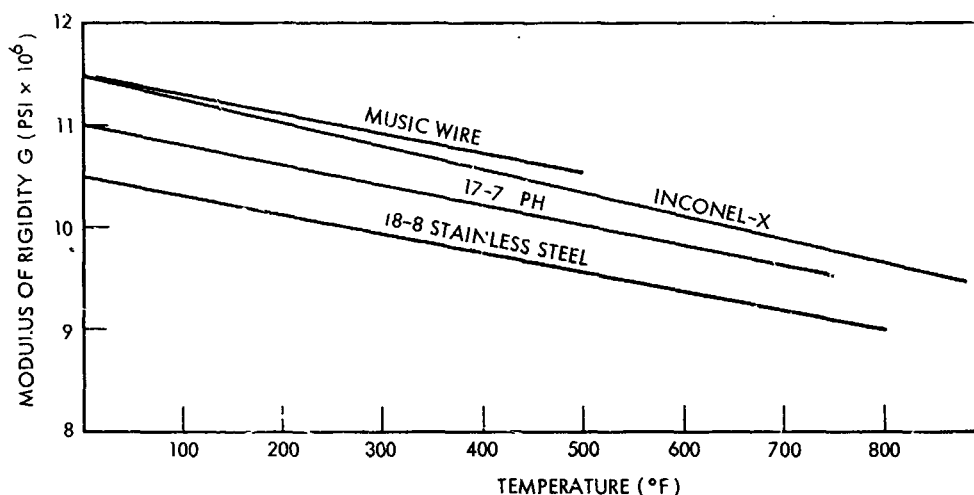


Figure 2 Modulus of Rigidity Versus Temperature

range shown. They can be expressed in a straight line equation as follows:

$$G = (K - at) 10^6 \quad (4)$$

where t is the temperature in °F. Values of K and a are shown in table 1 for various materials:

Table 1
VALUES OF K AND a IN EQUATION (4)

Material	K	a
Music wire	11.5	0.00193
18-8 stainless steel	10.5	0.00188
17-7 PH	11.0	0.00195
Inconel-X	11.5	0.00230

Equation (4) can be incorporated into equations (2) and (3) to develop a generalized expression for deflection and spring rate as a function of temperature.

Relaxation at High Temperatures

The term, "high temperature," when applied to springs, generally refers to temperatures above 400° F for steel and above 900° F for Inconel-X. Springs designed to operate at these temperatures must also be designed for limited life, inasmuch as relaxation continues until a spring collapses completely.

All springs, when subjected to high temperatures, creep or relax in time if in a loaded condition. This increase in strain (creep) or loss of load (relaxation) is due to several changes that occur in time under load. At temperatures below those causing metallurgical change, the four most important factors are:

- Anelastic strain
- Relief of residual stress
- Transient creep
- Steady-state creep

Anelastic strain is a reversible process (as shown in figure 3a) in which the permanent change of dimension is zero in time after the load is removed. This change of dimension is relatively small, and its contribution to the relaxation process is generally slight.

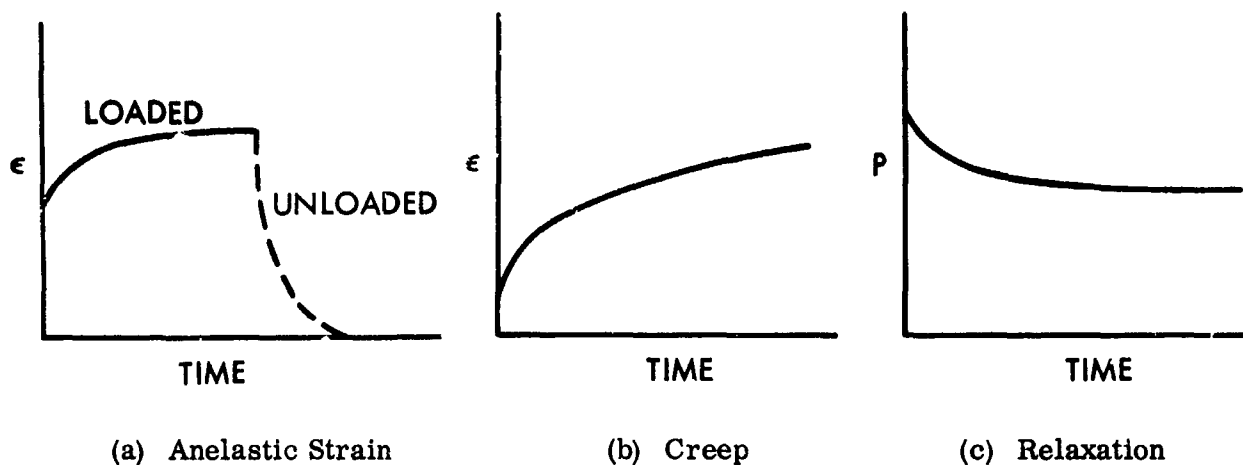


Figure 3 Strain Versus Time

Residual stresses are present in the spring wire prior to manufacture, and additional residual stress is introduced in the process of forming the spring. Residual stresses result from cold-working processes and generally contribute to spring strength.

Increased temperature causes relief of residual stress. The higher the temperature, the less the time required, and the larger the reduction of residual stress. Most spring materials are relieved of all residual stress at temperature above 900° F. Reduction of residual stress has the effect of loss of strength, and thereby contributes to the relaxation process.

Transient and steady-state creep account for permanent or inelastic dimensional changes. These are shown in figure 3b and in figure 3c as relaxation.

The foregoing factors, which contribute to loss of load and dimension under load, may act concurrently. Tests run on springs have yielded data representing the sum of these effects, which, although partially recoverable, can be considered as spring relaxation.

It is possible to predict analytically with accuracy the relaxation of springs that operate at very high temperatures and stresses, where relaxation is due primarily to steady-state creep, and the effect of anelastic strain and release of residual

stresses is small. At such temperatures, the creep rate does not become zero, but continues until the spring reaches solid height.

Relaxation at Moderate Temperatures

At moderate temperatures — to about 400° F for steel and to about 900° F for Inconel-X — relaxation proceeds rapidly at first, and continues at a rate that finally approaches zero. The time to attain a practically zero rate, and the magnitude of the loss of load are functions of several factors as follows:

- Temperature
- Initial stress
- Type of metal
- Heat-treatment history
- Degree of cold-work
- Spring and wire size
- Type of load and temperature cycle

Relaxation at moderate temperatures is due to the combination of anelastic strain, transient creep, and relief of residual stresses. Analytic predictions based on a process involving so many variables are not dependable because of insufficient data. Relaxation data are available, however, for compression springs of various materials under several loading conditions and at a limited number of temperatures. The most commonly used spring materials are music wire (carbon steel), 18-8 stainless steel, 17-7 PH stainless steel, and Inconel-X. Assuming a power relationship for relaxation, the constants K, m, and n can be evaluated from the available data. The relaxation equation can be assumed to be:

$$L = K \left(\frac{S_o}{1000} \right)^m \left(\frac{T}{100} \right)^n \quad (5)$$

Evaluation of constants based on a large amount of the available data results in values for K, m, and n, as shown in table 2.

Table 2
VALUES FOR K, m, AND n*

Material	K	m	n
Music Wire	52×10^{-10}	0.6	8.63
18-8 Stainless Steel	81.2×10^{-12}	0.44	10.0
17-7 PH	34.5×10^{-16}	1.13	12.3
Inconel-X	26.4×10^{-10}	0.453	7.5

*See equation (5)

The log - log plots of equation (5) and table 2 are shown in figures 4 and 5. The curves are straight lines which agrees well with the data from which the equations were derived. As mentioned previously, relaxation is a function of spring size, heat treatment, and degree of cold-work. The test data therefore vary with the variation in the specimens tested, and the curves of figures 4 and 5 thus vary to some extent with data from different sources. The curves and the table 2 data are intended primarily for illustrative purposes and for use in preliminary design. For situations requiring accurate relaxation predictions, relaxation tests should be run on springs similar to the ones to be used.

In table 2 and in figures 4 and 5, the relaxation L is the percent loss of stress, load, and deflection Δ of equation (2).

The curves of figures 6 and 7, derived from the relaxation equations, illustrate the variation with temperature of the ratio of the longtime stress S to initial stress for various values of initial stress.

Design for Moderate Temperatures

Data and theory are presently insufficient to predict precisely the behavior of a spring when it is subjected to specific design conditions. Design depends on selection of the

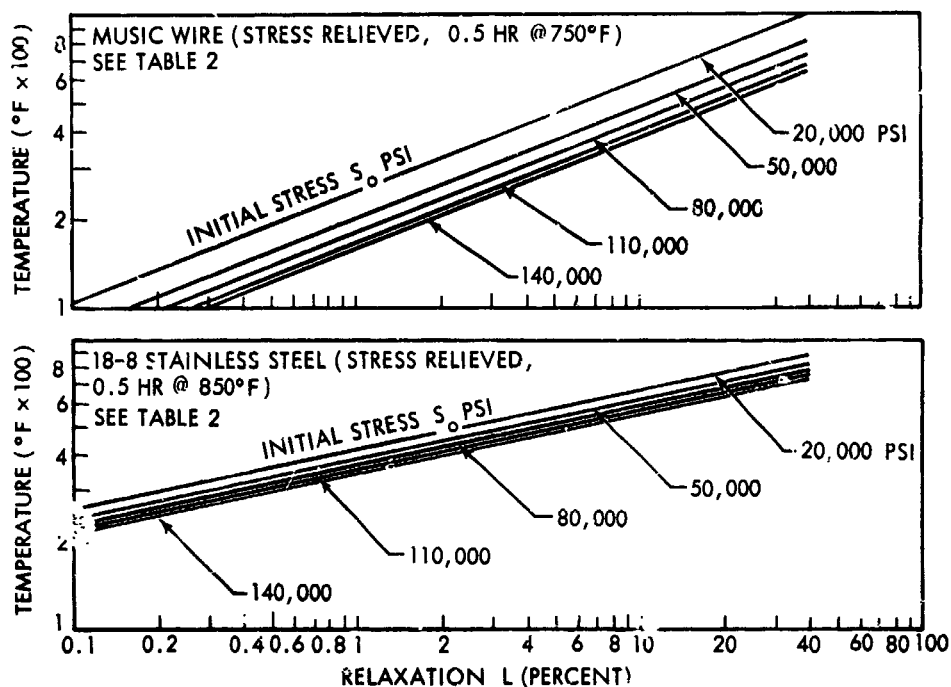


Figure 4 Percent Relaxation Versus Temperature – Music Wire and 18-8 Stainless Steel

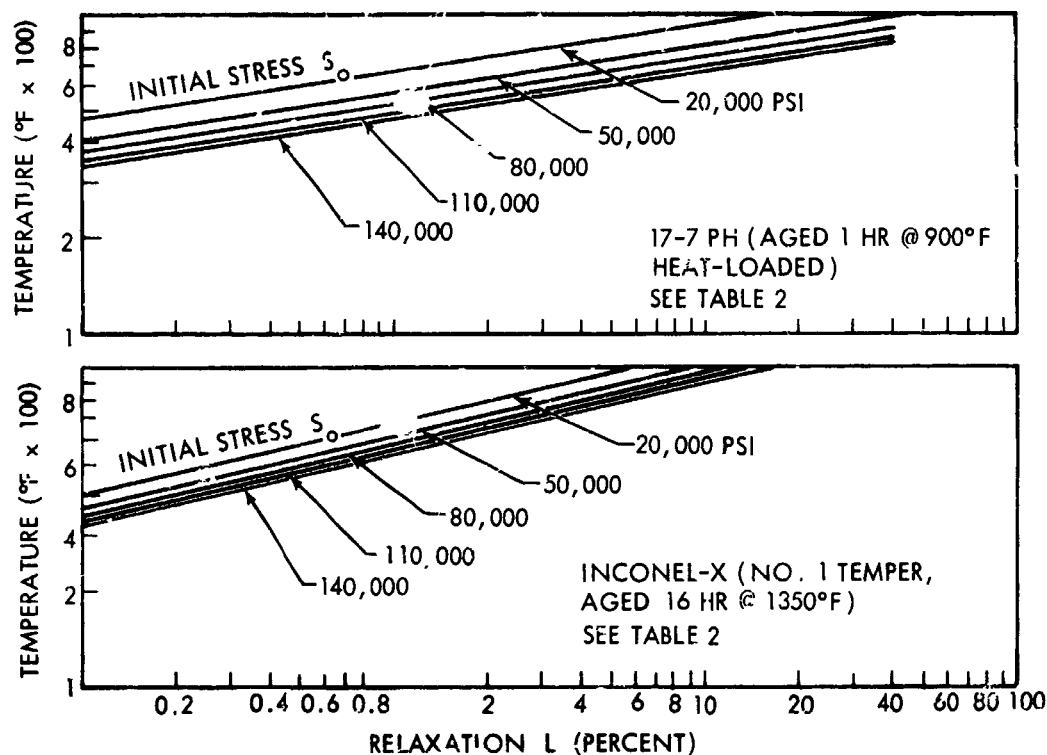


Figure 5 Percent Relaxation Versus Temperature – 17-7 PH and Inconel-X

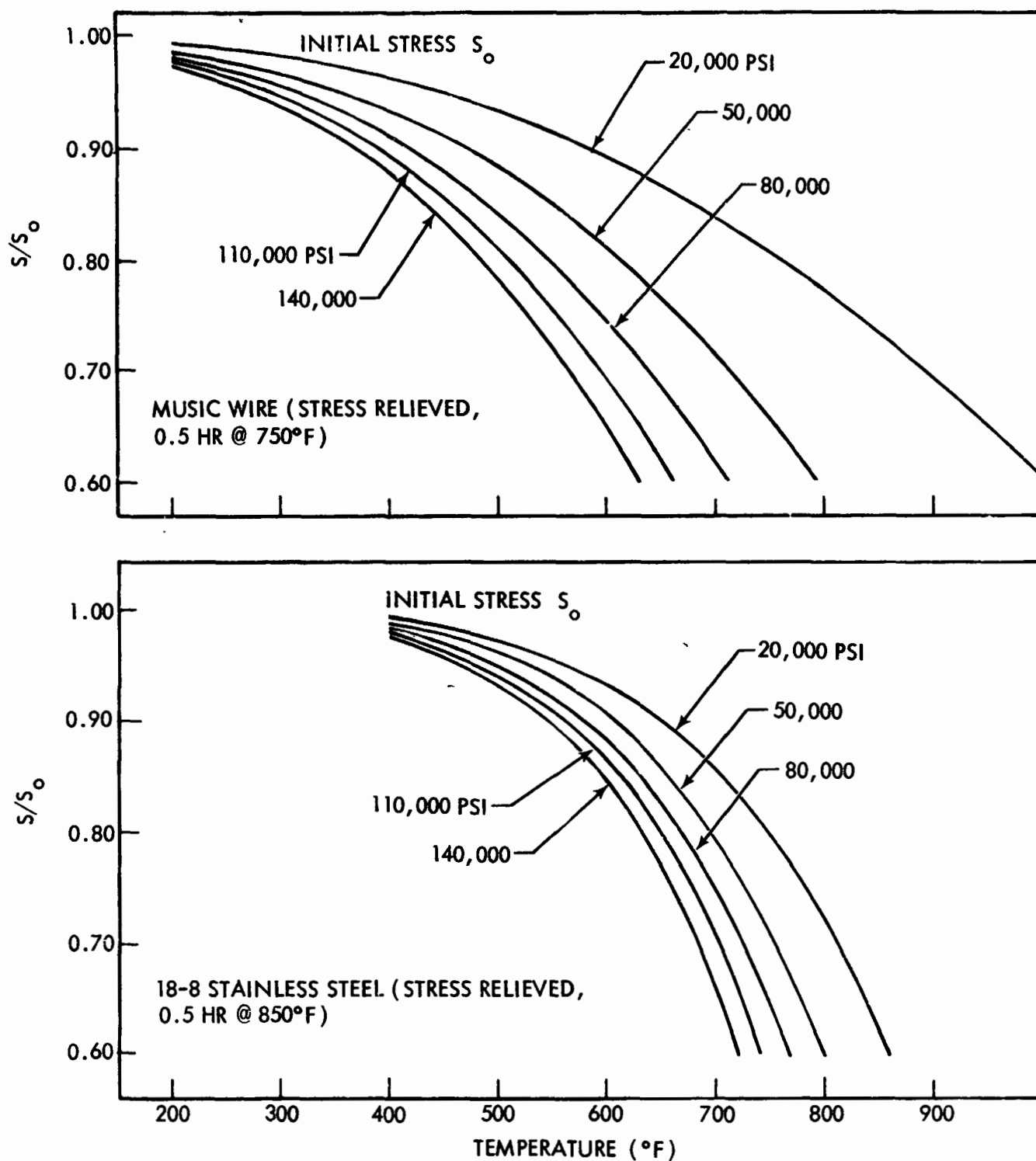


Figure 6 Ratio Between Long-Term Stress and Initial Stress Versus Temperature - Music Wire and 18-8 Stainless Steel

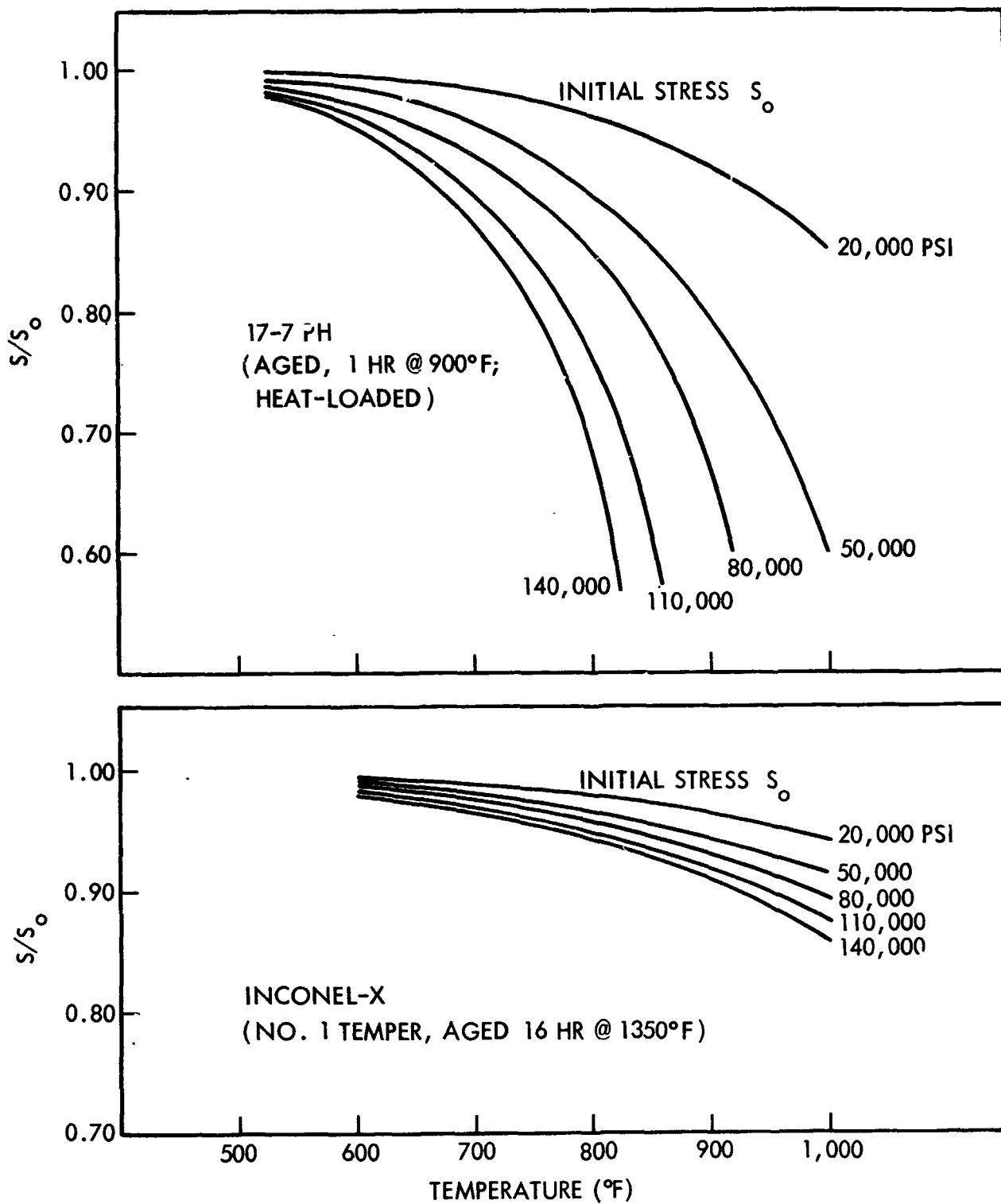


Figure 7 Ratio Between Long-Term Stress and Initial Stress Versus Temperature - 17-7 PH and Inconel-X

proper combination of material, heat treatment, and stress level. These factors are interdependent, and a variety of combinations are possible in meeting design requirements.

To a large extent, the selection of material depends on the chemical environment in which the spring will be used. The presence of fuel or acid vapors, or of oxidizing fluids, may limit the permissible materials to 18-8 stainless steel, Inconel, or other compatible alloys. Further, availability, cost, and delivery schedules may impose additional restraints on material selection.

The mechanical properties of springs are related to the degree of cold-work and the type of heat treatment to which they may have been subjected both before and after manufacture. During the spring-forming process, the wire cold-works, with an associated increase in mechanical properties and introduction of residual stresses. This increase in strength and residual stress adds to that present in the wire because of cold drawing. Often carbon steel and other low-alloy springs are used, as wound, or with a minor stress relief.

Precipitation-hardening metals, such as 17-7 PH and Inconel-X, are reheated after fabrication, since the aging temperature is generally greater than the stress-relieving temperature, and residual stresses are minimal. The greater the initial degree of cold-work, the higher the initial mechanical properties and the less the high-temperature stability. Spring-temper wire should not be used for springs that are to be subjected to environmental temperatures above 250 to 300° F.

To aid in material selection, table 3 indicates temperature limits for the several commonly used spring materials; it should be emphasized that the listed temperatures are approximations and should be used only as general guides to selection.

Table 3

MAXIMUM DESIGN TEMPERATURE

Material	Temperature (° F)
Music wire	300
Alloy steel	400
18-8 stainless steel	550
Inconel, 17-7 PH	650
Inconel-X	900

Improvement in the relaxation properties of springs can be obtained by heat soaking. Heat soaking consists of heating the spring under load (approximately equal to the service load) to a temperature in excess of the service temperature. The soak time and temperature are functions of the type of material, stress level, and temperature level. Heat soaking is accompanied by some reduction in both the length and the mechanical properties of the springs at room temperature. However, heat soaking reduces the relaxation at service temperature sufficiently to warrant its use, particularly where stability is important.

Design Stresses

The permissible stress level for a given material depends on the service temperature and the allowable relaxation. As relaxation cannot be eliminated, it must be anticipated in design and limited to a tolerable value, for which compensation is necessary.

Using the curves of figures 5 and 6 or table 2 data — or other available data — for a specified temperature and an allowable value of relaxation, a design stress S_0 can be obtained. If the applied load is cyclic, the stress S_0 should be less than the endurance limit for the material at the service temperature in order to avoid fatigue failure. For applications involving continually varying temperatures and stresses, the design stress selection should be based on the maximum temperature and stress for a permissible relaxation.

Sample Calculation

A representative problem and its solution are as follows:

- Problem. The wire size and the number of active turns of a compression spring made of 18-8 stainless steel for use in a safety-relief valve are selected to meet the following specifications: mean diameter = 2 in., load = 99 ± 1 lb, service temperature = 540°F , and spring rate = 300 lb/in.
- Solution. Since the required load may vary from 100 lb to 98 lb, a relaxation of 2 percent is permissible.

Substituting into equation (5),

$$2 = 81.2 \times 10^{-12} \left(\frac{S_o}{1,000} \right)^{0.44} \left(\frac{540 + 460}{100} \right)^{10}$$

$$2.46 = \left(\frac{S_o}{1,000} \right)^{0.44}$$

$$S_o = 7,750 \text{ psi}$$

From equation (4) and table I

$$\begin{aligned} G &= (10.5 - 0.00188 \times 540) 10^6 \\ &= 9.5 \times 10^6 \end{aligned}$$

Substituting into equation (1),

$$7,750 = \frac{8 \times 100 \times 2}{\pi d^3}$$

the wire diameter $d = 0.403$ in.

Substituting into equation (3),

$$\begin{aligned} N &= \frac{9.5 \times 10^6 \times (0.403)^4}{8 \times 2^3 \times 300} \\ &= 13 \text{ turns} \end{aligned}$$

CONCLUSIONS

The amount of relaxation exhibited by springs at elevated temperatures is affected by many factors and is not often analytically predictable. The design approach is governed primarily by the temperature level. The two basic high-temperature regimes result in either constant relaxation with an associated limited life (measured in min or hr) or a decreasing relaxation rate resulting in long life (measured in thousands of hours or longer). Limited life occurs at temperatures above 400° F for steel and 900° F for Inconel-X. Long life can be attained at temperatures below those shown in table 3. Based on existing data, the amount of relaxation for various materials can be predicted, at least for preliminary design, by using equation (5).

In cases where the loads and temperatures cycle, and where precise values or relaxation are required, tests should be run under the service conditions. By use of appropriate heat-soak techniques, the effective relaxation at moderate temperatures can be reduced. The selection of soak temperature, load, and time are related to the design parameters and can best be optimized by testing various combinations. As a preliminary indication, soak temperature and stress should exceed the service temperature and stress.

SIMPLIFIED SPACE MECHANISMS USING SUBLIMING SOLIDS

By Howard M. Kindsvater
Lockheed Missiles & Space Company

SUMMARY

N67 16921

The subliming solids technique can sometimes be utilized to solve difficult spacecraft design problems. In this connection, comparison is made of the characteristics and the suitability of subliming-solid and conventional aerospace devices in 17 spacecraft operations requiring 4 classes of mechanisms. To provide meaningful conclusions, a matrix methodology is utilized.

INTRODUCTION

As spacecraft operational lifetimes and travel in deep space are increased, devices requiring mechanical operation must be carefully evaluated to ensure that space exposure problems, such as lubrication loss, radiation effects, or cold welding, will not affect the operational integrity of these devices. At the same time, new techniques that minimize the need for or do not require mechanical operations should be sought, and the operational characteristics of these new devices should be compared with established equipment to ascertain where the new devices should be utilized. The use of subliming solids is proposed as a new technique that requires a minimum number of moving parts (or none at all), and the potential of this technique in the resolution of certain aerospace problems will be evaluated. Subliming solids have been used, or are being developed, for a number of spacecraft operations, including the following:*

- Applied Physics Laboratory Satellite (gravity-gradient damper spring-release mechanism)
- Naval Research Laboratory Satellite (station-keeping system)

*Other aspects of previous work in this field are described in references 1 through 4.

- NASA-Goddard AIMP-E Satellite (attitude-control system)
- NASA-Goddard ATS Satellite (station-keeping system; satellite inversion system)

Since the subliming-solid systems have already proved useful for certain satellite operations, this paper describes the evaluation of other potential uses for subliming solids and presents a parametric evaluation of the several candidate mechanisms suitable for a selected operation. Finally, the relative effectiveness of the various mechanisms for the selected operation is indicated.

Four general classes of mechanisms are considered.

- Energy-release mechanism
- Flow-control devices
- Timing devices
- Force device

METHOD OF PRESENTATION

The methodology employed consists of the following steps:

- For a given aerospace operation or requirement, applicable devices or mechanisms are established.
- For a given requirement, parameters or factors that influence the successful utilization of the mechanism are established. The relative importance of the parameters is weighted on a scale of 1 to 5.
- Using the parameters defined in the preceding step, the relative effectiveness of each mechanism is weighted on a scale of 1 to 5.
- By the matrix technique, utility of the different mechanisms for each requirement is indicated in order of effectiveness.

This methodology has been applied to 17 separate requirements in the 4 general classes of mechanisms under study. The results are summarized in the following sections.

ENERGY-RELEASE MECHANISMS

Spacecraft requirements on operations using energy-release mechanisms are listed in table 1. The relative importance of different parameters in the various requirements, and the relative characteristics of various mechanisms with respect to the parameters are also shown.

Table 1
ENERGY-RELEASE MECHANISM STUDY

Aspect	Parameters				
	Response Time	Power Required	Reliability	Adaptability	Debris Formation
Operational Requirements					
Spacecraft Operation					
Spring Release Operation	3	3	5	2	4
Solar Panel Release	3	3	5	3	5
Antenna Extension	3	3	5	2	3
Stage Separation	5	3	5	3	2
Mechanism Characteristics					
Mechanism					
Solenoid Device	3	3	4	5	5
Explosive Bolt	4	4	4	5	4
Squib-Actuated Cable Cutter	4	4	4	4	4
Shaped-Charge Device	5	4	4	3	3
Primacord Device	5	4	4	3	3
Subliming-Solid Mass	2	5	5	2	5
Subliming-Solid Support Pin	3	3	5	5	4

Selection of the values cited is based on the experience and knowledge of the requirements. In rating the characteristics of the different mechanisms, however, it was assumed that one or more of the devices produces the highest weighting factor for each parameter and that the ratings of the other mechanisms are incrementally lower.

The calculations required to complete the matrix were accomplished to provide relative ratings of the energy release mechanisms, and related results are given in table 2.

Table 2
RELATIVE RATING OF ENERGY-RELEASE MECHANISMS

Spacecraft Operation	Mechanism						
	Solenoid Device	Explosive Bolt	Squib-Actuated Cable Cutter	Shaped-Charge Device	Primacord Device	Subliming-Solid Mass	Subliming-Solid Support Pin
Spring Release Operation	68	70	68	65	67	70	69
Solar Panel Release	78	79	76	71	71	77	78
Antenna Extension	63	66	64	62	62	65	65
Stage Separation	69	75	72	72	72	66	72

These results may be summarized as follows:

	<u>Energy Release</u>	<u>Solar Panel Release</u>	<u>Antenna Extension</u>	<u>Stage Separation</u>
Best Mechanism	Explosive bolt Subliming-solid mass	Explosive bolt	Explosive bolt	Explosive bolt
Second-Best Mechanism	Subliming-solid support pin	Solenoid device Subliming-solid support pin	Subliming-solid mass Subliming-solid support pin	Squib-actuated cable cutter Shaped-charge device Primacord device Subliming-solid support pin

The explosive bolt appears to be the best mechanism for any of these spacecraft operations, but the solenoid-actuated device and the subliming-solid devices appear of interest where response time is less critical.

FLOW-CONTROL DEVICE

Parameter ratings for operational requirements and mechanism characteristics of flow-control devices are shown in table 3. Relative ratings of the flow-control mechanisms for the different spacecraft operation are presented in table 4.

Table 3
FLOW-CONTROL MECHANISM STUDY

Aspect	Parameters					
	Response Time	Power Required	Reliability	Adaptability	Debris Formation	Number of Function
Operational Requirements						
Spacecraft Operation						
Propellant Dump	3	2	5	2	2	1
Attitude Control	5	4	5	5	5	5
Station-Keeping	2	5	5	2	5	3
Fail-Safe Flow Stoppage	3	2	5	2	4	1
Mechanism Characteristics						
Mechanism						
Solenoid Valves	3	4	3	5	5	5
Squib Valves	4	5	4	4	4	3
Shaped-Charge Device	5	5	4	3	3	3
Frimacord Device	5	5	4	3	3	3
Subliming-Solid Plug Device	2	4	5	4	5	4

Table 4
RELATIVE RATINGS OF FLOW-CONTROL MECHANISMS

Spacecraft Operation	Mechanism				
	Solenoid Valve	Squib Valve	Shaped-Charge Device	Primacord Device	Subliming-Solid Plug Device
Propellant Dump	57	61	60	60	59
Attitude Control	120	115	110	110	116
Station-Keeping	91	90	82	82	94
Fail-Safe Flow Stoppage	67	69	66	66	71

The following is a summary of the findings:

	<u>Propellant Dump</u>	<u>Attitude Control</u>	<u>Station-Keeping</u>	<u>Fail-Safe Flow Stoppage</u>
Best Mechanism	Squib valve	Solenoid valve	Subliming-solid plug device	Subliming-solid plug device
Second-Best Mechanism	Shaped-charge device Primacord device	Subliming-solid plug device	Solenoid valve	Squib valve

For one-function operations (propellant dump and fail-safe flow stoppage) the squib valve, the shaped-charge or primacord devices, and the subliming-solid plug devices are of interest. For multifunction operations (attitude control and station-keeping), the solenoid valve and subliming-solid plug formation device are best, the former being of particular importance when response time is critical.

TIMING DEVICES

There are many requirements for timing devices in spacecraft operations. Only four representative operations, however, have been selected for consideration here.

Table 5 provides parameter ratings for the various operations and for the different mechanisms. The wide rating differences, both in requirements and characteristics, should be noted. The relative abilities of the various timing mechanisms to meet the spacecraft operations are shown in table 6.

Table 5
TIMING DEVICE STUDY

Aspect	Parameters					
	Time Accuracy	Temperature Effect	Reliability	Adaptability	Number of Simultaneous Events	Residue Left
Operational Requirements						
Spacecraft Operation						
Sequence Timer	5	4	5	2	2	1
Multiple-Event W/Short Delay	3	1	5	2	2	1
Multiple-Event Without Delay	5	3	5	3	5	1
Single-Event Long Delay	4	3	5	2	1	5
Mechanism Characteristics						
Mechanism						
Electric Timers	4	5	3	5	1	1
Electronic Counters	5	5	3	5	1	1
CDF Time Train	3	4	4	1	5	2
Pyrotechnic Delay	3	3	4	3	4	2
Alloy Delay	3	3	4	3	4	2
Subliming-Solid Delay	2	3	5	2	1	5

Table 6
RELATIVE RATING OF TIMING MECHANISMS

Spacecraft Operation	Mechanism					
	Electric Timer	Electronic Counter	CDF Time-Train	Pyrotechnic Delay	Alloy Delay	Subliming-Solid Delay
Spacecraft Sequence Timer	68	73	65	63	63	58
Multiple-Event W/Short Delay	45	48	47	48	48	45
Multiple-Event Without Delay	71	76	77	75	75	60
Single-Event Long Delay	62	66	58	61	61	73

Results of these studies may be summarized as follows:

	<u>Spacecraft Sequence Timer</u>	<u>Multiple Event W/Short Delay</u>	<u>Multiple Event Without Delay</u>	<u>Single Event W/Long Delay</u>
Best Mechanism	Electronic counter	Electronic counter Pyrotechnic delay Alloy delay	CDF time train	Subliming-solid delay
Second-Best Mechanism	Electronic counter	—	Electronic counter	Electronic counter

The electronic counter or electric timer are excellent timing devices where high time accuracy and single events are requirements. These devices are usually less desirable for multiple events since several mechanical operations may be involved in initiating the multiple events. The pyrotechnic delay or the alloy-burning delay are advantageous in that several events may be started with one signal, and the built-in delay permits subsequent initiation without additional signal. Timing accuracy for these pyrotechnic devices is lower because of burning rate variation as a function of temperature. The confined detonating-fuse time train is excellent for simultaneous initiation of several events because one signal may be transmitted to many points quite rapidly through the confined detonating fuse. The subliming-solid delay has the advantage that the device can be maintained

indefinitely during launch preparation and countdown and further, it is not actuated until the nozzle heater is activated to permit proper functioning of the thrusting device. The subliming-solid plug is completely evaporated so that no residue remains to interfere with the nozzle operation.

FORCE DEVICES

The requirements for force devices can be highly varied in spacecraft operations. Parameter ratings required by the operations and providing definition for mechanism characteristics are presented in table 7. The relative ratings of the force mechanisms for the various spacecraft operation are given in table 8.

Table 7
FORCE DEVICE STUDY

Aspect	Parameters				
	Force Constancy	Reliability	Adaptability	Power Required	Number of Functions
Operational Requirements					
Spacecraft Operation					
Payload Separation	4	5	3	2	1
Nose Fairing Removal	2	5	3	1	1
Spacecraft Attitude Control	5	5	3	3	5
Satellite Despin	5	5	1	3	2
Environmental Controller	3	5	3	5	5
Mechanism Characteristics					
Mechanism					
Compressed Spring	3	5	2	5	1
Bimetallic Element	2	4	1	5	5
Yo-Yo Device	4	4	1	5	1
Subliming-Solids System	5	4	2	1	5

Table 8
RELATIVE RATING OF FORCE MECHANISMS

Spacecraft Operation	Mechanism			
	Compressed Spring	Bimetallic Element	Yo-Yo Device	Subliming-Solid System
Payload Separation	54	46	50	53
Nose Fairing Removal	43	37	37	42
Spacecraft Attitude Control	66	73	63	79
Satellite Despin	54	56	58	60
Environmental Controller	70	79	65	71

The results of the table may be summarized as follows:

	Payload Separation	Nose Fairing Removal	Spacecraft Attitude Control	Satellite Despin	Environmental Controller
Best Mechanism	Compressed spring	Compressed spring	Subliming-solid system	Subliming-solid system	Bimetallic element
Second-Best Mechanism	Subliming-solid system	Subliming-solid system	—	Yo-Yo device	—

The specialized requirements of the operations and the unusual characteristics of the mechanisms selected for evaluation have limited backup mechanisms for all operations. The subliming-solid system is not competitive with the compressed spring device where a single function is required, but it is normally best where several repeated functions are required. The yo-yo device would normally be rated best for the satellite despin operation if only one operation was required. The use of the bimetallic

controller for environmental control capitalizes on the unique character of this device. When the spacecraft faces the sun, the heat on the bimetallic element causes a shutter to close, which excludes the radiation. As the angle of the spacecraft changes so the radiation is reduced, the bimetallic element opens the shutter, allowing more heat to be introduced into the spacecraft. This simple mechanism for environmental control proved highly successful for various space flights.

CONCLUSION

Comparing the relative effectiveness of various aerospace mechanisms in meeting the requirements of the many spacecraft operations indicates that the subliming-solid devices offer advantages for certain types of application. These devices are highly versatile and can be utilized in many forms (e.g., as an energy storage device, a support pin, a flow-control device without moving parts, an unusual timing device, and a force-producing system), and other applications can undoubtedly be proposed for this concept. Characteristics of the subliming-solid devices should be evaluated together with those of conventional aerospace mechanisms to establish the best candidate device for the requirement.

REFERENCES

1. Mobley, F. F.; and Fischell, R. E.: Orbital Results From Gravity-Gradient Stabilized Satellites. Preprint, Symposium on Passive Gravity-Gradient Stabilization, NASA Ames Research Center, May 10 - 11, 1965.
2. Hardt, A. P.; Foley, W. M.; and Brandon, R. L.: The Chemistry of Subliming Solids for Microthrust Engines. Preprint 65-595, AIAA Propulsion Joint Specialist Conference (Colorado Springs, Colo.), June 14 - 18, 1965.
3. Jonath, A. D.: Gas Dynamic Problems in Low-Pressure Microthrust Engines. Preprint 65-616, AIAA Propulsion Joint Specialist Conference (Colorado Springs, Colo.), June 14 - 18, 1965.
4. Steger, R.: Measurement of Very Low Thrust Associated With Reaction Control Systems. Preprint 17.19-6-65, 20th Annual Conference, Instrument Society of America (Los Angeles, Calif.), Oct. 4 - 7, 1965.

PRECEDING PAGE BLANK NOT FILMED.

ZERO-G TESTING OF SATELLITE INSPECTION MECHANISMS*

By R. N. Lahde
Lockheed Missiles & Space Company
and J. W. Lebold
Lockheed-California Company

INTRODUCTION

N67-16922

In most present and future space programs, civilian or military, rendezvous and docking operations play a major role. This paper describes some of the results of a study (ref. 1) concerned with the methods and means of testing the mechanisms needed in support of such docking operations, with particular emphasis on inspection of noncooperative targets. **

The emphasis on noncooperative targets introduces an element of uncertainty and risk into the docking operation, which reflects in the flexibility and versatility necessary for the docking systems. It also reflects on methods and types of facilities required to test components and systems for such operations.

DOCKING CONCEPTS AND MECHANISMS

It was necessary first to define these docking concepts and systems. The result of a literature search was supplemented by additional docking concepts based on a study of the characteristics of chase and target vehicles, and of docking missions typical of space systems scheduled to be operational by 1970.

Among the mechanisms considered in the study, one of the most promising for handling a variety of targets is an extendable and storable boom (figure 1). Attached to the boom is a manipulator capable of rotation and making possible the attachment

*This paper presents some of the results of a study conducted by the Lockheed-California Company under Contract AF 33(657)-10466, sponsored by the Air Force Dynamics Laboratory.

**Orientation guidance to the Lockheed-California study, provided by W. C. Buzzard, Air Force Flight Dynamics Laboratory, Aeronautical Systems Division, Wright-Patterson Air Force Base, Ohio, is gratefully acknowledged.

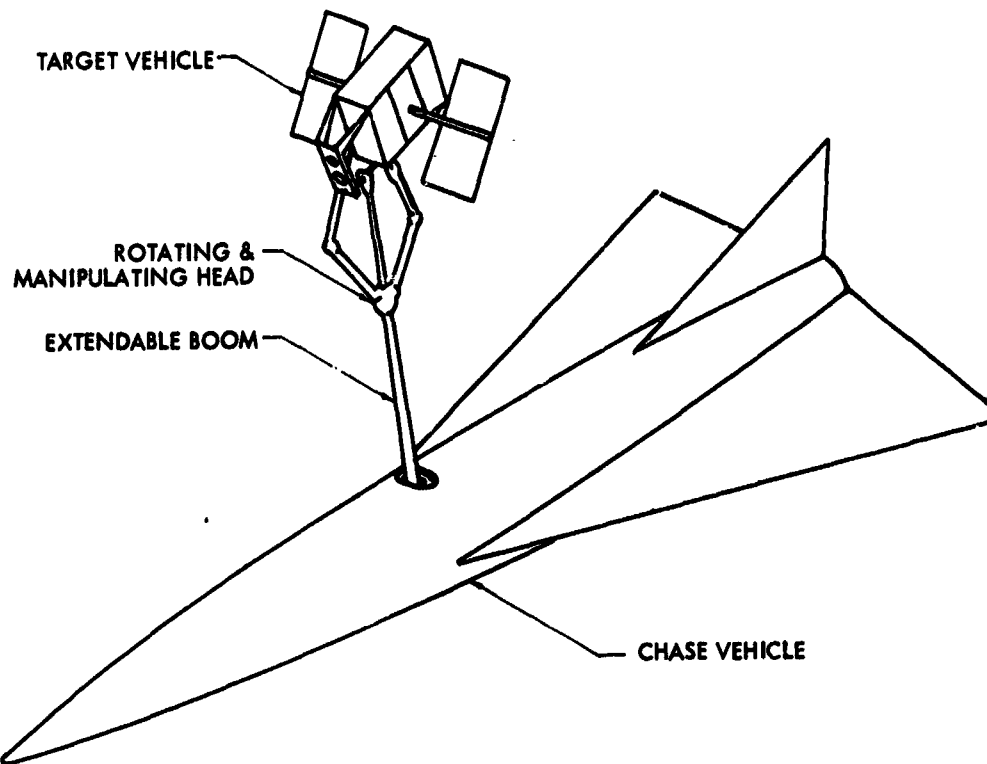


Figure 1 Boom and Manipulator

of its arms to a rotating target. The boom is a ribbon-type design permitting storage inside a rotating drum. The entire unit can be swiveled for alignment with the target. In extension of this design principle, various interchangeable heads can be provided to suit particular target characteristics.

One important prerequisite for a docking operation in the case of a spinning or nutating target is the despinning of the target, regardless of whether or not physical contact is involved in the docking mission. These targets are likely to have such protuberances as antennas or other sensors, solar panels, and/or attitude jets. An important consideration of a despinning mechanism is to avoid damaging the target. One mechanism considered for this purpose uses electromagnetic braking by means of a large, dc-energized electrical coil. The chase vehicle is controlled so as to place the spin axis of the target in the plane of the electrical coil. Eddy currents are then generated in the target by movement through the magnetic field, tending to reduce the rate of spin.

The coil is superconductive and cooled with LH_2 , and it generates a magnetic field of approximately 60 gauss at its center. The coil, which can be folded for storage, would be approximately 30 ft in diameter, have a cross section of 3 sq in., and weigh 100 to 150 lb. It was calculated that a target 8 ft in diameter, with an aluminum skin cross section of 6 sq in. would have a time constant of spin decay of approximately 7.5 min. Preliminary design indicates that, to further decrease the time constant, the coil would have sufficient structural strength to permit active spinning against the target spin. Electrical power required to overcome losses in the non-superconductive portions of the circuit is approximately 1 kw. The method requires the chase vehicle to have an adequate sensor and maneuvering control system. The chaser's attitude control would also cancel the effect of the despinning torque transmitted to the chaser.

The preceding examples are typical of the large number of docking mechanisms examined as part of the Lockheed study. Most of these mechanisms were extracted from existing literature, and extensive use was made of an Air Force report on space vehicle attachment and connection (ref. 2). Additional guidelines for docking systems were found in reference 3.

This survey aspect of the study had two main results: it narrowed down the number of systems likely to be used in future docking operations, and provided a basis for establishing design requirements for verification methods and systems.

TESTING METHODS

Following determination of a model of the verification needs of docking systems in general, three methods of verification were studied:

- Analytical verification
- Ground testing of components and systems
- Flight testing

In accordance with the purpose and limited scope of this paper, only ground testing of complete docking systems will be considered, and some results of design studies on such systems will be presented in more detail.

From the standpoint of classification of testing, four primary methods have been considered:

- Fixed-base simulators
- Buoyancy of a static fluid
- Drag of a moving fluid
- Mechanical support systems

Briefly, only the mechanical support-systems approach combines the characteristics of technical feasibility with flexibility of test applications and dynamic accuracy of testing; therefore, it appears to be superior to the other methods. Fixed-base simulators are widely used and are considered to be excellent where the main objective of the docking simulation is to test or train the human operator or to examine specific docking concepts. However, for the task of general verification testing of docking mechanisms, such simulators lack the flexibility and versatility necessary for such a facility.

ZERO-G SIMULATION CONCEPTS

One of the main difficulties in simulating the docking operation with mechanical support systems is the disturbing influence of gravity. A basic approach to the problem is to create forces equal and opposite to the weight of the simulated vehicles and all gravity-affected components of importance. One rather accurate method of balancing the effects of gravity consists of suspending the two vehicles in mechanical gimbals and using other mechanical means to provide the translational motions. Facilities can further be classified with respect to the method used to create the dynamic motions of the two vehicles. In one concept, termed "computed motion," the motions of the two vehicles are generated by servos controlled by a computer, (analog or digital) which treats the equations of motions and receives measurements of the contact forces as inputs. In the other concept, termed "natural reaction," the vehicles are free to follow the forces and torques applied in the docking process as if they were actually under the weightless, free-floating conditions of space.

It has not been possible to establish a clear-cut superiority of either concept because some of the factors involved in the comparison are sensitively dependent on assumptions which cannot be assessed with sufficient accuracy, and which are rapidly changing with technological progress.

The computed motion concept features relaxed requirements regarding mass and inertia duplication, balancing, and gravity compensation. Gravity compensation of parts of certain complex docking mechanisms, however, may be just as important as in the natural reaction concept, depending on the characteristics of the mechanism to be tested.

The computed motion concept is burdened with greater computer complexity. Another disadvantage is the methodology of instrumenting the docking system and the vehicle simulators in order to determine all forces required for computation of dynamic motions. Instrumentation can be particularly difficult for extended, flexible docking mechanisms, and practically impossible for some mechanisms. To set up this elaborate instrumentation will also require much time, and the tendency to keep testing complexity within reasonable limits will lead to reduced accuracy of the simulation.

In contrast, the natural-reaction concept is not burdened with these problems; however, it requires careful balancing and full-scale duplication of the mass and inertial values of the simulated vehicles. The gimbal system suspending the vehicles must be rigid and friction must be kept very low or servo-compensation of friction effects must be provided. Further, the actual propulsion and attitude control forces must be duplicated in full scale.

In designing in accordance with the natural-reaction concept, it is sometimes difficult to duplicate the moment of inertia or the mass in one particular axis when gimbal and attached components add unequal amounts of inertia or mass to different components of motion.

This difficulty can be overcome through the application of the concept of "artificial mass." In this concept, a servo adds or subtracts a force or torque to the particular component of motion or rotation in proportion to the longitudinal or angular acceleration of that motion as measured, for example, by an accelerometer. Required in this concept is a force servo, a device which generates a force or torque output proportional to an input signal independent of output position. Various solutions are available for performing this task.

Ground-Supported Vehicle Simulator

To obtain the necessary high degree of dynamic realism in simulating the two vehicles, the chaser and target, each must be capable of accurate dynamic motion in six degrees of freedom.

A good method of providing the three translational motions for the vehicle simulator is to support it from a smooth plane and level floor by means of a truck equipped with cycloid drive units (figure 2). These units are commercially available and are readily adaptable to both the computed-motion and natural-reaction concepts. Also, smooth operation of the cycloid drive unit was demonstrated in actual tests. Typically, the

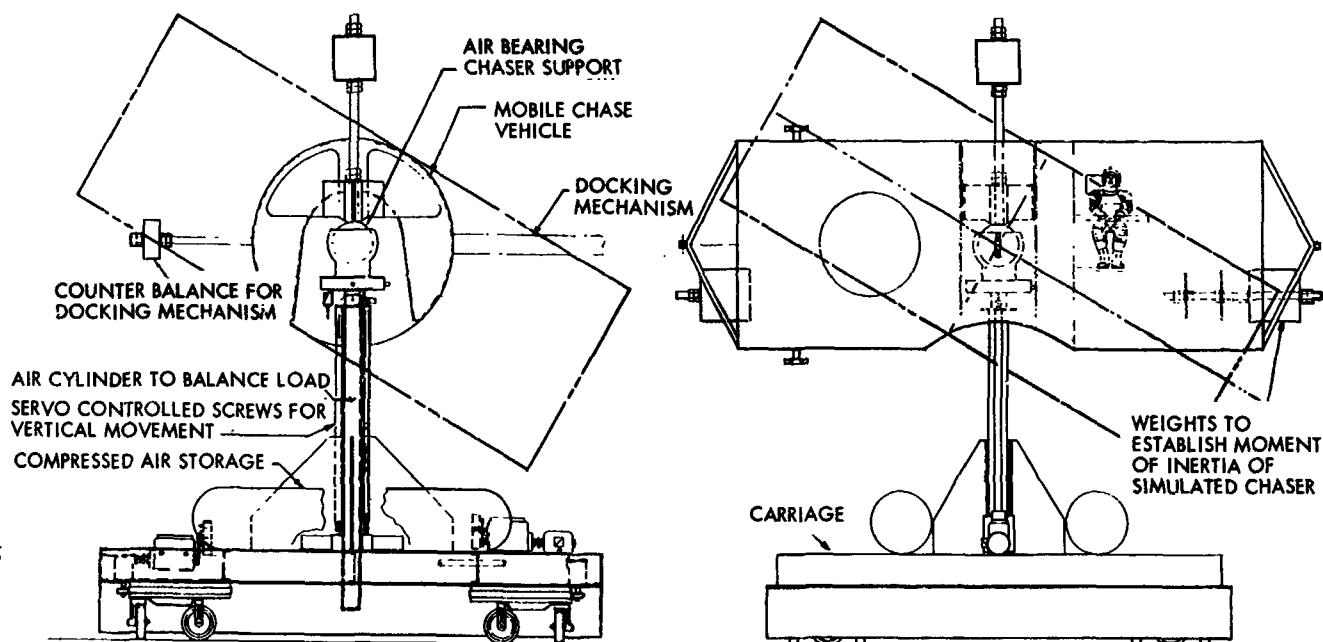


Figure 2 Floor-Supported Cycloid Drive Chase Vehicle

vehicle simulator is supported by three cycloid drive units. Each drive unit features a horizontally oriented disc, motor-driven at constant speed, to which three supporting coaster wheels are attached. Axis orientation of the wheel is controlled by means of linkage to a control point located near the center of the drive unit and moved by servos. Moving the control point in the horizontal x-y plane, in the x or y direction, generates drive-speed components proportional to the displacement of the control point in the y and x directions, respectively. The drive unit need not, therefore, change orientation in order to change direction of travel. For computed motion, the computer output can control directly the servos driving the control point of the cycloid drive. For natural reaction, a horizontal, low-friction bearing is used with a follow-up system controlling the cycloid-drive servos.

Vertical motion is controlled by a servo system and a motor-driven ball-lead screw. This configuration represents a completely natural-reaction type of simulator. The chase vehicle consists of a cylinder 26 ft long and 10 ft in diameter, and contains properly distributed weights to simulate moments of inertia of the lifting re-entry chase vehicle. The cylinder is gimballed and balanced around all three gimbal axes. It contains provision for installation of the docking system to be tested. A propulsion system capable of providing thrust for all six degrees of freedom, along with the necessary control, is incorporated. The two operator stations represent a universal setup whereby the controls for the docking system can easily be removed to accommodate various docking mechanisms. To counteract the effect of unbalance by a cantilevered docking structure, an adjustable weight is mounted along the centerline of the docking mechanism.

An airpad system could be used instead of a cycloid drive, and may eventually surpass the cycloid drive in accuracy and smoothness of operation. Disadvantages of the airpad system are the difficulty of adapting it to the computed-motion mode of operation, and the need for more power for its operation.

Overhead, Suspended Vehicle Simulator

Another promising configuration is suspension of the vehicle simulator from an overhead carriage or crane bridge. This overhead support principle, as in floor

mounting, lends itself to the computed-motion as well as natural-reaction concept of operation. Many ways to mechanize overhead support were studied and parametrically compared.

An overhead suspension using a servo-balanced beam is illustrated in figure 3. As shown, the servomotor providing the vertical motion is used to counterbalance the weight, which leads to rather high but not impractical power requirements for this motor. Various means, such as hydraulic or pneumatic springs, have been investigated to reduce this power requirement.

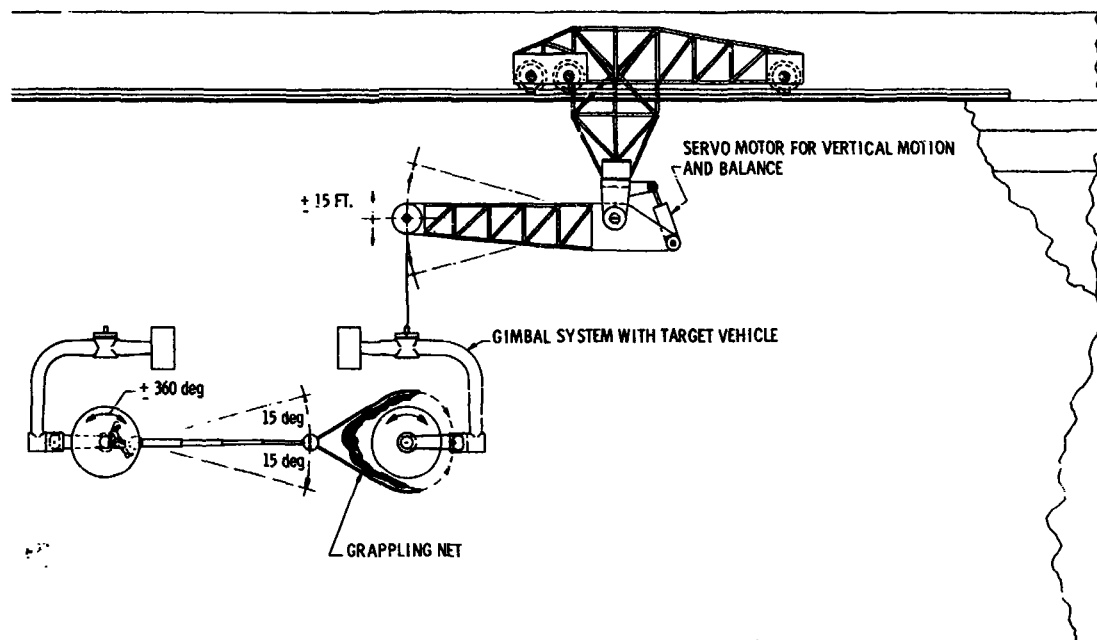


Figure 3 Servo-Balanced Overhead Beam

PARAMETRIC ANALYSIS

A parametric comparison placed the types of vehicle simulators into two categories: mechanical configuration, i.e., airpad, cycloid drive, etc., and a method of generating the simulated motion, i.e., computed motion, natural reaction, and combinations thereof. The listing of simulator characteristics thus forms a two-dimensional matrix. Further, all pertinent configurations in the matrix were rated in accordance with four

rating factors — utilization, cost, authenticity, and versatility. These factors are actually headings, each summarizing a number of contributions, which are discussed in more detail in the Air Force report documenting this study (ref. 2).

This parametric comparison showed, in general, that the natural-reaction concept achieved higher total scores than the computed-motion concepts, a consequence due mainly to high weighting of the authenticity factor. It must be emphasized that the method is somewhat arbitrary and that selection of the best vehicle simulator may be changed by changing the weighting factors; for example, if cost-factor weighting is increased relative to authenticity factor, the computed motion concept becomes more attractive.

For selection of the entire facility, other factors appear in addition to those considered in the matrix of vehicle simulators. In particular, it appears that the combination of one floor-mounted chase-vehicle simulator with one overhead-supported target simulator provides special advantages to the facility not possessed by the choice of either two floor-mounted or two overhead-supported simulators. The advantages exist with regard to overall test flexibility and freedom of action, i. e. , motion of the two vehicles relative to each other, because this combination alone allows the simulated test vehicles to pass over, under, and around each other. Also, this type of facility appears to have a greater growth potential.

ASSUMPTIONS AND FUTURE WORK

The assumptions upon which this study was based may not have been accurate and complete in all respects. Also, if such a facility is to be built, changes of assumptions warranted by better definition and advances in technology must be taken into account before construction begins because, in many areas, they will significantly influence optimum technology of docking system testing. Typical of such areas are:

- Definition of target characteristics
- Docking system design
- Docking loads and influence on structures
- Advances in attitude and maneuvering technology
- Advances in sensor technology
- Advances in computer technology

SUMMARY AND CONCLUSION

The following desirable characteristics for a versatile docking system validation facility have emerged as a result of this study:

- Use of true time scale, as essential for human operator control
- High fidelity in producing true dynamic motion of both vehicle simulators by providing the possibility of using the natural reaction concept in angular as well as in translational modes
- Full-scale duplication of masses and moments of inertia of both vehicles
- Possibility of using actual docking hardware
- Six degrees of freedom of motion for each vehicle simulator
- Largest possible range of motion
- Maximum freedom of relative motion between target and chase-vehicle simulator
- Accuracy of balancing and freedom of friction such that the maximum error force due to unbalance or friction is $1/3,000$ of the weight of the vehicle
- Flexibility of installation of different types of mechanisms
- Flexibility of testing a variety of target configurations

The facility which was finally recommended features a floor-mounted cycloidal drive truck for the chaser (figure 2) and an overhead-supported target suspended from a carriage which travels on an overhead bridge. Counterweights balance the vertical load of the target vehicle. The realism of simulation and freedom of relative motion obtainable with the proposed combination floor-mounted overhead-supported vehicle simulators is shown in figure 4.

REFERENCES

1. Lebold, J. W., and Lahde, R. N.: Methodology for Evaluating and Validating Mechanical Rendezvous Subsystems. RTD-TDR-63-4292, Lockheed-California Co., Feb 1964
2. Muscolino, C. J.; Berger, R. T.; and Weiss, M.: Space Vehicle Attachment and Connection. ASD-TDR-62-950, American Machine and Foundry Co., Nov 1962
3. Buzzard, W. C.: Design Considerations for Orbital Attachment, Connection and Docking Systems. FDFM-TM-63-18, Research and Technology Division, Air Force Systems Command, Sep 1963

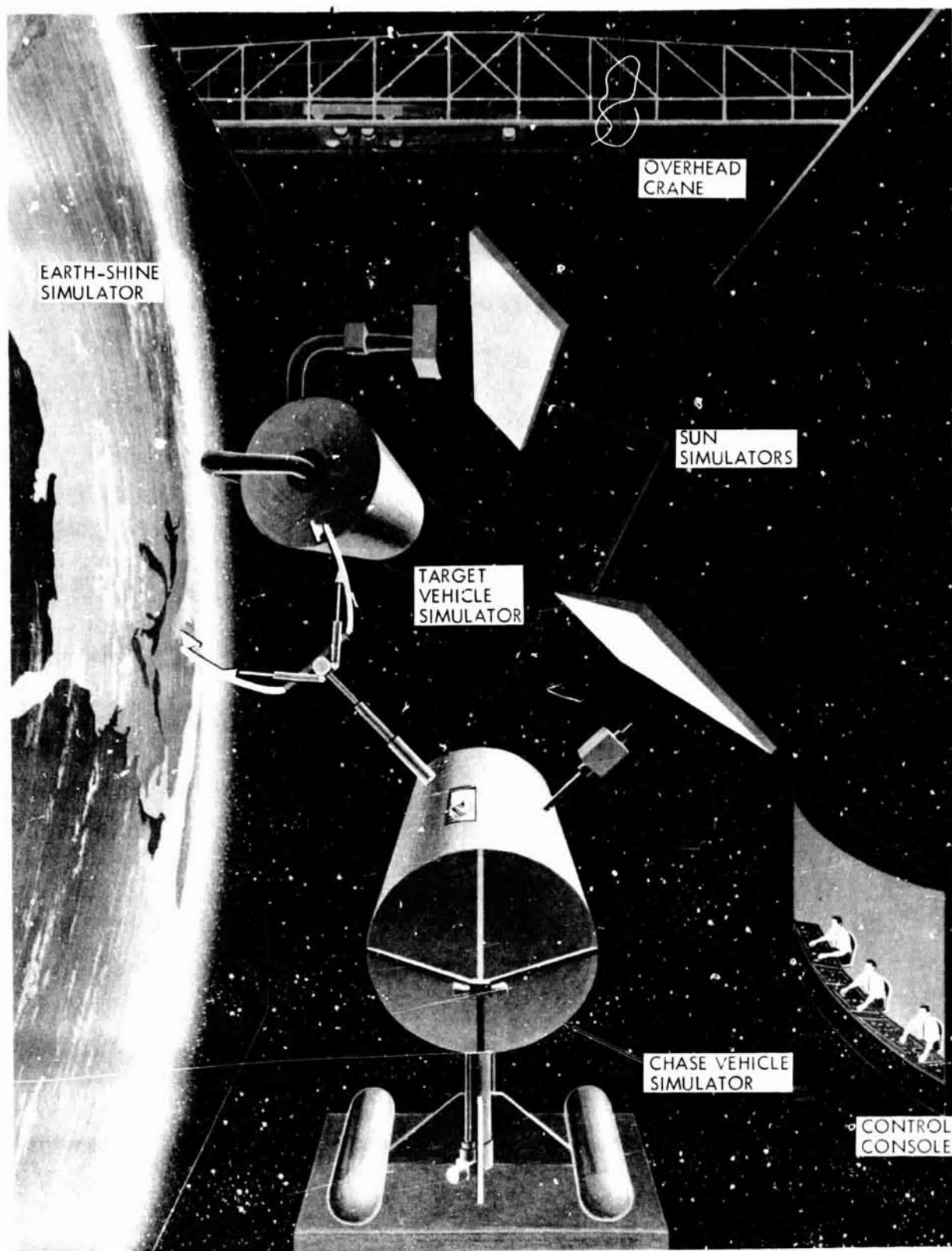


Figure 4 Proposed Docking System Validation Facility

A CONCEPT FOR THE DESIGN OF VARIABLE-VISCOSITY,
VARIABLE-STIFFNESS DAMPERS

By Jerome J. Lohr
Ames Research Center
National Aeronautics and Space Administration

SUMMARY

N67 16923

This paper discusses a design concept for damping mechanisms which permits an order-of-magnitude increase in damping efficiency compared with that of existing dampers. The concept utilizes polymeric materials at temperatures in the region of their glass transition temperatures. In this region (which may extend over a bandwidth of 10° to 50°C or more), configurational rearrangements of the polymer chain backbones allow very high mechanical energy absorption. Both free- and forced-vibration systems were used to study the properties of mechanical systems employing such dampers.

INTRODUCTION

Aerospace systems often are exposed to extreme shock or vibration. Typical sources of shock and vibration are booster ignition, retro-rocket firing, docking maneuvers, and planetary impact. The effects of these environmental parameters are often accentuated by the design configuration and weight limitation.

For example, solar cell panels must be light in weight and easily deployed. Shaker tests on Ranger Block III solar cell panels (ref. 1) have indicated panel-tip structural gains of 50 times the input at the spacecraft base. These high gains could result in structural yielding and failure if they occurred during a mission. As another example, planetary impact – whether soft or hard – imposes severe restraints (ref. 2) on design of instruments capable of withstanding impact decelerations.

In each of the above examples, vibration or shock-attenuation devices will be used to decrease the stress on various system components. Shock and vibration damping systems, if they are to be used in the aerospace environment, must be both reliable and efficient. Reliability is often enhanced if the design can be kept simple. Efficiency normally means high energy absorption relative to the weight of the damping mechanism.

The proposed damping mechanism concept, promising to fulfill the requirements for simplicity and efficiency, utilizes polymeric materials at temperatures in the region of their glass transition temperatures. This region is characterized as that wherein the polymeric material changes from a relatively stiff material to a relatively soft, rubbery material. The damping capability often increases by an order of magnitude in this region (ref. 3).

The concept is not entirely new in that manufacturers have compounded various special materials which permit very high damping at ambient temperatures. Actually, the compounders were formulating materials that have near-ambient glass transition temperatures.

In the aerospace environment, temperatures may deviate widely from earth ambient temperature; thus these materials might be relatively ineffective dampers. However, by understanding the concept of the damping material operating in its glass transition range, a designer could choose efficient damping materials simply by selecting materials whose glass transition temperature range coincided with the operating temperature of the system. Alternatively, the designer could control the temperature of the damper so that it would operate in its glass transition region. The purpose of this paper is to indicate the increase in damping capacity that occurs in the glass transition region of several thermoplastic materials, and to suggest some ways in which this capability might be utilized.

ANALYSIS

Free oscillations of a body supported by a viscous damping isolator may be described by the equation (ref. 4)

$$m\ddot{y} = -ky - c\dot{y} \quad (1)$$

where m is the mass of the body, y is its displacement, k is the damper spring stiffness, and c the damper viscosity. The ratio of the amplitude of successive free oscillations is commonly used to indicate the degree of damping in a system. The logarithm of this ratio is known as the logarithmic decrement Δ and is related to the viscosity c by the relation

$$\Delta = \frac{2\pi (c/c_c)}{\sqrt{1 - (c/c_c)^2}} \quad (2)$$

where $c_c = 2\sqrt{km}$ and is called the critical viscosity. Damping capacity greater than c_c does not allow oscillatory motion of the vibrating member. The damping ratio c/c_c may be determined from measurements of the logarithmic decrement Δ and by use of equation (2).

For a forced-vibration system, the motion of a body mounted on a vibration isolator which is itself attached to a vibrating support, may be described by the equation

$$m\ddot{y} = k(s - y) + c(\dot{s} - \dot{y}) \quad (3)$$

where, as schematically shown in figure 1, m is the mass of the vibrating body, k is the spring stiffness, c is the viscosity of the dashpot, and y and s are displacements as shown.

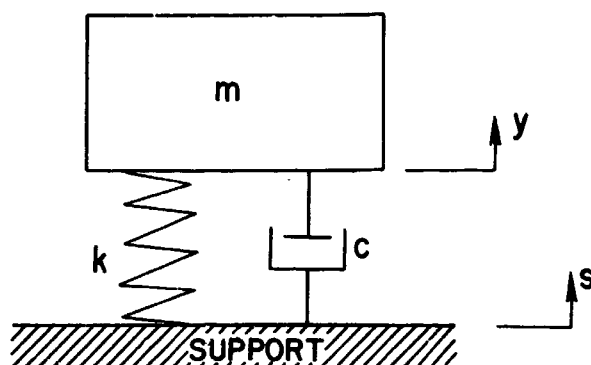


Figure 1 Schematic Diagram of Viscously Damped Single-Degree-of Freedom System

The initial transient vibration is assumed to disappear as a result of the damping, and the mounted body is assumed to oscillate with forcing frequency ω . If the amplitude of motion of the support is s_0 and that of the body y_0 , then the ratio y_0/s_0 , called the transmissibility T_D , is given by the equation

$$T_D = \frac{y_0}{s_0} = \sqrt{\frac{1 + \left[2(\omega/\Omega)(c/c_c)\right]^2}{\left[1 - (\omega^2/\Omega^2)\right]^2 + \left[2(\omega/\Omega)(c/c_c)\right]^2}} \quad (4)$$

where Ω is the resonant frequency of the system. Comparison of experimentally determined transmissibilities by use of a plot of T_D versus ω/Ω at various values of c/c_c allows determination of the damping ratio. The damping ratio should be a basic property of a material at a specified temperature.

EXPERIMENT

Free-vibration measurements were made with a torsional pendulum (ref. 5). The measurements were made in the approximate frequency range from 0.4 to 2.5 cps at temperatures accurate to within $\pm 1/2^\circ\text{C}$.

A system that loads disks of polymeric material in shear was used for the forced-vibration experiments. The significant portion of the system is shown in figure 2.

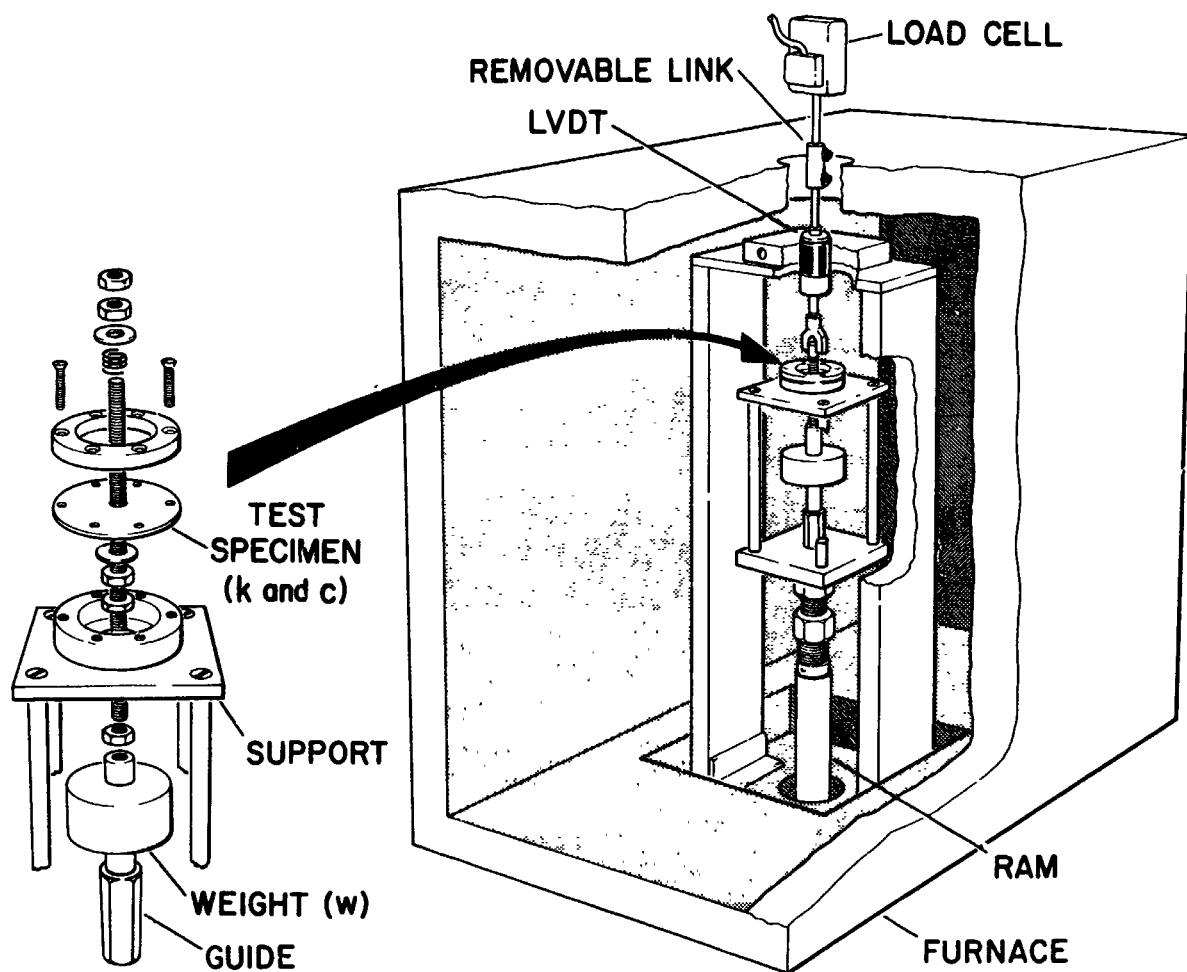


Figure 2 Test Fixture for Forced-Vibration Experiments

The disk acts as a spring and supports the weight immediately beneath it. The disk and its supporting flanges can be replaced by various commercial isolators. The linear variable differential transformer (LVDT) immediately above the disk is used to measure displacement of the disk core as the disk and its support move up and down under sinusoidal excitation. The cage holding the disk, weight, and LVDT was mounted on a hydraulic ram. Sinusoidal oscillations over a frequency range from 1 to 100 cps were programmed with a closed-loop servo-controlled hydraulic system. The output of the

ram-control LVDT and the disk-core-displacement LVDT was recorded on an oscillograph. The test fixture was enclosed in a chamber where temperatures were controlled within $\pm 1/2^\circ\text{C}$.

The system was allowed to equilibrate for 20 min at a given test temperature. The rod extending out of the furnace was then connected, through a removable link, to a load cell and the system oscillated at 0.1 and 1 cps to measure the sample stiffness. In all cases, ram displacement was 0.050 in. or less. The load cell was then disconnected. With the weight supported only by the disk, the frequency spectrum was then scanned, with amplitudes of vibration recorded at 10-cps increments. For all forced-vibration tests reported here, the total weight used was 0.597 lb.

RESULTS AND DISCUSSION

The increased damping that occurs in the range of the glass transition temperature T_g may be seen by examining the free-vibration curves for poly-methyl methacrylate (PMMA) shown in figure 3.

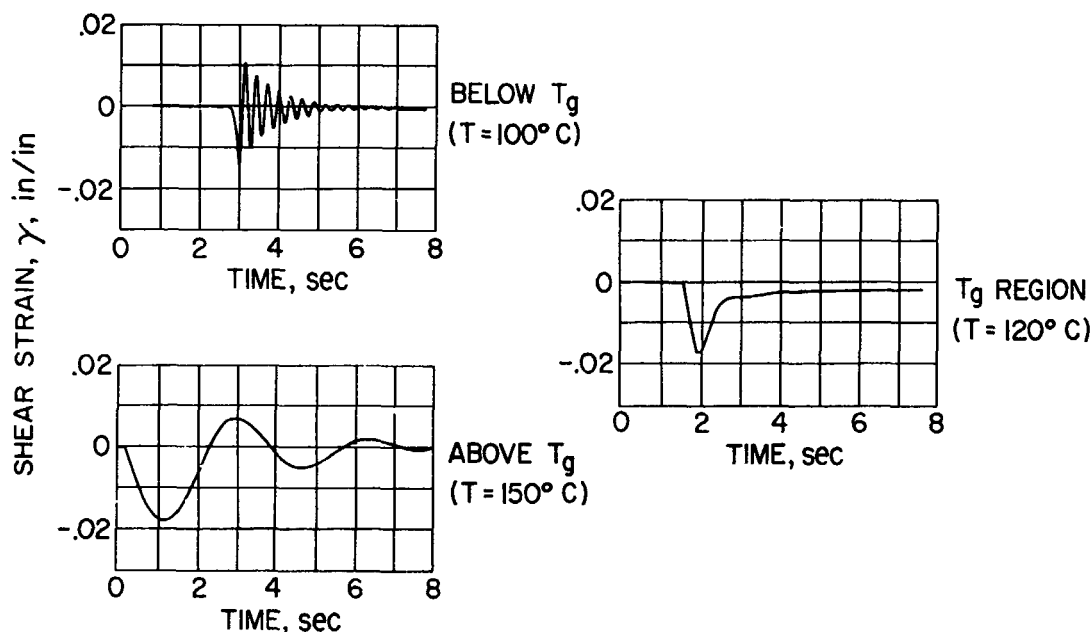


Figure 3 Typical Free-Oscillation Decay Curves for PMMA

The left curve is a typical vibration-decay curve determined at temperatures below T_g . The middle curve shows that damping at 120°C is so high that essentially no oscillation occurs after the material returns from its initial perturbation; this would correspond to a damping ratio of 1.0 or greater. The curve measured at 150°C, which is above the T_g region, shows decreased damping capability and a lower resonant frequency, owing to the decrease in stiffness of the PMMA.

An indication of the magnitude of the T_g region and the increase in damping that occurs in the region may be seen from figure 4, where logarithmic decrements and damping ratios are shown as a function of temperature for several different materials.

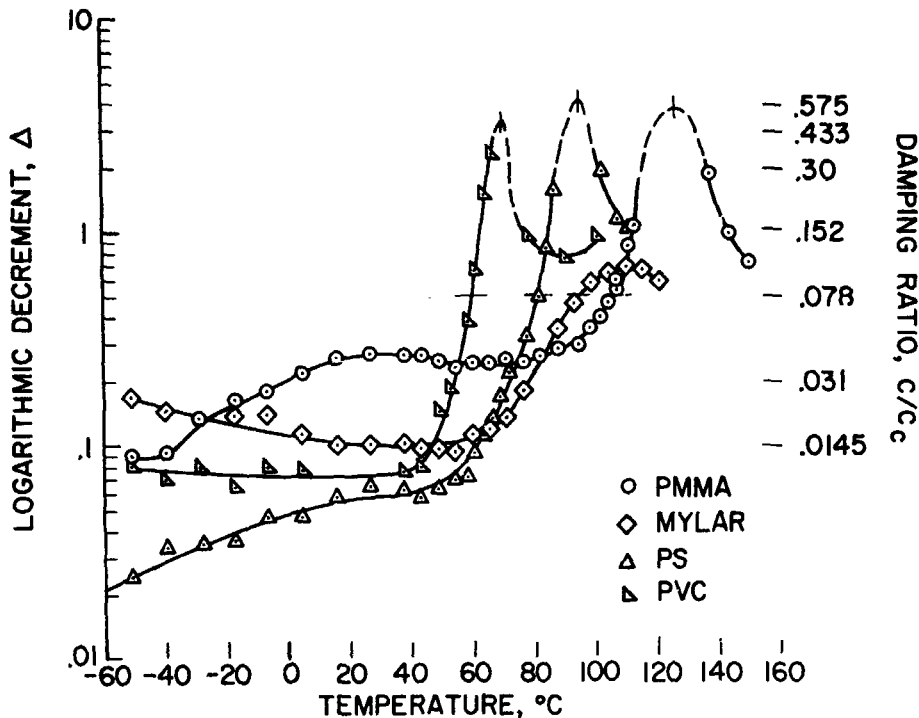


Figure 4 Logarithmic Decrement and Damping Ratio as a Function of Temperature for Various Materials

The data for this plot are the same as those used in ref. 6, wherein they were used to determine T_g . The dashed lines indicate that, with the torsional pendulum system which was used, it was impossible to measure damping ratios above about 0.4. Depending on the damping level of interest, the temperature range of greatly increased damping may be seen to be from 10° to 50°C in extent.

One limitation on using thermoplastic materials for isolators is their tendency to creep or slump after carrying a load at temperatures in the T_g region. If the materials are lightly cross-linked, they will have a built-in memory and return to their original shape when heated to temperatures above T_g . These cross-linked materials still show essentially the same damping behavior, as shown in figure 5 where Δ and c/c_0 are again indicated as functions of temperature. These materials were synthesized

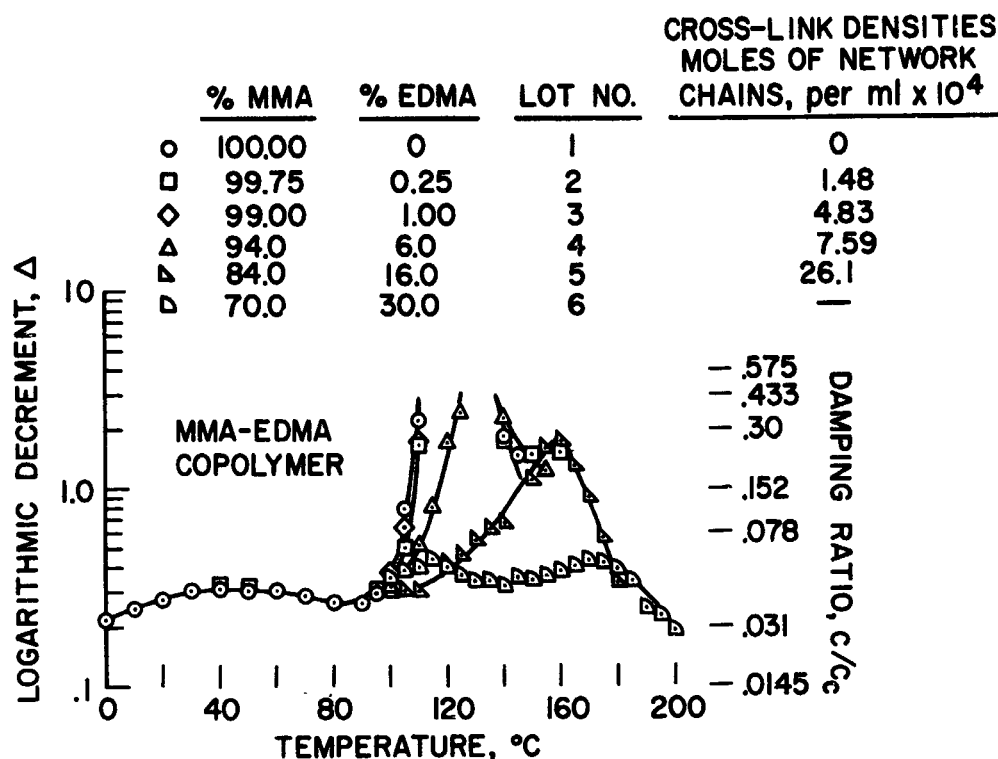


Figure 5 Logarithmic Decrement and Damping Ratio as a Function of Temperature for Cross-Linked PMMA

from varying ratios of methyl methacrylate (MMA) and ethylene glycol dimethacrylate (EDMA), a trifunctional monomer, which allows formation of cross-links. The cross-link densities were measured under contract to NASA (ref. 7). Materials numbered 2, 3, and 4 have cross-link densities in the range of commercially available rubber materials.

A graphic method of comparing the damping capability of materials in their T_g range with that of commercial isolators from Lord Manufacturing Company is shown in figure 6. The data were measured with the system shown in figure 2, except that the

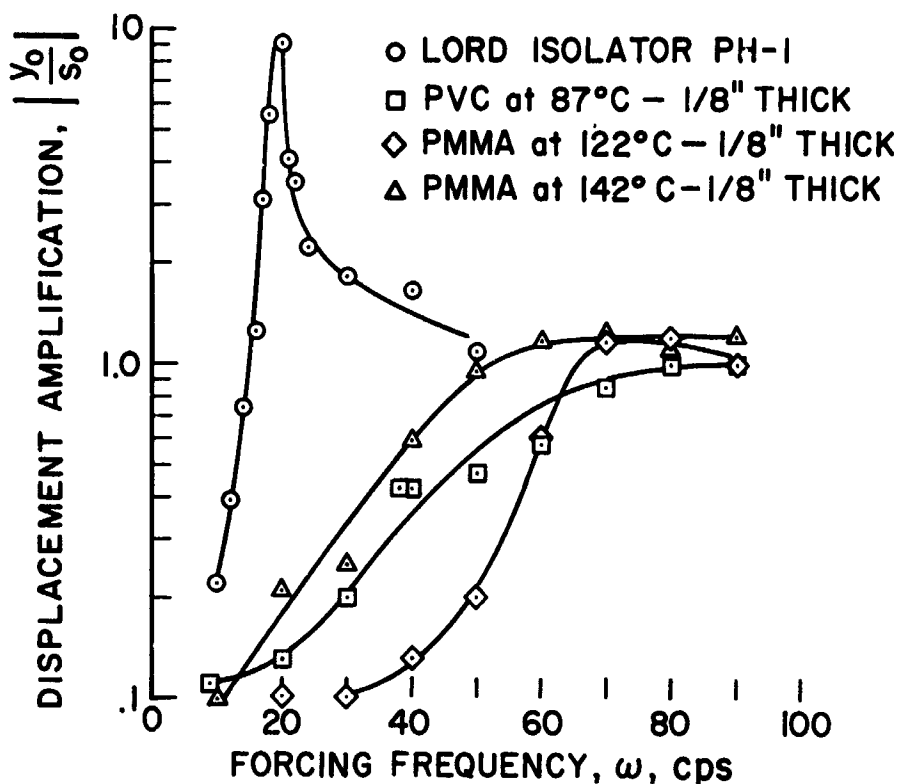


Figure 6 Displacement Amplification Versus Forcing Frequency for Different Damping Systems

specimen LVDT was mounted directly on the vibrating system. Thus, the displacement amplification y_0/s_0 is a measure of how much the damping disk deflects. As may be seen from figure 6, resonance for the commercial isolator occurred at about 20 cps. Although it cannot be seen in this figure, resonance for the polyvinyl chloride (PVC) and PMMA occurred at frequencies varying from 30 to 55 cps with corresponding displacement amplifications of 0.3 to 0.4. Above the resonance point, the displacement amplification approaches 1.0 because the body is effectively motionless. Figure 6 shows graphically that the position of the driven body, when the PVC or PMMA is used as a damping material, is well controlled at all frequencies.

Using damping materials in their T_g regions also allows some stiffness variation. The T_g region coincides with the temperature region where there is a marked decrease in stiffness of the material. The stiffness is related to the resonant frequency by the equation (ref. 4)

$$\Omega = \sqrt{\frac{k}{m}} = 3.13 \sqrt{\frac{k}{w}} \quad (5)$$

where w is the weight of the vibrating mass. Resonant frequencies for various materials were calculated from the measured stiffness and are shown in table 1. In general, they agree with the measured values quite well. In the next paragraphs, more will be said about the results in this table.

Table 1
COMPARISON OF CALCULATED AND EXPERIMENTALLY DETERMINING
RESONANT FREQUENCIES

Specimen	Temperature (°C)	Frequency for Stiffness Measurement ω (cps)	Ω_{cal} (cps)	Ω_{exp} (cps)
Lord PH-1	Ambient	0.1	18.5	20.5
Lord PH 377-3	↓	0.1	29.5	29.5
Lord PH-12	↓	0.1	56.8	55.0
1/8 in. PVC	78	0.1	45.8	~ 60
		1.0	55.5	
	87	0.1	34.0	~ 45
		1.0	39.2	
	96	0.1	35.1	43.0
		1.0	38.3	
	106	0.1	34.5	42.0
		1.0	38.8	
1/32 in. PVC	78	0.1	25.1	~ 38
		1.0	34.5	
	87	0.1	22.1	27.0
		1.0	24.4	
	96	0.1	17.13	22.5
		1.0	21.2	

Transmissibilities measured with the system shown in figure 2 were normalized by dividing the forcing frequency by the resonant frequency. These results for commercial isolators, as well as theoretical transmissibility values from equation (4), are shown in figure 7. A damping ratio of c/c_c equal to zero is, of course, the solution for an undamped system. As may be seen from figure 7, the amplitude of the driven member increases to as much as 9 times the driving amplitude. This corresponds to damping ratios of approximately 0.05 to 0.10.

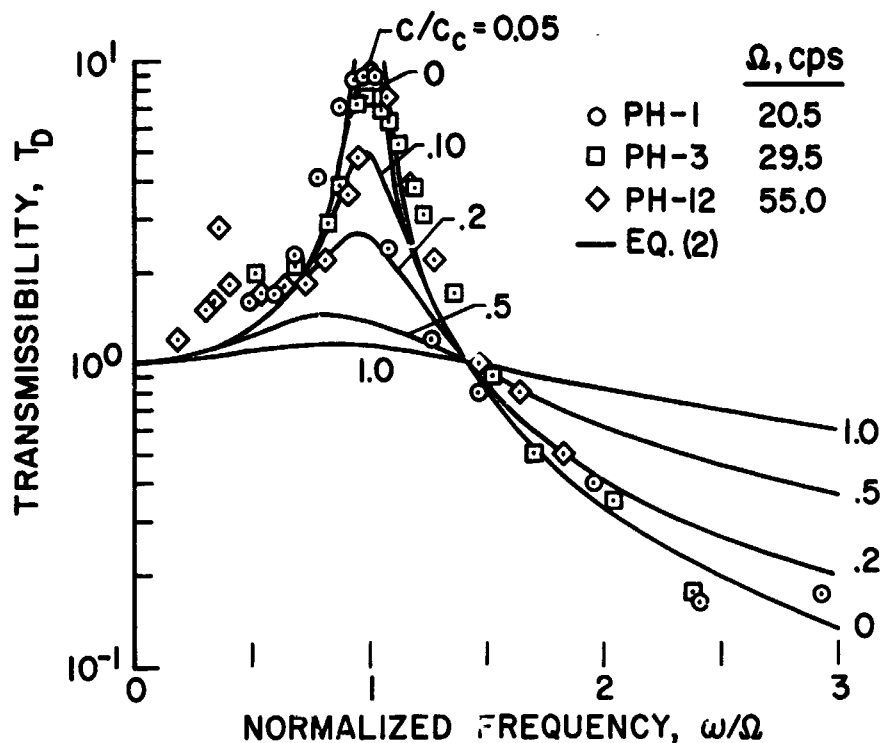


Figure 7 Transmissibility as a Function of Normalized Frequency for Commercial Isolators

Transmissibilities of a nominally 1/8-in. thick sheet of commercial PVC as a function of normalized frequency are shown in figure 8. These show that at temperatures of 78° and 87°C, which are in the T_g region, the transmissibilities near resonance are of the order of 1.25 or less, which corresponds to a damping ratio of approximately 1. As

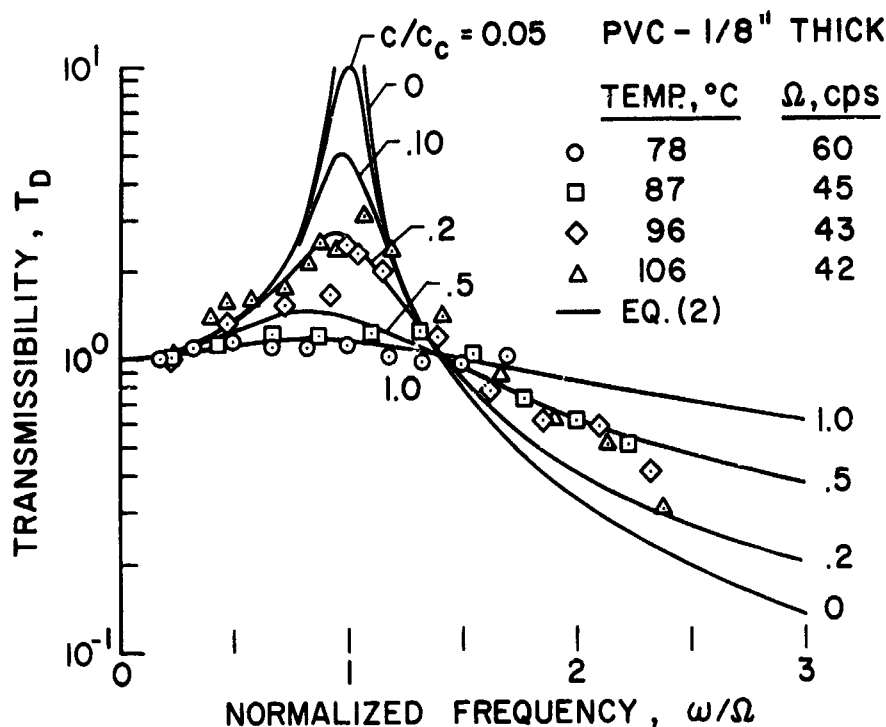


Figure 8 Transmissibility as a Function of Normalized Frequency for 1/8-in. PVC

the temperature is increased to above the glass transition region, to 96° and 106° C, the transmissibility increases, as one would expect, because the material is now in its rubbery region. As we saw in figure 7, in the rubbery region the damping ratios are much lower.

An interesting aspect of forced-vibration tests of these high-efficiency damping materials is that it is difficult to observe where resonance actually occurs because there is so little amplification of displacement. Even observing the change in the phase angle between the forcing and the following displacement is difficult, because for highly damped systems the phase angle changes slowly (ref. 4). Consequently, the frequency used to normalize the data was calculated from the measured stiffnesses using equation (5). This presented a minor difficulty, in that the stiffness is frequency dependent. This does not lead to a major error, however, because the resonant frequency calculated from equation (5) changes only about 10 percent for a one-decade increase in forcing frequency, as may be seen from table 1.

For those combinations of temperature and material where the resonant frequency could be experimentally observed, it was found to be about 10 percent higher than the calculated resonant frequency. Thus, the calculated frequency was increased by 10 percent to normalize the 78° and 87°C data in figures 5 and 6. For the forced-vibration tests, damping at temperatures just below the glass transition temperature region was not determined. This was because available test specimens were not thin enough to give stiffnesses that would produce resonant frequencies below the 100 cps capability of the test equipment.

In summary, increased damping capability shown by materials in their T_g region presents a designer with many possibilities. There is a wide choice of available polymeric materials, so he may choose one whose T_g region corresponds with his application temperature. Alternatively, he may plasticize materials to lower their T_g regions to his operating temperature. Or, he might imbed heating wires in the damping material, and by controlling temperature, control both stiffness and viscosity. By controlling the temperature of the damper, he could also use the damping materials as near-rigid supports for part of a mission, and as very efficient damping materials for another part. Understanding the phenomenon of increased damping in the T_g region of polymers therefore gives the designer an additional degree of freedom in designing reliable and efficient systems that can significantly surpass those formerly available.

REFERENCES

1. Gayman, M.: Jet Propulsion Laboratory, TR 32-793, 1965.
2. Adams, J. L.: Jet Propulsion Laboratory, TR 32-844, 1966.
3. Ferry, J. D.: Viscoelastic Properties of Polymers, Wiley, New York, 1961.
4. Crede, C. E.: Vibration and Shock Isolation. Wiley, New York, 1951.
5. Dudek, T. J.; and Lohr, J. J.: J. Appl. Poly. Sci., vol. 9, 1965, p. 3795.
6. Lohr, J. J.: Trans. Soc. Rheology, vol. 9, no. 1, 1965, p. 65.
7. Frederick, J. E.; Tschoegl, N. W.; and Smith, T. L.: Stanford Research Institute Final Report, Contract NASr-49(13), 1966.

PRECEDING PAGE BLANK NOT FILMED.

ANALYSIS OF A SATELLITE ANGLE-OF-ATTACK SENSOR

By William E. Frye
Lockheed Missiles & Space Company

N67 16924

SUMMARY

The direction of the deceleration due to airdrag on an attitude-stabilized satellite is sensed by a simple pendulum immersed in a damping fluid. This paper considers the manner in which the device responds to perturbations caused by attitude oscillations, variations in air density, orbit eccentricity, gravity gradient, and internal instrumental perturbations. Restrictions on the location of the device relative to the center of mass of the vehicle and the choice of damping fluid are also discussed.

INTRODUCTION

Since satellite drag force caused by the residual atmosphere is directed along the negative velocity vector, any device that can detect the effect of this force can be used, in principle, to determine the satellite attitude in pitch and yaw relative to the velocity vector, i.e., the angle-of-attack. The drag force will cause a small deceleration (acceleration in the negative velocity direction) proportional to the air density, the speed of the satellite, and the projected area normal to the velocity (since the satellite is moving in a medium where free molecular flow prevails). By the Einstein Equivalence Principle the effect of this deceleration on a pendulum can be illustrated by a pendulum with its support point at rest in a weak uniform gravitational field with the gravitational acceleration equal to the drag deceleration. If the satellite is in a circular orbit, if the air density is constant at that altitude, and if the area of the

satellite projected normal to the velocity vector remains constant (i.e., a well-stabilized vehicle), then the drag deceleration is constant, and the equation of motion of the pendulum is the well-known one for a simple pendulum suspended by a flexible string from a fixed support in a weak gravitational field. If damping is present (e.g., the pendulum is immersed in a fluid that offers viscous resistance to motion of the pendulum bob) the pendulum should eventually hang at rest in the direction opposite to the drag force vector, regardless of any initial angular velocity or position that the pendulum might have had.

Several perturbing influences can disturb this ideal equilibrium position of the pendulum. If the point of support is displaced from the center of mass of the vehicle, attitude oscillations of the vehicle will cause lateral accelerations of the support. This will affect the position of the bob relative to the support point. Similarly, thrust pulses from attitude-control jets in pitch and yaw that do not form pure torque couples will cause acceleration of the support point.

Variations in the density of the air through which the vehicle is passing (ref. 1) will cause variations in the drag deceleration and, under certain conditions, parametric excitation of the pendulum. Density variations can arise from such causes as the day-night influence on air-pressure altitude, influence of solar particle bombardment variations on the upper atmosphere, and the altitude variations of an eccentric orbit.

Variations in projected area presented to the airstream because of attitude oscillations will cause variations in the drag force, and result in variations in the equivalent acceleration acting to restore the pendulum bob to its equilibrium position. If the attitude excursions are small (as for a well-stabilized vehicle), it can be expected that this effect will be small and can be neglected.

Earth gravity and gravity-gradient effects on the pendulum can be expected to be negligible if the instrument is located close to the center of mass of the vehicle. The pendulum will normally lie close to the local horizontal, and, since the pendulum is quite short, the gravity gradient forces will be negligible.

Perturbation effects internal to the pendulum instrument can occur if care is not taken in the design. The support thread for the pendulum bob should be perfectly flexible so that the tension of the thread passes through the point of support, and no spurious forces or torques act on the bob. Proper choice of material for the thread can, hopefully, minimize this perturbation.

Because of the almost zero-g environment, convection currents in the fluid surrounding the pendulum, caused by localized heating, should not be a problem. In any event, the effect can be minimized by proper thermal isolation and stabilization of the instrument.

DYNAMIC ANALYSIS

The simplest form of damping of the pendulum motion can be provided by immersing the pendulum in a hermetically sealed can containing a fluid. A gaseous type is preferable since no bubble problem exists with a gas. Because the pendulum will move very slowly, the Reynolds number is small — typically less than one. Stokes' Law of viscous drag (ref. 2) should be valid. Thus

$$\text{Drag force} = 3\pi\mu vd = K_F v$$

for a sphere of diameter d moving at a speed v in a medium having a viscosity coefficient μ . Typical values of viscosity coefficient for several gases are listed in table 1.

Table 1

VISCOSITIES OF VARIOUS GASES AT 20°C^(a)

Gas	Viscosity (micropoise)
Air	180
Argon	220
Helium	194
Krypton	246
Neon	311
Xenon	226

(a) Handbook of Chemistry and Physics, 44th ed.

Of the common gases, neon has the largest value at room temperature, and it can therefore be assumed that it will be used to fill the pendulum container. Since viscosity is independent of the pressure and density of the gas, there is no advantage to high pressure and a subatmospheric pressure can be used (e.g., 5 psi).

Vehicle attitude oscillations about the center of mass (measured in pitch and yaw relative to the velocity vector) tend to be somewhat random, as the attitude control system functions whenever the dead band is exceeded. For our purposes the oscillations can be approximated by a sinusoidal function of time with a period of typically 100 sec and an amplitude equal to the dead band, typically 1 deg. These motions have the following effects:

- If the pendulum support is displaced from the vehicle center of mass, acceleration of the support point $R\ddot{\psi}$ occurs.
- Rotation of the case causes a force on the pendulum through the damping of the gas in the case $(-K_F r \dot{\psi})$ where R is the distance of the pendulum support from the vehicle center of mass, and ψ is the vehicle angle-of-attack.

From figure 1, the equation of motion of the pendulum, including the effects of vehicle deceleration, vehicle attitude oscillations, orbit eccentricity, and damping of the pendulum motion can be written as follows:

$$m(r\ddot{\theta} + R\ddot{\psi}) = -m a \sin \phi - K_F r \dot{\theta}$$

where the drag deceleration is approximately $a = a_0 + b \sin \omega t$ for elliptic orbits and m is the mass of the pendulum. If the angles are small, this equation applies equally well to motion in pitch and yaw.

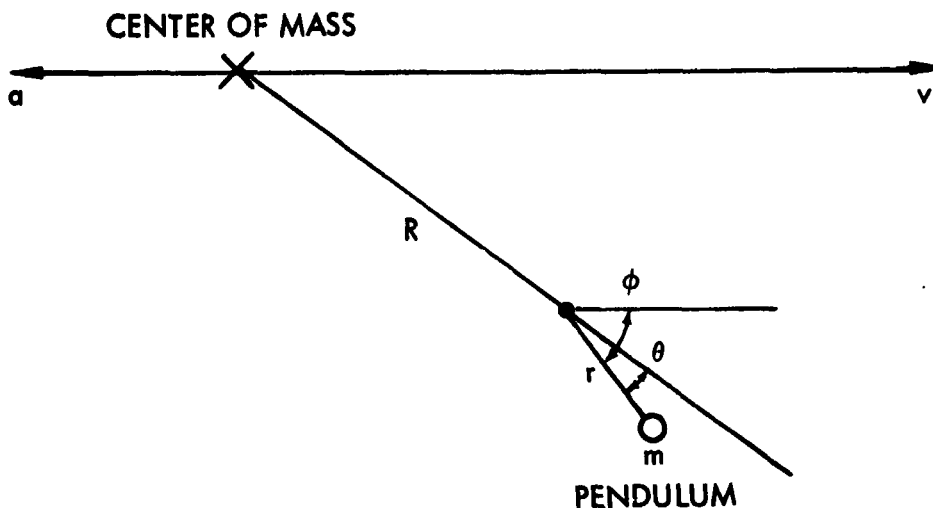


Figure 1: Pendulum and Vehicle Configuration

The desired motion of the pendulum is for ϕ to damp out to zero and for θ , the measured quantity, to indicate the angle of attack ψ .

The equation of motion in terms of ϕ is

$$\ddot{\phi} + \frac{K_F}{m} \dot{\phi} + \frac{a_0 + b \sin \omega t}{r} \sin \phi = \frac{R}{r} \omega_v^2 \psi_0 \sin \omega_v t + \frac{K_F}{m} \omega_v \psi_0 \cos \omega_v t$$

where $\psi = \psi_0 \sin \omega_v t$ represents the attitude oscillations of the vehicle. This equation is nonlinear and has a time-dependent coefficient. It can, of course, be programmed on a computer and solved for particular values of the parameters and conditions. The boundedness of the solution for the homogeneous equation (right-hand side equal to zero, or no attitude oscillations of the vehicle) can be tested by the method of Petty and Leitmann (ref. 3).

An alternative approach consists of linearizing the equation by replacing $\sin \phi$ by ϕ (small angle approximation) and transforming the equation into the form of the Mathieu differential equation, and then applying the Floquet theorem (ref. 4) to investigate the stability and boundedness of the solutions.

In lieu of a more exact treatment, the linearized equation can be solved for the particular case of the vehicle in a circular orbit with constant air density. The steady state error can easily be estimated, assuming typical values for the constants in the equation. Such an analysis indicates that the distance R of the instrument from the center of mass of the satellite should not exceed 10 cm if the steady state error is not to exceed 1 deg.

INSTRUMENT DESIGN

Pendulum Suspension

The pendulum string must be flexible enough so that in the steady state the bob hangs along the resultant acceleration direction. It is necessary, of course, that the string also be strong enough to withstand the launch accelerations. Experience with pendulums that hang in such a low acceleration field as 10^{-5} to 10^{-6} g is so limited that it is difficult to predict the behavior of any particular string material. One suggestion is to make the string as a chain of small links, each coated with Teflon to minimize friction. Since the instrument is basically simple (figure 2), it is suggested that a test program of orbiting several units with different suspensions to obtain experimental data would be relatively easy and economical.

Pendulum Position Sensor

The position of the pendulum bob can be measured optically in a straightforward way by using the Radiation Tracking Transducer (RTT) XY20.* Figure 2 shows how it is used in the instrument. The surface of the spherical bob (a hollow aluminum sphere or aluminized ping-pong ball) is highly polished. The image of the "point light source" reflected in the sphere is focused by the lens on the RTT. The output from the RTT is in the form of a pair of signal voltages giving the orthogonal coordinates of the focussed spot. These voltages are proportional to the orthogonal angular deflections of the pendulum bob.

For an angular range of pendulum motion of ± 15 deg for a pendulum length of 10 cm, a lens of 6.5-mm focal length can be used. A standard wide-angle lens for 8-mm movie

*Micro Systems, Inc., San Gabriel, Calif.

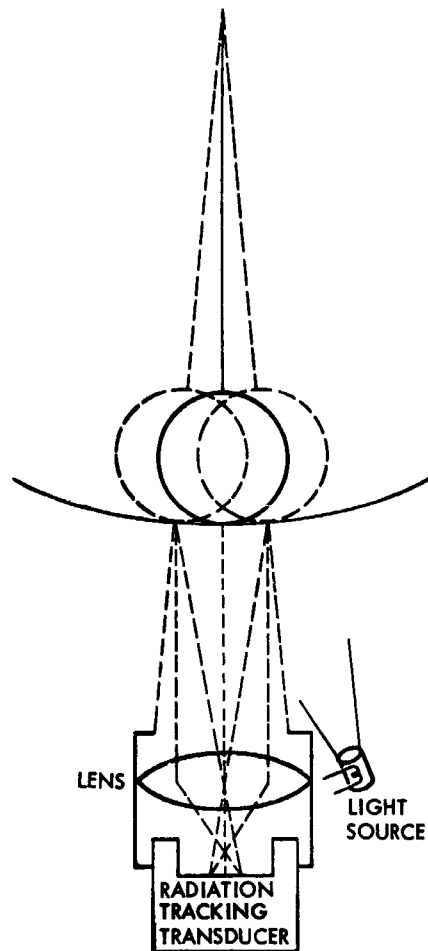


Figure 2 Angle-of-Attack Instrument

cameras could probably be used. The external case of the instrument could be cylindrical with a length of about 20 cm and a diameter of about 10 cm.

CONCLUSIONS

Compared with other methods of sensing satellite attitude, such as force balance accelerometers, a horizon sensor, or a star tracker, this device has the following advantages:

- Simple principle, straightforward design, and inexpensive to build
- Radiation link to external world not required
- Low mass
- Small volume

- Low power requirement
- Direct measurement of angle-of-attack

Disadvantages and limitations of this device can be summarized as follows:

- Limited accuracy (not a high-precision instrument)
- Limitation on location (must be close to vehicle center of mass)
- Uncertain performance of pendulum-supporting thread under low acceleration
- Limitation to relatively low satellite altitudes that assure sufficient drag deceleration

Analysis of the application of the angle-of-attack sensor as an element in the satellite attitude-control loop has not yet been attempted, and a model of the sensor has not yet been built or tested.

REFERENCES

1. Anon: U.S. Standard Atmosphere. Prepared under sponsorship of NASA/U.S. Air Force/U.S. Weather Bureau. Government Printing Office, 1962.
2. Streeter, V.L., ed.: Handbook of Fluid Dynamics. McGraw-Hill, 1961.
3. Petty, C.M.; and Leitmann, G.: A Bondedness Theorem for a Nonlinear, Nonautonomous System, Monatshefte für Mathematik. Vol. 68. 1964, p. 46.
4. Strutt, M.J.O.: Lamesche-Mathieusche und Verwandte Funktionen in Physik und Technik. Julius Springer (Berlin), 1932, p. 14.

EXPLOSIVELY ACTUATED (PYROMECHANICAL) DEVICES FOR SPACECRAFT APPLICATIONS

By A. G. Benedict
Jet Propulsion Laboratory
California Institute of Technology

N67 16925

SUMMARY

The lightness, compactness, and variety of available explosively actuated devices make them attractive for many spacecraft applications, but their inherent "single-shot" characteristic makes adequate reliability attainable only by avoiding misapplications, by scrupulous attention to good design practice, and by intelligent testing.

In this paper, rough guidelines are given for application, design, test, and economy; emphasis is placed on avoidance of nonanalytic devices.

INTRODUCTION

The compact energy-storage quality of explosives lends itself to the design of a wide variety of explosively actuated (pyromechanical) devices which are often much lighter and smaller than their mechanical, electromechanical, or pneumatic counterparts — particularly if a single-shot operation is acceptable. Pyromechanical devices are therefore attractive for stage separation, latch release, fuel-valve operation, and other comparable functions on board a spacecraft.

The single-shot characteristic of the pyromechanical device is an important design consideration because it precludes proof testing of flight hardware. A faulty electromagnetic release can hopefully be detected by preflight operation whereas a faulty pyromechanical release can provide no such inexpensive feedback to the designer.

Pyromechanical devices require unusual attention to detail in design, fabrication, inspection, and test. It is particularly important that samples consumed in destructive testing be substantially identical with units intended for service in actual flight.

The cost per unit of pyromechanical devices often compares favorably with electro-mechanical or other equivalent systems. However, the sample quantities needed to demonstrate the reliability of space-qualified hardware are usually relatively large, tending to make the overall cost extremely high for short-run applications.

APPLICATION

It is convenient to classify pyromechanical devices into two general groups -- analytic and nonanalytic. Devices that use propellant-type explosives for development of a high-pressure gas expanding adiabatically in a piston and cylinder (heat engine) arrangement are usually analytic, in that their mechanical design lends itself to analysis; devices that use detonating explosives must be designed on a cut-and-try basis (all reassurances to the contrary). Operation of nonanalytic devices is analogous to the trick of jerking a tablecloth from beneath a group of water glasses; if the trick works -- Bravo! Let's do it again!

Analytic Devices

Analytic devices, of which pin pushers and cable cutters are typical, tend to have marginal qualities in the smaller sizes. Electrical initiation (e.g., a 1-w, 1-amp squib)* or percussion initiation (e.g., a spring-driven firing pin) typically requires an input on the order of 1 in.-lb of energy; this input may in itself be adequate for direct (nonexplosive) actuation of small mechanisms such as lens-cover latches.

The mechanical work available from explosive mixes is typically of the order of 10 ft-lb per 0.001 cu in. of explosive; the design of devices requiring less than 10 ft-lb of energy may involve practical problems in manufacturing tolerances.

*In this paper, "cartridge" refers to both electrically and mechanically initiated cartridges, and "squib" is loosely used in reference to electrically initiated cartridges.

Nonanalytical Devices

Devices that use detonating materials (developing peak pressures possibly well over 10^5 atm) and those depending heavily on structural details such as crimped joints, are typical of designs that may be classified as nonanalytic. Some nonanalytic devices have remarkable and tantalizing performance characteristics, but development and proof of reliable designs can be an extremely expensive process.

General Guidelines for Application

The following guidelines are offered for achieving maximum economy, schedule adherence, and reliability in the application, design, and testing of pyromechanical devices:

- Careful comparisons should be made against reasonable alternative devices, such as electromechanical actuators, before specifying a pyromechanical device.
- Pyromechanical devices may not offer easy solutions to problems for which other types of device do not seem particularly suitable.
- Envelopes should not be restricted so that necessary peak pressures are much greater than about 25 percent of practical seal strengths.
- Caution should be exercised when specifying pyromechanical devices where the necessary work output is less than about 10 or 20 ft-lb.
- Nonanalytic devices should be used only after careful review of the potential problems they present.
- Noncritical acceptance of information relating to proven reliability of pyromechanical devices should be avoided.

DESIGN

The design of analytic devices is rather straightforward, but it requires careful attention to detail. The designer must foresee trouble rather than wait for a failure in service to highlight a design weakness.

Particular attention should be paid to the following aspects:

- Adverse combinations of dimensional tolerance stackups
- Variations in manufacturing processes
- Lack of uniformity in raw materials
- Specified environmental exposures and operating conditions
- Possible adverse effects resulting from variations in heat-treating
- Possible hydrogen embrittlement (which may occur during heat treat or plating)
- Possible acoustical resonance
- Stress concentrations resulting from threads, small fillets, rough surface finishes, etc.
- Assembly and mounting stresses
- Differential thermal expansion
- Reduction in firing-pin energy as the result of high g-loading, friction, or over-stressing of springs
- Low-temperature reduction of notch strength
- High-temperature reduction of yield strength
- Thrust and couples on mounting bolts
- Possibility of O-rings freezing at reduced temperatures, or extruding at high temperatures
- Details lending themselves to error or confusion in manufacture, field assembly, installation, or field checkout
- Breakaway friction
- Variations in strength of shear pins, rupture diaphragms, etc.
- Possibility of vacuum welding
- Practical limits of inspection and test
- Need to ensure that results of sample tests are meaningful
- Reduction of percussion primer sensitivity as the result of firing-pin eccentricity, or of damage to the primer during assembly

Most of the foregoing items represent established engineering precepts which are often ignored in the interest of what might best be described as faulty economy. If a design is good, there should be no room for buy-off in procurement of flight items (other than for apparent deviations, such as workmanship, which may have to be based on opinion).

TESTING

Test programs should be devised to achieve the following goals:

- Explore worst-case design tolerances
- Make maximum use of non-destructive techniques
- Take advantage of tests by variables rather than tests by attributes in order to obtain maximum information from a minimum number of samples

- Explore each potential failure mode so that limiting failure rates can be established for each mode
- Isolate failure cases when combined environments are involved
 - Avoid applying needlessly severe test criteria
 - Ensure that Bruceton-type tests,* if any, are conducted and interpreted in a defensible manner
- Ensure that test operating conditions are comparable with those anticipated in flight; and that these can be duplicated in the event of failure

Too many test programs involve little more than the indiscriminate firing of a large number of samples at low, room, and high temperature after exposure to a range of environments. The criticism that can be leveled at such a test program for a pin-puller latch release might include the following:

- The tests are tests by attributes for which, as an example, over 3,200 no-fail tests are required to demonstrate a reliability of 99.95 percent at 80-percent confidence; as few as 30 or 40 samples may be sufficient to demonstrate the same reliability if tested by variables.
- The test results may be meaningless unless the test items bear some analytical relationship to flight items.
- The tests give no indication of how marginal the device may be, and the results cannot be extrapolated to cover last-minute changes in operating conditions.

It is not uncommon to hear a claim such as "2,000 of these units have been tested without a failure," which raises a need for defining failure; for example, the pin-puller latch release may cause partial or complete mission failure if released prior to initiation because its shear pin is broken by vibration. Similar failure might result if the device unlatched successfully, yet caused one or more of the following malfunction conditions:

- Rupture following release, with consequent damage to adjacent wiring
- Venting of smoke, contaminating nearby optical surfaces

*Princeton University, Statistical Research Group: Statistical Analyses for a New Procedure in Sensitivity Experiments. Applied Mathematics Panel Report No. 101, Princeton Press, July 1944, p. 40.

- Rebound of latch release, jamming the cover it was intended to free
- "Tearing free" of the pin-puller latch release from its mounting
- Imposition by release of unrevealed dead short, preventing the operation of other mechanisms
- Disturbance of a magnetic field
- Operation slower than required
- Premature operation resulting from r-f field or static discharge
- Operation only because of inadvertent "undertorquing" of mounting bolts

Sample Size

Well-designed pyromechanical test programs are characterized by the comparatively large number of expensive samples consumed in test, a characteristic resulting from the one-time quality of the cartridge if not of the device itself.

The number of samples required to demonstrate high reliability at a high confidence level in destructive tests by attributes is so large as to make such tests almost economically impractical. As previously noted, the demonstration of 99.95-percent reliability at 80-percent confidence requires a sequence of over 3,200 no-fail tests; a sample size twice as large is needed if even one failure is recorded.

As a rough guide only, a qualification test program based on tests by variables, for a pin puller and squib combination, may require a total of about 250 squibs (costing possibly \$50 to \$100 each) and about 20 or 30 pin pullers (costing possibly \$100 to \$200 each). The high proportion of squibs is attributable to the fact that many squib tests are, of necessity, destructive.

Control Samples and Spares

The troubleshooting of anomalies in pyromechanical test results is not always easy, and duplication of yesterday's test results before proceeding with today's tests is almost certainly the most reassuring way of approaching this problem.

Such an approach requires not only that the test program provide for systematic use of control samples, but also that a liberal quantity of spares be carried to allow investigation of the anomalies. Spares should also be carried through all environmental exposures to allow prompt coverage of such contingencies as instrument failure or an error in test techniques leading to a loss of results during a destructive test. Control samples of squibs or cartridges should also be kept on hand to allow comparison with new lots which may have to be purchased later.

Types of Tests

Tests in which pyromechanical devices may be involved include those conducted for developmental, design evaluation, calibration, quality control, quality assurance, lot acceptance, and qualification purposes.

Calibration tests for cartridges are conducted to determine quantities of a particular lot of explosive material required to meet a performance specification; quality control tests may be viewed as in-process tests of production items, and quality assurance tests as tests on finished lots prior to delivery.

Qualification tests should always be preceded by lot acceptance tests, if for no reason other than to prove that lot acceptance tests have no significant adverse effect on the items.

100-Percent Inspection

Many qualities of pyromechanical devices lend themselves to complete nondestructive testing, and every advantage should be taken of this possibility, partly to minimize the risk of accepting a faulty item for flight, and partly to ensure that there are no significant differences in items which would negate the value of destructive tests performed later on a random sample basis.

Design and production engineering should take into account the desirability and usefulness of 100-percent inspection, e.g., the designer should consider the practical

difficulties involved in precise inspection of the radius of a stress-relief fillet at the bottom of a hole -- can the radius be measured reliably within the limits imposed by the drawing ?

Tests by Variables

Tests by variables involve estimating such parameters as the mean and standard deviation of an assumed distribution curve, and the use of the estimated parameters to make reliability-confidence calculations.

In the absence of evidence to the contrary, the log-normal distribution may be found useful for this purpose. The risk entailed in such an assumption is part of the penalty we pay for the reduction in sample size that tests by variables allow as compared with tests by attributes; every effort should be made to ensure that test results are indeed consistent with the assumed distribution.

The other part of the penalty associated with tests by variables is that the reliability confidence calculations must be pessimistic; this penalty factor decreases very rapidly with sample size up to a quantity of about 5 or 6, and very slowly with sample sizes above 10 or 12. Once the sample size has grown to 10 or 12 it may be economically prudent to discontinue testing and start again with a less marginal design.

One attractive feature of tests by variables is that they are sometimes tolerant of one wild test result which may be quantitatively outside specification limits but still within statistical limits. Further, specification of tests by variables for lot acceptance provides a strong and fair incentive for the manufacturer to achieve uniformity.

Analytic Versus Nonanalytic Devices

From a test or inspection standpoint, the main difference between analytic and nonanalytic devices is that the former typically allow a larger proportion of non-destructive tests and hence a smaller sample size. The cost of samples for a thorough evaluation of a nonanalytic device may be prohibitive at times, particularly since tests by variables may require fabrication of special components involving

pecially preselected dimensional variations. Nonanalytic devices may also create difficult problems in the establishment of adequate quality control procedures, and in the establishment of economical quality assurance tests.

ECONOMY

The "necessary" prices for procurement and test of a comparatively simple analytic device (e. g. , a pin puller) complete with squib could be estimated as follows:

<u>Item</u>	<u>Cost</u>
Proposal	3, 000
Engineering*	10, 000
Fabrication Costs**	
Flight Units and Spares (50 assemblies)	6, 000
Developmental Units	1, 000
Calibration, Quality Control, and Quality Assurance	2, 000
Lot Acceptance Test	1, 000
Qualification Test	12, 000
Test	
Quality Control and Quality Assurance	3, 000
Acceptance Tests	500
Qualification	10, 000
Documentation	
Quality Control and Quality Assurance	2, 000
Acceptance Tests	100
Qualification Tests	1, 500
	<u>\$52, 100</u>

*The allowance for engineering assumes that the cartridge involves only a minor modification of a proven unit; development and qualification of a new cartridge to high standards could easily cost over \$200, 000.

**Fabrication, including all associated overhead and profit, at \$80 per device and \$40 per squib. The prevailing prices to cover engineering quality control, etc. , might be \$120 for the device and \$80 for the squib.

Three elements of the foregoing cost breakdown are as follows:

- The flight units at \$6,000 represent only about 12 percent of the total cost.
- The example is for an analytic device; comparable figures for a simple nonanalytic device could easily be higher by a factor of 3 or more.
- The total cost, even for an analytic device, is so high as to make consideration of alternatives very desirable.

In addition to the necessary costs, economy may be viewed from the standpoint of possible additional but "unnecessary" costs. These costs can be considered with respect to five areas of expense — proposals, engineering, fabrication, testing, and documentation.

Proposals

The inherent costliness of proposal preparation is apparent. If, for example, each of six companies competing for business habitually spends \$5,000 per proposal, and each company wins only one in every six proposals, the cost figure per company for that winning proposal is \$30,000. (The estimate previously presented allowed for \$1,000 proposals from each of three companies.)

Since the bidder for contracts must prepare proposals matching those of his competitors in scope and quality, in order to be competitive, there is little he can do beyond improving his internal efficiency in proposal preparation. Hence, the initiative for economy in proposal preparation rests with the customer who should utilize every opportunity to limit the number of bids sought and the volume and finish of acceptable proposals.

Engineering

The assumed cost of \$10,000 for necessary design* is about 20 percent of the total, and is not a high figure for a short-run item. This figure allows \$9,000 for actual

*As indicated previously, the \$10,000 is associated mainly with development of the device, it being assumed that only minor modifications to a "proven" cartridge are required.

design, and \$1,000 for insurance against faulty design. (Every Ordnance company makes mistakes which sometimes lead to redesign, to discarding of a large lot of faulty items, and possibly to the need for repeating several months of work on qualification tests.)

In the face of price competition, the manufacturer may prefer to assign possibly only \$3,000 to design and \$5,000 to insurance, for a potential reduction of \$2,000 in the total cost. However, his design effort will be so marginal that his designers will have time only to meet the superficial rather than the basic requirements of the specification, and an important oversight in the specification may not be noticed by anyone until near the end of the qualification program. This oversight could lead to redesign and loss (to the customer) of possibly \$40,000 worth of work — a high price to pay for a saving of \$2,000. (It should be noted that the \$5,000 insurance adopted by the manufacturer is intended to cover oversights by his designers, not error or oversight in the specifications.)

Fabrication Costs

With test samples representing about 30 percent of the total cost, it is obvious that economy depends on well-planned test programs directed toward extracting the maximum amount of useful information from the minimum number of samples. Underestimation of quantity requirements, for example, can prove very expensive because an additional 20 assemblies would cost not only \$2,400 for fabrication of delivered assemblies but a further sum (e.g., \$6,000) to cover hardware for delivery, calibration, quality control, quality assurance, and lot acceptance tests, plus the associated testing and documentation.

As previously noted, ill-devised test programs can increase costs by useless increases in sample size; the effect on direct testing costs is self-evident.

Documentation

As with all other spacecraft hardware, it is easy to waste money on needless documentation. Qualification test reports on pyromechanical devices, for example, tend to be bulky because of the number of individual tests involved, and editing problems tend to cause report costs to increase exponentially with entries (and pages). Voluminous test reports may look impressive, but the related effort to produce it costs money, and few if any people have time to examine thick reports in detail. (As a rough guide, test-report compilation costs about \$30 to \$100 per page.) An alternative approach to achieve economy in this area is simply to ensure that raw data sheets are stored safely and available for reference, and to allow test reports to present data in compressed form.

The Potential for Waste

The following tabulation demonstrates how a "reasonable" cost of \$52,100 for the pin puller and squib could increase to \$138,000 by ignoring economies:

Necessary costs		\$52,100
Waste on many elaborate proposals	\$27,000	
Waste attributable to inadequate engineering	40,000	
Waste attributable to underestimating quantities	6,000	
Waste attributable to ill-devised test programs	10,000	
Waste attributable to excessive paperwork	<u>3,000</u>	<u>86,000</u>
Total cost		\$138,100

DEVELOPMENT OF A PASSIVE DAMPER FOR A GRAVITY-GRADIENT STABILIZED SPACECRAFT

By E. J. Buerger
Spacecraft Department
General Electric Company

SUMMARY

N67 16926

Gravity-gradient stabilization is possible only if existing oscillatory motions of a spacecraft can be damped out by some form of energy dissipation. This paper describes the configuration of a component that combines two forms of magnetic, passive damping: an eddy-current damper and a hysteresis damper. These dampers are so constructed that either one may be engaged, and the other disengaged, upon command. These dampers and the auxiliary components for switching, a roll rate angle indicator, and a caging device (used during the launch environment) are housed within a single envelope designated as the Combination Passive Damper.

INTRODUCTION

In 1967, NASA will place in orbit a gravity-gradient stabilized satellite — one of a series of spacecraft known as Applications Technology Satellites (ATS). One of the primary purposes of the ATS series is to evaluate the characteristics of gravity-gradient stabilization as a means of satellite attitude control.

The General Electric Company (GE) designed the stabilization systems for this series. The systems utilize four 132-ft primary gravity-gradient rods (in the form of an "X") rigidly attached to the satellite, and a secondary or damping boom (consisting of two 45-ft collinear rods) coupled to the spacecraft by a damping mechanism and a torsional spring. Gravity-gradient control utilizes the differences in gravitational forces acting upon the distributed masses of the primary booms to maintain a constant attitude with respect to earth.

Stabilization for ATS is possible only if oscillatory motions of the vehicle can be damped by some form of energy dissipation. Coupling of the damper boom array to the ATS and its primary stabilizing booms is accomplished by a Combination Passive Damper (CPD). Figure 1 is a schematic of the CPD functions; figure 2 is an isometric view. The CPD contains two forms of damping. Either may be selected, and either is capable of damping out the oscillations. One of the primary functions of this ATS flight is to evaluate the two types of magnetic passive damping contained within the CPD: eddy-current damping with diamagnetic suspension, and hysteresis damping with torsion-wire suspension. (Because of the inherent long life of gravity-gradient stabilization systems, only passive damping devices without wear-producing friction were considered for the three-year flight of ATS.)

The CPD package is designed to permit selection and operation of either damper by an appropriate command to the spacecraft telemetry system. In addition to housing the two dampers, the CPD must also provide for boom shaft alignment to the dampers and spacecraft and a means of caging the damper boom and boom shaft of the CPD during launch.

COMPONENT DESCRIPTION

Eddy-Current Damper

The damping, suspension, and torsional nulling characteristics of this system are as follows:

- Damping. The torque developed by an eddy-current damper is proportional to the comparative velocity between the elements whose relative motion is being damped. It can be said, therefore, that eddy-current damping is velocity dependent, i.e.,

$$T_d = C_d \omega$$

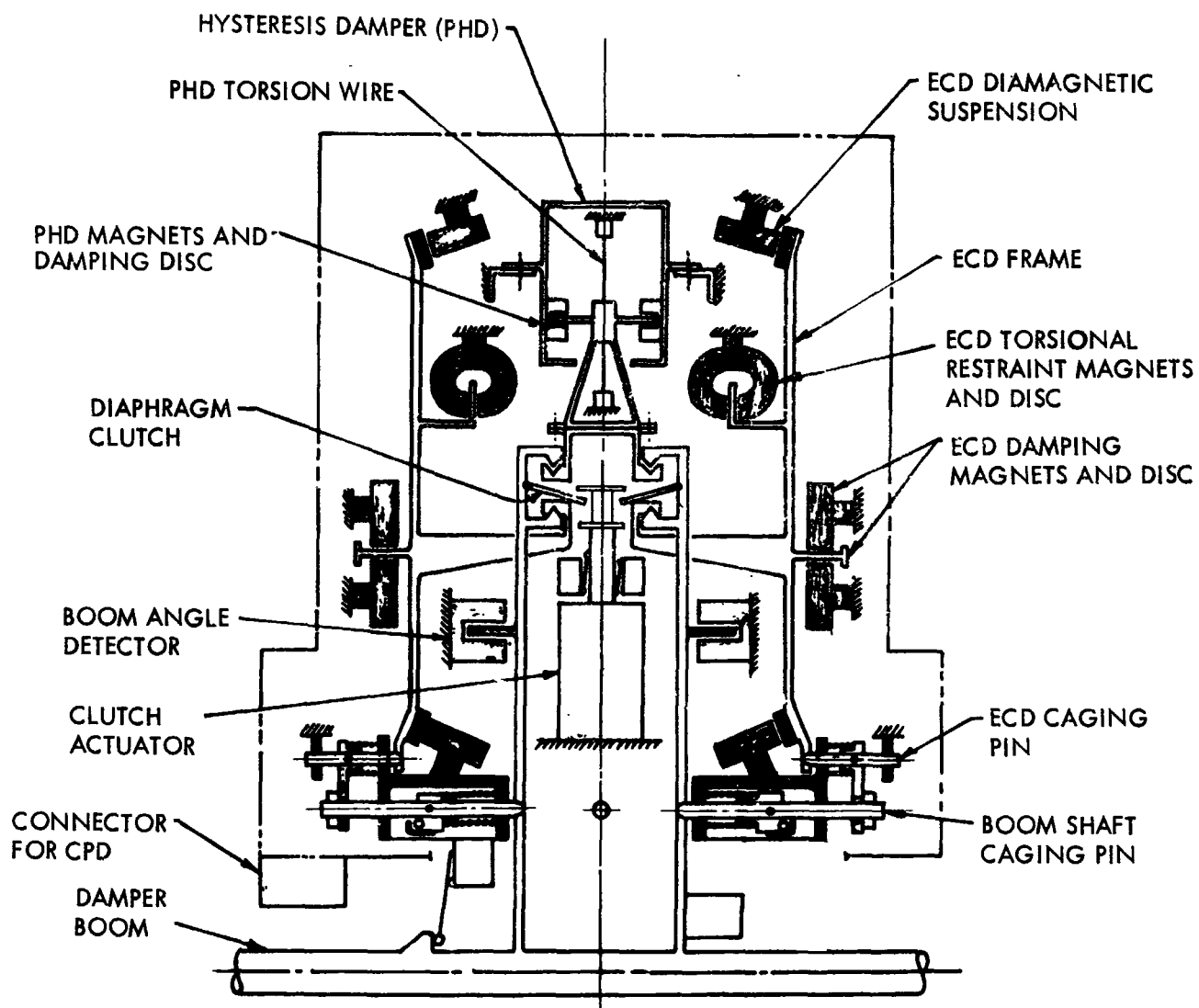


Figure 1 Combination Passive Damper for Applications Technology Satellite - Schematic

ALLOW $\frac{1}{4}$ PICAS
Margin to trim

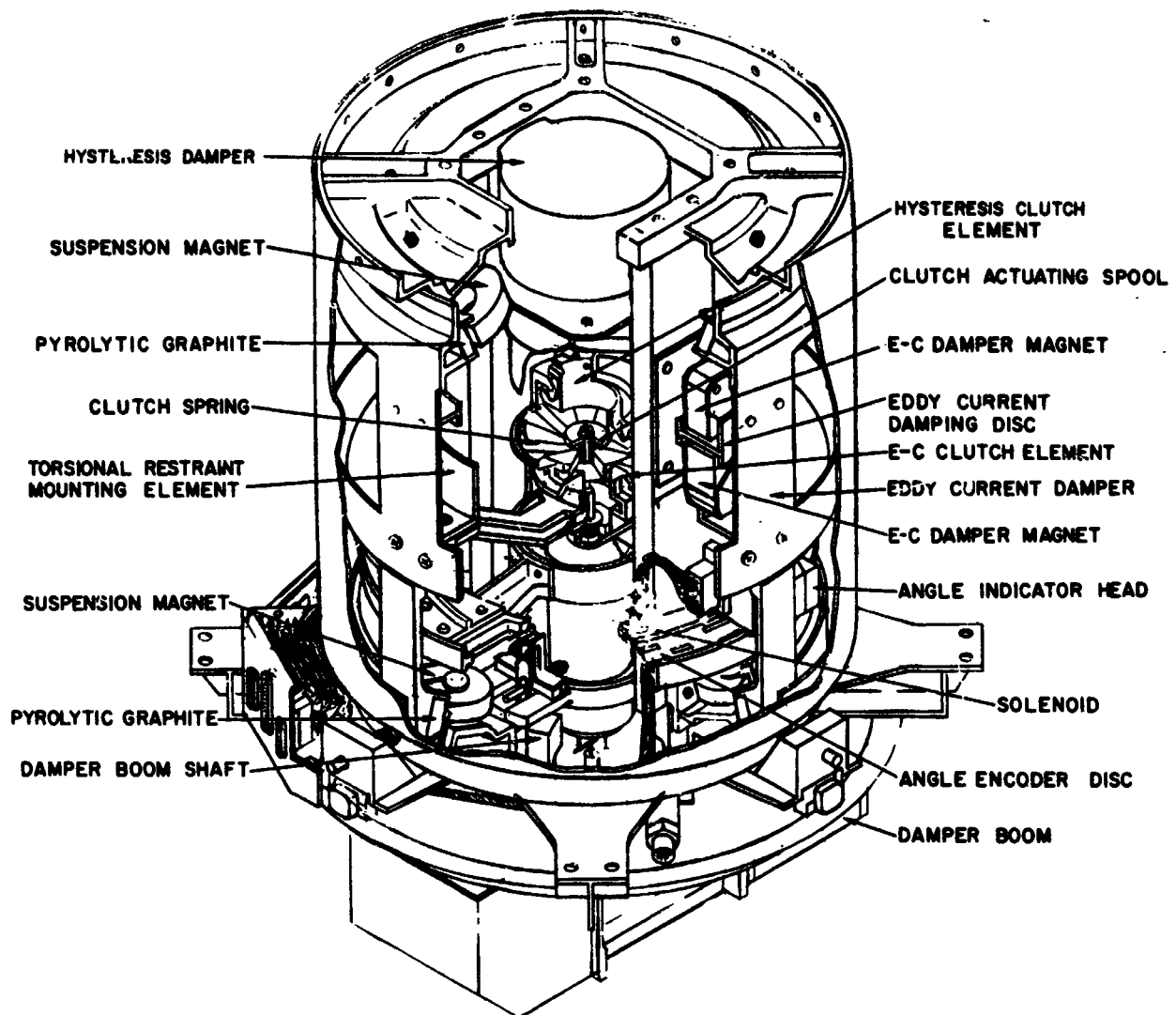


Figure 2 Combination Passive Damper for Applications Technology Satellite - Isometric

where T_d = Damping torque

C_d = Damping coefficient

ω = Relative angular velocity

In the CPD for the ATS, eddy-current damping is generated by the interaction of an aluminum disc that moves in the fields of appropriately placed magnets as shown in figure 2. In this figure, the two sets of Alnico V magnets and the damping disc can be seen.

- Suspension. Since the damper is to be used in the essentially zero -g field of the orbiting spacecraft environment, only very small suspension forces are required to maintain proper spacing between the rotor and stator of the damper. It has been found that a stable bearing, using a constant magnetic field, could be attained only if the suspended element had a permeability of less than unity, i. e., a diamagnetic material. For the ATS-CPD, pyrolytic graphite is used. In figure 1, the elements of the suspension system can be seen to include the pyrolytic graphite placed in the field of two groups of magnets to achieve radial support in two perpendicular directions as well as the axial direction of the CPD. For the ATS, system studies showed that the radial force in any direction would never exceed 50 dynes (a dyne being about 1/30,000 of an oz) nor the axial force, 10 dynes. The cocking torque that might be applied externally to the damper boom was calculated to be 2,500 dyne centimeters (a dyne-cm being about 1/70,000 of an oz-in.). Performance testing of the damper has shown that the suspension system, as designed, meets the specified value.

In this design, pyrolytic graphite is mechanically held in place by a metallic snap-ring arrangement and bonded with a flexible epoxy to the rotating structure. The design has successfully withstood 19-g vibration forces with no adverse effects. Mechanical stops are used to prevent the magnets from making contact with the pyrolytic graphite during launch environments.

- Torsional Nulling. This particular configuration of diamagnetic suspension has no restoring torque or preferred angular orientation. (This fact was used by GE in the earlier development of a truly frictionless bearing capable of continuous rotation.) It was therefore necessary to develop a torsional restraint technique with very low hysteresis loss and lateral force characteristics, but with the required tangential force levels. System studies showed that the minimum torsional restraint requirement would be 3.5 dyne cm/deg. A suitable element for this purpose was achieved in the CPD (figure 2) by the use of a properly shaped pattern of magnetic material. Two of these shapes were then placed in the fields of two sets of magnets.

In table 1, the requirements for the types of damper have been summarized. Separate values are given for medium-altitude and synchronous-altitude dampers. The initial flight is a medium-altitude orbit, with the two successive flights to be at synchronous altitude. From this chart it can be seen that the damping torques involved in the synchronous-altitude configuration are much lower than those for the medium-altitude flight.

Hysteresis Damper

The damping, suspension, and torsional nulling characteristics of this system are as follows:

- Damping. Characteristically, hysteresis damping torque is independent of relative velocity between the damped members. In the hysteresis damper for the ATS, the torque developed is constant over the limits of angular travel that may occur between the rotating and stationary parts of the damper. The hysteresis damping element is an annular disc of 0.003-in.-thick chrome steel. This disc is on the rotor and placed so that the flux of two sets of permanent magnets can pass through the disc. As this disc is moved through the magnetic field, magnetic domains in the disc are subjected to a reversal of the magnetic field environment. Energy is dissipated in proportion to the area of the hysteresis loop of the material used for the disc. The disc is a

Table 1
DAMPER SPECIFICATION REQUIREMENTS

Aspect	Eddy-Current Damper			Hysteresis Damper		
	Medium Altitude	Synchronous Altitude	Dimension	Medium Altitude	Synchronous Altitude	Dimension
Damping	15,800	9,900	$\frac{\text{Dyne-cm-sec}}{\text{Deg}}$	173	50	Dyne-cm
Spring Constant	21	3.5	$\frac{\text{Dyne-cm}}{\text{Deg}}$	21	3.5	$\frac{\text{Dyne-cm}}{\text{Deg}}$
Radial Force Axial Force Boom Cocking Torque	All Cases = ± 50 dynes All Cases = ± 10 dynes All Cases = ± 2500 dyne-cm					

magnetic material attracted to the permanent magnets with a relatively high force level; therefore, a diamagnetic suspension system of a reasonable size for a magnetic hysteresis damper cannot be used.

- Suspension and Torsional Nulling. In the hysteresis damper, a torsion wire provides suspension and torsional nulling. As an indication of the magnitude of the torque involved for both dampers, the torsion wires for the medium-altitude and synchronous-altitude configurations are about 1.0 in. long, with diameters of 0.005 and 0.0035 in., respectively. These diameters are only slightly larger than that of a human hair. To keep the torsional wires taut, cantilever springs are used at each end of the suspension wires to attach the rotor to the stator. A suspension system for the hysteresis damper with the specified spring constant is several orders of magnitude stiffer than one for the eddy-current damper. In fact, no caging is required for the hysteresis damper rotor when the boom is not attached to it – which is the configuration of the CPD at launch.

The hysteresis damper as configured for the ATS-CPD is a separate, self-contained unit which, as shown in figure 1, is attached to structural elements of the CPD so as to position it coaxially with the eddy-current damper and other rotatable elements of the package.

Switchover

One of the more intriguing problems to be solved in developing the CPD was that of providing a means for switching over, or clutching, between the two dampers. Because of the very low levels of damping forces associated with these dampers, there could be no frictional drag from any type of clutch-actuating device. The torque that had to be transmitted through the clutch was very low. However, because the CPD must be tested in earth's gravitational field, the forces holding the clutch elements together had to be sufficient to support the weight of the eddy-current damper during testing.

- Clutch. The clutching scheme utilized in the CPD can be seen in figure 2. It is shown in cross section in figure 3a. The clutch housing is directly attached

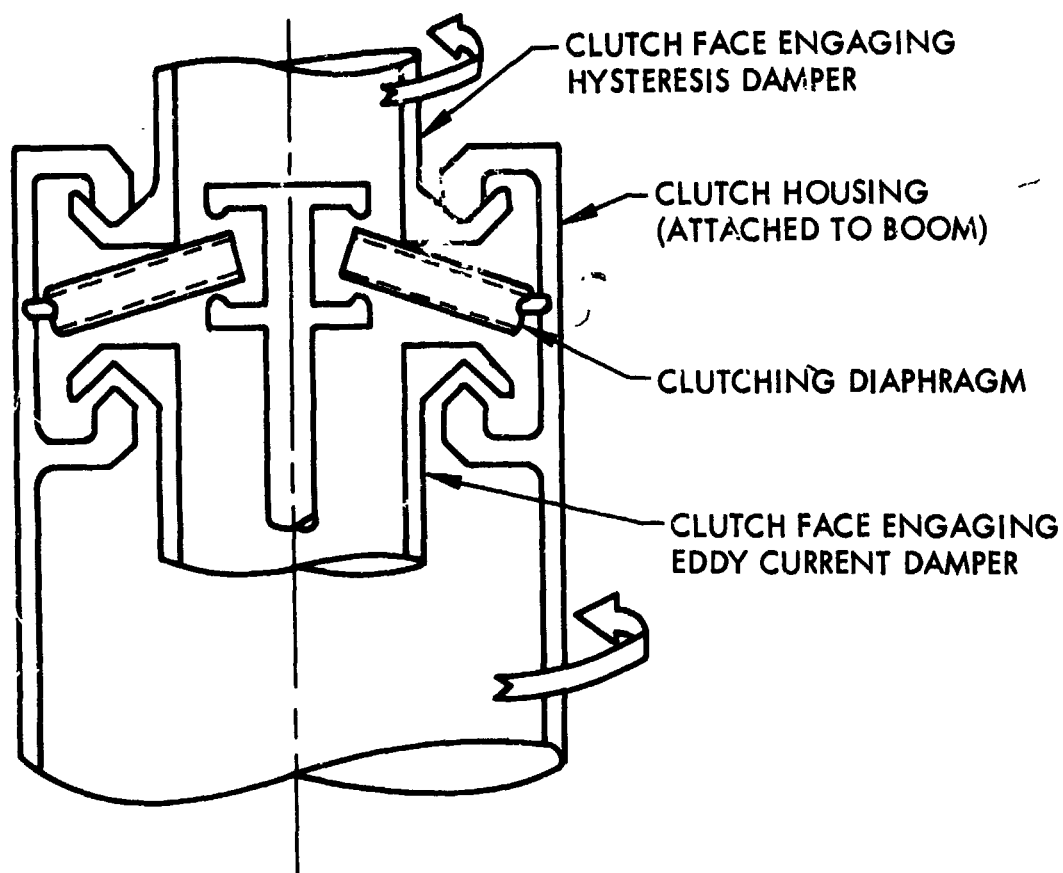


Figure 3a Clutch Cross Section

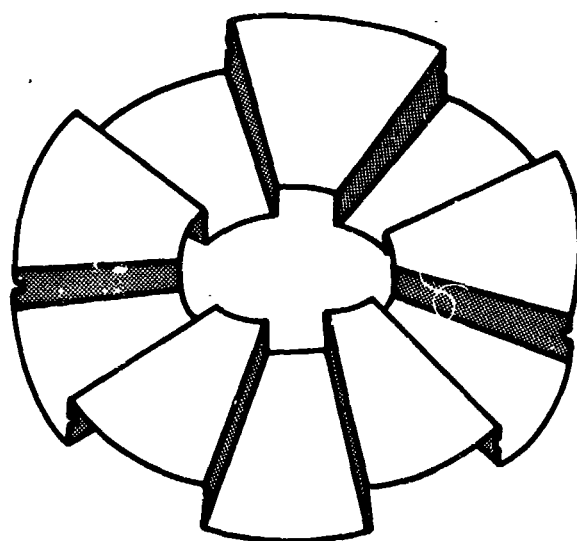


Figure 3b Clutching Diaphragm

to the damper boom and has a mating clutching surface for each of the dampers. The halves of the clutch faces associated with each of the dampers are in juxtaposition with the corresponding housing clutch face. The clutch faces are V-shaped in cross section and are circular in planform. The force to hold the two halves of the clutch in the engaged position is provided by a specially designed diaphragm spring, somewhat resembling a Belleville washer when in use. This square, fluted diaphragm is shown in detail in figure 3b in its flat, as-formed condition. In the assembly, this diaphragm is constrained by the clutch housing so that its outer diameter is less than when it is in the flat form. When thus constrained, it behaves as an over-center toggle mechanism, assuming one of two stable, conical positions; this precludes the possibility of the clutch "hanging up" at an intermediate position with neither damper engaged. The diaphragm, clutches, and clutch housing are designed to provide approximately 8 lb of holding force when the clutch is in either of its two stable positions.

- Solenoid. The actuating element for the clutching system is a double-acting solenoid. The end of the solenoid plunger is fitted with a spool designed so as not to be in contact with the diaphragm at either end of the solenoid travel. When the solenoid is actuated (by supplying electrical power to one of the two coils) to either "push" or "pull" the diaphragm, the spool must travel about 0.1 in. before it makes contact. A detent at each extreme of travel in the solenoid holds the plunger at that position (and out of contact) until actuated.

Angle Indicator

To permit evaluating the performance of the dampers, an indication is required from the CPD of the angle between the damper boom shaft and the stator of the CPD. This angle is a direct measure of the position of the damper boom relative to the spacecraft. Again, because of the low level of forces associated with the CPD, there cannot be any physical contact or reaction torque between the rotor and stator due to the angle indicator. Another factor that complicated the design of this indicator arose from the relatively large movements that can occur between the centerlines of the damper boom shaft and the stator when the damper is in the eddy-current mode. In this mode, the shaft can move ± 0.10 in. axially and ± 0.06 in. in any radial direction.

Angle indication is accomplished by mounting on the damper boom shaft an encoding disc, with appropriately arranged slits, through which light is passed onto an array of phototransistors to provide a digital readout of angular position. The arrangement of the elements is shown in figure 4. Encoder disc slits are arranged in a Gray binary code. By taking advantage of the fact that the accuracy requirement decreases as the shaft moves away from null, only five tracks or code bits are required for the ± 45 -deg rotation. The angle indicator is designed to provide an accuracy of ± 1 deg for the angles from 0 to ± 4 deg; ± 1.50 deg from ± 4 deg to ± 20 deg; and ± 10 percent of the reading ± 0.5 deg from ± 20 deg to ± 45 deg. The angle indicator as applied here therefore is designed to use a minimum number of bits (and thus minimize spacecraft telemetry requirements) and yet give the system analyst the accuracy required to evaluate performance of the spacecraft stabilizing system.

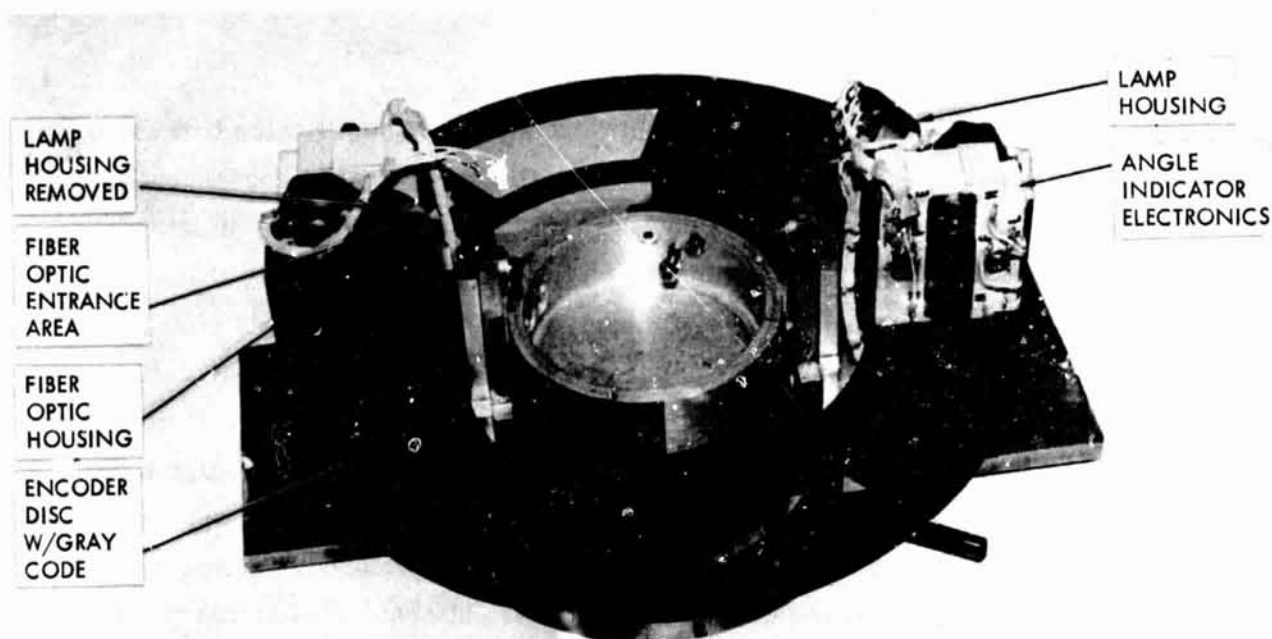


Figure 4 Angle Indicator

An incandescent lamp with redundant filaments provides the necessary light. Immediately adjacent to the lamp is the entrance aperture of a fiber optic assembly that was developed for the angle indicator. Because of the non-uniformity of the light output emanating from the lamp, it was necessary to divide the entrance area into the smallest possible increments and randomly distribute these increments to the five

exit areas. To achieve this randomization, the entrance fiber-optic bundle was divided into approximately 250 incremental elements (each about 0.005 in. in diameter). The light from each exit bundle is focused by a short-focal-length lens onto phototransistors mounted in the same structure as the light transmission system.

Interposed between the exit lenses and the phototransistors is the thin (0.010 in.) beryllium copper encoder disc, mounted in a suitable support structure attached to the rotor of the CPD. The encoder disc consists of two sets of identical patterns located diametrically opposite each other. By utilizing a separate angle indicator head with each of these patterns, the required accuracies are achieved regardless of lateral motion between the rotor and stator of the CPD. In addition, the important element of redundancy was obtained.

Boom Shaft Caging

The relatively large mass of the CPD damper shaft and damper boom dictates that these elements be securely fixed or caged with respect to the CPD stator (and, consequently, the spacecraft structure) during launch. As shown in figure 5, the caging is an integral part of the baseplate by which the CPD is mounted on the spacecraft. Caging of the boom shaft (to which the damper boom is attached by means of a mounting flange) is effected by four pins constrained in guides on the baseplate. A tensioned stainless-steel cable forces the tapered ends of the caging pins into mating recesses on the boom shaft when it is caged. Auxiliary pins, constrained by the shaft caging pins, are used to cage the eddy-current rotor during launch. Both sets of pins have powerful retraction springs to withdraw them from engagement when tension on the cable is released. To uncage after launch, a command signal fires the pyrotechnic cable cutters. This action releases all tension on the cable (retained on the baseplate by appropriately placed clips) which, in turn, allows the various springs to withdraw all caging pins and permit the rotor to float free. The desired damping mode can thus be selected, and damping of the spacecraft motions will start.

DEVELOPMENT STATUS

Two engineering models and a flight prototype unit have been built. One of the engineering models has been subjected to the entire qualification testing program,

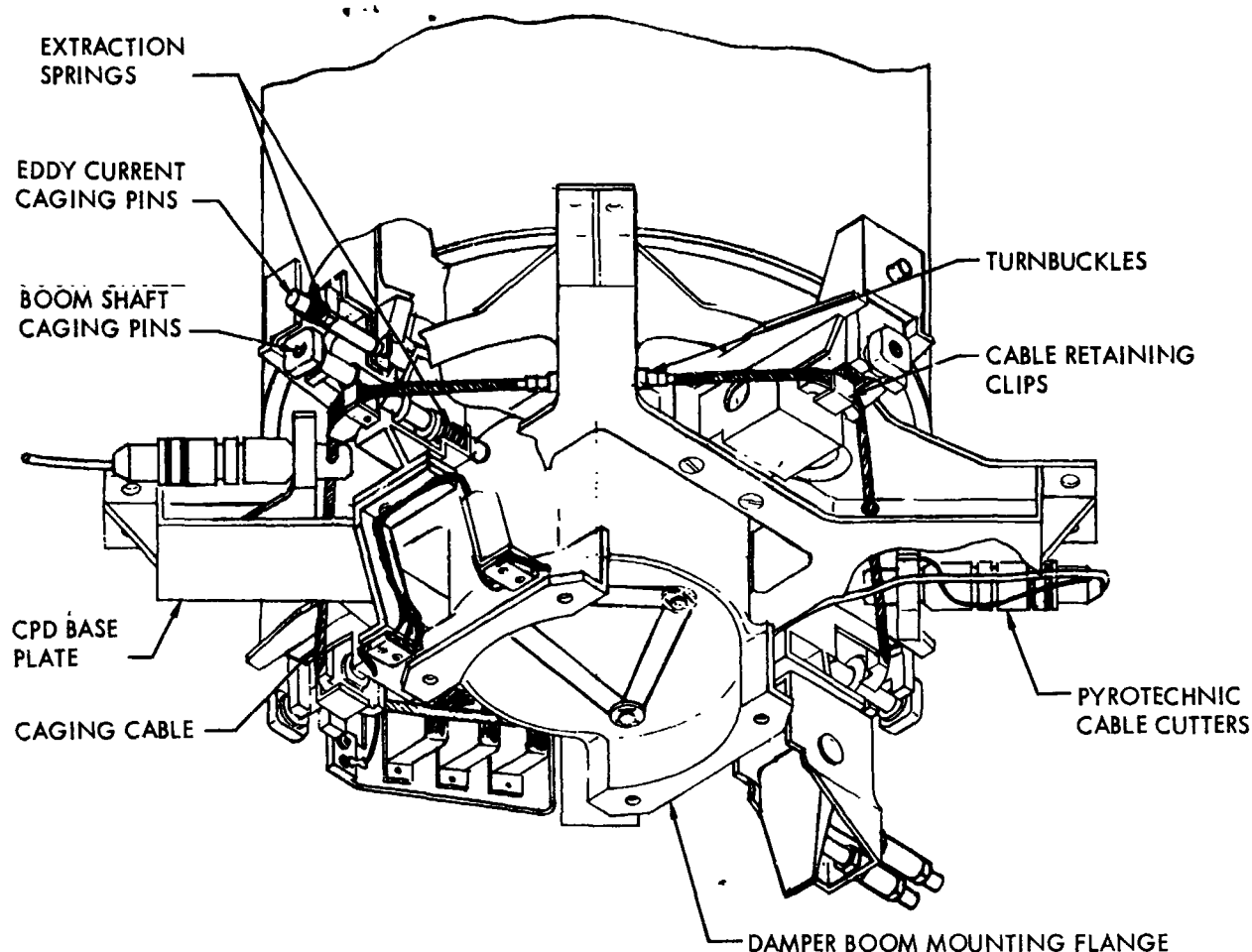


Figure 5 Baseplate of Combination Passive Damper for Applications Technology Satellites

including both functional and environmental performance evaluation. Functional performance has met or exceeded all established specification values. In spite of its complexity, this unit also successfully passed acceleration and vibrational testing, which subjected the CPD to accelerations as high as 19 g. Testing of the other two units is in progress, as is the fabrication of a second prototype and the three flight units.

Very sophisticated and highly specialized test equipment has also been designed and developed to measure the miniscule forces associated with the eddy-current and hysteresis types of damper. A discussion of the configuration and performance of this test equipment could well be the subject of another paper.

Page intentionally left blank

AN EXTENDIBLE STRUCTURE FOR SOLAR ELECTRIC POWER IN SPACE

By D. E. Lindberg
Lockheed Missiles & Space Company

SUMMARY

N67 16927

This paper describes an extendible structure used to angularly position four planar surfaces of solar-sensitive cells for a spacecraft electric power system. It includes the system requirements, the type of mechanisms used, and the ascent support structure. Since the assembly cannot be operated in a 1-g environment without support, a description of the equipment used for ground test is also included.

INTRODUCTION

The needs of certain space experiments have required the development of a mechanism capable of extending solar array panels from a spacecraft in orbit, and of positioning the panels so they function effectively as solar collectors. Rather stringent design requirements were imposed by the power and configuration requirements of the spacecraft itself. Further, since high reliability was essential, a simple mechanism was called for.

The resulting design can be described as four "jack-in-the-box" modules, each containing a simple slider-crank device which extends and positions a solar panel in a single, continuous cycle. The modules have been fabricated and qualification-tested and will be flight-tested in the near future.

MECHANICAL DESIGN REQUIREMENTS

The design requirements for the extendible structure for the solar electric power system were developed on the basis of spacecraft power and configuration requirements. It was therefore necessary to design, fabricate, and flight-test a solar array system consisting of 4 independent modular assemblies (with arms positioned as shown in figure 1).

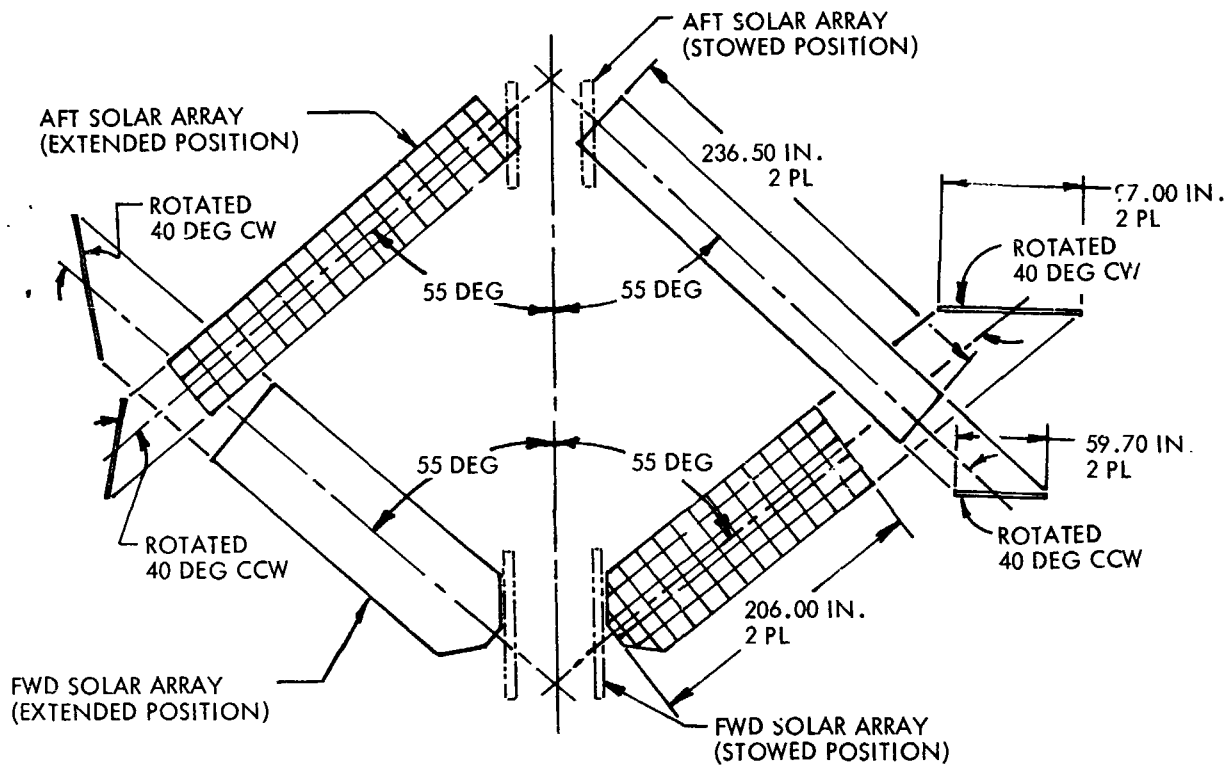


Figure 1 Solar-Array System Configuration

Each module assembly consists of 3 parts:

- An arm assembly capable of mounting standard solar-collector panels (and with the external dimensions shown in figure 1)
- An erection mechanism for extending and positioning each arm assembly within 30 to 90 sec
- A support structure for supporting and retaining the folded arm assembly and the erection mechanism during ascent and for supporting the extended arm assembly while in orbit

The centers of mass of each arm assembly are controlled with prescribed parameters compatible with the spacecraft attitude-control requirements.

DESCRIPTION OF THE SOLAR ARRAY SYSTEM

After a series of studies, a solar array configuration was designed in the form of four jack-in-the-boxes, each with four mechanical tie-downs and an electrical interface. Each box contains an extendible arm assembly powered entirely by springs and controlled by liquid damping. The lid on the box, also spring loaded, is released by the action of two squib-operated pin pullers. When the lid is released, the arm automatically extends to a prealigned position.

Two features are typical of each component in the modules. First, all rotating or sliding joints have either the shaft or the journal coated with a baked-on, solid-film lubricant to minimize friction and prevent electrochemical action. This protection is necessary since each joint has dissimilar metals. Second, all exposed surfaces of the structure are finished to specific thermal-control requirements for collector-panel temperature control.

STANDARD COLLECTOR PANEL

The standard panel used in each arm is an assembly approximately 14 by 18 in. Its surface is covered with photovoltaic cells which, in turn, are covered with glass slides for reducing the effects of radiation and temperature. The cells are assembled into submodules and then bonded to a magnesium grid. The back of the panel is coated with a thermal-control finish to maintain specified panel-operating temperatures.

THE EXTENDIBLE STRUCTURE

The extendible arm is simply a "lazy-tong" type of mechanism, consisting of a number of connecting links (figure 2). One-half of the links (leaves) are hinged together in one continuous assembly, providing support for the collector panels. The other half of the links (inriggers) are hinged together and pivot about pins fixed within each leaf assembly.

When fully extended, the leaf sections are in line, forming one planar surface; the inriggers remain at an angle of 150 deg with each other (15 deg with the leaves). With this linkage arrangement, the assembly is less flexible and the leaves are held in a flatter position than would be possible with the inriggers in the leaf plane. Although this arrangement causes some shadowing of the panels adjacent to the inriggers, the resulting power losses are actually quite small because the inriggers are designed to a minimum-diameter cross section.

To give an indication of strength capability, the assembly in this position has been designed to withstand 1-g load across its width and 0.1-g cantilever load when supported by its inboard links.

In a folded position, the array arm envelope is made as thin as possible by nesting the inriggers into their respective leaves. This also assures that mounting-bed preloads are directed through the leaves and not sidetracked into the inriggers. Tapered grooves are cut normal to the hinge lines on each side of the folded assembly to accommodate the mounting-bed center fittings.

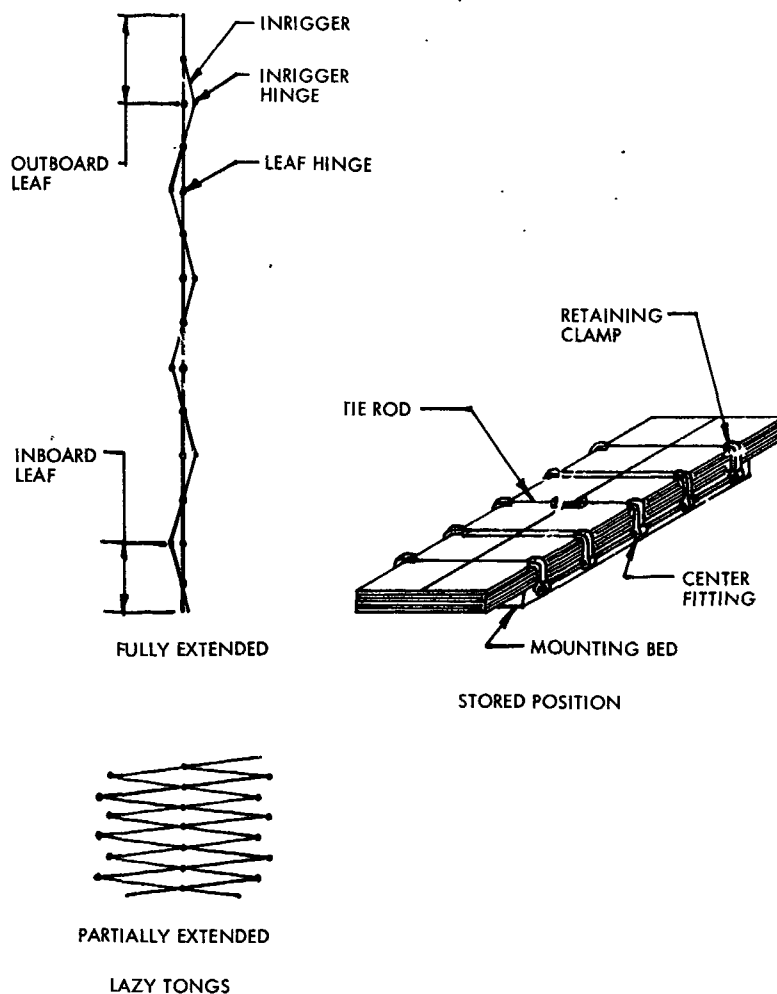


Figure 2 Solar-Array Arm Positions

Internal vibration of the components is minimized by stiffening the outboard leaf with additional structure and preloading it over spacers as it is assembled into the mounting bed. Also, small elastic pads are bonded to the cell side of each collector panel to slightly deflect and assure panel separation when the arm is folded.

The power for extension of the arm is distributed over the entire arm assembly. Small torsion springs replace two or three lobes at each hinge section. These are complemented by larger torsion springs installed at each inrigger joint. The load is uniformly distributed in this manner because of the size of the arm and the very thin sections from

which it is fabricated. The forward arm assembly is 8 ft wide, 16 ft long, and only 0.5 in. thick; the aft assembly is 5 ft wide 20 ft long, and 0.5 in. thick.

The wiring of an extendible structure can be quite difficult, but the lazy tong design lends itself fairly well to solution of this problem. The wires are installed along the backs of the leaves, opposite the cell side. Where hinge lines occur, they pass either through or around the hinge in such a way that a loop is formed. This loop is bonded in place, but enough flexibility remains so that repeated extension and retraction of the arm will not result in failure.

The forward and aft solar array arms are identical in principle and construction. They differ, however, in capability and tilt angle. The forward arm assembly can carry a total of 61 collector panels with a 40 deg clockwise tilt angle; the aft arm assembly can carry 45 collector panels with a 40 deg counterclockwise tilt angle (figure 1). Before each panel is installed into the arm, it is weighed and positioned so as to provide control of the center-of-mass of the arm.

ERECTION MECHANISM

The erection mechanism is the heart of the jack-in-the-box, and therefore requires ultimate simplicity for maximum reliability. It is a simple slider-crank device that rotates under the action of a single liquid-damped spring actuator, thus extending and angularly positioning the array in a single, continuous cycle (figure 3). The mechanism consists of a frame, an adjustable liquid-damped spring actuator, a bell-crank, a slider, and a support assembly. The inboard leaf is rotated about a fixed pivot on the support assembly. The inriggers are attached through a single fitting to the slider. During a cycle, the actuator rotates the bell-crank, which forces the slider along the support assembly tube until the full-extension position is attained.

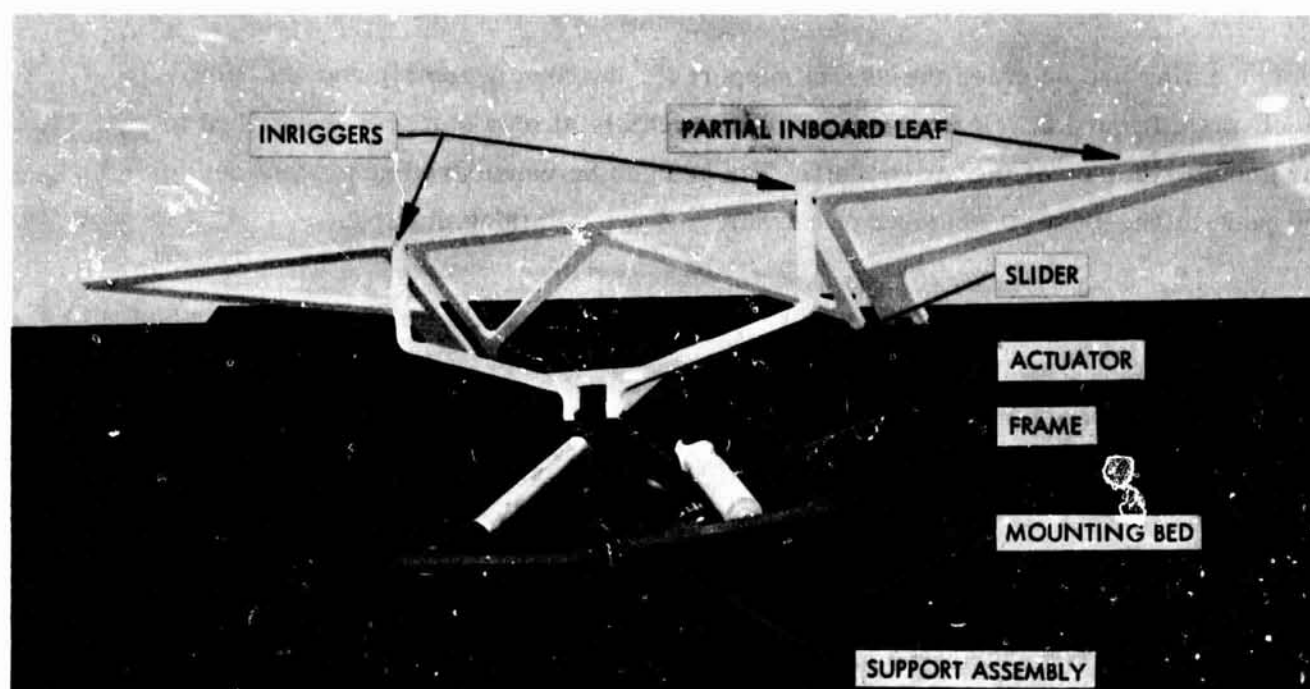


Figure 3 Erection Mechanism

The actuator is used to control the extension rate and complement the array arm forces when they are approaching their minimum output. A fluorosilicone fluid is used as the damping medium because of its relatively stable temperature characteristics. Rate control is adjusted by throttling the fluid flow with a needle valve within the piston rod. A compression spring surrounding the actuator, aided by the mechanical advantage of the mechanism, complements the forces built into the arm assembly.

Full arm extension and position is accomplished by adjusting the erection mechanism when it is installed in the mounting bed. Since it is not practical to adjust the mechanism with the arm attached, a tool that simulates the inboard leaf linkages is used. This tool is aligned to the mounting-bed feet.

ASCENT SUPPORT STRUCTURE (MOUNTING BED)

The mounting bed supplies the ascent support for the arm assembly and erection mechanism (figure 3). It interfaces with the vehicle at four surfaces prealigned to the geometric axes of the spacecraft. The bed can be considered as a container for the jack-in-the-box. It consists of a frame and two retaining clamps.

The mounting-bed frame is an integral structure with journals for the retaining clamps along each side. The retaining clamps are integral spring-loaded structures which rotate in the frame journals. Each fitting of the retaining clamps contains a set screw, tightened to specific torque requirements for retaining the folded arm assembly.

The center fittings on each retaining clamp mate with the grooves on the arm assembly to provide major acceleration support for the arm. The groove and the clamp fitting are both tapered to assure free separation. A tie rod is fastened to the outboard leaf of the arm and links the two retaining clamps. A squib-operated pin puller mounted to each center clamp joins the tie rod and the retaining clamps. When the arm and erection mechanism are assembled into the mounting bed, the tie rod is preloaded with an adjustment nut. The retaining clamp set screws are then torqued to preload the arm assembly. Once the pin pullers are fired, the retaining clamps are released, and the array arm is free to extend.

GROUND TESTING

Since the array system could not be extended without support in a 1-g environment, a series of studies was conducted to establish the best techniques and equipment for use in extension testing. The studies resulted in a system of support powered only by the spring forces in the solar-array module (figure 4). In this system, the array arm is supported at the center of each leaf by low-friction roller assemblies that ride in an overhead track. Each roller assembly is adjusted to support only the weight of the leaf to which it is attached. The inboard leaf is held so that only rotation can occur, and the remaining leaves are allowed to both rotate and translate along the overhead

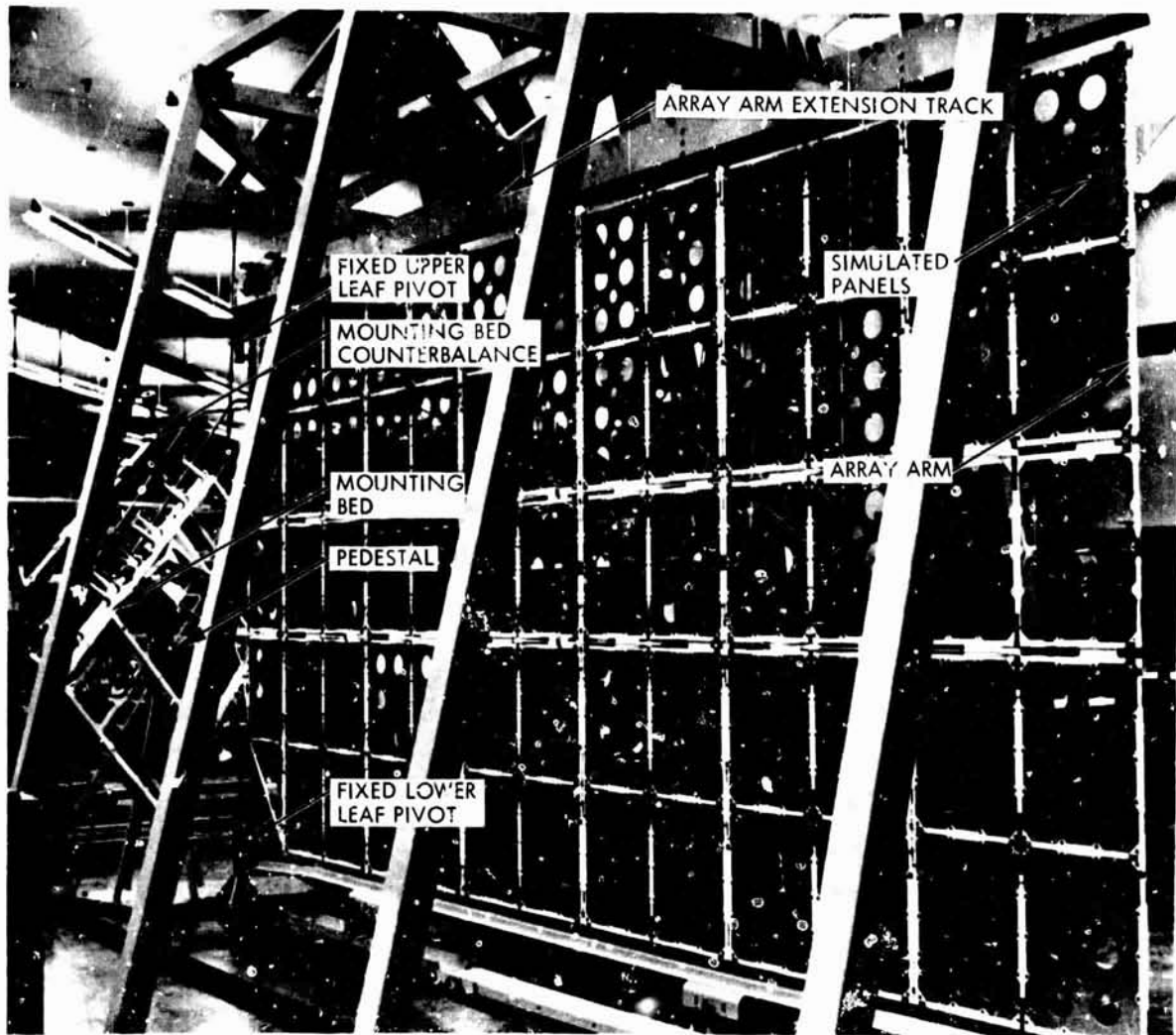


Figure 4 Qualification Test Module – Ground Extension

track. While the array arm is extending, the mounting bed is allowed to orient itself freely to its prealigned position. The bed is supported by a pedestal and counterbalanced about the support point to reduce the loads imposed on the array assembly. The only remaining loads are then the friction and inertia of the moving array module and ground-test equipment components.

An operation cycle of this system consists of extension and retraction of the arm assembly. Extension is initiated by remotely operating the flight pin pullers with a

pneumatic actuator. This action releases the mounting-bed retaining clamps and allows free extension of the array assembly. Retraction is then accomplished by applying hand pressure at the tip of the arm assembly while manually operating a mechanical device that forces the erection mechanism actuator to close. The two retraction operations are coordinated to prevent the induction of excessive loads into the arm assembly.

The array module and extension equipment system has successfully completed more than 200 test cycles. Included were the acceptance tests of the first flight modules. During these acceptance tests, recordings of the pin-puller operation, retaining clamp operation, rate of extension, and time required for complete extension were obtained by the flight instrumentation of each module. Eventually these data will be compared to flight data for performance evaluation.

CONCLUSIONS

The extendible system feasibility has been demonstrated by the actual design, fabrication, and test of the forward and aft modules. Both module types have been qualified by test to their predicted flight loads and functioned to demonstrate their operating capabilities. The first flight units have also been fabricated and acceptance-tested and will be flight-tested in the near future.